FUNGAL-MEDIATED SYNTHESIS OF NANOPARTICLES: CHARACTERIZATION, ANTIMICROBIAL ACTIVITY AND IMPACT ON APPLE PLANT HEALTH

Thesis Submitted for the Award of the Degree of

DOCTOR OF PHILOSOPHY

in

Botany

By

Shahnaz Anjum

Registration Number: 12116713

Supervised By

Dr. Ashish Vyas (12386)

Department of Microbiology & Biochemistry (Professor)

Lovely Professional University, Punjab

Co-Supervised by

Dr. Tariq Ahmad Sofi

Department of Plant Pathology (Assistant Professor)

SKUAST-Kashmir

LOVELY PROFESSIONAL UNIVERSITY, PUNJAB

2025

DECLARATION

I, hereby declared that the presented work in the thesis entitled "Fungal-mediated Synthesis of Nanoparticles: Characterization, Antimicrobial Activity and Impact on Apple Plant Health" in fulfilment of degree of **Doctor of Philosophy (Ph. D.)** is outcome of research work carried out by me under the supervision of Dr. Ashish Vyas working as Professor in the Department of Microbiology & Biochemistry of Lovely Professional University, Punjab, and co-supervision of Dr. Tariq Ahmad Sofi working as Assistant Professor in the Division of Plant Pathology, of SKUAST-Kashmir, India. In keeping with general practice of reporting scientific observations, due acknowledgements have been made whenever work described here has been based on findings of the other investigator. This work has not been submitted in part or full to any other University or Institute for the award of any degree.

(Signature of Scholar)

Name of the scholar: Shahnaz Anjum

Registration No.: 12116713

Department/school: Botany

Lovely Professional University,

Punjab, India

CERTIFICATE

This is to certify that the work reported in the Ph. D. thesis entitled "Fungal-mediated Synthesis of Nanoparticles: Characterization, Antimicrobial Activity and Impact on Apple Plant Health" submitted in fulfilment of the requirement for the award of degree of **Doctor of Philosophy (Ph.D.)** in the School of Bioengineering and Biosciences, is a research work carried out by Shahnaz Anjum, Registration number 12116713. It is a bonafide record of her original work carried out under my supervision and that no part of thesis has been submitted for any other degree, diploma or equivalent course.

(Signature of Supervisor)
Name of supervisor: Dr. Ashish Vyas Sofi
Designation: Professor
Department/school: Microbiology
University: LPU, Phagwara, Punjab, India

(Signature of Co-Supervisor)
Name of Co-Supervisor: Dr. Tariq Ahmad
Designation: Assistant Professor
Department/school: Plant Pathology
University: SKUAST-Kashmir, J&K, India

ABSTRACT

Nanotechnology has emerged as one of the most promising and rapidly advancing fields of the 21st century. In the past decades, a rapid progress has been found to take place in this area. Nanotechnology influences every dimension of scientific discipline, economic system, and various aspects of life, involving the design, synthesis, and manipulation of nano-sized materials for a range of applications such as disease management (in both plants and animals), drug and gene delivery, imaging and sensors, catalysis, electronics and other emerging technologies. Nanotechnology has the potential to advance agriculture by providing innovative tools that might boost food production and protect crops from diseases, pests, and other hazards. Metallic nanoparticles have attracted significant attention over the past decade due to their unique properties, which enable their use in a wide range of applications. Researchers have recently placed a great deal of emphasis on creating effective biological processes that use natural reducing, capping, and stabilizing agents to synthesize nanoparticles with the appropriate size and shape. Developing green and environmentally acceptable methods for synthesizing metallic nanoparticles is a crucial need in the field of nanotechnology. The applicability of myco-nanotechnology in every scientific discipline have made its continued growth in recent decades unavoidable. In comparison to the other biological entities usually engaged in the synthesis of nanoforms, the production of nanoparticles mediated by fungi has been the subject of several investigations as it is highly beneficial due to its high reaction rate, stability of particles up to several months and rapid uptake of organic bio-molecules. The fungi, therefore, position themselves to be the appropriate precursors for the nanoparticle synthesis on account of fiscal viability, sophisticated levels of tolerance towards metals, resource efficiency, resilient harvest of a fungal biomass besides presenting a reduced amount of toxic residual mass. Amongst the kingdom fungi, mushrooms are recognized as promising candidates for the production of infrequent and pharmacologically active secondary biometabolites. Additionally, they serve as excellent precursors for the biogenic synthesis of therapeutically potent, biocompatible, and stable nanostructures.

The current investigation focuses on the myco-synthesis of Zinc, Magnesium, Manganese and Combination nanoparticles using three fungal species - *Pleurotus*

sajor-caju, *Agaricus bisporus* and *Lentinus edodes* by incorporating their mycelia. A total of twelve nanoparticles were synthesized (four from each fungus). Metal ions of zinc, magnesium and manganese when exposed to the fungal mycelial extracts, were reduced and resulted in a color change indicating the formation of ZnO, MgO, MnO_2 and CNPs respectively. The physicochemical characterization of nanoparticles was done employing a blend of microscopic and spectroscopic procedures. The techniques as Ultraviolet–Visible (UV-Vis) Spectroscopy accounted for initial physicochemical characterization of nanoforms whereas Fourier Transform Infra-red (FT-IR) Spectroscopy, X-Ray diffraction (XRD) and Field Emission Scanning Electron Microscopy (FE-SEM) along with Energy Dispersive X-Ray (EDX) Spectroscopy were undertaken for in-depth portrayal of nanoparticles. These twelve samples of nanoparticles were further evaluated for detailed antifungal screening in comparison to the comparative controls i.e., Zinc, Magnesium and Manganese metal salts, besides respective reference standards. The nanoparticles were then applied to the apple plants so as to check the efficacy of different nanoparticle concentrations on gas exchange parameters including stomatal conductance (gs), net photosynthesis (Pn), intercellular CO_2 concentration (Ci), and transpiration rate (E); and chlorophyll content. The UV-Vis spectra showed peaks in the range of 307-391 nm in ZnONPs, 304-307 nm in MgONPs, 308-320 nm in MnO_2NPs and 309-329 nm in CNPs, which are the distinctive peaks of these nanoparticles accordingly. FT-IR spectroscopy showed chemical interactions of the nanoparticles with various molecules and peaks with bonds showcasing the capping and effective stabilization of nanoparticles. The respective peaks depicted in XRD patterns were in line with the crystalline phases of nanoparticles thus supporting the UV-Vis spectroscopy data and confirming the crystalline state of the nanoparticles. SEM micrographs showed the presence of irregularly shaped, angular, somewhat spherical and agglomerated nanoparticles with the average particle size of 13-92 nm, 29-99 nm, 13-90 nm, 8-63 nm, 6-76 nm, 13-84 nm, 12-63 nm, 14-61 nm, 12-71 nm, 9-73 nm, 13-72 nm, 12-73 nm in ZnO-Psc, ZnO-Ab, ZnO-Le, MgO-Psc, MgO-Ab, MgO-Le, MnO_2-Psc, MnO_2-Ab, MnO_2-Le, CNP-Psc, CNP-Ab and CNP-Le respectively. On the scale of 100-500 nm, the average size of nanoparticles came out to be in the range of 0-100 nm, thus again confirming the synthesis of desired nanoparticles. Agglomeration was observed as a result of the presence of remnants or

metabolites from fungal biomass. Energy Dispersive X-Ray (EDX) showed absorption peaks, weight percentages and atomic percentages of the elements with respect to the nanoparticles thus confirming the elemental composition.

Apple scab, caused by *Venturia inaequalis*, and Alternaria leaf blotch (ALB), caused by *Alternaria mali*, are two diseases that severely reduce apple crop production in apple-growing regions worldwide, including the Kashmir Valley. Therefore, the current study focused on using myco-synthesized nanoparticles to treat these two common apple plant diseases. The study focused on the antifungal efficacy of myco-synthesized nanoparticles and chemical fungicides against these two fungal pathogens of apple plant under *in vitro* conditions employing poison food technique and spore germination test respectively. The nanoparticles presented a broad spectrum as well as a dose and time-dependent antifungal potential against both pathogens. The highest inhibition of *A. mali* was shown by MnO_2NP-Le (96.04%) followed by ZnONP-Psc (94.57%) at the concentration of 0.30%, while as, in *V. inaequalis*, the highest inhibition of spore germination was shown by CNP-Ab (68.82%) followed by CNP-Le (62.67%) and MnO_2NP-Le (62.30%) at the same concentration. In both the cases, nanoparticles proved effective at the concentration of 0.30%. The antifungal efficacy of nanoparticles was observed to be largely comparative to the applied positive controls but certainly substantial than the comparative controls.

Gas exchange parameters were studied using Infra-Red Gas Analyzer (IRGA). Readings were taken twice (after 6 hours and 24 hours of spray). Stomatal conductance showed a positive response with the application of nanoparticles. With every increase in concentration from 0.10% to 0.30%, the value of stomatal conductance increased respectively. Metal salts showed a negative effect with the increase in concentration. In case of net photosynthesis, values increased with every increase in concentration of the nanoparticle samples. The metal salt concentrations showed a slight decrease in net photosynthesis. Intercellular CO_2 was decreased with the increase in concentrations of ZnO/MgO/MnO_2/CNPs. Similar effect was observed on the intercellular CO_2 with the increase in concentration of metal salts. There was a negligible to minimal effect on the transpiration rate of apple plants treated with all the concentrations of nanoparticles, metal salts or controls. The chlorophyll content of the apple plants was monitored Soil Plant Analysis Development (SPAD). After the controlled application of different

concentrations of nanoparticles, metal salts, and fungicides on the apple plants, the effect on chlorophyll content was quite unnoticeable, but in case of metal salts, a slight decrease in chlorophyll content was shown by the leaves with the increase in concentration from 300 ppm to 700 ppm. After the application of nanoparticles to the apple plants at even higher doses, nanoparticles did not show any adverse effect on growth rather enhanced the growth in field conditions. However, nanoparticle accumulation in plants has chances of their transfer to animals which is a major concern that needs to be addressed. The experimental results presented in this thesis are on the effects of different concentrations of ZnO/MgO/MnO_2/C-NPs on Apple plant both *in vitro* and *in vivo*. Through this research study, it is clear that the impact of nanoparticles on Apple plants is dependent on the concentrations of nanoparticles, type of growth media and the pathogen or plant parameter studied.

Conclusively, three fungi – *P. sajor-caju*, *A. bisporus* and *L. edodes* were responsible for the synthesis of twelve potential nanoparticles. The nanoparticles synthesized by extracellular mycelial fractions of these fungi emerged as the most favourable candidates in terms of the antifungal efficiency along with their preliminary effects on apple plant parameters approving the significance of this study. Therefore, these pristine, green, low-cost, therapeutically efficient besides possibly safe and easily synthesized, mycologically defined ZnONPs, MgONPs, MnO_2NPs and CNPs can be thought of to contribute a towards the enormous field of already standing or new found therapeutics. They might be perhaps well-thought-out as an additional or likely element for any proposed therapeutical conceptualization besides being utilized in other allied domains for the times to come. In this context, advanced therapeutic investigations besides a comprehensive toxicological assessment are undoubtedly mandatory.

Acknowledgment

To the experiences I never expected,
and the paths that were redirected.
To the friends and family I found along the way.

Setting a tone of gratitude, perseverance, and faith!

First and foremost, I would like to begin by expressing my heartfelt gratitude to Almighty Allah for guiding me through this significant journey, granting me the strength to embark upon, pursue, and fulfill this endeavor with integrity. The completion of this academic pursuit was marked by numerous challenges, yet, with the unwavering support and guidance of Allah, I was able to bring this extensive project to a successful conclusion with a sense of satisfaction.

The concept behind this study was both novel and pioneering, venturing into unexplored areas that offered a chance to contribute to the vast and advancing realm of research. With utmost humility, I now take this opportunity to extend my sincere gratitude to those who made this journey memorable. Their presence and support made a profound impact, enriching this experience in ways I will always cherish.

To my Mentors

It makes me proud and privileged to convey my heartfelt gratitude to my supervisor, Dr. Ashish Vyas, Professor and Head, Department of Microbiology & Biochemistry, Lovely Professional University, Phagwara, Punjab, for his benevolent encouragement, insightful guidance, and constructive criticism during my research. I am deeply grateful for his inspiring ideas, vast knowledge, and enthusiasm for scientific research, from which I have learned immensely. I would also like to thank him for his constant and unwavering support, which has been invaluable throughout this journey. Equally, I would like to extend my deepest appreciation to my co-supervisor, Dr. Tariq Ahmad Sofi, Assistant Professor, Division of Plant Pathology, FoH, Sher-e-Kashmir University of Agricultural Sciences and Technology, Kashmir, whose profound knowledge and expertise, endless motivation, invaluable suggestions and feedback have played a pivotal role in shaping my understanding and approach to this research. I take this

opportunity to thank him for his unfailing generosity, moral support and patience; for showing me where this work could go, for pushing me to take it there, and for trusting me to choose my own path forward.

I am enormously obliged to Dr. Anjali Khare, Assistant Professor, BFIT, Dehradun, affiliated with HNB Garhwal University, Uttarakhand, who introduced me to the world of research and taught me how to approach it with ease, dedication, and perseverance. A special mention and profound gratitude to Dr. Aijaz Ahmad Wani, Professor, Department of Botany, University of Kashmir, J&K, India, for his invaluable assistance, for teaching me the nuances of research in every possible way. I want to thank all the academics especially Prof. Syed, though not my supervisors but played a significant role in my development as a researcher. I am equally grateful to Dr. Asiya for her guidance being a young academic entering the profession—her advice has been enormously helpful. There have been numerous occasions where I remember feeling disheartened and stumped about the direction of my research, but inevitably, the teachings received from these wonderful mentors would reinvigorate my enthusiasm and raise my spirits immeasurably.

To my Colleagues and Labmates

I am profoundly thankful to my colleagues and labmates Mr. Kamran, Mr. Junaid Paul, Ms. Aarifa, Ms. Tabasum, Ms. Mehak Mohi-ud-Din, whose camaraderie, assistance, and encouragement have been quite stimulating for discussions and have made my time in the lab both productive and enjoyable. To the whole group of Agri-Nanotechnology Laboratory of SKUAST-Kashmir, since we all moved into the lab, there has been wonderful support and collaboration, and I thank you all for that. I am especially grateful to my colleague and friend, Ms. Arfa Ji for her insightful comments, constructive criticism, and constant support. Her distinct perspectives enriched my work and challenged me to push the boundaries of what can be achieved with research. My enduring thanks to Mr. Shabir Ahmad Bhat for all the assistance, suggestions and for fostering a lab environment that has been truly rewarding and memorable. I also unreservedly thank the technical and support staff at SKUAST-Kashmir, Mr. Bashir Ahmad, Mr. Imtiyaz, Mr. Sameer and Mr. Bilal for persistently lending their help.

To the supporting Institutes and Authorities

My indebtedness cannot ever equate the liability for which I am extremely obligated to SKUAST-Kashmir, India, for throwing open the laboratory and resources for my work besides always extending the full backing and genuine cooperation throughout this gruelling journey. Without their benevolence the work would not have been carried out successfully. I am equally and eternally grateful to my parent institute, Lovely Professional University, Phagwara, Punjab, India, for providing me with a wonderful opportunity to work, learn and grow independently.

It is my utmost privilege to place on record for a huge obligation and deepest thanks I owe to Prof. Shaheen Kauser Jan, Principal Scientist (Biochemistry), and Ex-Head, Division of Plant Pathology, SKUAST-Kashmir, J&K, India, for providing resources, and boundless assistance all throughout my work over there. I also thank Prof. M. D. Shah, Professor and Head, Division of Plant Pathology, SKUAST-Kashmir, J&K, India, for outspreading his guidance and help, whensoever required.

I owe immense gratefulness to the Central Research Facility Centre, National Institute of Technology, Srinagar, Kashmir, India, for providing me the chance to conduct various measurements like, UV-Vis spectroscopy, SEM, FT-IR, and XRD at their Centre with special acknowledgment to Prof. M. A. Shah, Professor, Department of Physics, NIT, Srinagar, J&K, India, and Mr. Tasaduq Hussain for their assistance at the institute.

I would like to sincerely express my appreciation to the Centre for Research Degree Programmes (CRDP), Lovely Professional University, for all the support and facilitation. Very special thanks to Ms. Aarti for her assistance, positive attitude and dedicated time with all the paper work and technical support that has made this journey more streamlined.

To my family

I would like to extend my appreciation and huge debt of gratitude to my parents, Mr. (Er.) Ali Mohamad Mirza and Hameeda Bano for their wholehearted and unreserved support in every aspect of my journey and in whatever I chose to do; for their

selflessness, for believing in me and providing the foundation necessary to chase my dreams.

The paucity of words does not compromise for extending my deepest gratitude to my sister, Dr. Urfeya Mirza, for her invaluable support, selfless contribution, and encouragement throughout this research. She has been a steadfast rock beside me since the beginning and has been inspiring me to do better with every new day. None of my efforts would have materialized without the unflinching support I received from her.

A special mention goes to my partner, Er. Majid Ali, for his endless patience, understanding, encouragement, intellectual guidance and unwavering moral support that has been instrumental in keeping me focused and motivated, even during the most challenging times.

Lastly, the chain of my everlasting appreciation and earnest acknowledgment goes to all those who have contributed to my research directly or indirectly. Through your silent prayers, and just by being there, this challenging endeavor has been successfully completed and transformed into a fulfilling and enriching learning experience. Indeed, a journey to be remembered, one that on moments must have turned turbulent but, in so many aspects, an evolving journey of its own where each and every person associated has been a source of encouragement. For all good things, this academic pursuit must end, but it has left life-lasting, often difficult, but ultimately valuable lessons—lessons that not only contributed to my academic growth but also strengthened my individuality and fostered my personal development.

This is the thesis, which should be a testament for many, but I am really glad to thank you all for your contribution.

I would like to thank the authors of various research articles and books whose work has been consulted, utilized and cited in my thesis.

As rightly quoted:

“It always seems impossible until it's done" *– Nelson Mandela*

Much obliged.”

S Anjum

Table of Contents

List of Tables

List of Figures

Abbreviations

ZnONPs	Zinc Oxide Nanoparticles
MgONPs	Magnesium Oxide Nanoparticles
MnO_2NPs	Manganese Dioxide Nanoparticles
CNPs	Combination Nanoparticles
Psc	*Pleurotus sajor caju*
Ab	*Agaricus bisporus*
Le	*Lentinus edodes*
nm	Nanometre
ppm	Parts per million
mM	Millimolar
mg	Milligram
kg	Kilogram
L	Litre
MT	Metric Ton
N	North
E	East
UV-Vis	Ultra Violet-Visible
XRD	X-Ray Diffraction
FT-IR	Fourier Transform Infra-Red
SEM	Scanning Electron Microscopy

EDX	Energy Dispersive X-Ray
FE	Field Emission
PDA	Potato Dextrose Agar
PDB	Potato Dextrose Broth
LPCB	Lacto-Phenol Cotton Blue
ZAD	Zinc Acetate Dihydrate
MNH	Magnesium Nitrate Hexahydrate
MD	Manganese Dioxide
SPR	Surface Plasmon Resonance
°C	Degree Centigrade
ALB	Alternaria Leaf Blotch
gs	Stomatal Conductance
Pn	Net Photosynthesis
Ci	Intercellular CO_2
E	Transpiration Rate
IRGA	Infra-Red Gas Analyzer
SPAD	Soil Plant Analysis Development
RCBD	Randomized Complete Block Design
CO_2	Carbon Dioxide
H_2O	Water
As	Arsenic

Ag	Silver
Co	Cobalt
Cu	Copper
Cr	Chromium
Cd	Cadmium
Hg	Mercury
H_2S	Hydrogen Sulfide
SeO	Selenium Oxide
Ni	Nickel
Pb	Lead
NO_2	Nitrite
NO_3	Nitrate
LD	Lethal Dosage
ROS	Reactive Oxygen Species
FWHM	Full Width at Half Maximum
ANOVA	Analysis of Variance
SD	Standard Deviation
CRD	Completely Randomized Design
DMRT	Duncan's multiple range test

Chapter 1

Introduction

1.1. Historical development of nanotechnology

The backdrop of nanotechnology dates back to early 1200-1300 BC when Chinese people used soluble gold and Romans used Lycurgus cup in 290-330 AD (Bayda *et al.*, 2019). In 1618, first colloidal gold book was released. Naturally existing nanoforms can be normally instituted within the volcanic residue, marine mist, and fine silt besides dust, in addition to organic matter e.g., viruses. In olden times people consumed colloidal gold or silver solutions as healthiness stimulants precisely to cure high fevers besides lues venerea (https://sustainable-nano.com/2013/03/25/nanoparticles-areall-around-us). A comparative outcome was too observed in late middle age church windows, the latter displaying glistening and brilliant red-yellow hues, as a result of the infusion of Silver and Gold nanoforms within the glass. Throughout the 9th -17th centuries, the shining brilliance of ceramic coverings used in the Islamic structures, or as seen in Europe, were basically imbibed with silver, copper or other nanoforms (Pradell *et al.*, 2007). During the 16th century, the Italians utilized nanoforms in manufacturing of the Renaissance pottery (Morachevskii *et al.*, 2006). In 1857, Michael Faraday, disclosed how gold nanoparticles form solutions of various colors when the former is subjected to specific lighting conditions (Bayda *et al.*, 2019). In 1902 SPR (surface plasmon resonance) was demonstrated. W. Wood, United States, 1908, G. Mie showed a nanosphere to scatter and absorb electromagnetic fields. In 1931, Transmission Electron Microscope (TEM) was found. In 1937, equipments like Scanning Electron Microscope (SEM) was discovered. In 1959, Richard Feynman gave an address “There’s Plenty of Room at the Bottom,” which paved way for the study of Nanotechnology. In 1960, I. Igarashi and T.H. Maiman effectively created Micro Electro Mechanical Systems (MEMS) oscillating a laser. Professor Norio Taniguchi, a Japanese researcher at Tokyo Science University, 1974, was the first one to utilize the expression "Nanotechnology". In 1986, K. Eric Drexler came up with the foremost book on Nanotechnology "Engines of Creation: The Coming Era of Nanotechnology", which prompted the concept of "Molecular Engineering" to become more well-known. In 1991, another book "Unbounding the Future: The Nanotechnology Revolution" was issued by Drexler, Peterson, and Pergamit, where the trio was able to utilize the expressions "Nanobots" or “Assemblers” with respect to the use and applications of

Nanotechnology inmedicine or more specifically being defined as “Nanomedicine” for the very first time (Drexler *et al.*, 1991).

1.2. Nanoscience

Richard Feynman, a renowned Nobel laureate in Physics (1959), created the notion of nanotechnology in his notorious speech at the American physical society conference held at California Institute of Technology on 29th December, 1959, saying “There is plenty of space at the bottom”. In this specific sector, there has been a revolutionary growth since. Norio Taniguchi (1974) developed the term “Nanotechnology”. Norio Taniguchi miniaturized optoelectronic, mechanical devices thus introducing the “top-down approach”. Around 1985, Eric Drexler stated, “The future of nanotechnology is the formation of larger objects from their molecular and atomic elements” thus introducing “bottom-up approach”. This lead to pioneering applications in the fast-growing fields for an evolving society (Henini, 1998). The term ‘nano’ has been derived from the Greek word meaning ‘dwarf’ i.e. small things. The science and technology of small things known as Nanotechnology is a comparatively new division of science, and deals with materials of smaller dimension that reveal size dependent quantum effect and their properties are completely distinct from the characteristics of macro-scale materials. It also exhibits unusual properties of the functions and phenomenon because of the small size of materials synthesized.

“Nanoscience is defined as a study of materials that exhibit remarkable properties, functionality and phenomena due to the influence of small dimension.”

(Filipponi & Sutherland, 2010).

1.3. Nanotechnology

Nanotechnology, which deals with particles as small as 1 to 100 nm, is based on interdisciplinary approaches from material science, biology, physics, chemistry, and medicine. The growing body of research in this field has concentrated on diverse nanomaterial fabrication techniques and their potential uses. Nanotechnology has two major components: the first is the production of nano-sized particles, and the other is the application of these nanoparticles for their intended purposes. The synthesis process

involves converting macro-sized materials into nano-sized particles. Nanoparticle generation is a complicated process that requires certain expertise and facilities, depending on the technique employed. Following synthesis, the next critical step ensuring the requisite particle size and relative homogeneity of the nanomaterials is characterization. Nanoparticles can be synthesized using several processes, including chemical reduction, electrochemical method, sonochemical method, micro-emulsion/colloidal method, microwave method, solvothermal breakdown, and biological synthesis. Soil microorganisms and plant extracts are vital for nanoparticle biogenesis and have an extensive range of potential and applications. The development of efficient and environmentally friendly nanoparticle synthesis procedures is a key feature of bio-nanotechnology (Khan and Rizvi, 2014). The aforementioned issues have been significantly addressed by the development of innovative agricultural products and ideas as a result of nanotechnology. Nanotechnology is now being investigated in agriculture for plant hormone delivery process, seed germination, management of water, targeted gene transfer, nano-barcoding, nano-sensors, and controlled agrichemical release (Hayles *et al.*, 2017). As agricultural nanotechnology advances, the possibility for developing a novel generation of insecticides along with additional actives for the management of plant diseases will grow significantly.

"Nanotechnologies are the design characterization, production and application of structure, device and systems by controlling shape and size at nanometer scale."

(Filipponi & Sutherland, 2010).

1.4. Nanoparticles

One of the most significant developments in nanotechnology has been the development of Zero dimensional novel materials in the nanometer scale called "Nanoparticles" (Biswas and Wu, 2005). These entities are invisible to human eyes yet they can be projected by intensely sophisticated instruments having a high resolution (Ramesh *et al.*, 2014). At the point when the size of a material decreases to miniature and nanoscale, its properties totally change in comparison to the bulk material (Sharma *et al.*, 2020). Decreasing the size to the nano range can alter their synthetic, mechanical, electric, organizational, morphologic, in addition to the optical features (Xu *et al.*, 2021).

Nanoparticles can enhance pesticide shelf-life, improve solubility, reduce toxicity, and increase site-specific absorption by the target insect. Nanocarriers may enhance the effectiveness and durability of nano-pesticides under light and rain conditions, minimizing the need for several applications and lowering toxicity and costs. Nanoparticles can be sprayed directly to plant seeds, leaves, or roots to protect them from pests and diseases like bacteria, fungi, viruses, and insects. Various metallic nanoparticles including titanium dioxide, zinc oxide and copper have been thoroughly investigated for their antifungal, antibacterial, and antiviral activities.

The unique features of nanoparticles include numerous applications ranging from environmental research to medical care, including metal sequestration, hazardous waste management, and environmental remediation. Pollutants in a variety of environmental matrixes, including soil, sediment, and wastewater, have been identified and removed using nanomaterials with a high surface area to volume ratio. The sequestration of As, Ag, Co, Cu, Cr, Cd, Hg, H_2S, Ni, Zn, Pb, and chlorine-based pollutants has been successfully investigated through a number of batch and column tests involving nanomaterials (the nanoscale zerovalent iron, nano-polymers, iron complexes, etc.) using adsorption, oxidation-reduction, surface complexation, and other mechanisms. The bulk of nanomaterials utilized in sequestration techniques, however, were produced chemically, endangering both animal and environmental health. Due to their advantageous environmental conditions throughout both the manufacturing and sequestration phases, fungus-mediated biosynthesised nanomaterials might be a good choice for this application. With an expanding population, the agri-food business has grown into a substantial burden on society. Future technologies, including nanotechnology, may serve as a solution to relieve the strain on this region. As technology advanced, we gained better understanding of nano-dimensional characteristics, which opened up new possibilities for the use of fungal-mediated nanomaterials in fields such as food and agriculture. With extensive funding for nanotechnology research in almost every field, the agricultural sector has only scratched the small part, with food nanoscience expanding. As reported by Duncan (2011), packaging in agricultural products appears to be a strongly motivating factor. The vast majority of the investigation is still in its early stages and is yet to be

commercialised. It does, in fact, bring honours to the field of nanotechnology by assuring to revolutionize the food and agricultural sector through novel crop enhancement tools, competent delivery techniques for monitored and intended agrochemical release, agricultural precision, prospective disease detection, nano-sensors in innovative packaging, and nano-antimicrobials for pathogen detection in food (Prasad *et al.*, 2013, 2017).

1.5. Methods for nanoparticle synthesis

Nanoparticle synthesis and manufacturing may be done using two approaches which vary in grades of quality, speediness, and monetary value (Majumder, 2013; Baig *et al.*, 2021).

1. Top-down approach

2. Bottom-up approach

The top-down approach involves dividing a bulk substance into nano-sized particles. The techniques aimed at the breakdown of the crude mass materials into nanoforms include interferometric lithography, high-energy ball milling and grinding, evaporation, condensation, chemical etching, pulsed laser ablation, sputtering, photo reduction, and so forth (Singh *et al.*, 2010; Chang *et al.*, 2013). This approach has advantages as it delivers enhanced yields, steadiness in terms of morphology of nanoparticles, a monodisperse populace, licenses scale-up of manufacturing, stability of preparation, etc. (Aryal *et al.*, 2019). However, this approach cannot be exploited for the generation of nanoparticles on a wider scale in light of the fact that it reflects incomplete topography besides it being a luxurious way out. Because of this method requiring cutting of material to make it nano-sized, the particles obtained may be unsatisfactory in terms of crystal structure.

The bottom-up strategy is the inverse of the previous method, relying on the idea of molecule self-assembly. Using this method, a nanoparticle is constructed atom by atom, yielding molecules or clusters until the desired dimensions are achieved. The various kinds of techniques utilized in this approach are the wet-chemical methods, co-precipitation, spinning, solvothermal and electrodeposition procedures, chemical vapor

deposition, pyrolysis, microemulsion, solid-gel chemistry, etc. (Mazari *et al.*, 2021). This approach results in nanoparticles that appear more homogeneous and properly organised. The drawbacks of this approach are increased consumption of energy along with long response time and ever-increasing cost, invariably poor particle size in addition to agglomeration issues. Subsequently, it requires the utilization of additional capping and stabilization agents including polymers e.g., polyethylene glycol, polyvinyl pyrrolidone, polyvinyl alcohol, and so on (Mukherji *et al.*, 2018), surface-active agent as sodium dodecyl sulfate, cetyltrimethylammonium bromide besides phospholipids (Talib and Wu, 2016). The usage of potentially perilous and unsafe reducing chemicals e.g., sodium borohydride, sodium citrate, or hydrazine, etc., further adds to toxicity both on ecological and physiological grounds hence, confining its utilization on a massive scale. The bottom-up method to metal nanomaterial production is significantly more common due to its obvious benefits (Thakkar *et al.*, 2010).

These two methodologies incorporate a variety of traditional or conventional methods like physical, chemical, or biological method, so as to manufacture nanoforms with explicit forms and sizes (Patil *et al.*, 2021). The former methods are conventional procedures employing high levels of radiation as well as concentrated reducing and stabilising chemicals that are harmful to human health and produce non-ecofriendly byproducts. In addition to that, the physical and chemical methods are really costly and can put down toxic imports on the biological systems, therefore; these are less favorable methods to synthesize nanoparticles (Thivasanthi and Alagar, 2012). The three methods are briefly discussed as follows:

1.5.1 Physical method

These methods for the development of nanoparticles comprise photo irradiation, radiolysis, solvated metal atom diffusion, ultrasonication, chemical vaporization, inert gas condensation, electrochemical methods, ion implantation, arc discharge method, spray pyrolysis and vapour-phase synthesis. The primary disadvantage of physical techniques is that managing the reaction parameters is extremely important in determining the size and form of the nanoparticles synthesized. Nanometals with significant melting points can only be synthesized using methods such as the Arc

discharge process. The main drawback of physical procedures is that they require high-quality pure source materials. Another issue with these conventional approaches is the fact that the distributions of particle sizes are quite broad and not uniform. Scaling up these procedures is tough. The nanoparticles created have an extremely limited shelf life, making the incorporation of capping agents necessary. The nanoparticles generated are extremely thermally unstable (Kruis *et al.*, 1998; Swihart, 2003; Raab *et al.*, 2011).

1.5.2. Chemical method

Chemical techniques for nanoparticle production entails a Gaseous phase and a Liquid phase, wherein the gaseous phase is further classed into pyrolysis and gas condensation whereas the liquid phase has subcategories as co-precipitation, solvothermal synthesis, sol-gel, micro-emulsion, electrochemical, colloidal method, oil microemulsion system and photochemical irradiation (Naveed Ul Haq *et al.*, 2017). The benefits associated with this strategy are the usage of a lesser amount of time to harvest massive yield of nanoforms, conception of monodisperse, pure, and highly stable nano entities, improved production rate along with the generation of diverse and size-specific nanoforms, etc. The shortcomings of chemical approaches include the difficulty of regulating the size and shape of nanoparticles, the existence of toxic byproducts during the chemical process, and the shorter shelf life of the nanoparticles created by these methods (Vaidyanathan *et al.*, 2009; Mosfegh *et al.*, 2011; Korbekandi and Iravani, 2012). The chemical reactions encompass the usage of highly noxious chemicals that can prove risky and perilous to the surrounding atmosphere and the health of a person dealing with such processes (Goyal and Pawar, 2018).

1.5.3. Biological Method

The biological method of nanoparticle synthesis is an emerging topic of nanotechnology (Roy and Barik, 2010; Rafique *et al.*, 2017). It directs us to the currently emerging and a highly trending branch of material science termed as ‘Green Nanotechnology’ or the biological synthesis of nanoparticles. Considering the drawbacks of physical or chemical methods, biological methods of nanoparticle synthesis have proven to be a boon to the field of nanotechnology, outperforming the other methods (Jain *et al.*, 2010; Kaler *et al.*, 2010; Natarajan *et al.*, 2010; Korbekandi

and Iravani, 2012). This methodology is referred so, since here the synthesis of nanoforms is carried out at mild pH, pressure, besides temperature and without the usage of any poisonous, perilous, or detrimental synthetic chemicals (Sharma *et al.*, 2015). The biological method of nanoparticle synthesis employs the bottom-up approach for metal atoms so as to fashion clusters and ultimately ultra-fine particles (Pandit *et al.*, 2022). The nanoforms are shaped as an outcome of the oxidation or reduction reactions of the metal ions into their corresponding nanoparticles through various organic biomolecules e.g., carbohydrates and proteins (Cavalu *et al.*, 2020). Some resources supposed to be environmentally acceptable for the biological synthesis of nanoparticles, include plants and plant parts (Jha *et al.*, 2009a; Mallikarjuna *et al.*, 2011; Prasad 2014; Sinha *et al.*, 2015; Ahmed *et al.*, 2016), algae (Aziz *et al.*, 2015), bacteria (Jha *et al.*, 2010; Seshadri *et al.*, 2012), actinomycetes (Sowani *et al.*, 2015), seaweeds, enzymes (Wilner *et al.*, 2006; Iravani, 2011; Patel *et al.*, 2015; Gayathri *et al.*, 2021) and fungi (Jha *et al.*, 2008; Korbekandi *et al.*, 2014; Muhsin and Hachim, 2014; Prasad 2016). Toxic, dangerous, and costly materials are not required in biosynthesis, making it easier to maintain and monitor optimal process conditions. The biological method is a one-step bio-reduction approach that produces non-toxic, clean, cost-effective, biocompatible, and ecofriendly or sustainable nanoparticles while using less energy (Sathishkumar *et al.*, 2009; Patil and Kim, 2017). During biological production, the nanoparticles are instantly covered by a protein molecule, creating a natural cap that prevents aggregation. Natural capping results in an extension of shelf life as well as stability for the synthesized nanoparticles.

Biological synthesis consuming microbes is beneficial over use of plants as the former can be effortlessly reproduced (Yusof *et al.*, 2019). Biological synthesis of precious metal nanoforms namely Gold, Silver, Platinum, Palladium, Silica, Titanium, Zirconia, Selenium, Tellurium, Magnetite, Uraninite, and Quantum dots (QDs) using various microbes, has been previously testified (Narayanan and Sakthivel, 2010). Amongst the diverse metals, Zinc draws additional attention on account of its sturdy reducing potential, and reasonable reactivity, besides inherently claiming five stable isotopes (Ali *et al.*, 2018). The biological synthesis of metallic and metal oxide nanoforms rests on the ability of microorganisms to endure heavy metals. Under conditions of stress,

the microorganisms produce enzymes and other organic or cellular biomolecules. The latter leads to an effective bio-reduction of the metallic ions thereby, causing the generation of stable and less noxious metallic NPs (Singh *et al.*, 2018). The benefits of biological synthesis of nanoparticles are that it is a rapid and one-step process, energy-efficient in addition to cost-effectivity, biocompatibility as well as harmlessness (Sharma *et al.*, 2015). The raw materials utilized in the nano biosynthesis typically have higher amounts of amino, carboxyl, or hydroxyl radicals that frequently serve as capping and stabilizing entities hence, setting off the formation of nanoparticles whilst preventing their aggregation. The resulting nanoforms have improved shelf life, higher stability, noteworthy catalytic activity (Agarwal *et al.*, 2017), augmented pharmacological dynamics along with an extensive variety of dimensions, forms, compositions as well as physicochemical features (Mohanpuria *et al.*, 2008). It also allows the large-scale generation of nanoforms devoid of any additional impurities (Agarwal *et al.*, 2017).

1.6. Mycogenic synthesis of nanoparticles

Fungi are eukaryotic primordial creatures that include yeasts, moulds, and the more common mushrooms. Their mode of sustenance is heterotrophic, including some parasites and a few saprophytes. Fungi are worldwide in distribution, thus they may be found in a variety of environments such as air, water and soil, as well as on various sections of plant bodies such as leaves, fruits, seeds, stems, and roots, as well as inside tissues of plants such as endophytes. Fungal nanotechnology, also known as 'myco-nanotechnology' is a subfield of nanotechnology that aims to understand fungi-mediated nanofabrication (Rai *et al.*, 2009). It also defines a clear borderline amongst arenas of "Mycology" in addition to "Nanotechnology" and has a noteworthy potential, on account of the widespread range besides the diversity of the fungal kingdom (Mohmed *et al.*, 2017). Mycogenic synthesis of nanoforms suggests the formulation of nanoforms via utilizing fungi along with their related metabolites and consequently their application principally in therapeutics (Salem and Fouda, 2020). It has been confirmed that synthesizing nanoparticles biologically can be made possible using the dissimilar properties of a eukaryotic organism such as fungus. Fungi may be the most beneficial biogenic source for nanoparticle production due to their enrichment with

extracellular enzymes (Ingle *et al.*, 2008), simplicity of preservation (Honary *et al.*, 2013a), solvent-free synthesis (Duran and Seabra 2012), and ease of scaling up (Yadav *et al.*, 2015). Fungal frameworks are considered to be “Bio-nanofactories", upon being biological and cost-effective resources for producing a lot of reducing enzymes accordingly, serving in the orchestration of nanoforms pertaining to numerous metals as Gold, Silver, Platinum, Iron, Zinc, Titanium, Copper and so forth (Hanafy, 2018). Fungi can function as efficient bio-reductants for the extra- and intracellular synthesis of metal nanoparticles because of the presence of enzyme hydrogenases, organic acids, proteins, and nitrate-dependent reductases. The production of nanoparticles by the extracellular release of enzymes has enhanced the handling and processing of biomass downstream. While intracellular synthesis entails transporting ions into microbial cells in order to produce nanoparticles in the presence of enzymes, making it challenging to retrieve the nanoparticles in pure form, extracellular synthesis entails trapping metal ions on the cell surface and reducing them with the involvement of enzymes, which are easily recovered from the process (Narayanan and Sakthivel, 2010). The cell wall of fungus and its carbohydrates are thought to be crucial for metal ion lowering (Mukherjee *et al.*, 2001). Fungi also offer a clear advantage in terms of metabolic processes and cellular level organisation for nanofabrication. These factors led to a rise in publications and the investigation of myco-nanotechnology for a range of applications pertaining to diverse fields such as the biomedical industry, pharmaceutical, agriculture, electronics, and so on (Youtie *et al.*, 2008; Jha *et al.*, 2009a; Gade *et al.*, 2010). Some of the most often used fungi for nanoparticle biosynthesis *Cladosporium* sp., are *Trichoderma* sp., *Aspergillus* sp., *Fusarium* sp., *Penicillium* sp. and *Trichothecium* sp. belonging largely to the phyla Basidiomycetes, Ascomycetes, and Phycomycetes. Mushrooms are higher fungi that lack chlorophyll, which means they cannot use solar energy to produce food in the same way that green plants can. However, mushrooms can manufacture an extensive variety of enzymes that deconstruct the complicated substrate on which they develop, allowing them to absorb the water-soluble substrate for their own sustenance. The term "mushroom" describes a macrofungus with a distinct fruiting body that may appear as epigeous or hypogeous, sufficiently sized to be seen with an unassisted eye, and harvested with hand (Chang and Miles, 1993). Mushrooms are classified within the phyla Ascomycotina and

Basideomycotina (Alexopolous et.al., 1996). They exist naturally and periodically in a variety of habitats and nicks across the world. The mushrooms are a huge diverse group with a wide range of forms, sizes, and colours, each with its own distinct character, appearance, and edible properties. From this enormous group of around 2000 edible species, over 300 species within 70 genera have been documented from India. However, just a handful have been cultivated commercially. Out of 2000 species of prime edible mushrooms, approximately 80 have been grown experimentally, 20 have been cultivated commercially, and six, *Agaricus bisporus*, *Lentinus edodes*, *Pleurotus* spp., *Auricubria*, *Valvarella*, and *Flammulina*, have undergone industrial production (Chang and Miles, 1991), earning them the nickname "the big six mushrooms."

The chief paybacks of mycogenic synthesis (Khandel and Shahi, 2018; Messaoudi and Bendahou, 2020; Salem and Fouda, 2020) are as follows:

1. Fungi may be easily isolated from many environmental sources and grown on simple, low-nutrient medium such as PDA and Czepekdox's broth in a laboratory setting, where they can be easily maintained.

2. Fungi offer an extensive range and diversity along with easy accessibility.

3. Maximum fungi need a wide variability of growth parameters as pH, temperature, as well as salt concentration, etc., that facilitates any variation in culture conditions so as to generate homogeneous nanoforms (Guilger Casagrande and Lima, 2019).

4. They may readily go through downstream processing for extracellular and intracellular manufacture of nanoparticles and generate additional extracellular production of reductive proteins (Absar *et al.*, 2005; Musarrat *et al.*, 2011).

5. The rate at which fungi reduce metallic ions to create highly monodispersed nanoparticles with distinct size and shape is remarkably quick (Kashyap *et al.* 2013; Chokriwal *et al.*, 2014).

6. Fungi have clearly defined nuclei and are genetically modified to release a large number of enzymes essential for nano-conversions, resulting in an enormous amount of nanoparticles with smaller particle sizes (Jha and Prasad, 2016).

7. Mycological mycelia comparatively offer a greater surface area for interaction along with easy handling of the fungal biomass.

8. The cell wall of fungi offers mechanical strength to endure changes in the environment and osmotic pressure (Durán and Nombela, 2004; Yadav *et al.*, 2015).

9. Fungi are considered to be biocompatible, less harmful, cost-effective and facile as well as eco-friendly.

10. Developed efficacy of fungal metabolites to create various habitually monodispersed nanoforms with a well-defined morphology besides diverse chemical compositions (Dhillon *et al.*, 2012).

11. Fungi generally exhibit slower kinetics hence, propose ease in manipulation and regulation over the morphology of nanoparticles alongside long-time stability (Zhao *et al.*, 2018).

12. Mycological cells appear to be more resilient to dealing with the procedural settings and variations, e.g., high compression, rate of flow and mixing, etc., that improves their probable usage for extensive synthesis of nanoforms (Narayanan and Sakthivel, 2010).

13. Fungi can possibly be manipulated for the synthesis of nanoforms at large-scale as they particularly harvest enormous quantities of extracellular enzymes, readily able to catalyse the heavy metallic ions to produce the corresponding nanomaterial.

14. Mycological candidates generate nanoparticles on an extracellular route thus, resulting products can be easily purified and right away utilized in varied applications (Gaikwad *et al.*, 2013).

15. Myco-fabrication makes downstream processing easier for product purification and recovery along with an additional benefit of producing a large number of nanoparticles due to the release of several extracellular enzymes (Kumar *et al.*, 2007; Gade *et al.*, 2008; Ingle *et al.*, 2008; Birla *et al.*, 2009; Rai *et al.*, 2009; Zhang *et al.*, 2011a; Honary *et al.*, 2013b; Quester *et al.*, 2013; Yadav *et al.*, 2015; Prasad *et al.*, 2016).

16. Maximum fungi carry a greater acceptance of metals, a higher wall-binding ability, and substantial competence for intracellular metal intake (Alghuthaymi *et al.*, 2015).

17. Fungi possess more intricate proteins and bioactive metabolites, that can easily reduce metal ions and stabilize corresponding nanoparticles for longer time frames (Mohanpuria *et al.*, 2008).

18. Fungi are known to synthesize chemicals such as anthraquinones and naphthoquinones (Siddiqi and Husen, 2016), that can specifically reduce a particular metal, for example, nitrate reductase is essential for reducing ferric ions into iron nanoforms.

19. Fungi produce various secondary metabolites such as vitamin C, peroxidases, proteins, etc., which have classified them as efficacious bioresources for heavy metal reduction in industries.

To synthesise nanoparticles, extracts from three fungal species- *Pleurotus sajor-caju*, *Agaricus bisporus*, and *Lentinus edodes* were employed.

1.7. Description of targeted fungi for nanoparticle synthesis

1.7.1. Systematics of *Pleurotus sajor-caju*

Domain	Eukaryota
Kingdom	Fungi
Division	Basidiomycota
Sub-division	Basidiomycotina
Class	Agaricomycetes
Order	Polyporales
Family	Polyporaceae
Genus	*Pleurotus*
Species	*P. sajor-caju*

Fruiting body of *Pleurotus sajor -caju*

This *Pleurotus* strain originated in India. In 1974, it was found growing in the foothills of Himalayas on the succulent tissue of *Euphorbia royleana* Boiss (Jandail, 1974; Jandail and Kapoor, 1976). Dr. Z. Bano gave this fungus, known as "*Pleurotus sajor-caju*," to Professor S.-T. Chang, a prominent mushroom biotechnologist, in 1980. *P. sajor-caju* is a basidiomycete, and the basidiocarp is edible as well as nutritious. It belongs to the order Polyporales and the family Polyporaceae. The sporophores of *P. sajor-caju* are usually grown in groups. *P. sajor-caju* is commonly known as oyster mushroom because the fruiting bodies look like oyster shells. *Pleurotus* species include a high concentration of proteins, minerals, and vitamin B and C complexes. They can be utilised to address dietary deficiencies in impoverished nations when the diet lacks high-quality minerals and proteins (Kumar *et al.*, 2020). Oyster mushrooms are a great source of nutrients. Crude protein content was calculated using dry weight (Yang *et al.*, 2001). They have around 60% carbohydrates (dry weight), which is consistent with other culinary mushrooms (Crisian and Sands, 1978; Bano and Rajarathnam, 1988).

Oyster mushroom contains no carbohydrates, minimal sugar, and a high fibre content, making it among the least fattening foods (Osei, 1996).

1.7.2. Systematics of *Agaricus bisporus*

Domain	Eukaryota
Kingdom	Fungi
Division	Basidiomycota
Sub division	Basidiomycotina
Class	Agaricomycetes
Order	Agaricales
Family	Agaricaceae
Genus	*Agaricus*
Species	*A. bisporus*

Fruiting body of *Agaricus bisporus*

Agaricus bisporus, sometimes referred to as the white or button mushroom, stands as the most frequently cultivated edible fungus worldwide and is mostly accessible to consumers through commercial cultures, with yields that make up 70% of the total edible fungi (Kalac *et al.*, 2013). The culinary and therapeutic properties of *A. bisporus*, which result from its wide range of metabolites and physiologically active ingredients, are among its most noteworthy traits. *A. bisporus* is rich in essential and semi-essential amino acids, dietary fibre (chitin), and antioxidants (phenolics, sterols, and indole compounds, vitamins, ergothioneine, and selenium) (Elmastas *et al.*, 2007; Foulongne-Orio *et al.*, 2013). Fruiting bodies of the fungus contain a high concentration of amino acids. Eighteen of these chemicals have been studied and reported, however several are not found in sufficient quantities to constitute *A. bisporus* as a means of supplementation. Aspartic acid, alanine, arginine, glutamic acid, serine, lysine, leucine, phenylalanine, proline, tyrosine, and threonine are among the many amino acids found

in *A. bisporus* (Bernaś *et al.*, 2006a; Muszyńska *et al.*, 2013a). But the least common ones are still valine, methionine, and cysteine (Bernaś *et al.* 2006b). The cell walls of *A. bisporus* consist of fibres and matrix elements that are abundant in mannans, β-D-glucans, and chitin (Cheung, 2013; Liu *et al.*, 2013). The fact that *A. bisporus* contains both primary and secondary metabolites suggests that phytochemicals are crucial for its therapeutic properties (Bhushan and Kulshreshtha, 2018). Saponins are a broad class of structurally similar chemicals that include steroids and terpenoids. Saponins have been shown in studies to have anti-inflammatory, anti-malarial, anti-cancer, and anti-diabetic properties (Wandati *et al.*, 2013). *A. bisporus* extract contains phenolic chemicals that function as antioxidants as well as anti-cancerous and anti-inflammatory effects (Jagadish *et al.*, 2009). *A. bisporus* mushrooms have a carbohydrate content of 4-13% by dry weight (Colak *et al.*, 2007). The soluble glucoside level was much lower than the protein quantity. *A. bisporus* has significant amounts of alkaloids and flavonoids, which may explain its antioxidant, anticancer, as well as anti-inflammatory properties.

1.7.3 Systematics of *Lentinus edodes*

Domain	Eukaryota
Kingdom	Fungi
Division	Basidiomycota
Sub division	Basidiomycotina
Class	Agaricomycetes
Order	Agaricales
Family	Omphalotaceae
Genus	*Lentinus*
Species	*L. edodes*

Fruiting body of *Lentinus edodes*

Lentinus edodes, commonly referred to as black forest or oak mushroom (Shiitake in Japanese and Xiang-gu in Chinese), is considered as the most essential edible mushroom produced worldwide and the most widely consumed fungus in China and other Asian countries. *L. edodes* is a wood-decaying fungus that thrives in warm, moist climates on fallen or dead wood from a wide range of deciduous trees, particularly chestnut, oak, maple, beech, oplar (aspen, cottonwood), sweet gum, hornbeam, palder, chinquapin, ironwood, and mulberry. The natural distribution of shittake extends across northeast Asia, however, the precise boundaries are unknown. For a long time, people have valued this mushroom for its distinct aroma and taste as well as its use as a medical tonic. Wood logs or artificial substrate logs can be used to cultivate it (Quimio *et al.*, 1990; Stamets, 2000; Chang and Miles, 2004). It also has a high nutritional value and components that strengthen the immune system. Various therapeutic values such as anti-inflammatory effects, anticancer activity, and anti-diabetic properties are attributed mostly to the β-glucan found in lentinan (Wang *et al.*, 2016a). Many chemicals with health-promoting properties have been isolated from *L. edodes* via scientific research (Mizuno, 1995; Wasser and Weis, 1997; Hobbs, 2000). Longvah and Dosthale (1998) reported that the fruiting bodies of *L. edodes* contain 88-92% water, lipids, protein, carbs, vitamins, and minerals. The mushroom is high in vitamins, particularly provitamin D2 (ergosterol), which converts into calciferol (vitamin D2) when exposed to ultraviolet (UV) light and heat. Besides, it includes B vitamins, such as riboflavin, thiamine, and niacin (B12) (Hobbs, 1995; Mizuno, 1995; Hobbs, 2000; Mattila *et al.*, 2001; Mattila *et al.*, 2002). From the chemical standpoint, the physiochemical characteristics and structures of *L. edodes* polysaccharides, such as their average molecular dimensions, monosaccharide concentration, and glycosylation type, are often what determine their biological activity. The existence of normal β-glucans is necessary for the considerable host-mediated anti-cancer effect of lentinan, a polysaccharide with a high molecular weight β-1,3-D-glucan that contains β-1,6-glucopyranoside branches produced from *L. edodes* (Zhang *et al.*, 2011b). Recently, *L. edodes*-derived polysaccharides have been used as antimicrobial agents, pharmaceuticals, and nutritional additives in a variety of functional foods.

1.8. Mycosynthesis of Zinc nanoparticles

Inorganic compounds, such as Zinc Oxide (ZnO), outperform organic materials in terms of durability, selectivity, and heat resistance. ZnO is the most significantly manufactured and commonest compound of Zn found in nature besides having a wide array of uses (Greenwood and Earnshaw, 1997). It is a multipurpose inorganic material, typically showing up as a white precipitate and almost insoluble in water. It is the least expensive compound of Zn, appears to be well absorbed as it is solvable in dilute acid, and possibly dissolves in acidic gastric juices too (Klemm, 2013). Amongst the diverse kinds of inorganic nanoforms, zinc oxide nanoparticles (ZnONPs) are rated as the third largest nanoform, shaped all around the world besides being utilized in innumerable fields (Piccinno *et al.*, 2012). ZnO NPs have established themselves as a more competent metal oxide (MO), on account of their multifunctional nature (Al-Mohaimeed *et al.*, 2022). ZnO adopts a stable wurtzite configuration with several planes made up of tetrahedral synchronized Zn^{2+} and O^{-} ions arranged sequentially along the c-axis (Xu *et al.*, 2014). ZnO is a biocompatible and environmentally accessible material, which is essential, particularly for utilization in the biomedical industry (Miri *et al.*, 2020). There are several Zn-related nanomaterials as ferrite, phosphide, selenide, sulfide, telluride, etc., out of which ZnO nanostructures are of intense attention because of their striking properties such as outstanding biotic compatibility, nontoxicity, ease, and minimal cost involved in manufacturing, greater analytical performance with sensitivity, having an extensive array of antimicrobial activity, higher resistance to critical processing settings and so forth (Hatamie *et al.*, 2015). The main features accountable for applications of ZnONPs are higher concentration and large surface area (Ashrafi and Jagadish, 2007). Furthermore, because of their high photosensitivity, ZnONPs are thought to be a great photocatalysts for the breakdown of organic contaminants (Tripathy *et al.*, 2014).

1.9. Mycosynthesis of Magnesium nanoparticles

Magnesium oxide nanoparticles (MgONPs) are essential metal oxide nanoparticles due to their crystal structure, good stability, cost-effectiveness, biocompatibility, effective ionic properties and ability to operate as safe and potent contaminant adsorbents. MgONPs have been particularly interesting to researchers worldwide over the last two

decades due to their diverse uses and distinctive features (Khan *et al.*, 2020). MgONPs may be synthesized using a variety of chemical techniques, including solvent transformation, sol-gel, co-precipitation, and hydrothermal processes; nevertheless, these procedures have detrimental environmental impacts (Duong *et al.*, 2019). The biological production of nanoparticles using fungi has recently become the best method due to its adaptability, rapid development, multiplication, wide variety of species (more than 1.52 million species), novelty, cost-effectiveness, and ecological sustainability (Clarance *et al.*, 2020; Rai *et al.*, 2021). The most preferred method for synthesizing MgONPs is the extracellular biological synthesis utilizing fungi, which is quick, easy, and inexpensive method without the use of potentially hazardous substances (Saad *et al.*, 2018). MgONPs may be synthesised utilising fungi in two ways: intracellularly by transporting metal ions within the fungal cell and subsequently reducing them using enzymes, or extracellularly by reacting metal ions to the filtrate of fungal biomass (Bhardwaj *et al.*, 2020b). MgONPs have been estimated to be useful in a variety of applications, involving hazardous material removal, catalytic activity, antimicrobial activity, refractory substances and treatment of wastewater, ceramics, heavy-duty fuel oils, enhancing antioxidant properties and substrate potential in agriculture, biomedical fields, ferroelectric thin films, sensing, adsorbents, and lithium batteries (Din *et al.*, 2018; Jeevanandam *et al.*, 2019; Khan *et al.*, 2020; Rani *et al.*, 2020).

1.10. Mycosynthesis of Manganese nanoparticles

Manganese, one of the most prevalent elements on Earth, is essential for development in both plants and animals (Veeramani *et al.*, 2013; Asaikkutti *et al.*, 2016). Over the past ten years, manganese oxides have attracted a lot of scientific attention because of their distinct physical and chemical characteristics, as well as prospective uses in catalytic activity, exchange of ions, molecular adsorption, biological sensors, and storage of energy. According to recent studies, manganese oxides nanomaterials, may eventually replace rare element-based technologies like platinum catalytic converters for various uses (Katz, 1953; Zaki *et al.*, 1998; Han *et al.*, 2006; Iablokov *et al.*, 2010). However, their use is rare in plant research. Only a few techniques have been utilized for the synthesis of manganese, despite the fact that there are several approaches for the environmentally friendly synthesis of nanoparticles (Agarwal *et al.*, 2017). The

findings are in accordance with certain researchers who advocate manganese oxides as lesser toxic compared to other materials that are routinely used to make nanoparticles (Harish *et al.*, 2013). The current work intended to synthesise and characterise antimicrobial manganese nanoparticles (MnNPs) utilising fungal extracts, as well as explore their influence on apple diseases and plant parameters. Additionally, Mn-oxides have a high specific capacitance, are environmentally friendly, and are generally less hazardous than other chemicals such various chalcogenides that serve as the basis for nanoparticles (Chen *et al.*, 2010; Veeramani *et al.*, 2013). According to recent research, Mn-oxide nanoparticles have the potential to displace technologies that rely on rare elements, including platinum catalytic converters for automobile production (Veeramani *et al.*, 2013). The structural flexibility of Mn-oxide nanoparticles is made up of many physicochemical characteristics (Fei *et al.*, 2008). From an ecological perspective, manganese nanoparticles can be synthesized using green methods because they do not need stabilization or reduction as a specific chemical and can be prepared in mild conditions like room temperature and pressure (Vanaja *et al.*, 2013; Prasad and Patra, 2017). Natural substances, fruits and vegetables, plant extracts, microorganisms, and fungi have all been used to create Mn and Mn-oxide nanoparticles in the biological synthesis of manganese nanoparticles (Singh *et al.*, 2016; Ahmed *et al.*, 2017). Two significant issues in nanobiotechnology remain the regulation of the size and form of green synthesised manganese nanoparticles and their uses (Quester *et al.*, 2013). Manganese nanoparticles are employed in a variety of applications, including water treatment, purification, catalysts, solar cells, and magnetic materials (Zayed and Eisa, 2014; Gehrke *et al.*, 2015; Singh *et al.*, 2016; Zayed *et al.*, 2017).

1.11. Apple plant - fungal diseases

In agriculture, nano-pesticides, nano-herbicides, and nano-fungicides are used (Owolade *et al.*, 2008). In order to increase their activity, a number of companies created formulations that included nanoparticles in the 100–250 nm size range, which may dissolve in water more effectively than current ones. Additional companies employ nanoscale particle suspensions, also known as nano-emulsions, which can be oil-based or water-based and consist of homogeneous suspensions of herbicidal and pesticidal nanoparticles in the 200–400 nm range. These suspensions have a number of potential

uses for treatment, harvest preservation, and preventive measures (Rickman *et al.*, 1999; Goswami *et al.*, 2010). Significant problems have been brought about by pathogenic fungus in both plant and animal systems. Although widespread use of antimicrobial compounds has greatly slowed the spread of fungal diseases, dangerous fungi have developed resistance to antifungal drugs over time. These antifungal substances are also detrimental to humans, plants, and the ecosystem as a whole (Vandeputte *et al.*, 2012). When compared to studies on bacteria, the possible negative effects of antifungal substances may be one of the main reasons why reports on antifungal research have become less frequent (Doughari and Nuya, 2008). According to numerous studies, a variety of nanoparticle materials have antimicrobial qualities against bacteria, viruses, and eukaryotic microorganisms. These materials include copper (Cioffi *et al.*, 2005), zinc oxide (Sui *et al.*, 2013), silver (Adeli *et al.*, 2013), gold (Gu *et al.*, 2003), magnesium, and titanium dioxide (Yah *et al.*, 2015). In the current investigation, we established the inhibitory activity of zinc, magnesium, manganese, and combination nanoparticles on the pathogenic fungi- *Alternaria mali* and *Venturia inaequalis*. Furthermore, the anti-mycelial efficacy of all twelve forms of nanoparticles was investigated against *A. mali* and *V. inaequalis*, damaging the apple crop.

Since the beginning of time, apple (*Malus domestica* Borkh.) has been the most widely grown temperate fruit across Europe and Asia (Wang *et al.*, 2016b). Globally, more than 65 million tonnes of apples are grown each year. India ranks seventh in terms of apple fruit output, with 2163400 MT produced year (FAO, 2012). In India, apples are mostly cultivated in Himalayan states such as Jammu and Kashmir (J&K), Himachal Pradesh, and Uttaranchal, which account for over 90% of total output (Anonymous, 2000). The Kashmir Valley in the Union Territory of Jammu and Kashmir accounts for 60–65% of this production. The Kashmir Valley is home to hundreds of apple varieties, which account for the majority of apple genetic diversity in India. This germplasm may have essential agronomic features, such as resistance to diseases. It produced 1,372,973 metric tonnes of apples from 138,191 hectares of orchard land between 2010 and 2011 (FAOSTAT, 2021). Apples, like most horticultural crops, are attacked by a variety of diseases that reduce the fruit both in quantity and quality. However, fungal infections are mostly responsible for significant crop losses. Plant diseases originating from fungi are common and problematic for the agricultural sector. In addition to reducing crop

production and parameters, diseases caused by these fungi can result in a decline in produce quality because of the buildup of mycotoxins, which can be harmful to both humans and animals. Thus, pathogenic fungi remain the focus of attention for phytopathologists across the globe. The principal fungal diseases are scab, powdery mildew, *Alternaria* leaf blotch, root rot, collar rot, fly speck, and sooty blotch. The most commercially significant disease among them is *Venturia inaequalis*, which causes apple scab (Alaniz *et al.*, 2014). Regarding yield losses, *Alternaria mali*, which causes *Alternaria* leaf blotch, is one of the severe saprophytic and pathogenic genera that affects ripened as well as harvested produce (Yuan *et al.*, 2019). Although much research has been carried out on management of apple plant diseases like leaf spot and apple scab through chemicals, plant extracts and bio-control agents, yet no work has been carried out on testing various fungal-mediated metal nanoparticles against the diseases so far.

To manage these fungal infections, many insecticides and fungicides are utilised, and pathogenic organisms have developed resistance to such traditional chemical compounds. Over 15 fungicide applications are utilised to manage the fungi within a single season. Following infection, this is still the sole feasible technique for disease control. However, uncontrolled use of fungicides is producing major health and environmental issues since these fungicides are not biodegradable and accumulate in water, soil, and plants, imposing harmful effects on other organisms that are part of the ecosystem (Villa *et al.*, 2017; Pimentel *et al.*, 1993; Holb *et al.*, 2005). Alternative organic substances (bio-fungicides) are affordable, readily accessible, non-toxic, and biodegradable. Several researchers have lately expressed interest in employing plant products as bio-fungicides to combat fungal illnesses. Compared to conventional fungicides, bio-fungicides safeguard the soil, crop, and environment more effectively. Biological fungicides can also reduce the possibility of disease resistance (Zaker, 2016). A different approach to fungicide spraying is the adoption of resistant cultivars, that are not readily accessible in bulk. As a result, there is a dire need to develop additional cultivars that are resistant to scab and apple spot that may be employed in apple breeding.

1.12. Targeted fungi for antimicrobial activity

1.12.1. *Alternaria mali*

Domain	Eukaryota
Kingdom	Fungi
Division	Ascomycota
Class	Dothideomycetes
Order	Pleosporales
Family	Pleosporaceae
Genus	*Alternaria*
Species	*A. mali*

Alternaria leaf blotch (ALB), a foliar fungal infection caused by *Alternaria mali*, is found in all apple-growing regions of the world and is an economically significant disease. Roberts (1924) was the very first to identify *Alternaria mali* as the cause of Alternaria leaf blotch in the United States. This was initially reported in India by Gupta and Agarwala (1968) in Himachal Pradesh. Puttoo originally documented the disease in Kashmir in 1987 and identified *A. tenuissama* as the causal agent, while *A. mali* was later identified as the principal cause (Shahzad *et al.* 2002). In August 2013, the disease became widespread in Kashmir, affecting over 80 % of orchards (Bhat *et al.*, 2015). According to various reports based on a different study, the disease caused a projected loss of 40-60% this year, decreasing apple quality from Grade "A" down to Grade "C" (Annonymous, 2013). In apple-growing areas, the disease causes extensive foliar defoliation. Small, recessed, light or medium brown specks on ripe fruits indicate fruit spot indications (Persley and Horlock, 2009). Thus, growing pathogen sensitivity to synthetic fungicides, along with public pressure to limit pesticide usage, fuelled by heightened knowledge of environmental and health concerns, has shifted the emphasis to alternate pathogen control approaches. ALB is distinguished by irregular (although

initially nearly circular) light brown or blackish brown patches that gradually grow to 2-5 mm in diameter and are surrounded by a dark brown to violet-colored stripes (Bulajic and Babovic, 1997). It is crucial to remember because *Alternaria*-like symptoms, particularly leaf symptoms, might resemble those of physical damage or similar fungal infections. As a result, relying just on lesions of the leaves to diagnose *A. mali* is neither appropriate nor conclusive. ALB is defined by the fact that, under favourable environmental circumstances, the blotches might keep growing and leaves may fall untimely from the branches.

1.12.2. *Venturia inaequalis*

Domain	Eukaryota
Kingdom	Fungi
Division	Ascomycota
Class	Dothideomycetes
Order	Pleosporales
Family	Venturiaceae
Genus	*Venturia*
Species	*V. inaequalis*

The fungus *Venturia inaequalis* causes apple scab, which is one of the most devastating diseases in apple crops. The disease causes significant economic losses for producers specifically and the apple sector in general (Machardy, 1996). Infection can develop on foliage, fruits, stems, or young twigs, even though fruits and leaves are the most common sites of infection. Infection begins on the inner side of the leaf and eventually spreads to other areas. Young leaves are more susceptible to infestation than matured or older leaves (Thakur VS, Sharma 1999). The first noticeable signs are pinhead-sized water-soaked areas. Later, they grow and take on a black and smoky look. As the condition progresses, the skin ruptures, and the exposing tissue produces black or dark

velvety appearance. Finally, they become brownish-black. If fruits get contaminated before harvest, signs and symptoms do not appear until storage (Berrie and Xu, 2003). During storage, black, rough, and round lesions may form. The fungus produces upright, brown conidiophores and many conidia, which cause the lesions. The ascospores are the major cause of infection. These become active immediately as spring arrives (Holb *et al.* 2005). After 7 to 10 days, the biomass of the pathogen grows significantly, and asexual spores known as conidia infect other cells. In the Kashmir valley, ascospore discharge may commence as early as late March and last for a few weeks (Sharma, 2010). Further infections are caused by asexual conidiospores. Conidia propagate from branch to branch by raindrops and the wind. If the weather is favorable, the fungus spreads swiftly, resulting in a significant rise in the occurrence of scab. The pathogen is active even at extremely cold temperatures (Stensvand *et al.*, 1997), and it can spread at temperatures as low as 1°C in 40 hours. Temperature and moisture are closely linked to the occurrence of infection; hence, they may be utilized for estimating scab incidence (Mills and Laplante, 1951). Qazi *et al.* (2008) offer a change to Mills' table that is appropriate to the valley of Kashmir. Even various methods for estimating ascospore maturation have been created to aid in disease prevention (James and Sutton, 1982).

1.13. Antimicrobial activity of ZnONPs

ZnONPs have been shown to exhibit antibacterial and antifungal properties (Yamamoto, 2001; Sawai and Yoshikawa, 2004). Zinc compounds are mostly used as fungicides in the agriculture industry (Waxman, 1998). ZnO has a rather high 50% lethal dosage (LD50) of gastrointestinal toxicity; in rats, it reaches 240 mg/kg (South, 2002). Higher antibacterial action is believed to be associated with the smaller diameters of ZnO (Yamamoto, 2001). ZnONPs show antimicrobial effects against *Bacillus subtilis, Salmonella* spp*., Klebsiella pneumoniae, Staphylococcus epidermidis, Candida albicans, Malassezia pachydermatis, Enterobacter aerogenes* (Palanikumar *et al.*, 2014). Zinc nanoparticles were reported to show antifungal activity against *Penicillium expansum* and *Botrytis cinerea* (He *et al.*, 2011). Nagarajan *et al.* (2013) discovered that biosynthesised ZnO nanoparticles derived from fucoidan water-soluble pigments found in leaf extract of *Sargassum myriocystum* are more efficient as

antibacterial agents against the gram-positive bacteria than gram-negative bacteria. These pigments are accountable for the reduction and stability of ZnO nanoparticles. Food-related microbes *Bacillus subtilis*, *Escherichia coli*, and *Pseudomonas fluorescens* have all been studied in relation to the antimicrobial properties of ZnO NPs (Jiang *et al.*, 2009; Theivasanthi and Alagar, 2011). The plant pathogenic fungus *Fusarium oxysporum, Alternaria alternata, Mucor plumbeus,* and *Rhizopus stolonifera* have all been demonstrated to be susceptible to antifungal activity of ZnONPs. According to the *in vitro* investigation, ZnONPs have strong fungicidal activity and prevent spore germination, albeit at varying doses (Wani and Shah, 2012). Additionally, ZnONPs of various sizes have demonstrated effectiveness against *Aspergillus niger* and *Aspergillus flavus* (Rajiv *et al.*, 2013). According to reports, ZnONPs have strong antifungal qualities against the harmful fungus *Penicillium expansum*, which causes apple blue mould disease, and *Botrytis cinerea*, which damages a wide range of crops. ZnONPs negatively impact the cellular processes of the pathogen, which in turn inhibits the formation of fungal hyphae. Furthermore, ZnONPs stop conidiophores and conidia from growing, which ultimately results in the death of fungal hyphae and a significant morphological modification of the fungus following ZnONP treatment (He *et al.*, 2011). Therefore, ZnONPs may be employed as strong fungicides to manage plant diseases (Kairyte *et al.*, 2013). Because of their surface-chemical activity, nanostructured ZnO and MgO nanoparticles are biosafe, biocompatible, and have antibacterial and antifungal properties (Ruffolo *et al.*, 2010; Janaki *et al.*, 2015).

1.14. Antimicrobial activity of MgONPs

MgONPs have long-lasting antibacterial action, which can be linked to their capacity to withstand severe temperatures along with low volatility (Ammulu *et al.*, 2021). MgONPs have shown great antimicrobial effects for *Salmonella* spp. and *Escherichia coli.* The mechanism of antimicrobial activity of the MgONPs is yet unknown. The antibacterial action mechanism of MgONPs was described by a number of hypothesised processes, including the release of reactive oxygen species (ROS), the contact of MgONPs with the microbial cell, which subsequently destroys the pathogens, and an alkaline influence (El-Sayyad *et al.*, 2018). The microbial cell wall was being destroyed

as a result of the association with the harmful microorganisms. The electrostatic interactions among MgONPs and the microbial cell wall caused the cell loss (Stoimenov *et al.*, 2002). Furthermore, because of their failing nature and positive evaluation of their exterior, which results in a potent contact with negatively charged microorganisms, MgONPs may produce halogen vapours (Stoimenov *et al.*, 2002). Overall, because MgONPs produce hydrogen peroxide, they alter the permeability of microbial membranes, alter the architecture and composition of microbial cells, and induce the emergence of oxidative stress response genes inside the microbial cell. The total membrane loss suggests that the dissociation of membrane reliability in microbial cells and the activation of oxidative pressure genes are the causes of antimicrobial effects of MgONPs (He *et al.*, 2016).

1.15. Antimicrobial activity of MnO_2NPs

Nanomaterials made of manganese oxide may hold a lot of promise for environmentally friendly nanotechnology. Research on the biological synthesis of manganese nanoparticles was greatly needed in the field of nanotechnology because of the diversity of organisms and the availability of different structures for Mn-oxides (Prasad, 2017). Apart from the utilization of manganese oxide nanoparticles utilizing their electronic characteristics and catalytic activities, the majority of research papers concentrated on assessing their chemical, physical, and catalytic properties; its antibacterial effects were, however, hardly studied (Joshi *et al.*, 2020). Furthermore, it is never investigated if these nanoparticles have antifungal activities against the majority of fungi (Jayandran *et al.*, 2015). Furthermore, it has been suggested in the past to look into the possibilities of creating metallic nanocomposites (such ZnO-MnO_2, MgO-MnO_2, and others) in order to increase the uses of manganese nanoparticles (Moon *et al.*, 2007; Thankalekshmi *et al.*, 2011; Hsu *et al.*, 2013). Manganese nanoparticles work against an extensive range of fungi, for example, *Fusarium* wilt fungus and *Verticillum* wilt fungus and have caused a remarkable inhibition of the same (Elmer and White, 2016).

1.16. Apple plant parameters

The application of nanotechnology may significantly contribute to the long-term enhancement of agricultural productivity. The advantageous effect of nanoparticles used as fertilizers on crops is mainly reflected in increased yields, but nanoparticles

may also affect both the quantity and quality of secondary metabolites as well as various other parameters such as chlorophyll content, each of which contribute to improved crop quality. Foliar fertilisation involves applying nutrients, biostimulants, insecticides, and phytohormones to the aerial portions of plant (Laane, 2018). Spraying fertilizers, which include micronutrients such as zinc, iron, manganese, boron, copper, and silicon are both easy for field usage and effective, with an exceptionally quick plant responsiveness. The use of these substances can enhance the nutritional balance of plant, resulting in increased fruit output and quality, enhanced disease resistance, and greater drought and salinity tolerance (Fernandez *et al.*, 2013). Nanomaterials could be used to create new fertilisers (Mosanna and Khalilvand, 2015), ensuring effective delivery of nutrients to the plant and a rapid response from the plant (Fernandez *et al.*, 2013), with only one-third of the conventional equivalents added to the natural environment (Boutchuen *et al.*, 2019). In the same vein, it was shown that silicon is mainly hazardous to plants in its bulk form, but silicon nanoparticles are helpful to plants (Helaly *et al.*, 2017). There are currently very few studies on how nanoparticles affect fruit trees. Some studies focused on the effect of nanoparticles in mitigating the effects of stressful situations on fruit seedlings, while others focused on utilizing nanoparticles to boost the development, yield, and fruit nutritional value of trees grown in non-stressful environments. Over many years, the apple plant has had a significant impact on restrictions such as gas exchange parameters and chlorophyll content present in the leaves. Gas exchange could be measured using O_2 electrodes or infrared gas analysers, which can calculate CO_2 flux across the ecosystem, plant or individual leaf levels and canopy growth (Perdomo *et al.*, 2018). Net CO_2 flow is frequently calculated using CO_2 gas exchange evaluations for both response curves and point-in-time measurements of leaf photosynthesis. Gas exchange measurements are also considered the 'gold standard' for evaluating optical methods such as reflectance measurements (Ainsworth *et al.*, 2014; Silva-Perez *et al.*, 2017). Monitoring plant CO_2 uptake has long been a standard procedure. In previous methods, plant CO_2 absorption was measured by passing air from a plant chamber over CO_2 absorbing solutions. After then, conductance (Sproehr and McGee, 1924; Thomas and Hill, 1937) or titration measurements (McLean, 1920; Heinicke and Hoffman, 1933) were carried out. Later systems included infrared gas analyzers (IRGAs), which enhanced precision and

allowed for continuous tracking of an air stream (Mooney, 1972). The requirement for field measurements of photosynthetic rates led to the development of the first mobile labs (Strain, 1969; Mooney *et al.*, 1971). These devices were still bulky and challenging to transport to several field sites. The existing century-long history of gas exchange metrics has led to a widespread recognition of the system requirements for precise and accurate measurements (Bloom *et al.*, 1980; Long and Ireland, 1985; Long and Hällgren, 1993; Long *et al.*, 1996). Additionally, routine assessment of physiologically important parameters is made possible by mobile/portable commercial systems (Sharkey, 2016; Long and Bernacchi, 2003). The decrease in the amount of photosynthesis in apple plants during mild to severe drought conditions is mainly caused by stomatal restrictions, which limit the diffusion of CO_2 from the atmosphere into carboxylation sites (Escalona *et al.*, 2000; Marques da Silva and Arrabac, 2004). The current study represents one of the few that covers many targets, and the first on apple, to assess the involvement of zinc, magnesium, manganese, and combination nanoparticles in different gas exchange parameters and their effect on chlorophyll content of the apple crop. Most of the studies dealing with apple disease management have been considered with morphological, cultural, physiological, epidemiological and chemical features. A little is known about the botanical control of apple diseases in India. In addition, nanoparticle evaluation studies being a new aspect as antimicrobial agents, also need to be considered for their analysis at *in vitro* level.

Scope of the present investigation

Researchers have historically used metals nanoparticles like silver (Ag), gold (Au), Copper (Cu), Iron (Fe), and titanium (Ti), each with their own biological and catalytic roles (Mukherjee *et al*., 2001; Ahmad *et al*., 2003). Compared to these, Zn, Mg, and Mn are less toxic and more environmentally friendly, aligning with green synthesis principles (Abdelraheem et al., 2021; Ramezani Farani *et al*., 2023; Sharma *et al*., 2025). Their roles in biological systems also make them more compatible with fungal enzymes, leading to more controlled and sustainable nanoparticle production. Therefore, the current progress in nanotechnology has incited growing curiosity in the curative efficacy of ZnO, MgO, MnO_2 and Zn+Mg+Mn nanoforms besides navigating environmentally friendly courses through which these nanoparticles could be

effortlessly formulated. It could also be concurrently utilized to offer new insights into sustainable nanotechnology and in various branches of agriculture along with highest productivity. Consequently, the present effort was pursued as per an underlying objective to employ the biometabolites as mined from an array of three fungal species. This synergy of biomolecules was made to amalgamate with the broad-spectrum and multifunctional metals as Zn, Mg and Mn in order to realize a rapid, cost-effective and green synthesis route, so as to carve out various kinds of biological nanoforms. Additionally, the therapeutic worth of these mycogenic nanoparticles was investigated by exploring their underlying antifungal effectiveness on an *in vitro* scale against Alternaria leaf blotch and apple scab causing pathogens- *A. mali* and *V. inaequalis* respectively. Detailed investigations were conducted on the ability of myco-synthesized nanoparticles to alter the plant parameters of apple plant.

Organization of the thesis:

The thesis is split into five chapters. Chapter I offers an introduction regarding the importance and objectives of the study. Chapter II is the review of the literature which deals with a brief report on various synthetic methods, different characterization techniques, and various applications of zinc, magnesium, manganese and combination nanoparticles in short. Chapter III is the experimental part. It describes the method of myco-synthesis of twelve types of nanoparticles using three fungal extracts, antimicrobial studies and then the evaluation of plant parameters. It also gives the description of various characterization techniques used in the study. Results and discussions are summarized in Chapter IV. It is organized into seven sections, each of which details the synthesis, characterization, and antifungal properties of zinc, magnesium, manganese, and combination nanoparticles synthesized using the specific fungal extracts. The conclusions of the entire work are summarized in Chapter V.

Chapter 2

Review of Literature

2.1. Green synthesis of nanoparticles

Over the past few years, the environmentally benign characteristics of biologically synthesized nanoparticles and their prospective uses in a wide range of areas have attracted a lot of interest. Various researches have demonstrated how this method can be utilized for environmental remediation, particularly in the removal of pollutants (Cao *et al.*, 2020; El Messaoudi *et al.*, 2024; Mehmood *et al.*, 2024; Pal *et al.*, 2024; Shobana *et al.*, 2024;). This shift towards greener methods not only reduces environmental impact but also opens up new avenues for biomedical applications (Al-Darwesh *et al.*, 2024; Johnson *et al.*, 2024; Mariappan *et al.*, 2024; Netala *et al.*, 2024; Ragavendran *et al.*, 2024; Varshney and Gupta, 2024; Vinothini *et al.*, 2024), specifically anti-phytopathogenic effects (Abdelhady *et al.*, 2024; Bouqellah *et al.*, 2024; Dėnė *et al.*, 2024; El-Abeid *et al.*, 2024; El-Naggar *et al.*, 2024; Garibo and Khan, 2024; Ibrahim *et al.*, 2024; Ingle *et al.*, 2024; Jahan *et al.*, 2024; Jomeyazdian *et al.*, 2024; Konappa *et al.*, 2024; Narware *et al.*, 2024; Parada *et al.*, 2024; Tiwari *et al.*, 2024b; VS *et al.*, 2024) of nanoparticles synthesized from natural sources.

2.1.1. Plant-Based Synthesis

Plant extracts, abundant in phytochemicals, work as stabilizing and reducing agents during the synthesis of nanoparticles, enabling the environmentally friendly manufacture of nanoparticles without the use of hazardous chemicals (Bekele *et al.*, 2024; Dhanalakshmi and Losetty, 2024; Elkhateeb *et al.*, 2024; Fifere *et al.*, 2024; Hayat *et al.*, 2024; Johnson *et al.*, 2024; Moradnia *et al.*, 2024; Mousa *et al.*, 2024; Pahuja *et al.*, 2024; Sagar *et al.*, 2024; Sedefoglu, 2024; Bhardwaj *et al.*, 2020a).

2.1.2. Microbial Synthesis

Microorganisms provide a potential path for the eco-friendly fabrication of metallic nanoparticles (Bharose *et al.*, 2024; Liu *et al.*, 2024; Li *et al.*, 2024; Mandal and Sarkar, 2024; Ozdal, 2024; Singh and Chandra, 2024 and Soni *et al.*, 2024). Through enzymatic processes or direct interactions with metal ions in their environment, the metabolic activities of these microbes can lead to the reduction of metal ions into nanoparticles (Liu *et al.*, 2024; Nzithya *et al.*, 2024; Zahera *et al.*, 2024). The capacity of these microbes to generate nanoparticles with uniform size and shape makes them very

beneficial (Gericke and Pinches, 2006; Mandal *et al.*, 2006; Das *et al.*, 2010; Narayanan and Sakthivel, 2010; Sweet *et al.*, 2012).

2.1.2.1. Fungal-mediated Synthesis of Nanoparticles

Fungi have emerged as efficient systems for the manufacture of nanoparticles because of their exclusive characteristics, including high wall binding capacity, simplicity of culture, and ease of managing biomass (Yadav *et al.*, 2015). The fabrication of zinc nanoparticles has so far made extensive use of a variety of fungi like *Aspergillus niger* (Shamim *et al.*, 2019; Abdelkader, *et al.*, 2022), *Aspergillus fumigatus* (Rajan *et al.*, 2016), *Aspergillus aeneus* (Jain *et al.*, 2013), *Cordyceps militaris* (Dias *et al.*, 2022), *Phanerochaete chrysosporium* (Sharma *et al.*, 2021), *Dictyota dichotoma* (Kumar *et al.*, 2022), *Xylaria acuta* (Sumanth *et al.*, 2020); *Monascus purpureus* (Ammar *et al.*, 2021), *Fusarium keratoplasticum* (Mohamed *et al.*, 2019), *Fusarium chlamydosporum* (Hammad *et al.*, 2023); Magnesium nanoparticles like *Rhizopus oryzae* (Hassan *et al.*, 2021), *Penicillium chrysogenum* (El-Sayyad *et al.*, 2018), *Aspergillus niger* (Ibrahem *et al.*, 2017), *Aspergillus tubingensis* (Raliya *et al.*, 2014), *Erysiphe cichoracearum* (Fathy and Mahfouz, 2021), *Penicillium crustosum* (Amin *et al.*, 2024); and Manganese nanoparticles like *Arcopilus globulus* (Dhoble and Kulkarni, 2016; Zhang *et al.*, 2022), *Aspergillus niger* (Mohiudden *et al.*, 2023), *Alternaria alternata*, *Fusarium brachygibbosum*, *Penicillium verruculosum* and *Aspergillus niger* (Dhoble and Kulkarni, 2016). Figure 2.1 showcases the outline of mycosynthesis of nanoparticles. A broad outline of the fungal species utilized for the synthesis of Zn, Mg, and Mn nanoparticles along with the key characteristics of synthesized nanoparticles and the characterization techniques employed has been summarized in Table 2.1.

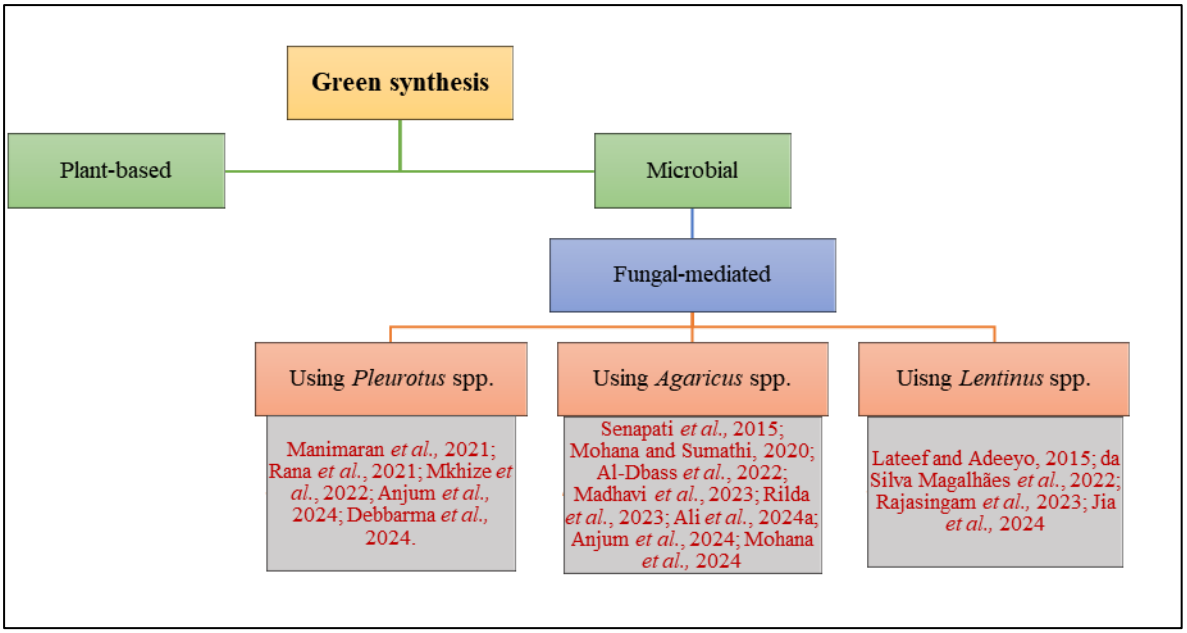

Figure 2.1: Schematic outline of fungal-mediated nanoparticle synthesis process

Table 2.1: Summary of synthesis and biophysical characterization of Zn, Mg and Mn nanoparticles via various fungal species

Fungi	NP	Characterization	NP characteristics	Applications	References
Aspergillus niger	Zinc	XRD, SEM, UV-Vis and EDX technique	• Shape: Hexagonal • Size: 40 nm	-	Shamim *et al.*, 2019
Aspergillus niger	Zinc	UV-Vis spectroscopy, FT-IR, XRD, SEM, TEM, EDX, DLS	• Shape: Hexagonal • Size: 23.97 ± 2.29 nm	In vitro and In vivo antibacterial activity (against *Staphylococcus aureus*).	Abdelkader , *et al.*, 2022
Aspergillus fumigatus	Zinc	UV-Vis spectroscopy, FT-IR, SEM	• Shape: Spherical • Size: 60-80 nm	Antimicrobial activity of *Klebsiella pneumoniae, Pseudomonas aeruginosa* and *E scherichia coli*, *Staphylococcus aureus* and *Bacill us subtilis*.	Rajan *et al.*, 2016
Aspergillus aeneus	Zinc	UV-Vis spectroscopy, FT-IR, XRD, TEM, EDX	• Shape: Spherical • Size: 100-140 nm	-	Jain *et al.*, 2013

Cordyceps militaris	Zinc	UV-Vis spectroscopy, FT-IR, XRD, SEM, EDX, TEM, zeta potential analysis	• Shape: Spherical • Size: 20-100 nm	Antibacterial activity against *Pseudomonas aeruginosa, Shigella flexneri, Proteus vulgaris, Rhodococcus equi.*	Dias *et al.*, 2022
Phanerochaete chrysosporium	Zinc	UV-Vis spectroscopy, FT-IR, XRD, PL, SEM	• Hexagonal (average size = 83.9 nm) • Spherical (average size = 59.5 nm)	Antimicrobial activity against bacterial strains (*Escherichia coli* and *Staphylococcus aureus*) and white rot fungus (*Phanerochaete chrysosporium*).	Sharma *et al.*, 2021
Dictyota dichotoma	Zinc	UV-Vis spectroscopy, FT-IR, SEM, EDX	• Shape: Spherical • Size: 80-100 nm	• Dye degradation efficiency (~90%) under photo illumination. • Antibacterial activity against *Bacillus subtilis* and *Klebsiella pneumonia.*	Kumar *et al.*, 2022
Xylaria acuta	Zinc	UV-Vis spectroscopy, FT-IR, XRD, SEM, EDX, DLS, TEM, SAED	• Shape: Hexagonal • Size: 34-55 nm	Antibacterial activity on *Staphylococcus aureus, Bacillus cereus, Pseudomonas aeruginosa* and *Escherichia coli.*	Sumanth *et al.*, 2020
Monascus purpureus	Zinc	UV-Vis spectroscopy, DLS, TEM, FT-IR, SEM	• Shape: Round • Size: 33.6-78.1 nm	Antifungal activity against *Fusarium solani*, *Fusarium sporotrichioides*, *Fusarium oxysporum*, *Rhizoctonia solani*, and *macrophomina phaseolina.*	Ammar *et al.*, 2021

Fusarium keratoplasticum	Zinc	UV-Vis spectroscopy, FT-IR, SEM, EDX, TEM, XRD, Zeta potential	• Shape: Spherical • Size: 6-36 nm	Antibacterial activity against *Staphylococcus aureus, Bacillus subtilis, Pseudomonas aeruginosa* and *Escherichia coli*.	Mohamed *et al.*, 2019
Fusarium chlamydosporum	Zinc	UV-Vis spectroscopy, FT-IR, XRD, SEM, EDX	• Shape: Spherical • Size: 19.3 nm	-	Hammad *et al.*, 2023
Rhizopus oryzae	Magnesium	UV-Vis spectroscopy, TEM, SEM, EDX, XRD, DLS, FT-IR, XPS analyses	• Shape: Spherical • Size: 20.38 ± 9.9 nm	Antimicrobial activity against *Staphylococcus aureus*, *Bacillus subtilis*, *Pseudomonas aeruginosa*, *Escherichia coli* and *Candida albicans.*	Hassan *et al.*, 2021
Penicillium chrysogenum	Magnesium	UV-Vis spectroscopy, XRD, DLS, TEM, FT-IR	• Shape: Spherical • Size: 10.28 nm	Antimicrobial activity against *Enterococcus faecalis, Candida albicans*, and *Klebsiella pneumoniae.*	El-Sayyad *et al.*, 2018
Aspergillus niger	Magnesium	UV-Vis spectroscopy, SEM	• Shape: Spherical • Size: 47.35-98.46 nm	Antibacterial activity against *Staphylococcus aureus* and *Pseudomonas aeruginosa.*	Ibrahem *et al.*, 2017
Aspergillus tubingensis	Magnesium	UV-Vis spectroscopy, TEM, WDS, DLS	• Shape: Spherical and slight edged • Size: 1-5.8 nm	-	Raliya *et al.*, 2014
Erysiphe cichoracearum	Magnesium	UV-Vis spectroscopy, FT-IR, XRD, DLS, SEM, and TEM	• Shape: Spherical • Size: 20-30 nm	Antimicrobial activity against *Escherichia coli* and *Candida albicans.*	Fathy and Mahfouz, 2021
Penicillium crustosum	Magnesium	UV-Vis spectroscopy, FT-IR, XRD, TEM, EDX, DLS, Zeta potential	• Shape: Spherical • Size: 8-35 nm	Chlorophyll and carotenoid contents; carbohydrate and protein contents;	Amin *et al.*, 2024

				free proline contents in *Nigella sativa.*	
Arcopilus globulus	Manganese	UV-Vis spectroscopy, FT-IR, XRD, SEM	• Shape: Spherical • Size: 24 nm	-	Dhoble and Kulkarni, 2016
Arcopilus globulus	Manganese	UV-Vis spectroscopy, TEM, EDX, FT-IR, XRD	• Shape: Spherical • Size: <200 nm	Antibacterial activity against *Escherichia coli.*	Zhang *et al.*, 2022
Aspergillus niger	Manganese	UV-Vis spectroscopy, XRD, SEM	• Shape: Spherical • Size: 87.39 nm	-	Mohiudden *et al.*, 2023
Alternaria alternata	Manganese	UV-Vis spectroscopy, FT-IR, SEM, XRD	• Shape: Spherical • Size: 20-30 nm	-	Dhoble and Kulkarni, 2016
Fusarium brachygibbosum	Manganese	UV-Vis spectroscopy, FT-IR, SEM, XRD	• Shape: Spherical • Size: 20-30 nm	-	Dhoble and Kulkarni, 2016
Penicillium verruculosum	Manganese	UV-Vis spectroscopy, FT-IR, SEM, XRD	• Shape: Spherical • Size: 20-30 nm	-	Dhoble and Kulkarni, 2016
Aspergillus niger	Manganese	UV-Vis spectroscopy, FT-IR, SEM, XRD	• Shape: Spherical • Size: 20-30 nm	-	Dhoble and Kulkarni, 2016

2.1.2.1.1. Utilizing *Pleurotus* spp.

The production of metal nanoparticles using fungal species belonging to the *Pleurotus* genus has emerged as a sustainable and eco-friendly approach in recent years. It has offered an environmentally benign alternative to chemical synthesis and also leveraged the natural biological processes of the fungi (Mkhize *et al.*, 2022). Studies have explored various species within the *Pleurotus* genus for the production of various metal nanoparticles, showing their versatility and efficiency (Rana *et al.*, 2021).

Zinc: Debbarma *et al.* (2024) demonstrated that *Pleurotus* extract-mediated selenium and zinc nanoparticles significantly improved the biofortified fruit body yield besides enhancing their protein and Se/ Zn contents. Anjum *et al.* (2024) synthesized ZnONPs using fungal cultures of *Pleurotus, Agaricus* and *Lentinus* spp. and evaluated their

biofungicidal properties. ZnONPs have been biosynthesized earlier using *Pleurotus ostreatus* and their cytotoxicity and antimicrobial activities have also been assessed against HepG2 and Hek293 cells thus offering a different, environmentally friendly way to produce ZnONPs with antimicrobial properties and may also be used to treat cancer (Mkhize *et al.*, 2022). Manimaran *et al.* (2021) evaluated the application (larvicidal, histopathology, antibacterial, antioxidant and anticancer activity) of ZnONPs from *Pleurotus djamor*. Rana *et al.* (2021) synthesized metal oxide nanoparticles using varying amounts of three metal salts—zinc, copper, and iron, that were created by incubating the salts with *Pleurotus florida* mycelium extracts.

Magnesium and Manganese: Specific studies focusing on the synthesis of magnesium and manganese nanoparticles using *Pleurotus* fungi are quite rare or may not be published yet. This presents a potential area for future study, given the demonstrated ability of *Pleurotus* species to facilitate the biosynthesis of various metallic nanoparticles that could include magnesium and manganese.

2.1.2.1.2. Utilizing *Agaricus* spp.

In recent years, significant amount of research has been done on the production of metal nanoparticles utilizing *Agaricus* spp. (Madhavi *et al.*, 2023; Ali *et al.*, 2024a). Nanoparticles derived from *Agaricus* are used to control plant diseases and produce non-toxic, eco-friendly pesticides and fungicides that increase agricultural output (Madhavi *et al.*, 2023). The use of *Agaricus bisporus* for the nanoparticle synthesis using green approach has also been demonstrated to exhibit significant antibacterial properties (Al-Dbass *et al.*, 2022).

Zinc: Mohana *et al.* (2024) attempted a bio approach (mediated by *Agaricus bisporus)* to synthesize zinc, copper and cobalt ferrite nanoparticles and evaluated their *in- vitro* cytotoxic effect. Using various fungal cultures from mushroom species, ZnONPs were produced and their possible antifungal efficacy against *Alternaria mali* was evaluated (Anjum *et al.*, 2024). Sol–gel–hydrothermal techniques were used to produce bioactive zinc oxide nanorods utilizing bioactive chemicals from the fungus *Agaricus bisporus* (Rilda *et al.*, 2023). Mohana and Sumathi (2020) synthesized ZnONPs using aqueous extract of *Agaricus bisporus* and evaluated its *in-vitro* biological effects. Senapati *et al.*

(2015) created zinc sulphide (ZnS) nanoparticles using button mushroom (*Agaricus bisporus*) extract which showed their structural, optical, and electrical characteristics.

Magnesium and Manganese: To the best of knowledge, there are currently no published studies that specifically address the synthesis of magnesium and manganese nanoparticles using *Agaricus* spp. This study aims to fill this gap by exploring the potential of *Agaricus* spp. in the biological synthesis of zinc, magnesium and manganese nanoparticles.

2.1.2.1.3. Utilizing *Lentinus* spp.

The *Lentinus* species, isolated from Amazon substrates, is a viable bioresource for the biological production of metal nanoparticles with pertinent antimicrobial properties (da Silva Magalhães *et al.*, 2022) and therefore *Lentinus* spp. can be used as potential industrially viable organisms, used for diverse biotechnological applications (Lateef and Adeeyo, 2015).

Zinc: Jia *et al.* (2024) coated and dispersed ZnONPs using the denaturation–renaturation process of a triple helix glucan lentinan, induced by changes in pH value within the reaction system. A polysaccharide called lentinan was extracted from the fruit body of shiitake mushroom (*Lentinus edodes*). The synthesized composites were further evaluated for antimicrobial activity and their inhibitory effect on various plant pathogens. Rajasingam *et al.* (2023) fabricated zinc-oxide nanoparticles using extract from *Lentinus sajor-caju*, which were then used as a carrier for natural substances. Their potential for application in biomedicine was proved by their significant inhibition of microorganisms.

Magnesium and Manganese: To the best of knowledge, the synthesis of magnesium and manganese nanoparticles using *Lentinus* spp. has not been previously reported, indicating a novel area for further exploration.

A broad outline of the Zn nanoparticles synthesized using *Pleurotus*, *Agaricus*, and *Lentinus* species has been presented in Table 2.2.

Table 2.2: Summary of Zn nanoparticles synthesized using *Pleurotus, Agaricus* and *Lentinus* spp.

Fungi	Characterization	Nanoparticle characteristics	Application	Reference
Pleurotus spp.	UV-Vis spectroscopy, FT-IR, SEM, XRD	• Shape: Spherical • Size: 84-91 nm	Improved yield of biofortified fruit bodies in mushrooms.	Debbarma *et al.*, 2024
	UV-Vis spectroscopy, FT-IR, SEM, XRD	• Shape: Irregular • Size: 10-100 nm	Antifungal activity against *Alternaria mali*.	Anjum *et al*., 2024
	UV-Vis spectroscopy, FT-IR, SEM, TEM, SAED, XRD, DLS	• Shape: Spherical • Size: 7.50 nm	Antibacterial activity and potential use in cancer treatment.	Mkhize *et al.,* 2022
	UV-Vis spectroscopy, FT-IR, XRD, SEM, EDX, TEM, PSA	• Shape: Spherical • Size: 70-80 nm	Anti-larvicidal, antibacterial, antioxidant and anticancer activity.	Manimaran *et al*., 2021
	UV-Vis spectroscopy, FT-IR, SEM, TEM	• Shape: Spherical • Size: 9.36 to 58.13 nm	Antibacterial activity against *Escherichia coli.*	Rana *et al*., 2021
Agaricus spp.	UV-Vis spectroscopy, XRD, FT-IR, SEM-EDAX, Zeta potential and DLS	• Shape: Spherical • Size: 65 nm	Hyperthermia Treatment and Drug Delivery	Mohana *et al.*, 2024
	UV-Vis spectroscopy, FT-IR, SEM, XRD	• Shape: Irregular • Size: 10-100 nm	Antifungal activity against *Alternaria mali*.	Anjum *et al.*, 2024
	UV-Vis spectroscopy, FT-IR, XRD, SEM, EDX	• Shape: Irregular • Size: 20-28 nm	Antibacterial activity against *Staphylococcus aureus* and *Pseudomonas aeruginous*	Rilda *et al.*, 2023
	UV-Vis spectroscopy, FT-IR, XRD, SEM, TEM, Zeta potential	• Shape: Irregular • Size: 32 nm	Antibacterial activity against *Bacillus subtilis*, *Staphylococcus aureus*, *Enterococcus faecalis*, *Proteus vulgaris*, *Klebsiella pneumoniae*, *Escherichia coli.*	Mohana and Sumathi, 2020

	UV-Vis spectroscopy, FT-IR, XRD, SEM, EDX, TGA	• Shape: Spherical • Size: 3.5-2.1 nm	-	Senapati *et al.*, 2015
Lentinus spp.	UV-Vis spectroscopy, FT-IR, XRD, SEM	• Shape: Needle-like • Size: 20 nm	Antimicrobial activity against *Candida albicans.*	Jia *et al.*, 2024
	UV-Vis spectroscopy, FT-IR, XRD, SEM, TEM	• Shape: Spherical • Size: 28 nm	Antimicrobial activity.	Rajasingam *et al.*, 2023

2.2. Characterization of Nanoparticles

Nanoparticle characterization is essential to determining their characteristics and applications. A large number of techniques namely atomic force microscopy, UV–visible spectroscopy, electron microscopy, dynamic light scattering, FT-IR spectroscopy, X-ray diffraction, X-ray photoelectron spectroscopy etc. can be utilized to characterize nanoparticles (Titus *et al.*, 2019; Wadhwa *et al.*, 2022). Mourdikoudis *et al.* (2018) provided a comprehensive review of these techniques and their applications in nanoparticle characterization.

2.2.1. Ultraviolet-Visible (UV–Vis) Spectroscopy:

Zinc: Singh *et al.* (2024) examined a number of theoretical and empirical techniques for estimating the size of ZnONPs and examining their properties by employing the UV-Vis spectroscopy. Mousa *et al.* (2024) synthesized ZnONPs employing a range of plant extracts, and they were characterized them by means of a number of techniques, such as X-ray diffraction, Ultraviolet-Visible Spectroscopy, Fourier-Transform Infrared Spectroscopy, Field Emission Scanning Electron Microscope, and High-Resolution Transmission Electron Microscopy. When exposed to UV light, the photocatalytic activity of green synthesized nanoparticles was tested using Methyl Orange (MO). The enhanced light absorption by the inter-band gap states and efficient charge transfer are responsible for the rise in photocatalytic efficacy. Yadav *et al.* (2024) used UV-Vis spectroscopy to examine the phytogenic production of ZnONPs from the aqueous extract of the *Evolvulus alsinoides* plant, and detected a peak at 264 nm. Takcı *et al.* (2024) used zinc acetate dihydrate as the precursor metal salt and sodium hydroxide with calcination to create bioaugmented ZnONPs from Uziza seed

extract. An UV-Vis spectrometer detected a prominent absorption peak at around 350 nm that was unique to ZnONPs. The Kubelka-Munk formula was used to estimate the optical bandgap of ZnONPs to be around 3.58 eV. Tiwari *et al.* (2024a) used *Calendula officinalis* leaf extract to produce ZnONPs in an ecologically friendly manner. The structure and stability of the nanoparticles were subsequently confirmed by analysis utilizing several spectroscopic methods. The UV-Vis spectra of the ZnONPs showed two noticeable absorption peaks at 355 and 370 nm respectively, with an energy band gap of about 2.986 eV. Fakhari *et al.* (2019) produced ZnONPs using aqueous extract of *Laurus nobilis* L. leaves and two distinct precursor zinc metal salts (zinc acetate and zinc nitrate), and studied them using a variety of methods. Because of their high excitation binding energy at ambient temperature, UV-Vis spectra displayed characteristic absorption peaks at about 350 nm. Shamim *et al.* (2019) synthesized ZnONPs using *Aspergillus niger* and zinc chloride ($ZnCl_2$) as precursors and and confirmed the synthesis using many characterization techniques including UV-Vis spectroscopy.

Magnesium: Singaram and Selvaraj (2024) used *Phyllanthus Emblica* fruit extract for synthesis of MgONPs and characterized them using various techniques. According to the UV-visible analysis, with the increase in calcination temperature from 200 to 600 °C, the peak also showed an increase to a longer wavelength at 350 nm, suggesting a decrease in the size of MgONPs. Al Musayeib *et al.* (2024) fabricated MgONPs and described using a variety of methods. The MgONPs were distinguished by a noticeable absorption peak in the UV-Vis spectra at 284 nm. Using acid orange 8 (AO-8) dye, the biosynthesized MgONPs demonstrated effective photocatalytic capability in an amount comparable to that of MgO powder when exposed to UV light. In a brief period of time, the degradation performance of MgONPs demonstrated a photocatalytic degradation efficiency of over 94% of acid orange 8 (AO-8) dyes. Radwan *et al.* (2024) biosynthesized MgONPs using seaweed aqueous extract and characterized the synthesized nanoparticles using various techniques including UV–Vis spectrometry. According to the UV-visible analysis, sharp peaks and a color shift in UV-Vis spectra between 200 nm and 800 nm at high absorption under various circumstances demonstrated the synthesis of MgO-NPs. MgONPs were produced and used to maize

by Abbas *et al.* (2024). Physiological evaluation using a UV-Vis spectrophotometer applied to the leaves and roots verified the effectiveness and absorption of MgONPs. Aung *et al.* (2023) used aqueous extracts of *Moringa oleifera* leaves to synthesize MgONPs. Following that, these particles were examined using contemporary spectroscopic techniques, such as UV-Vis absorption spectroscopy which confirmed the presence and stability of MgONPs and the strongest absorption peak was achieved at 261 nm. Essien *et al.* (2020) fabricated MgONPs using an aqueous extract of the leaves of plant - *Manihot esculenta*. The resulting MgONPs were then assessed using a number of methods, such as UV-Vis spectrophotometry. The UV-Vis result unequivocally demonstrated that the biomolecules with reducing ability in the leaf extract were capable of carrying out a bio-reduction function, which resulted in the synthesis of MgONPs.

Manganese: Ali and Karem (2024) synthesized the MnO_2NPs using manganese sulfate and plant extract from *Punica granatum*. These nanoparticles were further studied using a variety of methods, including UV-Vis spectroscopy. This absorbance peak of the spectrum at 348.0 nm was caused by the transition holes phase between Mn and O. Lohiya *et al.* (2024) produced manganese oxide nanoparticles using a methanolic extract of *Sapindus mukorossi* (reetha). Several approaches were used to analyze the synthesized MnO_2NPs, including UV-Vis spectroscopy (λ = 750 (Perkin Elmer) UV-Vis NIR Spectrophotometer). UV-Vis spectroscopy was used to analyze the optical characteristics of nanoparticles. The generation of MnO_2NPs was revealed by the electronic absorption spectra of the produced MnO_2NPs, which had absorption maxima (λ_{max}) at 380 nm. Amatya *et al.* (2021) investigated the use of a green synthesis of multifunctional manganese nanoparticles (MnNPs) by utilizing potassium permanganate ($KMnO_4$) as the precursor and the banana peel (*Musa paradisiaca*) aqueous extract. A double beam UV-vis spectrophotometer (Model LT-2802) was used to characterize the synthesized MnNPs at 5-nm intervals in the wavelength range of 200-700 nm. The surface plasmon resonance (SPR) of electrons present at the surface of nanoparticles was responsible for the greatest absorption at 450 nm in the UV-vis spectrum of the biosynthesized MnNPs. Hoseinpour *et al.* (2018) synthesized MnO_2NPs from *Yucca gloriosa* leaf extract and then characterized using many

techniques including ultraviolet visible spectroscopy. The band gap of the synthesized MnO_2NPs was identified as the cause of the absorption peaks at 410 nm in their UV–visible absorption spectra.

2.2.2. Fourier Transform Infra-Red (FT-IR) Spectroscopy:

Zinc: Mousa *et al.* (2024) produced ZnONPs using a variety of plant extracts and analyzed them using a number of techniques, including FT-IR spectroscopy, in order to identify the presence of certain biomolecules involved in the synthesis of ZnONPs. At room temperature, FT-IR spectra were generated for the pomegranate extract and the synthetic photocatalyst. Using FT-IR spectroscopy, Yadav *et al.* (2024) examined the phytogenic production of ZnONPs from the aqueous extract of the *Evolvulus alsinoides* plant. Takcı *et al.* (2024) used zinc acetate dihydrate as the precursor salt and sodium hydroxide with calcination to create bioaugmented ZnONPs from Uziza seed extract. The Kubelka-Munk formula was used to estimate the optical bandgap of ZnONPs to be around 3.58 eV. The existence of biofunctional groups that are in charge of the reduction of bulk zinc acetate to ZnONPs was revealed by FT-IR results. Tiwari *et al.* (2024a) used the *Calendula officinalis* leaf extract to synthesize ZnONPs in an environmentally friendly way. The structure and stability of the nanoparticles were then verified by analysis utilizing several spectroscopic methods. The FT-IR spectroscopy findings showed that pure ZnONPs were formed, with no detectable peak in the monitoring range and an absorption peak of the Zn–O link between 4000 cm−1 and 500 cm−1. Ammar *et al.* (2021) developed PEGylated zinc nanoparticles (PEGylated ZnNPs) by polygylation of zinc nanoparticles (ZnNPs), by using fungal filtrate of *Monascus purpureus,* and then characterized them by many techniques including FT-IR. The presence of rounded, evenly distributed nano-zinc with a size range of 33.6–78.1 nm was verified by all studies. Fakhari *et al.* (2019) produced ZnONPs using *Laurus nobilis* L. leaves aqueous extract and two distinct precursor zinc salts (zinc acetate and zinc nitrate), and studied them using a variety of methods. FT-IR spectroscopy examines the verified chemical bond forms of zinc oxides.

Magnesium: Singaram and Selvaraj (2024) synthesized MgONPs using *Phyllanthus emblica* fruit extract and characterized them using a variety of methods. The synthesis of MgONPs from $Mg(OH)_2$ was verified by FT-IR and XRD analysis, showing

spherical forms of around 20 nm in size. Muhaymin *et al.* (2024) used the gingerbread tree (*Hyphaene thebaica*) fruit extract to synthesize MgONPs in an environmentally friendly manner. FT-IR analysis identified distinctive Mg-O bonds via peaks at 560 cm−1 and 866 cm−1, while as, the Raman spectroscopy confirmed the cubic structure of MgONPs. Radwan *et al.* (2024) biosynthesized MgONPs using seaweed aqueous extract and characterized the synthesized nanoparticles using various techniques. Functional groups found in seaweed aqueous extract are analyzed using FT-IR spectroscopy (Agilent system Cary 660 FT-IR model). Abbas *et al.* (2024) synthesized MgONPs followed by their characterization through different techniques including FT-IR spectroscopy. The FT-IR spectra of synthesized MgONPs were examined, along with bioactive substances that may have anything to do with the stability and chemical production of the particles. Aung *et al.* (2023) synthesized MgONPs from aqueous extracts of *Moringa oleifera* leaves. These particles were then examined using FT-IR and other contemporary spectroscopy techniques. The FT-IR spectra of produced MgONPs showed distinct absorption bands at wavenumbers of 1090, 861, and 683 cm^{-1}, suggesting the presence of Mg-O interactions. It is evident from this spectrum that the synthesis and stability of MgONPs were demonstrated by the large peaks at 861 cm^{-1}, which were brought on by the stretching vibration of the Mg-O-Mg bond. MgONPs are made by Essien *et al.* (2020) using an aqueous extract of *Manihot esculenta* leaves. In order to supplement and validate the findings of the study with GC-MS, UV-Vis spectroscopy and XRD, FT-IR spectroscopy (FT-IR: Nicolet iS10) with a wavenumber in the 350–4000 cm−1 range was used to evaluate the kind of bonds existing in the MgONPs.

Manganese: Lohiya *et al.* (2024) synthesized nanoparticles of manganese oxide by methanolic extract of *Sapindus mukorossi* (reetha). Synthesized manganese oxide nanoparticles were characterized by many techniques including FT-IR spectroscopy (Spectrum 2 Perkin Elmer). The presence of chemical bonds was analysed by FT-IR spectroscopy. Ali and Karem (2024) synthesized MnO_2NPs using manganese sulfate and plant extract of *Punica granatum*. These were further analyzed using a variety of methods, such as Fourier transform infrared (8500S) type spectroscopy in the 400–4000 cm^{-1} range. Bands at 590 and 532 cm^{-1} are seen in the MnO_2 FT-IR spectra. Amatya *et*

al. (2021) investigated the use of a green synthesis method of multifunctional MnNPs by employing potassium permanganate ($KMnO_4$) as the precursor and an aqueous extract of banana peel (*Musa paradisiaca*). The FT-IR spectroscopy method was used to characterize the synthesized MnNPs. FT-IR spectroscopy was utilized to identify the functional group connected to the organic biomolecules of the BPE. The large peak at around 3240 cm^{-1} in the FT-IR spectra of MnNPs is attributed to the -OH bending vibration of the polyphenolic groups found in banana peel extract. MnO_2 nanoparticles were produced and described by Manjula *et al.* (2020) using leaf extract from *Gardenia resinifera*. FT-IR is one of the various methods used to characterize the produced manganese dioxide nanoparticles (MnO_2NPs). The findings indicate the existence of several functional groupings that might display a range of biological functions. MnNPs were created by Kamran *et al.* (2019) using bark extracts from *Cinnamomum verum*. FT-IR was one of the methods used to characterize the biosynthesized MnNPs. FT-IR spectrometer (Bruker Tensor) was utilized for the FT-IR study. Following dye degradation under UV irradiation, the FT-IR spectra of MnNPs showed peak shifting, indicating that the dye was destroyed by MnNPs and that the peaks were subsequently somewhat altered. Using a variety of methods, including FT-IR, Hoseinpour *et al.* (2018) produced MnO_2NPs from *Yucca gloriosa* leaf extract. The role of the plant extract in synthesis of MnO_2NPs was shown by FT-IR spectra.

2.2.3. X-ray Diffraction (XRD):

Zinc: Mousa *et al.* (2024) synthesized ZnONPs using various plant extracts, and characterized by means of various methods including XRD. A PANalytical diffractometer fitted with graphite monochromated CuKα radiation was used to gather data at room temperature. All of the produced ZnO samples possessed hexagonal structures, according to the XRD data. Using XRD, Yadav *et al.* (2024) examined the phytogenic production of ZnONPs from the aqueous extract of the *Evolvulus alsinoides* plant. Takcı *et al.* (2024) used zinc acetate dihydrate as the precursor salt and sodium hydroxide (with calcination) to produce bioaugmented ZnONPs from Uziza seed extract. XRD and SEM examinations of ZnONPs verified the hexagonal and spherical high purity crystalline structure with a mean size of 7.39 nm. *Calendula officinalis* leaf extract was used by Tiwari *et al.* (2024a) to synthesize ZnONPs in an ecologically

friendly manner. The structure and stability of the nanomaterial was then confirmed by analysis utilizing several spectroscopic methods. The XRD result of synthesized ZnONPs revealed the most intense peak (101) and a crystalline size of 28.23 nm with a wurtzite hexagonal structure. Fakhari *et al.* (2019) produced ZnONPs using the aqueous extract of *Laurus nobilis* L. leaves and two distinct precursor zinc salts (zinc acetate and zinc nitrate), and studied them using a variety of methods. The development of a hexagonal wurtzite structure was shown by the XRD data. Shamim *et al.* (2019) generated zinc oxide (ZnO) nanoparticles using *Aspergillus niger* and zinc chloride (ZnCl2) as precursors, which were then analyzed using a variety of methods, including XRD.

Magnesium: Singaram and Selvaraj (2024) synthesized MgONPs using *Phyllanthus emblica* fruit extract and characterized them using a variety of methods. The synthesis of MgONPs from $Mg(OH)_2$ was verified by XRD and FT-IR analysis, showing spherical forms of around 20 nm in size. Muhaymin *et al.* (2024) used the gingerbread tree (*Hyphaene thebaica*) fruit extract to synthesize MgONPs in an environmentally friendly manner. With a crystallite size of 32.6 nm, the XRD pattern showed strong peaks at two planes of (200) and (220), confirming the high crystallinity of MgONPs. Radwan *et al.* (2024) used seaweed aqueous extract to biosynthesize MgONPs and used a variety of methods, such as XRD analysis at a 2θ degree of 0°–80°, to characterize the produced nanoparticles. Strong diffraction peaks were visible in the XRD pattern at different values: 18.76°, 38.12°, 42.97°, 51.45°, and 54.17°. MgONPs were synthesized by Abbas *et al.* (2024) and then characterized using a variety of methods, such as X-ray diffraction. The XRD patterns were recorded in order to examine the phase and purity of the produced MgONPs. Aung *et al.* (2023) synthesized MgONPs using aqueous extracts of *Moringa oleifera* leaves. Following that, these particles were examined using contemporary spectroscopic techniques, such as XRD study. The crystalline structure and phase purity of the produced MgONPs were assessed using an X-ray diffractometer, and the diffraction patterns at 500, 600, and 700 °C were acquired. MgONPs are made by Essien *et al.* (2020) using an aqueous extract of *Manihot esculenta* leaves. An X-ray diffractometer was used to analyze the diffraction

pattern of MgONPs in order to determine their crystalline structure and investigate the kinds of phases that were present in the sample.

Manganese: Ali and Karem (2024) fabricated MnO_2NPs using manganese sulfate and plant extract from *Punica granatum*. These were further characterized using a variety of methods, such as X-ray diffraction type PW1730 (Phillips/Holland). Using the Debye Scherrer equation in XRD, the crystal size was determined to be 30.94 nm. The absence of impurity signals in the XRD tests indicates that the MnO_2NPs samples are very crystalline. Lohiya *et al.* (2024) synthesized nanoparticles of manganese oxide by methanolic extract of *Sapindus mukorossi* (reetha). Synthesized manganese oxide nanoparticles were characterized by many techniques including XRD analysis. The purity and product phase are examined by XRD. From the XRD pattern it is clear that MnO_2NPs synthesized were purely crystalline. The average particle size was found 16 nm obtained by XRD analysis. Amatya *et al.* (2021) investigated the use of a green approach for the synthesis of multifunctional MnNPs by employing potassium permanganate ($KMnO_4$) as the precursor and an aqueous extract of banana peel (*Musa paradisiaca*). XRD spectroscopy was used to analyze the synthesized MnNPs and the overall XRD result verified the formation of crystalline MnNPs. The estimated size of the crystallite is 8.92 Å (~ 1 nm). MnO_2NPs were produced and described by Manjula *et al.* (2020) using leaf extract from *Gardenia resinifera*. XRD was one of several methods used to characterize the produced MnO_2NPs. Since the nanoparticles were discovered to be poorly crystalline, the diffraction peaks were classified as being in the tetragonal phase. No further impurity-related diffraction peaks were seen, indicating that the produced MnO_2NPs were of high quality. Kamran *et al.* (2019) fabricated MnNPs using *Cinnamomum verum* bark extracts. The biosynthesized MnNPs were characterized by different techniques including XRD. An XRD diffractometer operating at 40 kV voltage and 40 mA current was used to do the analysis. It used Cu Kα radiation in the range of 20° to 80° with a scanning rate of 5° min^{-1}. The peaks at 28.33, 40.53, and 50.01 at 2θ in the XRD pattern of the MnNPs in the angle range of 10˚C to 80˚C are indexed as face centered cubic Mn. Hoseinpour *et al.* (2018) synthesized MnO_2NPs from *Yucca gloriosa* leaf extract then characterized using many techniques including XRD. XRD was also used to characterize the crystal phase of

MnO_2NPs, and the production of the crystalline forms of MnO_2NPs was verified. Additionally, the X-ray diffraction pattern showed that MnO_2NPs had an average size of almost 80 nm.

2.2.4. Scanning Electron Microscopy (SEM):

Zinc: Mousa *et al.* (2024) fabricated ZnONPs using a variety of plant extracts, and they were analysed using a series of techniques, including Field Emission Scanning Electron Microscope (FE-SEM). Green generated ZnONPs are spherical in shape, whereas chemically manufactured ZnONPs are homogeneously distributed and resemble nanorods. Using FE-SEM, Yadav *et al.* (2024) examined the phytogenic production of ZnONPs from the aqueous extract of the *Evolvulus alsinoides* plant. The findings from SEM analysis exposed spherical nanoparticles with size in the range of 100 nm. Takcı *et al.* (2024) used the precursor salt - zinc acetate dihydrate and calcinated sodium hydroxide to create bioaugmented ZnONPs from Uziza seed extract. SEM examinations of ZnONPs verified the hexagonal and spherical structure at high purity with a mean size of 7.39 nm. *Calendula officinalis* leaf extract was used by Tiwari *et al.* (2024a) to create ZnONPs in an ecologically safe manner. The structure and stability of the nanoparticles were then verified by analysis utilizing several spectroscopic methods. Both large and small agglomerated forms of the nanoparticles were seen using FE-SEM, which is frequently utilized to ascertain their external assembly, after initial confirmations of the anticipated ZnONPs. Fakhari *et al.* (2019) produced ZnONPs using the aqueous extract from the leaves of *Laurus nobilis* L. and two distinct precursor zinc salts, and studied them further using a variety of methods. According to the SEM studies, the nanoparticles produced by the reduction of precursor metal salts, had spherical shapes and average sizes of 21.49 and 25.26 nm. Shamim *et al.* (2019) synthesized ZnONPs using *Aspergillus niger* and zinc chloride ($ZnCl_2$) as precursors, which were then analyzed using the SEM method. The produced ZnONPs had a hexagonal shape and ranged in size in the nm range.

Magnesium: Muhaymin *et al.* (2024) used the gingerbread tree (*Hyphaene thebaica*) fruit extract to synthesize MgONPs in an environmentally friendly manner. With a size in the range of 20 nm - 60 nm, their agglomerated quasi-spherical form was validated by analysis using SEM. Al Musayeib *et al.* (2024) fabricated MgONPs and

characterized them using various techniques. The polyhedral shape and minor CP-MgONP aggregation of the nanoparticles was observed by SEM. Energy-dispersive X-ray (EDX) spectroscopy revealed that the composition consists of 48.64% oxygen and 40.47% magnesium by weight. Radwan *et al.* (2024) used seaweed aqueous extract to biosynthesize MgONPs and used a variety of methods, such as XRD analysis at a 2θ degree of 0°–80°, to characterize the produced nanoparticles. MgONPs were produced by Abbas *et al.* (2024), and SEM was used to determine if nanoparticles might have the greatest possible impact. With an average particle size distribution range of 5 nm, most of the MgONPs displayed uniform aggregation. MgONPs were created by Aung *et al.* (2023) using aqueous extracts of *Moringa oleifera* leaves. Following that, these particles were examined using contemporary spectroscopic techniques, such as SEM analysis. The generated MgONPs were morphologically examined using SEM. The high-resolution SEM image of the synthesized MgONPs showed that they are composed of spherical shapes with particle sizes ranging from 16 to 23 nm. The SEM image of MgONPs revealed that the majority of them were clumped together and had good surface features and a constant particle size distribution. The predicted magnesium nanoparticles have an average particle size of 18.5 nm, based on SEM images. MgONPs are made by Essien *et al.* (2020) using an aqueous extract of Manihot esculenta leaves. A morphological analysis was conducted in a SEM fitted with the EDX unit (SEM: JEOL JSM 7660F) to evaluate the microstructure, elemental content and particle distribution of the MgONPs. The sample was examined using a 15 kV accelerating voltage. The hexagonal shape of the particles, initially seen in the SEM micrograph, was found to be more noticeable in the TEM micrographs, indicating a crystalline composition.

Manganese: Ali and Karem (2024) utilized manganese sulfate and plant extract from *Punica granatum* to produce MnO_2NPs, which were subsequently examined utilizing a variety of methods, such as scanning electron microscopy. To ascertain the morphology and forms of nanomaterials, SEM was employed. SEM investigation revealed small quantities of rods in nanostructured, unconsolidated forms of MnO_2NPs. Lohiya *et al.* (2024) synthesized MnO_2NPs using a methanolic extract of *Sapindus mukorossi* (reetha). SEM was one of the methods used to characterize the synthesized manganese

oxide nanoparticles. The surface morphology of MnO_2NPs was investigated using the SEM method. The homogeneous dispersion of MnO_2NPs was demonstrated by the surface morphology. MnO_2NPs were produced and studied by Manjula *et al.* (2020) using leaf extract from *Gardenia resinifera*. SEM-EDAX analysis was one of the methods used to analyze the produced MnO_2NPs. The size and surface shape of MnO_2NPs were determined by the SEM examination findings. The SEM investigation revealed that the particles were spherical with the size ranging from 50 to 100 nm. Because of their bigger surface area besides greater quantity, MnO_2NPs aggregate and agglomerate to increase in size. MnNPs were created by Kamran *et al.* (2019) using bark extracts from *Cinnamomum verum*. SEM was one of the methods used to characterize the biosynthesized MnNPs. The development of spherically shaped nanoparticles with a range of sizes and an inclination to aggregate was validated by the SEM images. TEM examination was used to further clarify the size and structure of the biosynthesized MnNPs. The produced face-centered cubic MnNPs were spherical, crystalline, and aggregate-shaped, with a size of less than 100 nm. MnO_2NPs were produced by Hoseinpour *et al.* (2018) from *Yucca gloriosa* leaf extract and characterized using a variety of methods, including SEM. The synthesised MnO_2NPs were found to be spherical in form by investigation using field emission scanning electron microscopy.

2.3. Effect of Metallic Nanoparticles on Apple Plant Pathogens

The North-Western hill areas, particularly those in Jammu and Kashmir, Himachal Pradesh, and Uttarakhand, comprise almost 99 percent of India's apple (*Malus domestica* Borkh.) producing area. In the union territory of Jammu & Kashmir, apples are the main fruit crop, covering 1,57,280 hectares and yielding 13,48,155 metric tons annually. Pear and cherry, on the other hand, cover 13,702 and 3728 hectares, yielding 54,847 and 11,129 metric tons annually, respectively (Anonymous, 2013). It is well known that the Himalayan environment is particularly delicate and susceptible to the whims of nature, which is why its soils are typically deficient in nutrients. Because they can enhance knowledge of the horti-ecosystem and their function in assisting these plants in surviving under stressful situations, it is crucial to comprehend the biodiversity of related microfora, particularly arbuscular mycorrhizal fungus, in these soils.

However, the diversity and roles of fungi within this horticultural ecosystem have received limited focus (Burni *et al.*, 2009). Metallic nanoparticles have demonstrated significant effectiveness against plant pathogens (Rai and Ingle, 2012). Their antimicrobial properties help in managing plant diseases by disrupting microbial cell walls and interfering with metabolic processes (Ali *et al.*, 2020).

2.3.1. Effect on *Alternaria mali*

Anjum *et al.* (2024) used the poison food approach to test ZnONPs for possible antifungal efficacy against *Alternaria mali*. The results showed that ZnONPs, especially those derived from *Pleurotus*, significantly inhibited *Alternaria* growth with respect to the concentrations. Ahmad *et al.* (2020) assessed the antifungal efficacy of biosynthesized ZnNPs against the main phytopathogens that affect apple orchards. The fungal growth inhibition rate for *Alternaria mali* was reported to be 76.7% at 100 ppm of ZnNPs, whereas the rates for *Botryosphaeria dothidea* and *Diplodia seriata* were 65.4 and 55.2%, respectively. ZnNPs alter the topography of the fungal hyphal layers, which results in less hyphae contraction, according to microscopic studies of the treated fungal plates. The significant fungicidal action of ZnNPs against phytopathogenic fungi can significantly influence their use in managing fungal pests and protecting fruit crops. While extensive studies have explored the antimicrobial properties of zinc nanoparticles, against various plant pathogens, the potential effects of magnesium and manganese nanoparticles on *Alternaria mali* remain unexplored.

2.3.2. Effect on *Venturia inaequalis*

Zinc, magnesium and manganese nanoparticles have shown potential antimicrobial effects against various fungal pathogens; however, specific studies on *Venturia inaequalis*, the pathogen responsible for apple scab, are lacking. This gap in the literature highlights the need for further investigation into the potential antifungal properties of zinc nanoparticles against this significant agricultural pathogen.

2.4. Effect of Metal Nanoparticles on Plant Parameters

Metal nanoparticles influence the critical physiological parameters of plants such as stomatal conductance, net photosynthesis, intercellular CO_2 concentration, transpiration, and chlorophyll content. For example, zinc, magnesium, and manganese

nanoparticles can modulate stomatal conductance, thereby influencing the rate of gas exchange crucial for maintaining net photosynthesis (Hernandez-Viezcas *et al.*, 2013; Raliya *et al.*, 2018). These nanoparticles also significantly impact the concentration of intercellular CO_2, a vital component of the photosynthetic process (Rico *et al.*, 2011). The impact of these nanoparticles on transpiration rates have been observed, with variations depending on their type and concentration, showing that these particles can either enhance or inhibit water loss through stomata (Zhao *et al.*, 2015). A careful management of nanoparticle application is necessary to avoid phyto-toxicity while harnessing their potential to enhance plant growth and stress resistance (Dimkpa and Bindraban, 2017).

2.4.1. Effect on Stomatal conductance

Zinc: Ahmed *et al.* (2023) investigated the impact of foliar-applied ZnONPs on *Coriandrum sativum* L. under drought conditions, focusing on stomatal attributes and photosynthetic induction. Their study highlighted significant changes in biochemical parameters and how ZnONPs influenced stomatal conductance, thereby affecting photosynthesis and plant resilience under stress. Azhar *et al.* (2021) conducted a study investigating the effects of silicon dioxide (SiO_2), zinc oxide (ZnO), and composite nanoparticles on *Arabidopsis thaliana* and found that ZnONPs significantly influenced various physiological processes including growth, stomatal conductance, and overall plant health. The findings suggest that ZnONPs can modulate plant physiological functions through complex signaling mechanisms, impacting stomatal conductance and potentially other plant parameters.

Magnesium: Ali *et al.* (2024b) examined how *Brassica napus* cultivars responded differently to the dual effects of MgONPs. They found that while excessive nanoparticle levels negatively affected plant parameters like stomatal conductance, low doses of MgONPs (primarily 10 mg/L) significantly increased these parameters. Silva *et al.* (2023) investigated magnesium oxide and carbonate nanoparticles as possible ways to lessen the effects of drought stress on lettuce. Data demonstrated that unstressed plants stored more carbohydrates and displayed increased stomatal limits when exposed to nanoparticles; in contrast, water-stressed plants accumulated more chlorophyll and carotenoids. Faizan *et al.* (2022) stated that foliar application of MgONPs along with

the presence of arsenic boosted plant height and also improved the stomatal conductance by 13.4%.

Manganese: Huang *et al.* (2024) have explored manganese ferrite nanoparticles as a micronutrient fertilizer in wheat, showing promising results in enhancing plant growth and nutrient uptake. These nanoparticles may also affect physiological parameters such as stomatal conductance, given the role of manganese in enzyme activation and photosynthesis regulation. Elmer and White (2018) observed that MnONPs influenced stomatal conductance in tomatoes and eggplants, leading to changes in intercellular CO_2 concentration and photosynthetic efficiency. Sobańska *et al.* (2021) evaluated the biological activity and potential applications of manganese and manganese oxide nanoparticles, providing insights into their effects on various biological parameters, including stomatal conductance.

2.4.2. Effect on Net Photosynthesis

Zinc: Dang *et al.* (2024) examined how ZnONPs affected rice cultivated on sodic-saline soil. According to the study, application of ZnONPs to rice plants increased photosynthesis, strengthened their resistance to sodic-saline stress, and eventually aided in their overall growth and development. Mahawar *et al.* (2024) demonstrated that foliar spraying of ZnONPs in radish plants under NaCl stress was effective in enhancing the photosynthetic electron transport rate, leaf area, proton conductance, PSII quantum yield, and mineral content. The effect of ZnONPs in tomato plants was evaluated by Faizan *et al.* (2017), who found that ZnONP treatments considerably enhanced growth, photosynthetic efficiency, as well as the activities of antioxidant systems and carbonic anhydrase in a way that was dependent on both concentration and time.

Magnesium: Ali *et al.* (2024b) examined how *Brassica napus* cultivars responded differently to the dual effects of MgONPs. They found that while excessive nanoparticle levels negatively affected plant parameters like stomatal conductance, low doses of MgONPs (primarily 10 mg/L) significantly increased these parameters. In their evaluation of the ability of MgONPs to reduce arsenic toxicity in soybean plants, Faizan *et al.* (2022) found that foliar MgONP treatment increased net photosynthetic rate by 12.9% when arsenic was present. Nair *et al.* (2010) investigated the effects of several

nanoparticles, including MgONPs, on plant systems with an emphasis on metrics like net photosynthesis and the overall effect on plant physiology. It offers valuable insights into how magnesium nanoparticles influence photosynthetic efficiency and related plant growth metrics.

Manganese: Yue *et al.* (2022) stated that the application of $MnFe_2O_4$ nanoparticles on the tomato leaves resulted in a 13.3% improvement in photosynthetic efficiency by dramatically upregulating the expressions of ferredoxin, PsaA, and PsbA in these leaves, most likely due to their electron-donating properties. Elmer and White (2018) assessed the impact of MnONPs on net photosynthesis indirectly through their influence on stomatal conductance and intercellular CO_2 concentration. The researchers found that MnONPs altered stomatal behaviour, which in turn affected the availability of CO_2 for the Calvin cycle, thereby influencing the overall rate of photosynthesis.

2.4.3. Effect on Intercellular CO_2 Concentration

Zinc: Zhang *et al.* (2024) discovered that spraying wheat seedlings with ZnONPs solution administered as nanobubble irrigation enhanced the wheat's growth and nutritional condition. The intercellular CO_2 concentration decreased by 11.52% for gas exchange parameters and biological capabilities. Kaningini *et al.* (2024) examined the use of bush tea-mediated ZnONPs for chickpea fertilization and also assessed the cytotoxicity, antioxidant, and antibacterial properties of these compounds. The study showed that the application of ZnONPs had a considerable impact on the intercellular CO_2 concentration. According to Wang *et al.* (2016c), who evaluated the effects of ZnONPs exposure on biomass growth and photosynthesis in *Arabidopsis*, plants treated with 300 mg/L ZnONPs showed an intercellular CO_2 concentration reduction of more than 50%.

Magnesium: Faizan *et al.* (2022) assessed the efficacy of MgONPs for reducing the toxicity of arsenic in soybean plants and stated that foliar application of MgONPs in the presence of arsenic improved intercellular CO_2 concentration by 15.3%. Salcido-Martinez *et al.* (2020) demonstrated that the foliar application of magnesium nano-fertilizers significantly improved various physiological and biochemical parameters in green beans, including enhanced photosynthetic activity. This suggests that magnesium

nanoparticles could also modulate gas exchange processes such as stomatal conductance, which directly impacts intercellular CO_2 concentration and photosynthesis efficiency.

Manganese: Elmer and White (2018) investigated the efficacy of various metallic oxide nanoparticles, including MnONPs, on the growth and physiological processes of tomatoes and eggplants. While their focus included multiple aspects of plant growth, they noted that MnONPs influenced stomatal conductance and, as a result, the intercellular CO_2 concentration (Ci). This alteration in Ci was linked to changes in photosynthetic efficiency and the response of plants to stress factors in their environment. the effect of stabilized manganese oxide nanoparticles on plant growth parameters. Liu *et al.* (2016) assessed the effects of several metal oxide nanoparticles, including manganese, on plant growth parameters, which could encompass changes in intercellular CO_2 concentration as part of broader physiological responses.

2.4.4. Effect on Transpiration

Zinc: Kaningini *et al.* (2024) examined the use of bush tea-mediated ZnONPs for chickpea fertilization along with the cytotoxicity, antioxidant, and antibacterial properties of these compounds. According to the study, application of 25 mg/L ZnONPs resulted in greater values of transpiration efficiency and stomatal conductance. Wang *et al.* (2016c) documented the effects of ZnONP exposure on *Arabidopsis* biomass accumulation and photosynthesis. All plants treated with 300 mg/L ZnONPs had a transpiration rate reduction of greater than 50%.

Magnesium*:* Faizan *et al.* (2022) in the evaluation of the ability of MgONPs to reduce arsenic toxicity in soybean plants, found that foliar MgONP treatment increased transpiration rate by 14.7% when arsenic was present. Cai *et al.* (2018) explored the impact of MgONPs on tobacco plants. Their research demonstrated that the nanoparticles significantly influenced plant growth and enhanced morpho-physiological functions, including increased transpiration rates.

Manganese: Khalid *et al.* (2022) reviewed the role of nanoparticles, including manganese, in mitigating abiotic stresses such as drought, which directly influences transpiration rates in plants. They further emphasized how nanoparticles enhance plant

physiological responses under stress conditions, which could include modifications in transpiration as a coping mechanism. Liu *et al.* (2016) investigated how stabilized nanoparticles, including manganese oxides, influence various physiological parameters of lettuce, such as seed germination and overall plant growth. The study indicates that manganese nanoparticles can affect transpiration rates by altering stomatal behaviour and water uptake efficiency, which are crucial for understanding how these nanoparticles influence plant physiology under different environmental conditions.

2.4.5. Effect on Chlorophyll content

Zinc: Chen *et al.* (2024) evaluated that ZnONPs may improve the photosynthesis of tea plants, increase the accumulation of photosynthetic products, increase the growth of new shoots, upregulate the expression of certain genes linked to photosynthesis, and change the mineral elements present in the leaves and new shoots of tea plants. The effect of ZnONPs on the chlorophyll fluorescence in rice cultivated on sodic-saline soil was examined by Dang *et al.* in 2024. In line with the research findings, ZnONP treatment is more beneficial for increasing the amount of pigments present in chloroplasts. According to Venkatachalam *et al.* (2017), application of ZnONPs synthesized by algae to cotton plants enhanced yield, biomass, chlorophyll, soluble proteins, and carotenoids by as much as 179%.

Magnesium: Ali *et al.* (2024b) investigated the varying reactions of *Brassica napus* cultivars to the dual effects of MgONPs and found out that low doses of MgONPs significantly increased the levels of photosynthetic pigments by 14–27%. Silva *et al.* (2023) demonstrated the potential of magnesium oxide and magnesium carbonate nanoparticles to modify photosynthesis by encouraging plants to increase pigment formation under water stress and preventing possible defects in the photochemical phase of photosynthesis. Fatemi *et al.* (2022) assessed a number of physio-biochemical characteristics while conducting research on the use of magnesium nanoparticles in sunflowers (*Helianthus annuus* L.). The results showed that spraying magnesium nanoparticles during drought enhanced the enzymatic activity of antioxidants, soluble carbohydrates, chlorophyll and carotenoid, and water content. Salcido-Martinez *et al.* (2020) assessed the impact of magnesium nano-fertilizer on the production, and physiological and biochemical parameters of green beans and found that the largest

quantity of biomass and photosynthetic pigments were produced by foliar application of magnesium nanoparticles at 50 ppm.

Manganese: Tahir *et al.* (2024) evaluated the effects of tetragonal crystalline MnONPs on wheat plants under lead stress. They found that these nanoparticles significantly alleviated stress and improved various physiological traits, including chlorophyll content. This improvement is attributed to the ability of nanoparticles to enhance antioxidant enzyme activity, which in turn supports better chlorophyll retention and overall plant health. Siddiqui *et al.* (2024), demonstrate that MnO_2NPs can influence plant health and growth. The use of MnO_2NPs has implications for enhancing chlorophyll content in plants, which is critical for photosynthesis and overall plant vigour. According to Yue *et al.* (2022), $MnFe_2O_4$ nanoparticles raised the amount of chlorophyll in the leaves by 20% following foliar treatment before flowering.

2.5. Effect of Metallic Nanoparticles on Apple Plant Parameters

Montaño-Herrera *et al.* (2022) assessed the effects of foliar fertilization with Zn and Se nanoparticles on apple fruit yield and antioxidant compounds. They discovered that the treatments of these two nanoparticles increased the sugar content, ascorbic acid and yield of the apple fruit. The ZnNP treatment increased fruit output by the greatest amount (+193%) as compared to the control. Alizadeh and Dumanoğlu (2022) demonstrated that the nanoparticles loaded with auxins could increase the rooting success of apple plants with their physicochemical properties. Ahmad *et al.* (2020) assessed the antifungal efficacy of biosynthesized zinc nanoparticles against three main phytopathogens that affect apple orchards: *Alternaria mali, Diplodia seriata* and *Botryosphaeria dothidea*. Zn nanoparticles alter the topography of the fungal hyphal layers, which results in less hyphae contraction, according to microscopic studies of the treated fungal plates. The significant fungicidal effect of zinc nanoparticles against phytopathogenic fungi can significantly influence their use in managing fungal pests and protecting fruit crops. The impact of magnesium nanoparticles on apple plant parameters has not been the subject of any published research as of yet.

The lack of research on the possible effects of magnesium and manganese nanoparticles on the physiochemical characteristics of apple plants is underlined by this gap in the literature, demanding more thorough investigations.

2.6. Toxic effects of Metallic Nanoparticles on Plants and Environment

The ecological hazards and toxicological consequences caused by nanoparticles on plants or animals have since sparked intense societal concern. The physicochemical characteristics (size, shape, surface charge, and ion release), culture settings (exposure concentration, soil culture, and hydroponics), environmental variables (temperature, humidity, and light), and plant species all influence the threat posed by nanoparticles. Nanoparticles are primarily controlled by concentration dependency and can have either beneficial (Nekoukhou *et al.*, 2022) or detrimental (Zhang *et al.*, 2023) effects in specific concentrations. More significantly, an enormour number of contaminants, biomolecules, and other elements are present in natural ecosystems. Considering the increasing environmental exposure to nanoparticles, their combination with other environmental mediators may have antagonistic harmful effects (Banerjee *et al.*, 2023) or synergistic effects (Guo *et al.*, 2023) in organisms (Liu *et al.*, 2023). However, there are also major issues with the behaviour and toxicity of complexes of individual or combination nanoparticles in addition to the biotoxicity caused by individual nanoparticles. Plants, as essential species in both terrestrial and aquatic environments, serve as both ecological sensors for nanoparticles and as food chain intermediaries for transformation and bioconcentration. Furthermore, nanoparticles are mostly absorbed during the early phases of plant growth (Rico *et al.*, 2011), which puts seedling development at risk and increases the likelihood that they would be translocated to edible sections (Rajput *et al.*, 2020). The ambient nanoparticles can enter plant cells and travel to other tissues through root uptake and absorption through leaves or vesicles (Miralles *et al.*, 2012). Once there, they can change the physiology and morphology of the plant in addition to interacting at the cellular and subcellular levels (Khan *et al.*, 2019). A key mechanism for the toxicological effects of nanoparticles is revealed by the way the internalized nanoparticles interact with plants, causing nutrient component imbalance, photosynthetic impairment, oxidative stress response, metabolic disorders, and genotoxicity. While the activation of antioxidant systems is essential for preserving oxidative homeostasis, the production and scavenging of ROS dominate the toxicity of nanoparticles and are the focus of research into detoxification and tolerance mechanisms. Furthermore, complex antagonistic or synergistic phytotoxicity is induced

by composite exposures of nanoparticles with other compounds, raising questions about the possible hazards to the ecological safety of plants (Kang *et al.*, 2024).

Conventional synthesis methods frequently include hazardous stabilizers and solvents that can build up in the environment and be detrimental to plant health. These dangerous substances are removed by green synthesis, which lowers the risk of toxicity by utilizing biological resources such as bacteria, fungus, and plant extracts (Singh *et al.*, 2018). Nanoparticles synthesized this way have better biocompatibility and are therefore safer for use in agricultural applications. This is especially important for Zn, Mg, and Mn nanoparticles, as excessive quantities of these elements might otherwise interfere with plant metabolism (Kirubakaran *et al.*, 2025). The study of predicting and controlling the nanotoxicity of nanoparticles is still in its infancy phase. The use of smart sensors to identify the dangers and exposure hazards of nanoparticles to living things, which entails thorough exposure monitoring and possible toxicity evaluation, is still fraught with difficulties. However, competent assistance for risk assessment comes from efficient models that can forecast the behavior and possible impacts of nanoparticles in the environment and organisms. By using green synthesis techniques, toxicological concerns and environmental dangers are reduced while Zn, Mg, and Mn nanoparticles maintain their advantageous qualities. This strategy enhances crop production without jeopardizing ecological balance and is consistent with sustainable agriculture methods. To improve the stability, effectiveness, and safety of nanoparticles, further research is needed to concentrate on improving the synthesis conditions.

Chapter 3

Hypothesis

The hypothesis witnessing this philosophy goes as follows:

The biogenic preparation of Zn, Mg, Mn and Zn+Mg+Mn NPs can be successfully carried out using the biometabolites of three fungal species of *Pleurotus, Agaricus* and *Lentinus* in combination with the multifunctional metal salts of the nanoparticles synthesized. This facile process of myco-nanosynthesis can supposedly help out in the formulation of eco-friendly and cost-effective nanoforms. The resulting nanomaterial might hold a wide array of potential therapeutic applications as antimicrobial and might show positive effects of various plant parameters including gas exchange and chlorophyll content. These mycogenic nanoparticles might supposedly also have a lower toxicological profile as compared to their chemically synthesized counterparts as well as the already existent broad spectrum synthetic regime.

Chapter 4

Objectives

The following are the major objectives of the entire research work presented in this Thesis:

4.1. Screening of fungi for the synthesis of nanoparticles.

4.2. Characterization of the synthesized material.

4.3. Assessment of the anti-microbial activities of the synthesized material.

4.4. Evaluation of the efficacy of synthesized material on various Apple plant parameters.

Chapter 5

Materials and Methods

The synthesis of Zinc, Magnesium, Manganese and Combination (Zn+Mg+Mn) Nanoparticles, and their antifungal tests were conducted at the Division of Plant Pathology, Sher-e-Kashmir University of Agricultural Sciences and Technology, Kashmir (SKUAST-K), J&K, India. *Pleurotus sajor caju, Agaricus bisporus* and *Lentinus edodes* were taken from Mushroom Research Training Centre (MRTC), SKUAST-K, and the apple plants were collected from Jammu and Kashmir. UV-Vis spectroscopy, FT-IR, XRD, SEM studies were carried out at National Institute of Technology, Srinagar.

5.1. Experimental location

The study was carried out in the Laboratory of Plant Pathology, and the trial was maintained at the Experimental field located at SKUAST-K, Jammu & Kashmir (34˚8'42" and 34˚9'3"N latitudes and 74˚39'5" and 74˚53'5.6"E longitude). It is 23.8 hectares in size and has an average elevation of 1615 meters above sea level. The region witnesses moderate climatic conditions, with warm summers and cold winters. The average annual temperature is 19.53°C and the lowest is 6.80°C, while the average annual rainfall is 786.2 mm. Cereals, fruits, vegetables, and floriculture make up the majority of the vegetation. The experiment was set up at an average elevation of 1500 meters above the sea level. It has a cool, moderate climate. The selected plants for this investigation were set up in the field with 3 m × 1.5 m spacing. The Randomized Complete Block Design (RCBD) was used for the experiment.

Figure 5.1: A view of the experimental field at SKUAST-Kashmir

The brief outlines of the procedures implemented for tests as specified under each objective are as follows:

5.2. Screening of fungi for the synthesis of nanoparticles

5.2.1. Maintenance and identification of fungal strains

A total of three fungal strains (*Pleurotus sajor caju, Agaricus bisporus* and *Lentinus edodes*) were obtained from Mushroom Research Training centre (MRTC), Sher- e-Kashmir University of Agricultural Science and Technology of Kashmir. The cultures were sub-cultured on PDA (potato dextrose agar) media, and after the designated incubation period, preservation was achieved by carefully conserving each fungus at -4^0 C, besides continued sub-culturing onto fresh PDA slants and storing the latter again at 4-5^0 C, along with proper labelling (Ibrahim *et al.*, 2021). Moreover, the cultures were correspondingly authenticated. The tentative microscopic assessment of the fungi was carried out utilizing the Lacto-Phenol Cotton Blue (LPCB) stain (Treasure *et al.*, 2020).

5.2.2. Preparation of fungal biomass

The fungal strains were independently cultured in a liquid medium i.e., Potato Dextrose Broth (PDB). Further down maintaining aseptic settings, single mycelial discs were transferred into the Erlenmeyer flasks (250 mL), previously holding 100 mL of aseptic PDB. The flasks were appropriately plugged and raised in a BOD incubator at 26 ± 1ºC under dark conditions for 6-7 days, until even fungal mats developed above the broth. The fungal cultures were observed periodically to rule out any contamination. After incubation and undertaking comprehensive sterile conditions, the respective mycological biomass was cautiously separated from the liquid fractions of the respective fungi.

5.2.3. Preparation of fungal extract

The fermented liquids as obtained above were aseptically filtered using Whatman no. 1 filter papers. The mycelia then obtained was splashed 2-3 times using sterile de-ionized water and again aseptically suspended in 150 ml Erlenmeyer flasks containing 50 ml sterile de-ionized water for further growth at 26 ± 1ºC in dark conditions for 3 days (Mekky *et al.*, 2021). After incubation, the biomass was carefully detached using

Whatman no. 1 filter paper so as to obtain the cell-free fungal extracts of *P. sajor caju, A. bisporus* and *L. edodes* respectively. The filtrates thus obtained were stored in sterilized flasks and refrigerated at 4^0 C until further use for the synthesis of nanoparticles (Mohamed *et al.*, 2019).

5.2.4. Synthesis of Zn, Mg, Mn, Combination Nanoparticles

The production of Zn, Mg, Mn, and combination (Zn+Mg+Mn) nanoparticles was attained by taking 50 ml of each cell-free extract and adding it to a 250 ml Erlenmeyer flask containing 500 ml of the already dissolved 5 mM metal salts (Zinc acetate dihydrate (ZAD), Magnesium nitrate hexahydrate (MNH) and Manganese dioxide (MD) respectively (Hamad, 2019). Same procedure was followed for all of the nanoparticles and hence making the total sample flasks of twelve. The subsequent solutions were set on a magnetic stirrer with hot plate and left for stirring at 60°C for 1 hour. The reaction progress was continuously monitored by observing color changes from transparent to brackish in case of zinc and magnesium nanoparticles, black to brownish black in manganese nanoparticles, and black to grey in combination nanoparticles. The formation of nanoparticles was quite visible.

5.2.5. Production of powdered form of Zn, Mg, Mn, and Combination Nanoparticles

Biosynthesized Zn, Mg, Mn, and combination nanoparticles were hydrated and centrifuged at 10,000 rpm for 15-20 minutes. After centrifugation, the pellet was redispersed in sterile de-ionised water and centrifuged again at 3000 rpm (2 to 3 times) to remove the macromolecules and obtain the purified pellet of nanoparticles (Mary *et al.,* 2012). The liquid suspension of the nanoparticles was poured in sterile petri-plates which were placed carefully in the centre of hot air oven operated at 60°C for 24 hours. Thus, oven dried powder of nanoparticles was finally collected and stored in refrigerator at 4°C to be used for characterization and other analysis (Kirthika *et al.,* 2014).

5.3. Characterization of the synthesized material

The characterization of synthesized nanoparticles is an essential part of the assurance of shape, morphology, phase purity, crystalline nature, particle size and surface charge.

The synthesized material was characterized using UV-Visible (UV-Vis) Spectroscopy, Fourier Transform Infra-Red (FT-IR) Spectroscopy, X-ray Diffraction (XRD) and Scanning Electron Microscopy-Energy-Dispersive X-ray Spectroscopy (SEM-EDX) (Mittal *et al.*, 2013) (Table 5.1). To confirm the metal ion reduction, the solution was analysed using a UV-Vis spectrophotometer (Labtronics) from 200-800 nm and using distilled water as a blank sample. FT-IR spectroscopic analysis of biosynthesized metal nanoparticles was recorded using FT-IR (Perkin Elmer) spectrophotometer following KBr pellet production at room temperature. The range was kept at a resolution of 4 cm−1, between 4000 and 400 cm−1. The crystal structure, phase identification and particle size of the metal nanoparticles were analyzed by XRD on a SmartLab 3kW, RIGAKU, Japan, at 40.0 kV, 30.0 mA, and 2θ values between 20° and 100°, with a flow rate of 2°/min. The surface morphological properties of MgO NPs, such as form, size, and composition, were studied using SEM on FE-SEM, GeminiSEM 500, Carl Zeiss, Germany, with a spectral imaging system. FE-SEM was outfitted with the EDX spectrometer (Octane Elect Plus, Ametek USA) for EDX analysis.

Table 5.1: List of techniques and forms of nanoparticles used for characterization

Nanoparticles	**UV-Vis**	**SEM**	**XRD**	**FT-IR**
ZnONPs (*P. sajor caju*)	Liquid	Powder	Powder	Powder
MgONPs (*P. sajor caju*)	Liquid	Powder	Powder	Powder
MnO_2NPs (*P. sajor caju*)	Liquid	Powder	Powder	Powder
CNPs (*P. sajor caju*)	Liquid	Powder	Powder	Powder
ZnONPs (*A. bisporus*)	Liquid	Powder	Powder	Powder
MgONPs (*A. bisporus*)	Liquid	Powder	Powder	Powder
MnO_2NPs (*A. bisporus*)	Liquid	Powder	Powder	Powder
CNPs (*A. bisporus*)	Liquid	Powder	Powder	Powder
ZnONPs (*L. edodes*)	Liquid	Powder	Powder	Powder
MgONPs (*L. edodes*)	Liquid	Powder	Powder	Powder
MnO_2NPs (*L. edodes*)	Liquid	Powder	Powder	Powder
CNPs (*L. edodes*)	Liquid	Powder	Powder	Powder

5.3.1. *UV-Visible (UV-Vis) Spectroscopy*

This technique is employed to estimate the concentration of liquid nano-formulations using appropriate chemical reaction having absorption spectrum in the visible light. It is broadly used for identification of organic as well as inorganic substances. The synthesis of Zn, Mg, Mn, and combo nanoparticles was verified by collecting the aqueous component at various time intervals and using a UV-Vis spectrophotometer to scan the absorbance maxima at wavelengths between 200 and 800 nm. The nanoparticles were sonicated after being thinned in Milli-Q water. Using Milli-Q water as a blank, the absorption spectra of the samples were recorded. The reduction of metal salt ions in solution was supervised by periodically collecting aliquots of the aqueous component and evaluating the solutions using a UV-Vis spectrophotometer (Ibrahem *et al.*, 2017).

5.3.2. *Fourier Transform Infra-Red (FT-IR) Spectroscopy*

FT-IR is very helpful for identifying organic molecular groups and compounds because of the presence of a variety of functional groups. It is powerful tool for isolating and characterizing organic contamination. The FT-IR investigation was carried out to identify the active functional groups fabricating the Zn, Mg, Mn, and combination nanoparticles. The resulted absorption spectrum from bonds natural vibration frequency designated the presence of many functional groups in the samples (Chaudhuri and Malodia, 2017).

5.3.3. *X-Ray Diffraction (XRD)*

The crystalline nature and elemental conformation of the compounds was confirmed by X-ray diffraction. A thin film of the specimen was made by plunging a glass plate for XRD considers. A copper (Cu) anode operating at 30.0 mA and 40.0 kV was used in the analysis. The examination was performed at room temperature and samples were scanned at a rate of 2°/min throughout a 2θ range of 20° to 100°. The diffraction angle (2θ) was found to be a function of the diffracted X-ray intensity. The structural assignments for identifying minerals of the core materials were carried out using the Joint Committee on Powder Diffraction Standards (JCPDS) database files (Raut *et al.*, 2015).

5.3.4. *Scanning Electron Microscopy (SEM) with Energy Dispersive X-ray (EDX) Spectroscopy*

SEM microscopy utilizes the high energy electronic beam which can scan the given surface and provide information about shape, size and very fine details of the superficial morphology of the specimen investigated. The nanoparticle solutions were drop coated onto glass slides to create the samples, which were then sputter-coated with gold. Both backscattered electron images (BEI) and secondary electron images (SEI) were employed. Before being measured, the films on the glass slides were let to dry. To analyze the elemental configuration of the produced samples, EDX-SEM was used (Shamim *et al.*, 2019).

5.4. Assessment of the anti-microbial activities of the synthesized material

The antifungal potential of the synthesized metal nanoparticles was estimated using apple plant pathogens - *Alternaria mali* and *Venturia inaequalis* by poison food technique and spore germination test respectively. Water was used as the control in both cases, while flusilazole and mancozeb were used as standard checks. Aqueous suspensions of the synthesized nanoparticles were added to the media for making different concentrations for the antifungal assays.

5.4.1. *Tested plant pathogenic fungi*

The most commonly encountered, pathogenic yet standard fungi (*Alternaria mali* and *Venturia inaequalis*) *causing* the most dreadful and prominent diseases in apple crop, that is, Alternaria leaf blotch and apple scab respectively, were selected for this work. Maintenance of the pathogenic isolates was carried out by repeated sub-culturing. In order to select the best experiment technique for assessment of antifungal effects of the synthesized nanoparticles two different methods discussed below were used in present study.

5.4.1.1. Poison Food Technique (PFT)

a. Sample preparation

Alternaria mali culture was obtained from Division of plant pathology. To preserve and maintain the cultures for further use, they were sub-cultured on PDA media and then incubated for 5-7 days at 25-27 °C, to get the optimum growth. Zn, Mg, Mn and

Combination nanoparticles were prepared in working concentrations (0.10%, 0.20%, 0.30%) and appropriately sonicated. Simultaneously, PDA media was prepared in 150 ml Erlenmeyer flasks according to the working concentrations of nanoparticles.

b. Evaluation of mycelial growth inhibition via PFT

Alternaria mali was evaluated using the poison food technique (Sharvelle, 1961). PDA media was used to make the desired concentrations of 0.10%, 0.20%, 0.30% in all the nanoparticles respectively. The working concentrations of nanoparticles were added to the alreeady prepared flasks containing PDA media so as to make the poisoned media. The samples achieved were autoclaved, cooled at room temperature and then poured to sterile petri-plates (50 mm) to uniform depth. Once the media was solidified in the plates, wells were punched aseptically with sterile cork borer having 6 mm diameter. Uniform disks from 72 hours old culture of *Alternaria mali* were transferred to the wells and the petri plates were left for incubation under sterile condition at 25-27 ^{0}C for 5-6 days till the control gets full growth of the culture. The antifungal activity of the metal nanoparticles was determined by the measurement of mycelial growth around the inoculated well. The zone of growth was measured using a transparent ruler from the centre to the outer most edge of the growth area.

Growth inhibition as a percentage was computed using the formula (Vincent, 1947) given below:

$I = (\mathrm{C} - \mathrm{T}/\mathrm{C}) \times 10$

Where,

I = Inhibition (%)

C = Growth in control plate (mm)

T = Growth in treated plate (mm).

5.4.1.2. Spore germination test (SGT)

a. Sample preparation

Venturia inaequalis culture was obtained from Division of Plant Pathology, SKUAST-Kashmir. For 15 to 20 days, the fungus was maintained in an incubator at 25 to 28°C while being cultivated on solid PDA media. For the studies, a concentrated water suspension of fungal spores (5 × 106 spores/mL) was produced. The synthesized nanoparticles of Zn, Mg, Mn and Combination were prepared in working

concentrations (0.10%, 0.20%, 0.30%) in de-ionized water with proper sonication. Water agar was prepared for the petri-plates as a medium for spore germination. The *V. inaequalis* conidia were collected by pouring sterile de-ionized water (5 ml) into the fully grown petri-plate and gently scrapping the culture plate with a loop to release the *V. inaequalis* spores. The collected spores were sieved through three layers of sterile cheese cloth to eliminate any fragments of mycelia.

b. Evaluation of spore germination inhibition via SGM

Venturia inaequalis was evaluated using the Spore germination test (Turner *et al.*, 1986). For this method, working concentrations of nanoparticles were added to the water agar media containing flasks and autoclaved. The water agar was then poured into the petri-plates (80 mm) and left to solidify at room temperature. Once the plates were solidified, the water suspension of fungal spores of *V. inaequalis* was poured in vitro and spread on the petri-plates containing solidified poisoned media. The excess suspension was drained by turning the plates upside down in sterile conditions. The petri-plates were then left for incubation for 24 hours at 26±1 ^{0}C. A sterile water solution of spores dispersed on medium without any nanoparticles added was used to prepare control samples. After fungi grown on PDA medium were incubated with nanoparticles at working concentrations for 24 hours, the amount of spores produced by the fungal cultures was assessed. Conidia were considered to have germinated when their length matched or surpassed that of the germ tube. For the control samples, this was done once more. Pictures (10× and 40× magnification) were taken with a binocular microscope. The number of germinating spores in the nanoparticle treated petri-plates was determined after 24 hours of incubation. All experiments were replicated 3 times. The inhibition percentage of spore germination was estimated using the formula by Vincent, 1947:

$$I = (\mathrm{C} - \mathrm{T}/\mathrm{C}) \times 10$$

Where,

I = Inhibition (%)

C = Germination in control plate (mm)

T = Germination in treated plate (mm).

5.5. Evaluation of the effect on plant parameters

a. Sample preparation

To measure various parameters of the apple plants, working concentrations of the nanoparticles were prepared as 0.10%, 0.20%, 0.30% respectively (Table 5.2). Prior to the investigation, spray was done on the field of 120 apple plants. The concentrations were sprayed using a sprayer (150-200 ml) and the experiment was done in two replications.

b. Evaluation of plant parameters via IRGA and SPAD

A portable Infra-Red Gas Analyzer (TARGAS-1 CO_2/H_2O Analyzer) was used to measure the parameters. The middle leaflets of each apple plant were measured from the top for gas exchange metrics. Observations were carefully documented within 48 hours of the spray. Over the course of the experiment, the settings of the leaf chamber were consistently maintained. Observations were made from 9:00 to 11:00 a.m. The boundary layer resistance was 0.08 $ms.mol^{-2}$, and the gas flow rate in the leaf chamber was set at 250 $mL.min^{-1}$. Since the atmospheric CO_2 concentration was around 330 ppm at both locations, the CO_2 mode was set to ambient. Prior to the actual measurements, the CO_2 and H_2O instruments were calibrated. Parameters such as ambient pressure, PAR, leaf chamber and air temperatures, CO_2 and H_2O concentrations in reference and sample air, and leaf chamber gas flow rate are all measured by the device. The device computed and showed the intercellular CO_2 concentration (Ci), stomatal conductance (gs), transpiration rate (E), net photosynthesis (Pn), and biophysical formulas and gas constants (Harley *et al.*, 1992; Pons *et al.*, 2009; Tominaga *et al.*, 2018). Observations were carefully documented within 48 hours of the spray. Readings were taken on two consecutive days.

In addition to these parameters, the chlorophyll content of the treated apple plants was determined using SPAD (Konica Minolta) (Yamamoto *et al.*, 2002). For this, leaves at the tips of the branches were chosen for estimation. Observations were recorded within 48 hours of spraying. Over the course of the experiment, the settings of the leaf chamber were consistently maintained. On two consecutive days, observations were taken between 9:00 and 11:00 a.m.

Table 5.2: Treatments prepared for application on the apple plants maintained in the experimental field

Treatment	Nanoparticle	Conc. (%)	Treatment	Nanoparticle	Conc. (%)
T1	ZnONP-Psc	0.10	T10	CNP-Psc	0.10
	ZnONP-Psc	0.20		CNP-Psc	0.20
	ZnONP-Psc	0.30		CNP-Psc	0.30
T2	ZnONP-Ab	0.10	T11	CNP-Ab	0.10
	ZnONP-Ab	0.20		CNP-Ab	0.20
	ZnONP-Ab	0.30		CNP-Ab	0.30
T3	ZnONP-Le	0.10	T12	CNP-Le	0.10
	ZnONP-Le	0.20		CNP-Le	0.20
	ZnONP-Le	0.30		CNP-Le	0.30
T4	MgONP-Psc	0.10	T13	Zn-MS	300 ppm
	MgONP-Psc	0.20		Zn-MS	500 ppm
	MgONP-Psc	0.30		Zn-MS	700 ppm
T5	MgONP-Ab	0.10	T14	Mg-MS	300 ppm
	MgONP-Ab	0.20		Mg-MS	500 ppm
	MgONP-Ab	0.30		Mg-MS	700 ppm
T6	MgONP-Le	0.10	T15	Mn-MS	300 ppm
	MgONP-Le	0.20		Mn-MS	500 ppm
	MgONP-Le	0.30		Mn-MS	700 ppm
T7	MnO_2NP-Psc	0.10	T16	C-MS	300 ppm
	MnO_2NP-Psc	0.20		C-MS	500 ppm
	MnO_2NP-Psc	0.30		C-MS	700 ppm
T8	MnO_2NP-Ab	0.10	T17	Control	-
	MnO_2NP-Ab	0.20	T18	Man	-
	MnO_2NP-Ab	0.30	T19	Flu	-
T9	MnO_2NP-Le	0.10			
	MnO_2NP-Le	0.20			
	MnO_2NP-Le	0.30			

5.6. Statistical Analysis

A comprehensive statistical approach was employed to analyze the experimental data generated during the characterization of nanoparticles and evaluation of their antifungal properties. OriginPro 9.0 was utilized for data plotting, graphical representation, and preliminary statistical processing. ImageJ software was used for quantifying specific experimental outputs, including measurements of nanoparticles obtained in SEM micographs and other image-based analyses.

Prior to statistical analysis, the raw data were appropriately transformed to meet the assumptions of normality and homogeneity of variance, following the guidelines suggested by Gomez and Gomez (1984). These transformations ensured the reliability and accuracy of the subsequent statistical interpretations.

The processed data were subjected to statistical analysis using OPSTAT (2011), a reliable tool for agricultural and biological data analysis. Descriptive statistics, including mean and standard deviation (SD), were calculated for each treatment group to summarize the central tendency and variability within the dataset.

To determine the statistical significance of differences among multiple treatment means and % inhibition data, a One-Way Analysis of Variance (ANOVA) was employed. This test was particularly useful for comparing the effects of different concentrations and types of nanoparticles (Zn, Mg, Mn, and Zn+Mg+Mn) synthesized using Pleurotus sajor-caju, Agaricus bisporus, and Lentinus edodes, on fungal inhibition zones. The ANOVA allowed the evaluation of whether observed variations in antifungal activity were statistically significant.

Where necessary, post hoc comparisons (CRD, DMRT) were applied to further distinguish significant differences between individual treatment means. All results were expressed as mean ± standard deviation (SD), with triplicate biological replicates ($n = 3$), and statistical significance was considered at a confidence level of $p < 0.05$.

Chapter 6

Results and Discussion

In this study, we used the cell-free fungal extracts of *Pleurotus sajor caju*, *Agaricus bisporus and Lentinus edodes* for the synthesis of zinc, magnesium, manganese and combination nanoparticles. The latter were thoroughly characterized for their origin and further assessed chiefly on an in vitro basis for their probable therapeutic antifungal efficiency. The key results for each test along with the equivalent discussion for the same as per each objective goes as follows:

6.1. Collection of fungal cultures

When compared to other physical and synthetic chemical synthesis methods, it has been shown that biological synthesis of nanoparticles is less harmful, demands less efforts, and is environmentally friendly. Interactions among microorganisms and nanostructured materials are receiving more interest because they may be utilized to produce efficient nanoparticles with particular biological activities. Among all other micro-organisms, fungi produce the most metabolites and are also more resistant to pressure and flow-rate to encourage the production of nanoparticles on a larger scale. Fungi are able to remove and accumulate heavy metals because they possess multiple reductase enzymes with the ability to convert precursor metal salts into nanoparticles with a narrow size distribution and, therefore, better dispersity (Singh et al, 2016). In the study, three fungal extracts were utilized to synthesize the nanoparticles of ZnO, MgO, MnO_2 and the combination of three. Cultures of the fungi used - *Pleurotus sajor caju, Agaricus bisporus* and *Lentinus edodes*, collected from MRTC, SKUAST-Kashmir, were selected on the criteria of their extensive usage in nanoparticle production in addition to their easy accessibility and cost-effectiveness. Pathogenic fungi used for evaluation - *Alternaria mali* and *Venturia inaequalis* were collected from Division of Plant Pathology, SKUAST-Kashmir.

6.1.1. Preservation and identification of the fungal cultures

The fungal species selected and collected were purified via reinoculation as done upon fresh PDA plates and slants. Sub-culturing was repeated as so to preserve the cultures (Figure 6.1.1). The isolated fungi were then stored as PDA slants and *A. mali* and *V. inaequalis* were sub-cultured on petri-plates as well. Preliminary identification of the pathogenic fungi consisted of recognizing their microscopic characters. The individual fungal isolate was microscopically (40x) assessed via lactophenol cotton blue (LPCB)

mount to express the microscopic structures namely hyphae, conidiophores, conidia, etc. as shown in figure 6.1.2.

Figure 6.1.1: *in-vitro* slant cultures of *P. sajor caju*, *A. bisporus* and *L. edodes* after a) 1 day; b) 6 days; c) 12 days

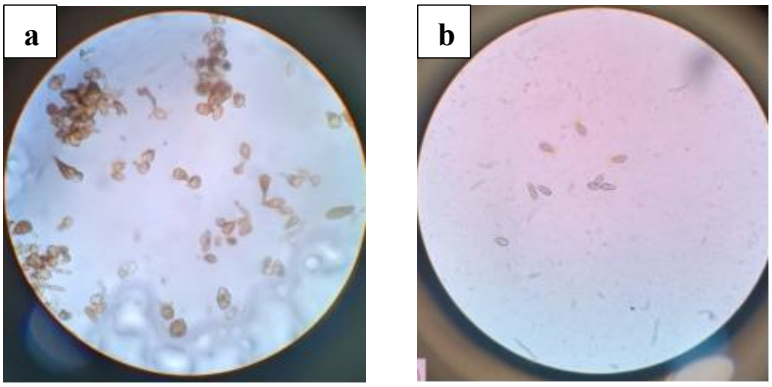

Figure 6.1.2: Microscopic view of the spores of a) *A. mali*; b) *V. inaequalis*

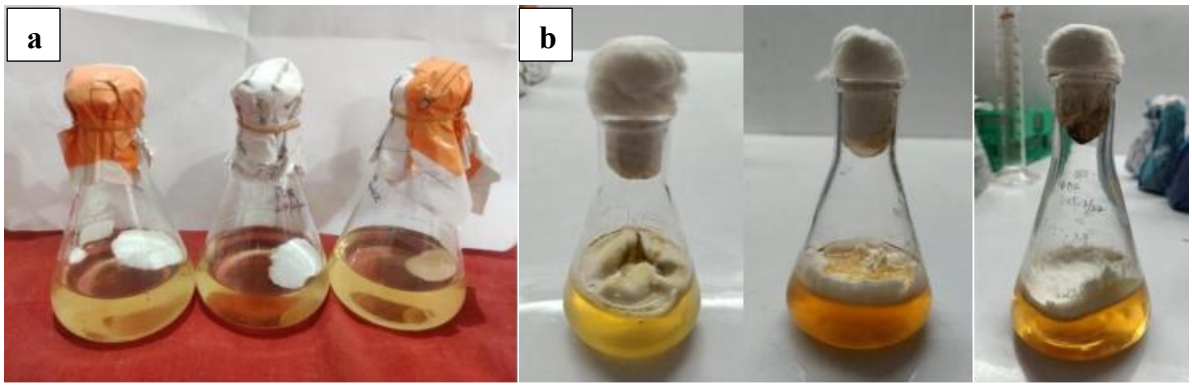

Figure 6.1.3: a) PDB media flasks inoculated with *P. sajor caju*, *A. bisporus* and *L. edodes*; b) Flasks showing mycelial mats of *P. sajor caju*, *A. bisporus* and *L. edodes* after 6 days

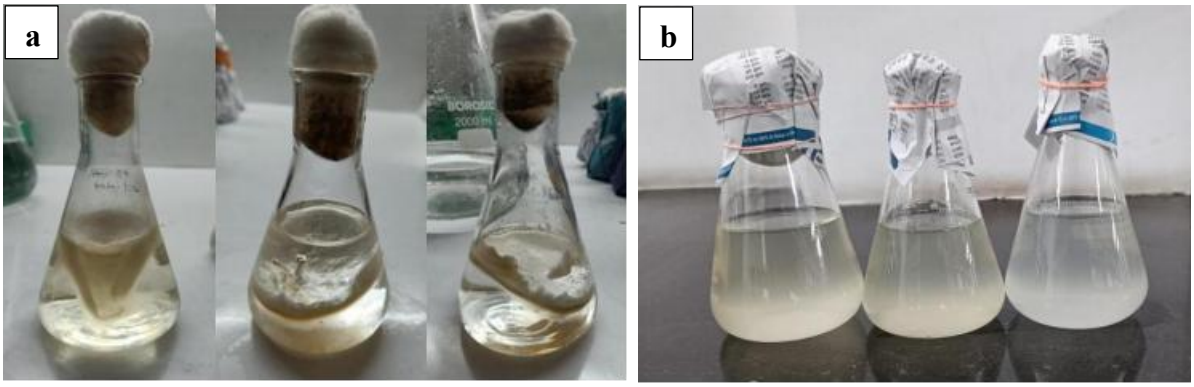

Figure 6.1.4: a) Fully grown fungal mycelia in flasks containing de-ionized water; b) Cell-free fungal extracts of *P. sajor caju, A. bisporus* and *L. edodes*.

6.2. Mycogenic synthesis of Zn, Mg, Mn and Combination (Zn+Mg+Mn) nanoparticles

Nanotechnology encompasses a range of methods for nanomaterials, including chemical, biological, and physical methods. The biological manufacturing approach has emerged as a viable environmentally friendly strategy to eliminate the adverse effects associated with physical or chemical fabrication methods (Alghuthaymi *et al.*, 2015). Accordingly, nanoparticles were biologically produced in the new field of nano-biotechnology using bioactive metabolites that were extracted from a range of biological entities, including bacteria, fungi, algae, and plants (Usha *et al.*, 2010; Chatterjee *et al.*, 2017; Makvandi *et al.*, 2020; Ragab and Saad-Allah, 2020). In order to lessen the hazardous nature of the product, these biological substrates are mostly utilized in place of chemical stabilizing and solving agents (Bandeira *et al.*, 2020). The biological method being commercially viable, eco-friendly, clean, and non-toxic is preferred over other techniques to synthesize nanoparticles applied in agriculture and medicine (Ogunyemi *et al.*, 2019; Salem *et al.*, 2020). The effort of this study started with the screening of all three fungal species (*P. sajor caju, A. bisporus* and *L. edodes*) to examine their potentiality for the biogenic synthesis of Zn, Mg, Mn and Combination nanoparticles. The mycelial mat of each of the three fungal colonies was individually grown on PDB and further utilized to extract their extracellular components (Jain *et al.*, 2013, with modification) (Figures 6.1.3, 6.1.4). The extracellular fungal extracts that reduced the metal salts into nanoparticles were produced from the fermented broth. Additionally, variables that impact the myco-synthesis of targeted nanoparticles, such

as pH, precursor concentrations, incubation temperature, and contact durations were adjusted.

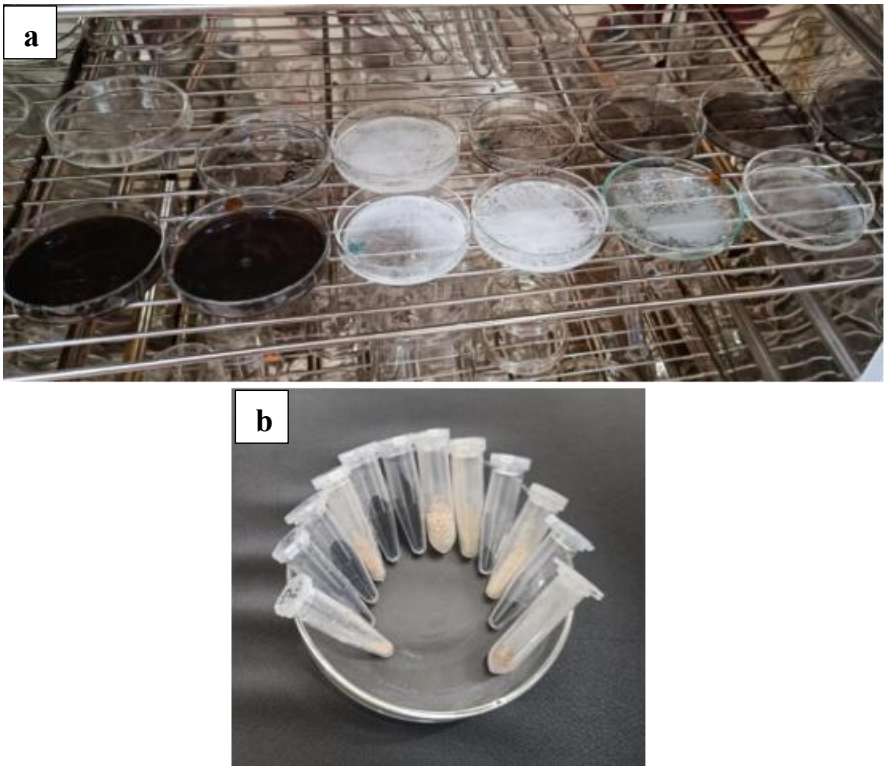

Figure 6.2: a) Nanoparticles put for oven-drying at 60 °C; b) Powdered form of nanoparticles

6.2.1. Mycogenic synthesis of ZnONPs

There has been increased interest in the myco-synthesis of metal or metal oxide nanoparticles recently because of their high metabolite secretions, ease of handling, and scalability. Furthermore, fungi are distinguished by their high biomass production, which is utilized to create highly active metabolites, as well as their increased accumulation and resistance to metals (Salem and Fouda, 2020). One of the main areas of focus for the study of biological nanostructures is the synthesis of ZnONPs with inorganic complex using naturally occurring ligating agents made from biological resources. Zinc oxide (ZnO) stands as one of the most important semiconducting resources because of its many uses and remarkable qualities (Singh *et al.*, 2011). A simple, economical, and biological technique was undertaken for the synthesis of ZnONPs which goes down well with the effort of El-Saadony *et al.*, 2021. The nanoparticles were synthesized following a one-hour reaction of the metal salt with

each fungal extract used leading to the visible production of ZnONPs. The latter was subjected to drying at 60^0 C (Figure 6.2a). The resultant powdered form of ZnONPs was ground to a fine powder, that was stored at -4^0 C for further use (Figure 6.2b). This was done for all the nanoparticles synthesized. Figure 6.3 shows the liquid form of ZnONPs before centrifugation.

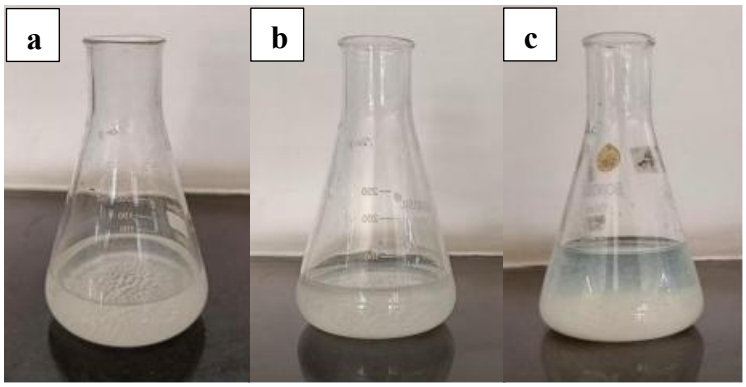

Figure 6.3: ZnONPs synthesized from
a) *P. sajor caju*; b) *A. bisporus*; c) *L. edodes*

The synthesis of ZnONPs includes the cationic bonding with the polymer networks of the fungal extracts of *P. sajor caju, A. bisporus*, and *L. edodes*. By producing nanoparticles, the intricate networks of reducing secondary metabolites present in the fungal extracts may be linked together. The reductants found in fungal extracts control the ZnO nucleation process, which is essential for the ordered development of ZnO nanoparticles (Healy *et al.*, 2004). The increase in the concentration of secondary metabolites, enzymes, and chemicals found in each fungal extract—which serve as essential chelating, stabilizing, and reducing agents in addition to gelling agents—could be the reason for variations in the size and structure of ZnONPs (Ganesan *et al.*, 2020). A similar work was conducted by Oyefusi *et al.* (2014) utilizing the peel of a rambutan fruit, where the p-track conjugation impact was customized by the ester group of oxygen atoms and the phenolic (OH−) groups present in polyphenols. The chelating action created the OH-groups together with the metal phenolate or zinc-ellagate complex. These ZnONPs produced using fungal extracts are also known to have advantageous antimicrobial potentials in addition to the previously listed ones (Ali *et al.*, 2016).

6.2.2. Mycogenic synthesis of MgONPs

Researchers have been very interested in employing biological approaches to produce MgONPs for the past decade. Less chemical use, cost-effectiveness, and environmental friendliness are key aspects in the development and significance of this specific sector (Wani *et al.*, 2012; Ali *et al.*, 2015; Das *et al.*, 2017; Jeevanandam *et al.*, 2017). MgONPs have been produced from any of the precursors, including magnesium nitrates, acetates, chlorides, and sulphates, due to the growing trend of greener techniques for creating nanoparticles employing plants, microorganisms, and biomolecules (Figure 6.4). The precursor is mixed with the formerly prepared biological extracts to form a homogenized solution, which is subsequently heated (Sugirtha *et al.*, 2015; Jadhav *et al.*, 2016; Das *et al.*, 2018; Singh *et al.*, 2019). The extracellular enzymatic secretion of the employed fungus is what produces MgONPs from the Mg precursor salt. It is highly successful in reducing magnesium salt to generate MgONPs when fungal spheres are extracted from the biomass culture (Raliya *et al.*, 2014). Additionally, MgONPs have been effectively produced using gamma rays and the melanin pigment of *Pencillium chrysogenum*. According to El-Sayyad *et al.* (2018), pH, ideal temperature, and an ideal media are some of the main factors contributing to the creation of MgO nanoparticles. For the first time, the biomass filtrates of *P. sajor caju, A. bisporus,* and *L. edodes*—which were used as biocatalysts—were used to create this economical green technique for MgONPs synthesis at room temperature (El-Batal *et al.*, 2017a; 2017b). The color shift of the solution from pale yellow to white upon mixing with the magnesium precursor salt served as the first indicator of effective production (Saad *et al.*, 2018). According to Khanra *et al.* (2015), color change signifies the action of metabolites present in biomass filtrate that convert nitrates (NO_3) to nitrites (NO_2) and the released electron that reduces Mg^{2+} to generate MgONPs. The enzymatic ability of nitrate reductase to reduce magnesium salt is essential to the extracellular process of nanoparticle production (Ingle *et al.*, 2008). The produced MgONPs are stabilized by the other proteins that are secreted in the fungal filtrate (Fouda *et al.*, 2017).

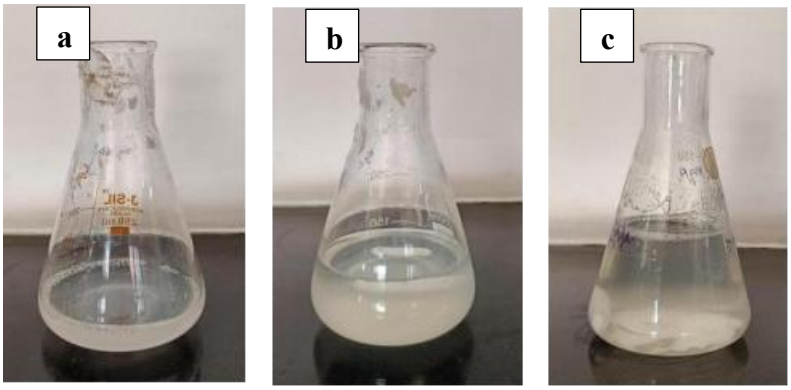

Figure 6.4: MgONPs synthesized from
a) *P. sajor caju*; b) *A. bisporus*; c) *L. edodes*

6.2.3. Mycogenic synthesis of MnO_2NPs

Manganese oxides have garnered particular attention among many 3D transition metal oxides because of their abundant structural and compositional variations, including MnO, Mn_5O_8, Mn_2O_3, MnO_2, and Mn_3O_4 (Prasad, 2017). According to Veeramani *et al.* (2013), MnONPs have a lot of potential for sustainable nanotechnology. Despite possessing a number of intriguing and useful features, Mn nanoparticles have not been employed extensively. Although the biosynthesis of MnONPs using bacterial and plant extracts has been the subject of several papers, no study has examined the production of MnO_2NPs utilizing bioactive metabolites that have been isolated from fungi, particularly mushrooms. The use of fungi as green producers for the biofabrication of nanoparticles with adequate antimicrobial activity has sparked a lot of interest in the nanobiotechnology community. In order to effectively produce MnO_2NPs, all of the aforementioned goals were statistically examined. The current study utilized fungal extracts of *P. sajor caju, A. bisporus,* and *L. edodes* in an attempt to manufacture and analyze MnO_2NPs. It was observed that the color of the solutions turned from normal black to brownish black after an hour of continuous stirring monitoring various parameters, which indicated the formation of MnO_2NPs (Figure 6.5).

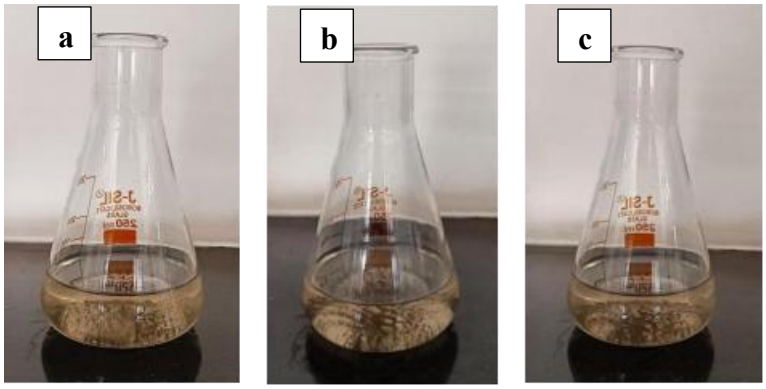

Figure 6.5: MnO_2NPs synthesized from
a) *P. sajor caju*; b) *A. bisporus*; c) *L. edodes*

6.2.4. Synthesis of Combination Nanoparticles (CNPs)

Enormous number of nanoparticles are being synthesized in combination. Mn- and Fe-doped ZnONPs have been synthesized using chemical co-precipitation method (Sharma *et al.*, 2016); Zn-doped MgO by sol-gel method (Sierra-Fernandez *et al.*, 2018); zinc oxide-doped selenium oxide (ZnO-SeO) nanoparticles via mycosynthesis using the fungus *Alternaria alternata* (Qanash *et al.*, 2024). But so far, trimetallic nanoparticles of Zinc, Magnesium and Manganese have not been synthesized from *P. sajor caju, A. bisporus* and *L. edodes* and could be therefore, considered as a novel approach. Figure 6.6 shows the liquid form of CNPs synthesized after one hour of reaction with continuous stirring at 60°C.

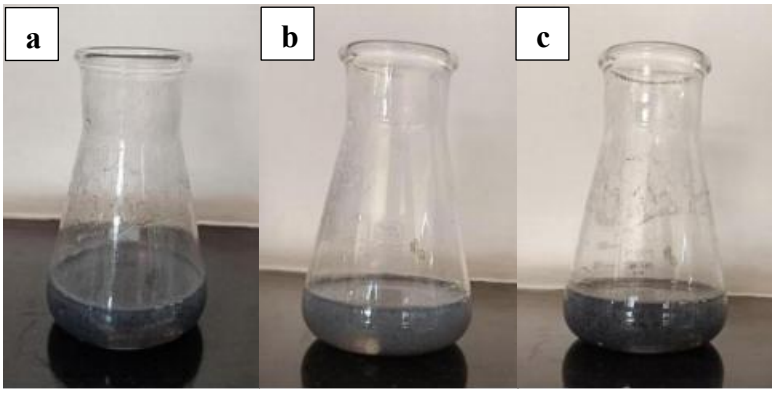

Figure 6.6: CNPs synthesized from
a) *P. sajor caju*; b) *A. bisporus*; c) *L. edodes*

6.3. Physicochemical characterization of Zn, Mg, Mn and Combination nanoparticles

The extracellular synthesis of nanoparticles is significantly influenced by the reducing components that microorganisms create. One fundamental and effective method for comprehending the optical characteristics of metal nanoparticles is spectroscopic investigation. UV-visible spectral analysis was performed for synthesized ZnONPs, MgONPs, MnO_2NPs and Combination nanoparticles synthesized from extracellular fungal filtrates of *P. sajor caju, A. bisporus* and *L. edodes* respectively. All types of nanoparticles synthesized via utilizing these specific fungal extracts were given suitable codes and further subjected to preliminary physicochemical characterization using procedures such as UV-Vis Spectroscopy, FT-IR Spectroscopy, XRD, SEM and EDX Spectroscopy. It was done to sieve out fungi and their respective extracts that were accountable for the potential formation of the nanoparticles besides proceeding for the in-depth characterization as well as primary assessment of the bioactivity of selective nanoparticles.

6.3.1. Ultraviolet-Visible Spectroscopy

UV-vis analysis is an important element of characterizing metal nanoparticles. The interaction amongst incoming photons and the electrons of metal nanoparticles results in sharp and intense surface plasmon absorption peaks in the UV-vis spectrum. Significant color shifts and distinct absorption peaks in the UV-vis absorption spectrum are indicators that nanoparticles have formed. Using a UV-vis absorption spectrum, the phytochemicals in the fungal extracts of *Pleurotus sajor caju, Agaricus bisporus*, and *Lentinus edodes* were shown to reduce metal ions into nanoparticles. The apparent color shift in the reaction mixture upon microwave irradiation provided the first indication that nanoparticles were being produced. The mixtures of zinc acetate dihydrate, magnesium nitrate hexahydrate and manganese dioxide solutions with that of the three fungal extracts were colorless, but the color changed afterwards. The reduction of Zn^{2+} ions to ZnONPs, Mg^{2+} ions to MgONPs and Mn^{4+} to MnO_2NPs by the reductase enzymes in the fungal extracts of *P. sajor caju, A. bisporus* and *L. edodes* was examined by recording UV-vis absorption spectra of the nanoparticles which revealed the occurrence of ZnONPs, MgONPs, MnO_2NPs and CNPs. It can be seen that the

appearance of peaks clearly indicates the formation of nanoparticles and observations clearly specify the successful reduction of metal salts to nanoparticles using *P. sajor caju, A. bisporus* and *L. edodes* extracts. The absorption spectra achieved in the study are summarised in Table 6.1.

Table 6.1: UV-Visible absorption wavelengths of the nanoparticles

S. No.	Nanoparticle	Absorption wavelength (λ_{max})
1	ZnONP-Psc	307.55
2	ZnONP-Ab	391.76
3	ZnONP-Le	309.70
4	MgONP-Psc	304.79
5	MgONP-Ab	305.99
6	MgONP-Le	307.34
7	MnO_2NP-Psc	309.96
8	MnO_2NP-Ab	320.98
9	MnO_2NP-Le	308.61
10	CNP-Psc	309.76
11	CNP-Ab	328.53
12	CNP-Le	329.04

6.3.1.1. *UV-vis spectroscopy of ZnONPs*

After 24 hours of incubation, the medium containing the zinc ions exhibits its highest intensity in the absorption spectrum at 300–400 nm. This outcome verified that ZnONPs were present. The apparent color shift in the reaction mixture apparent color shift upon microwave irradiation provided the first indication that nanoparticles are formed. The mixtures of zinc acetate dihydrate and the three fungal extracts were colorless, but the color changed to brackish after 1 hour of continuous shaking on the magnetic stirrer at a temperature of 50-60^0 C. Both direct absorption by the ZnO and enhanced scattering by the nanoparticles may be responsible for the general rise in absorption across the 200–800 nm range. A similar increase was observed in every condition tested, suggesting the synthesis of ZnO nanoparticles with the fungal filtrate.

Optical characteristics of the synthesized particles indicated towards nano size of ZnONPs as the absorption bands represented slight shifts with absorbance peaks at about 307 nm in ZnONP-Psc, 391 nm in ZnONP-Ab and 309 nm in ZnONP-Le (Figure 6.7.1) as recorded by UV-vis spectrophotometer.

6.3.1.2. *UV-vis spectroscopy of MgONPs*

UV-Vis spectroscopy was used to observe color change and determine the maximum surface plasmon resonance (SPR) and validate the production of MgONPs. After an hour of constant stirring, the translucent solutions became brackish due to the application of fungal extracts and magnesium metal salt. According to earlier reports, SPR typically had an effect on the shape, size, and good dispersion of myco-synthesized nanoparticles (Fedlheim and Foss, 2001). When the SPR is less than 300 nm, the size of biosynthesized MgONPs is typically small; but, for SPRs more than 300 nm, they may become more anisotropic (Jeevanandam *et al.*, 2017). Myco-synthesized MgONPs in the current study exhibited SPR at wavelengths of 304 nm, 305 nm, and 307 nm in MgONP-Psc, MgONP-Ab, and MgONP-Le, respectively (Nguyen *et al.*, 2021) (Figure 6.7.2). This suggests the existence of particles at the nanoscale. The current data is in line with previous works (Abdallah *et al.*, 2019; Nguyen *et al.*, 2021). As a result, it may be presumed that the metabolites in fungal filtrate are effective in reducing, capping, and stabilizing MgONPs.

6.3.1.3. *UV-vis spectroscopy of MnO_2NPs*

The addition of manganese metal salt solution to cell-free extracts of the fungi showed a decrease in the color intensity from black to brownish black after 1 hour of continuous stirring on the magnetic stirrer is a marker of MnO_2NPs production, according to UV-vis spectroscopy in the 200 nm to 800 nm region. This color change served as evidence that fungal enzymes were bioreducing manganese ions. Consequently, the UV-vis spectrum is used to verify the stability and generation of nanoparticles in an aqueous solution. Figure 6.7.3 demonstrates the UV–vis spectra of MnO_2NP-Psc, MnO_2NP-Ab and MnO_2NP-Le that were generated. An examination of MnO_2NP absorption shows distinct peaks at 309 nm, 320 nm and 308 nm in MnO_2NP-Psc, MnO_2NP-Ab and MnO_2NP-Le respectively. Due to the SPR, liquid formulations of MnO_2NPs show colour change and have a distinct absorption peak around 310 nm (Dessie *et al.* 2020).

6.3.1.4. *UV-vis spectroscopy of CNPs*

In the combination nanoparticles, the initial indication of the production of nanoparticles was the color shift from black to grey after the reaction of metal salts in combination with that of the fungal extracts individually. CNPs showed maximum absorption peaks in the wavelength range of 300-400 nm. *P. sajor caju* mediated CNPs (CNPs-Psc) showed the absorption peak at 309 nm, whereas *A. bisporus* and *L. edodes* mediated nanoparticles (CNPs-Ab and CNPs-Le) showed peaks at 328 nm and 329 nm respectively (Figure 6.7.4).

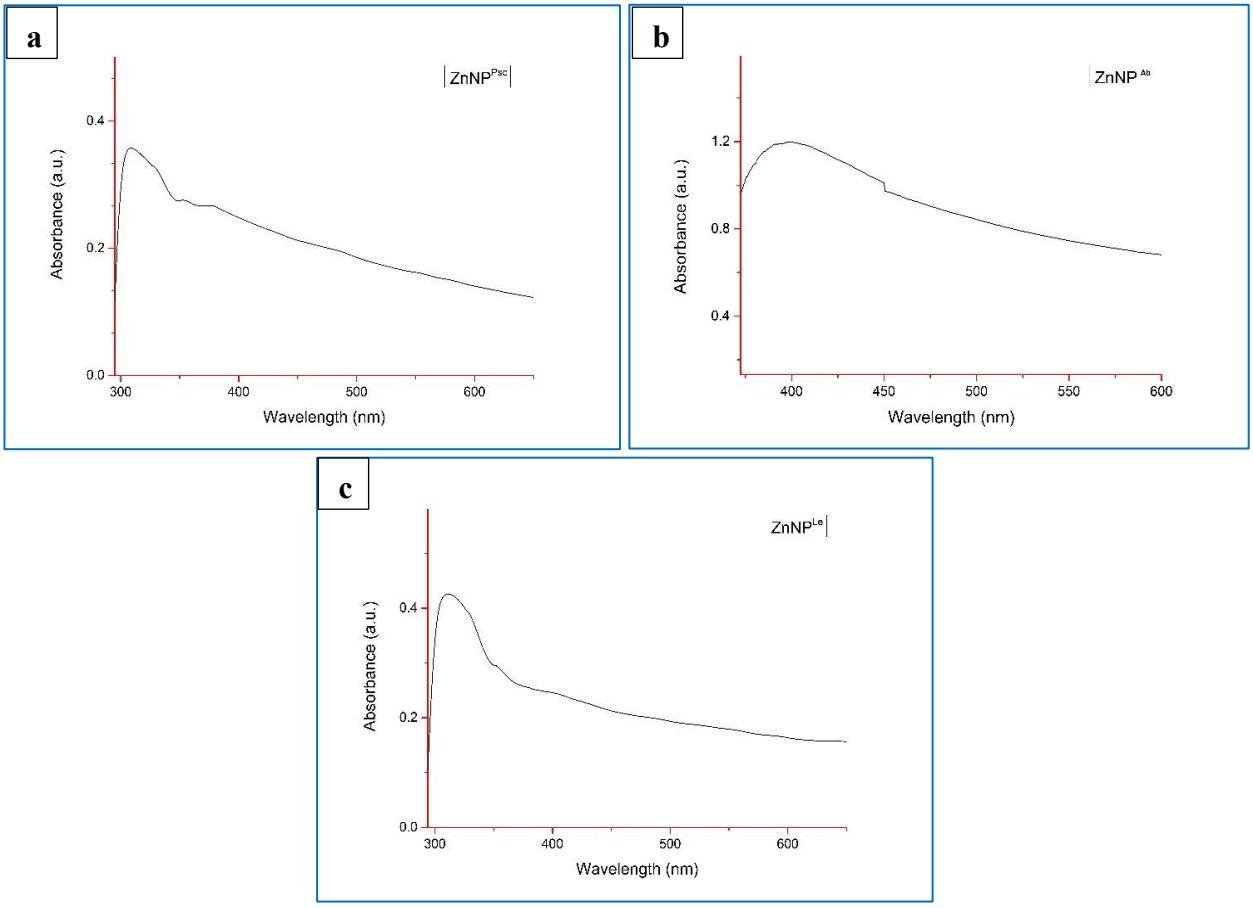

Figure 6.7.1: UV-Vis Spectrograms defining prospective synthesis of a) ZnONP-Psc; b) ZnONP-Ab; and c) ZnONP-Le

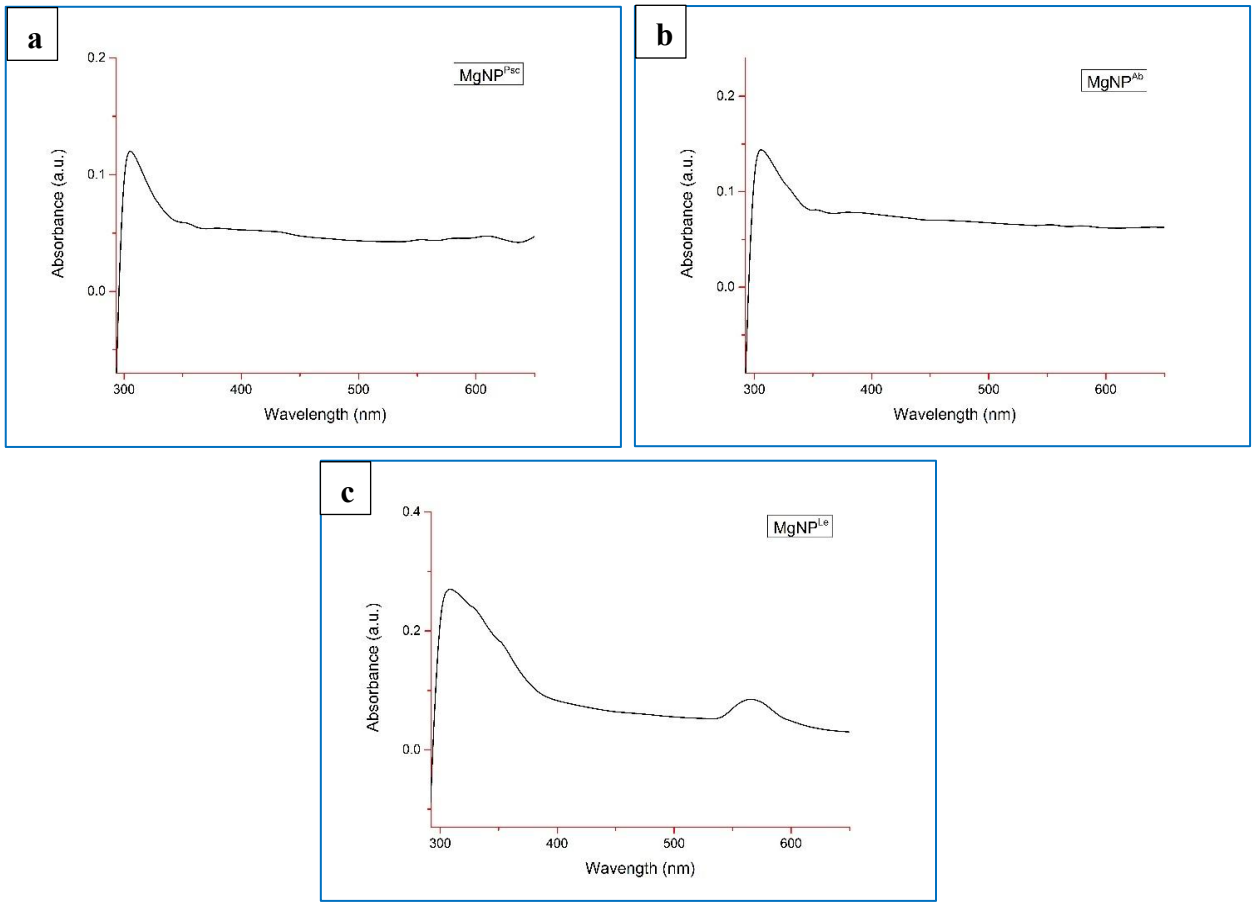

Figure 6.7.2: UV-Vis Spectrograms defining prospective synthesis of a) MgONP-Psc; b) MgONP-Ab; and c) MgONP-Le

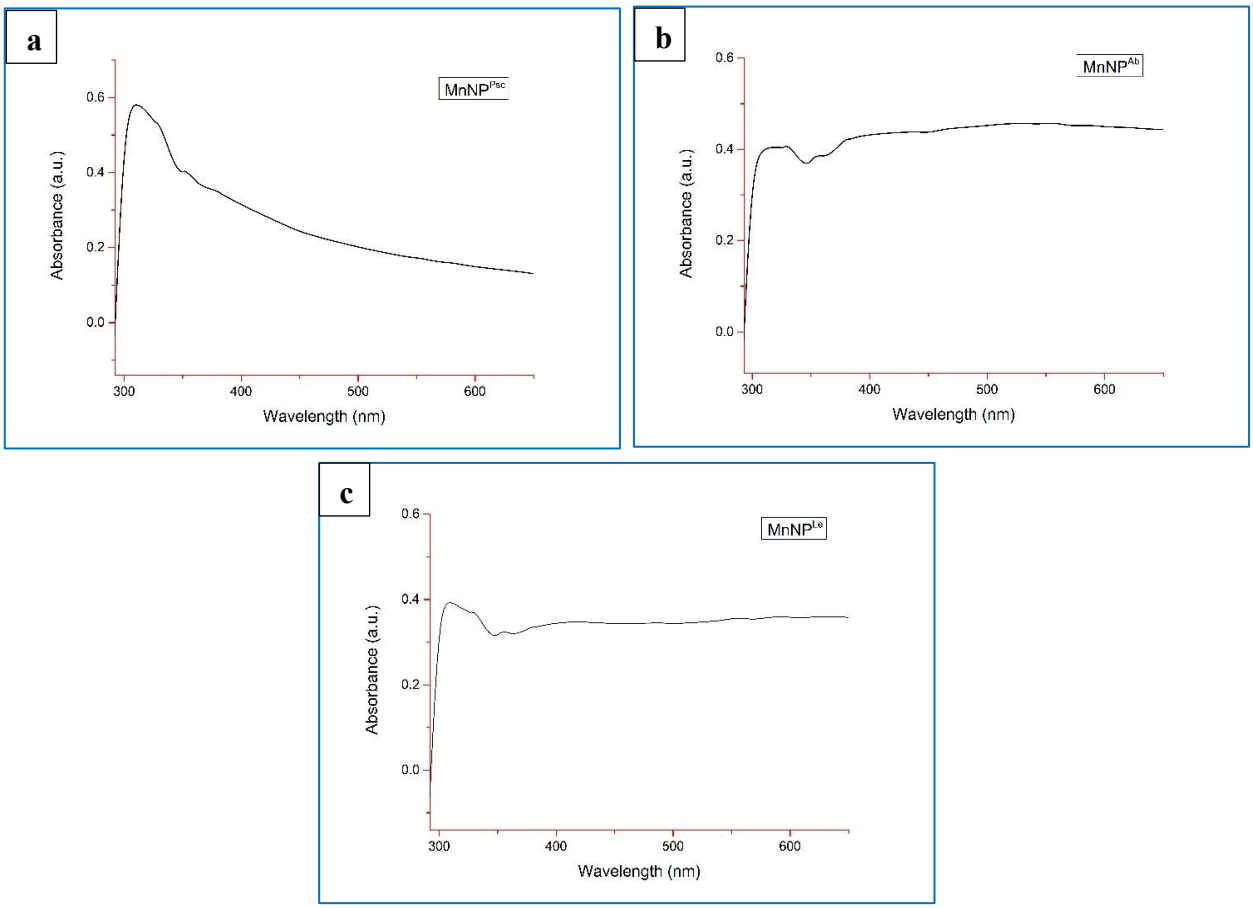

Figure 6.7.3: UV-Vis Spectrograms defining prospective synthesis of a) MnO_2NP-Psc; b) MnO_2NP-Ab; and c) MnO_2NP-Le

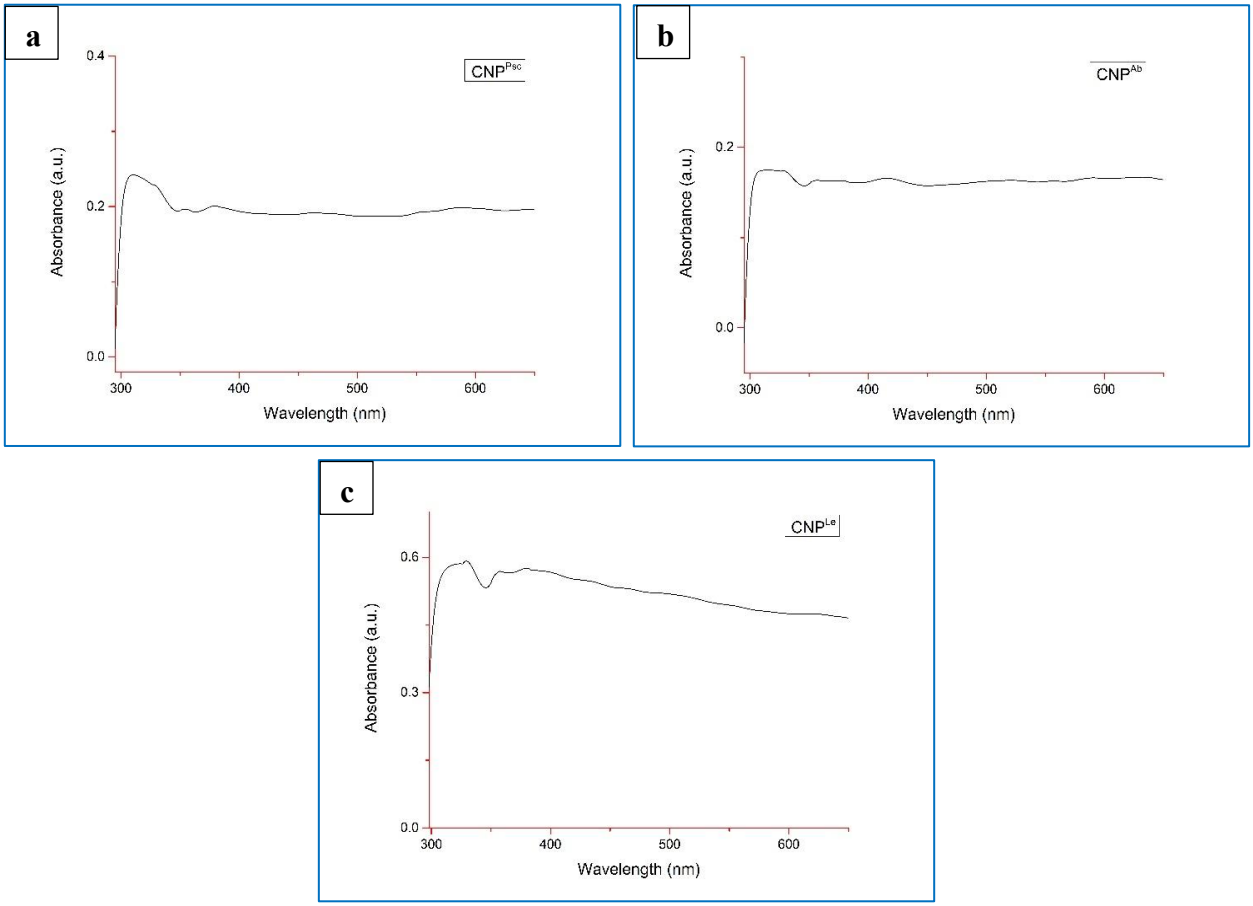

Figure 6.7.4: UV-Vis Spectrograms defining prospective synthesis of a) CNP-Psc; b) CNP-Ab; and c) CNP-Le

6.3.2. Fourier Transform Infra-Red (FT-IR) Spectroscopy

FT-IR spectroscopy is a practical method for measuring the secondary structure of metal nanoparticles and protein interaction, by using resonance of non-centrosymmetric (IR active) modes of vibration to absorb Infra-Red (IR) radiation. To investigate the functional groups of chemical compounds and find potential biomolecules in fungal extracts that are in charge of capping and effectively stabilizing ZnONPs, MgONPs, MnO_2NPs, and CNPs, FT-IR spectroscopy is often utilized. The bioactive chemicals found in the biomass filtrate of *P. sajor caju, A. bisporus,* and *L. edodes* strains—which in turn are in charge of reducing metal precursors to generate MgONPs—are discovered using FT-IR analysis, which records the wavenumber between 400 and 4000 cm–1. The spectra attained are quite comparable.

6.3.2.1. *FT-IR spectra of ZnONPs*

The FT-IR spectra of ZnONPs synthesized by using *P. sajor caju* (ZnONP-Psc), *A. bisporus* (ZnONP-Ab) and *L. edodes* (ZnONP-Le) showed the peaks in the region of 500–3700 cm −1 (Figure 6.8.1), which confirmed the presence of hydroxyl (O–H) groups. The characteristic spectra of peaks of about 588 cm−1 and 2295 cm−1 (ZnONP-Psc), 670 cm−1 and 2200 cm−1 (ZnONP-Ab) and 602 cm−1, 2196 cm−1 and 2285 cm−1 (ZnONP-Le) point towards the ZnO transverse optical stretching modes. In the case of ZnONP-Psc, ZnONP-Ab, and ZnONP-Le, sharp absorption peaks were attained at 2960 cm^{-1}, 2964 cm^{-1}, and 2967 cm^{-1}, which correspond to the methyl group stretching of C–H band present in proteins, while the major absorption peaks were achieved at 3200-3400 cm^{-1} for all ZnONPs, which correspond to the N–H stretching of secondary amides of proteins. The –CO stretching of the amide-I band of the protein is responsible for the peaks at 1490 cm^{-1} (ZnONP-Psc), 1550–1551 cm^{-1} (ZnONP-Ab), and 1497 cm^{-1} (ZnONP-Le). The C–N stretching vibrations of aromatic amines are responsible for the peaks at 1377 cm^{-1} in ZnONP-Psc, 1380 cm^{-1} in ZnONP-Ab, and 1387 cm^{-1} in ZnONP-Le. Some extracellular proteins found in the fungal filtrates may be the cause of the decrease in zinc ions (Gupta and Chundawat, 2020). These proteins also function as capping agents to add more stability and have a strong capacity to bind ZnONPs. The C–OH group of the phenols is accountable for the peaks at 825–1037 cm^{-1} in ZnONP-Psc, 815–1024 cm^{-1} in ZnONP-Ab, and 825–1024 cm^{-1} in ZnONP-Le. This indicates the role of polyphenols like terpenoids and flavonoids, that may also function as bio-reducing agents. Consequently, proteins serve as both reducing and stabilizing agents. The peaks at 588-667 cm^{-1}, 670 cm^{-1} and 602-677 cm^{-1} in ZnONP-Psc, ZnONP-Ab and ZnONP-Le respectively, are due to the Zn–O stretching. These findings aligned with previous studies of biological nanoparticle production (Netala *et al.*, 2016; Kadam *et al.*, 2019; Ogunyemi *et al.*, 2019; Ahmad *et al.*, 2020).

6.3.2.2. *FT-IR spectra of MgONPs*

The -OH stretching band is specified by the peak seen at 3698 cm^{-1} (Ramanujam and Sundrarajan, 2014). The vibration mode due to the O–H stretching in hydroxyl groups overlapped with the N-H stretching band of amines, which is shown by the broadness peak at 3252 cm–1 (Dobrucka, 2018). The bending mode of N–H (main amine)

overlapped with either amide or carboxylate salt is indicated by the medium detected peaks at 1800-2300 cm–1 (see XPS study). The C=O stretching of carboxylate salt and the adsorption of CO3 2– and CO2 at the surface of MgONPs are represented by the average peaks at 1431 cm^{-1} (MgONP-Psc), 1365 cm^{-1} (MgONP-Ab), and 1411 cm^{-1} (MgONP-Le) (Coates, 2006; Hamza *et al.*, 2021). Catalytic reactions depend critically on the adsorption of these functional groups on the exterior surface of MgONPs (Taourati *et al.*, 2020). In contrast, the Mg–OH stretching with the C-H band was matched by the peaks at 1044–1085 (Karthik *et al.*, 2019). The trans-C-H out-of-plane bend, C-O stretching, and P-O, or phosphate comprising molecules, are represented by the peaks at 842–843 cm–1 (Wei *et al.*, 2020). According to several published investigations, peaks seen at a wavenumber between 500 and 700 cm–1 further verified the effective synthesis of MgONPs (Ramanujam and Sundrarajan, 2014; Pugazhendhi *et al.*, 2019; Fouda *et al.*, 2021). The peaks demonstrated by FT-IR spectra show how metabolites from biomass filtrates of *P. sajor caju, A. bisporus*, and *L. edodes* contribute to the reduction and stabilization of MgONPs (Figure 6.8.2).

6.3.2.3. *FT-IR spectra of MnO_2NPs*

The biomolecules and functional groups of the nanomaterial may be identified by FT-IR analysis. FT-IR spectroscopy in the wavenumber range of 400–4000 cm−1 provided valuable information on the extract's chemical makeup and the surface functional groups of MnO_2NPs. The FT-IR characterisation of a few functional groups on MnO_2NPs is displayed in Figure 6.8.3. The principal peaks in the MnO_2NP-Psc FT-IR spectra were 1380 cm−1 (C-O and C-X expansion), 2824–2967 cm−1 (C-H vibration), 1613 cm−1 (aromatic C=C bond stretching), 921–1030 cm^{-1} (C-N and C-O stretching), and 3351 cm^{-1} (O-H bond stretching vibration). The Mn-O stretching was suggested by the strong peaks at 859 cm−1 (Kamran *et al.*, 2019). The Mn–O bond stretching characteristic in MnO_2NP-Ab and MnO_2NP-Le is represented by the vibrational frequency seen at 492 and 513 cm−1 (Salavati-niasari *et al.*, 2014; Nassar *et al.*, 2016). The OH molecules adsorbed on the surface of the atmosphere with Mn atoms are responsible for the band at a wavenumber of around 1538-1634 cm−1 (Rani *et al.* 2018). For the C=O, C-N stretch, the bands at 3678, 3673, 1724, 1024, and 1023 cm−1 are important. The bending frequency of the methylene group is shown by bands at

1369–1404 cm^{-1} (Abdel-Aziz *et al.* 2020). However, MnO_2NPs only exhibit a very broad and less intense absorption band at 3351-3773 cm−1 and a strong band at 490-600 cm−1, which is property of the O–Mn–O linkage, as a result of the O-H bond stretching of adsorbed H_2O molecules (Dessie *et al.* 2020). The purity of the sample is shown by the lack of any additional bands.

6.3.2.4. *FT-IR spectra of CNPs*

FT-IR studies were performed to determine the potential biomolecules in charge of the reduction of the bioreduced Combination NPs (CNPs). The peaks at 3311 cm^{-1} (CNP-Psc), 3684 cm^{-1} (CNP-Ab) and 3286 cm^{-1} (CNP-Le) are due to the stretching vibrations of O-H group. The ones at 2955 cm^{-1}, 2864-2960 cm^{-1} and 2944 cm^{-1} are due to the C-H bond stretching. The peaks at 1499-1641 cm^{-1}, 1480-1648 cm^{-1} and 1517-1637 cm^{-1} correspond to the C=C stretching while, the peaks at 1365 cm^{-1}, 1363 cm^{-1} and 1401 cm^{-1} correspond to the C-O stretching in CNP-Psc, CNP-Ab and CNP-Le respectively. The C-N stretching of amines is at 1027-1119 cm^{-1}. Vibrational peaks at 592 cm^{-1} to 674 cm^{-1} confirm the presence of Zn-O stretching (Ahmad *et al.*, 2020) whereas, the peaks at 936-1029 cm–1 in CNP-Psc, 928-1037 cm^{-1} in CNP-Ab and 938-1027 cm^{-1} coordinated with the Mg–OH stretching (Karthik *et al.*, 2019). Distinct peaks at 835 cm^{-1} (CNP-Psc), 821 cm^{-1} (CNP-Ab) and 849 cm^{-1} (CNP-Le) indicate the Mn-O bond stretching (Kamran *et al.*, 2019). Figure 6.8.4 shows peaks obtained by FT-IR analysis of CNPs.

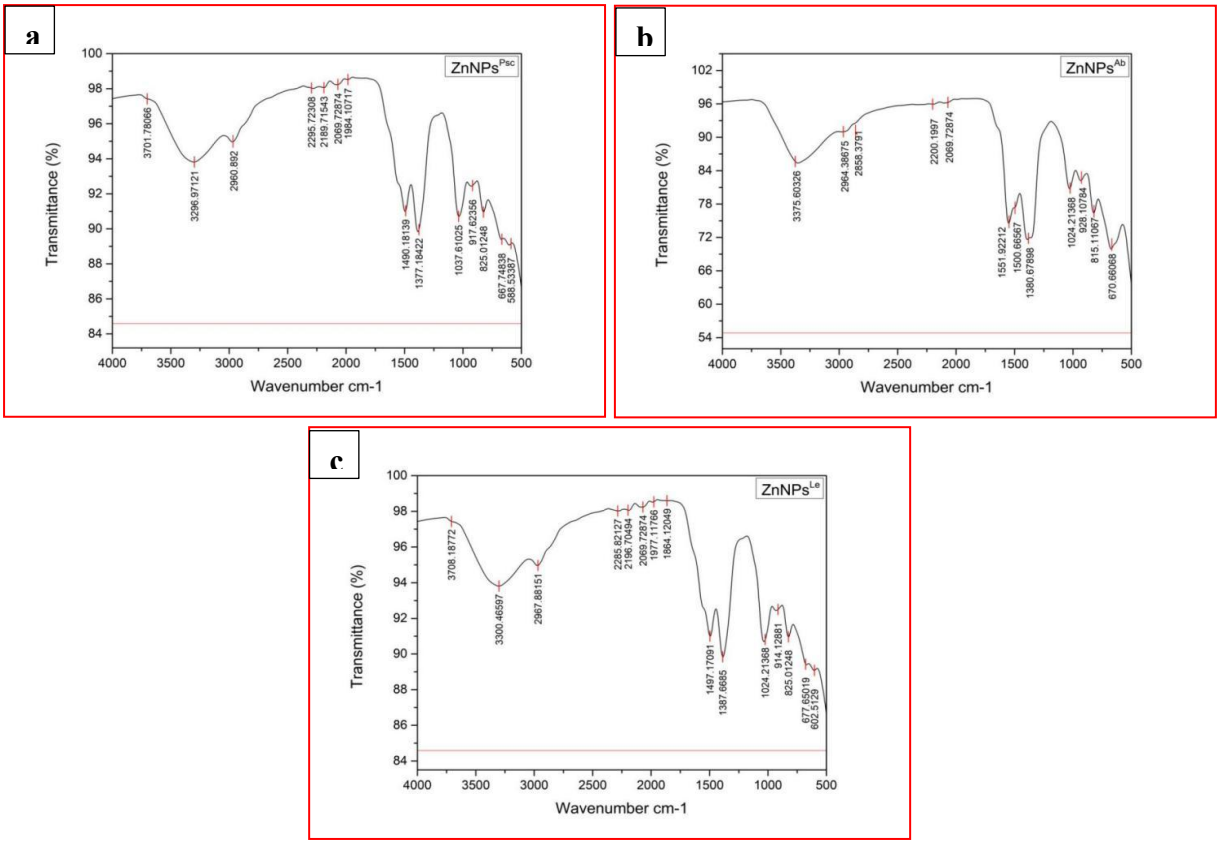

Figure 6.8.1: FT-IR spectra of ZnONPs synthesized using a) *P. sajor caju*; b) *A. bisporus*; and c) *L. edodes*

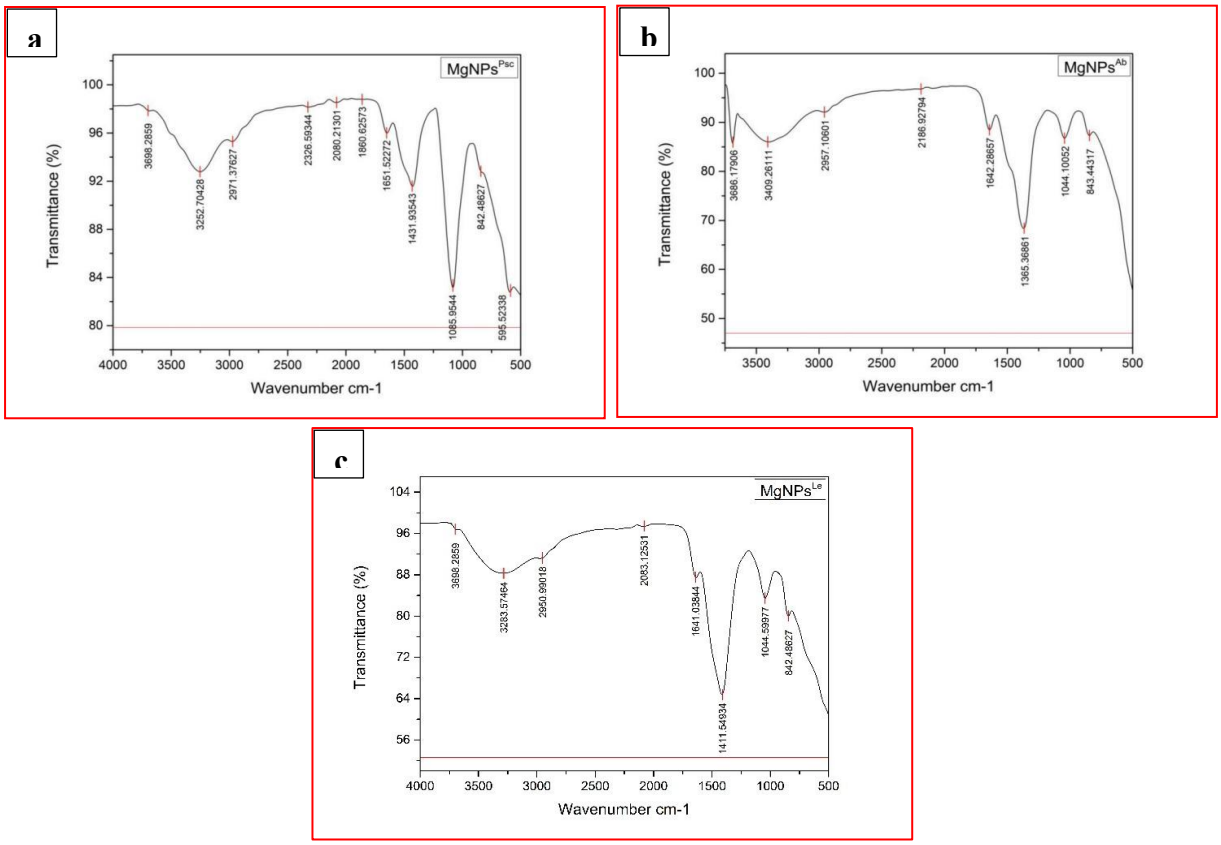

Figure 6.8.2: FT-IR spectra of MgONPs synthesized using a) *P. sajor caju*; b) *A. bisporus*; and c) *L. edodes*

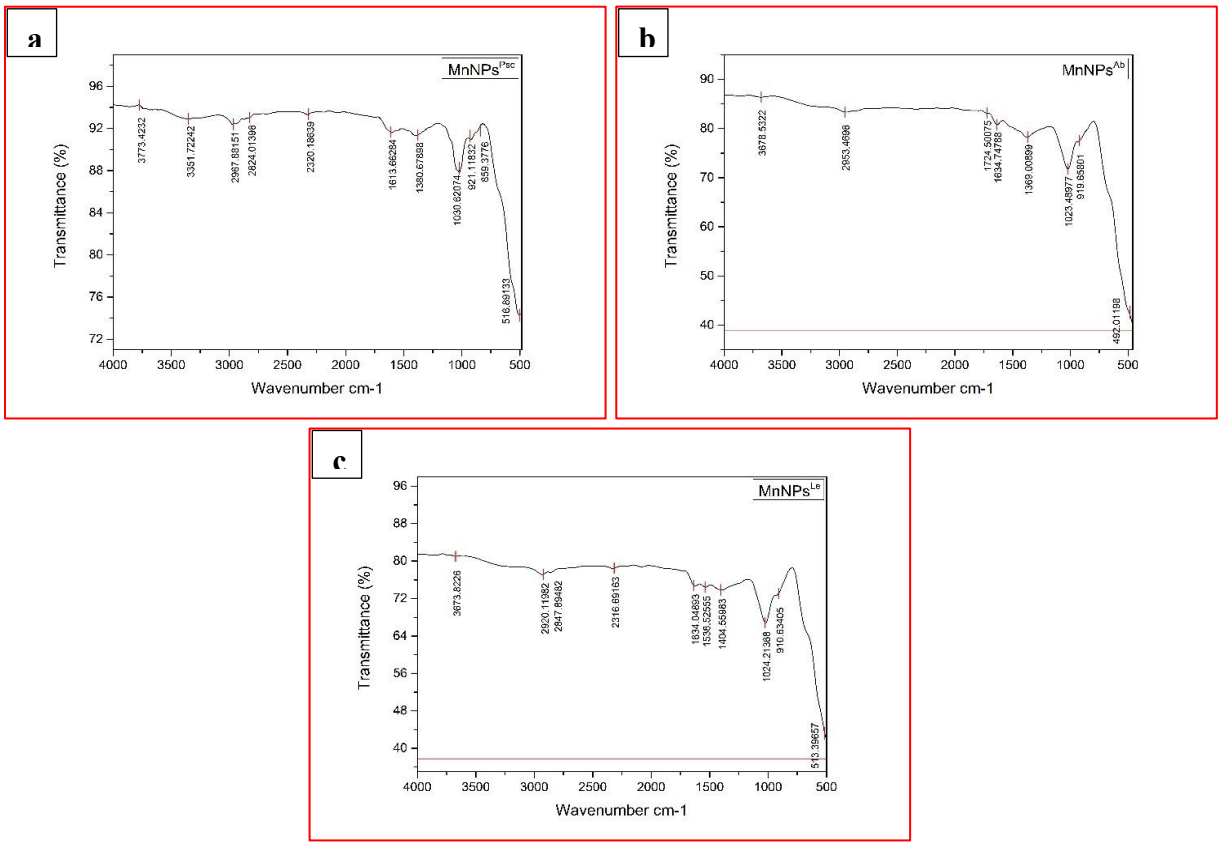

Figure 6.8.3: FT-IR spectra of MnO_2NPs synthesized using a) *P. sajor caju*; b) *A. bisporus*; and c) *L. edodes*

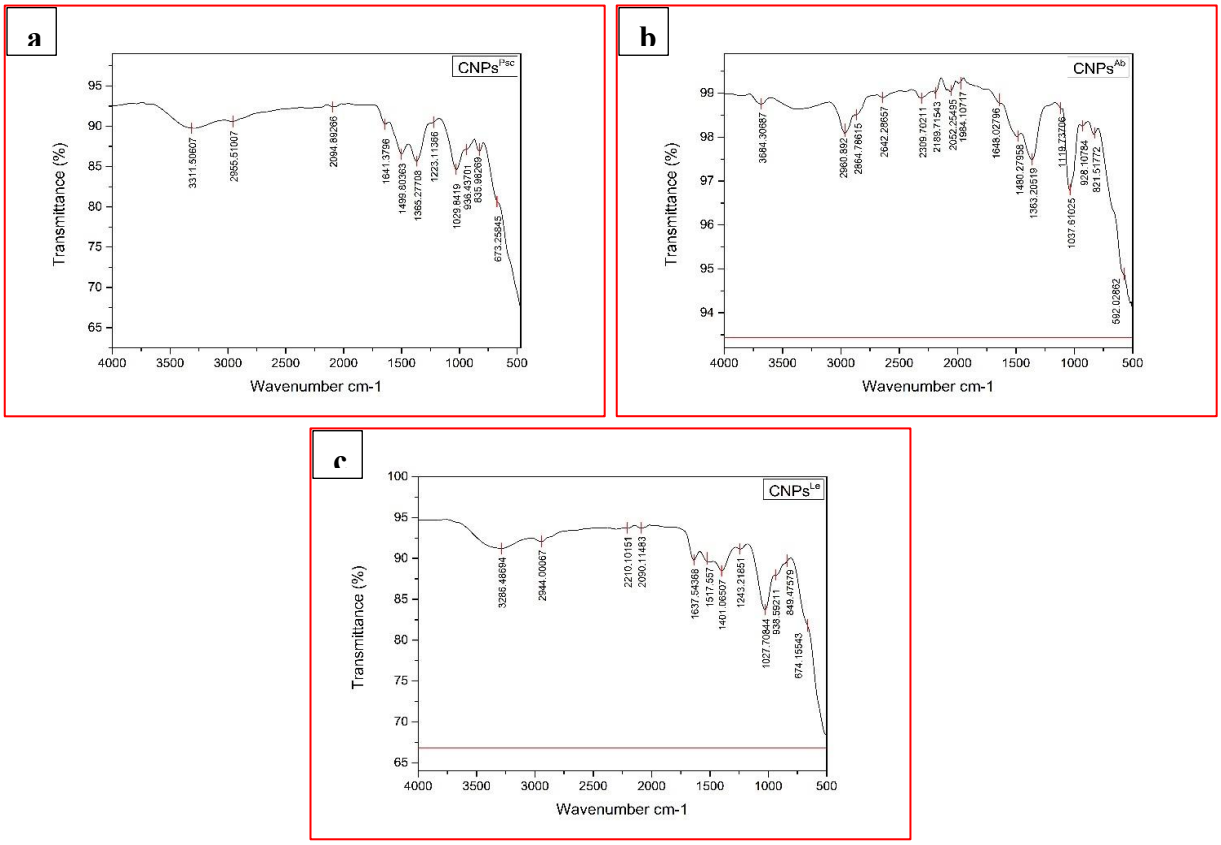

Figure 6.8.4: FT-IR spectra of CNPs synthesized using a) *P. sajor caju*; b) *A. bisporus*; and c) *L. edodes*

6.3.3. X-Ray Diffraction (XRD)

XRD analysis was carried out to validate the crystalline nature of myco-synthesized nanoparticles and complement the findings of the UV-visible spectrum. XRD examination was performed to examine the crystalline nature of the ZnONPs, MgONPs, MnO_2NPs and CNPs synthesized using all three fungal extracts. The results of UV-vis spectral analysis were verified using XRD examination. These reflections readily indicate the monophase cubic crystals of the NPs. All the spectra show well-defined peaks typical of ZnO, MgO and MnO_2 in the crystal structures. The sharp peaks indicate crystalline nature of the synthesized solids.

6.3.3.1. *XRD patterns of ZnONPs*

The considerable band broadening of the XRD peaks indicated that ZnONPs were present in the samples. Figure 6.9.1 shows the crystalline size and lattice strain of

ZnONPs while, Figure 6.9.2 shows the XRD diffractograms of synthesized ZnONPs. Narrow and strong peaks indicate that the produced nanoparticles are crystalline and extremely pure. In ZnONP-Psc, the peaks were comparatively leser in number with 2θ of 13.62°, 28.37°, 33.12°, 36.08°, 47.51°, 59.44° and 69.74°. In ZnONP-Ab, peaks were at 2θ of 13.20°, 21.58°, 25.30°, 28.02°, 31.13°, 31.66°, 33.25°, 34.34°, 36.16°, 41.61°, 47.44°, 48.29°, 56.61°, 59.53°, 62.91°, 66.32°, 67.88°, 69.06°, 72.57° and 76.92°. Similarly, ZnONP-Le showed the peaks at 2θ of 13.80°, 21.72°, 25.10°, 28.21°, 31.47°, 33.01°, 34.30°, 36.10°, 40.16°, 47.56°, 55.22°, 56.47°, 59.39°, 62.76°, 67.86°, 69.21°. The findings were verified by comparing them to standard International Centre for Diffraction Data (ICDD) card no. 01-083-6338 for ZnONP-Psc and ZnONP-Le, and card no. 01-080-3004 for ZnONP-Ab (Bodke *et al.*, 2018). The data obtained from the XRD analysis of ZnONPs is shown in Tables 6.2.1, 6.2.2 and 6.2.3 for *P. sajor caju, A. bisporus* and *L. edodes* respectively.

Table 6.2.1: XRD data for the prediction of miller indices of ZnONPs synthesized using *P. sajor caju*

S. No.	2-theta (deg)	d(ang.)	Height(cps)	FWHM (deg)	Int. I (cps deg)	Int. W (deg)	Asym. factor
1	13.62(11)	6.50(5)	1068(67)	5.3(3)	6269(364)	5.9(7)	3.4(13)
2	28.37(3)	3.144(4)	681(54)	0.47(9)	342(96)	0.50(18)	1.9(19)
3	33.125(5)	2.7022(4)	8355(188)	1.06(2)	17002(185)	2.03(7)	0.50(4)
4	36.08(2)	2.4871(15)	1550(81)	1.23(7)	3653(190)	2.4(2)	0.50(4)
5	47.51(19)	1.912(7)	426(43)	3.3(3)	2510(146)	5.9(9)	0.50(15)
6	59.44(3)	1.5537(7)	2777(109)	1.55(3)	5016(92)	1.81(10)	1.29(10)
7	69.74(12)	1.347(2)	603(51)	2.48(13)	2084(88)	3.5(4)	1.8(4)

Table 6.2.2: XRD data for the prediction of miller indices of ZnONPs synthesized using *A. bisporus*

S. No.	2-theta (deg)	d(ang.)	Height(cps)	FWHM (deg)	Int. I (cps deg)	Int. W (deg)	Asym. factor
1	13.2(2)	6.69(10)	1230(72)	2.11(18)	3101(308)	2.5(4)	0.8(3)
2	21.580(15)	4.115(3)	1611(83)	0.85(5)	2109(84)	1.31(12)	1.1(3)
3	25.3(6)	3.52(8)	262(33)	2.3(6)	728(209)	2.8(12)	0.7(7)

4	28.02(4)	3.182(5)	2026(93)	0.94(4)	2138(111)	1.06(10)	1.1(2)
5	31.13(9)	2.871(8)	1906(90)	1.40(17)	3475(566)	1.8(4)	0.84(4)
6	31.658(5)	2.8240(5)	10554(212)	0.422(15)	5812(369)	0.55(5)	0.84(4)
7	33.249(10)	2.6924(8)	16429(264)	0.970(12)	20772(248)	1.26(4)	0.84(4)
8	34.344(3)	2.6090(2)	16918(268)	0.280(7)	6175(116)	0.365(13)	0.84(4)
9	36.160(9)	2.4821(6)	21271(301)	0.524(11)	16343(185)	0.77(2)	0.85(7)
10	41.61(10)	2.169(5)	889(61)	1.75(9)	1658(127)	1.9(3)	0.63(16)
11	47.44(2)	1.9150(8)	3462(121)	0.90(5)	4934(345)	1.43(15)	1.10(14)
12	48.29(10)	1.883(3)	644(52)	0.89(18)	913(341)	1.4(6)	1.10(14)
13	56.608(5)	1.62460 (14)	6523 (166)	0.591(9)	4509(50)	0.69(3)	1.89(7)
14	59.533(14)	1.5516(3)	6730(169)	1.731(14)	13631(100)	2.03(7)	1.89(7)
15	62.908(7)	1.47619(14)	4670(141)	0.677(11)	3699(47)	0.79(3)	1.89(7)
16	66.32(3)	1.4082(6)	703(55)	0.75(11)	901(114)	1.3(3)	0.65(5)
17	67.882(15)	1.3796(3)	4620(140)	0.82(2)	6512(236)	1.41(9)	0.65(5)
18	69.06(2)	1.3590(4)	1723(86)	0.77(6)	2266(234)	1.3(2)	0.65(5)
19	72.57(3)	1.3016(5)	337(38)	0.38(11)	137(36)	0.41(15)	1.3(18)
20	76.92(15)	1.238(2)	312(36)	0.75(13)	287(42)	0.9(2)	1.4(11)

Table 6.2.3: XRD data for the prediction of miller indices of ZnONPs synthesized using *L. edodes*

S. No.	**2-theta (deg)**	**d(ang.)**	**Height(cps)**	**FWHM (deg)**	**Int. I (cps deg)**	**Int. W (deg)**	**Asym. factor**
1	13.8(3)	6.42(11)	484(45)	2.3(4)	1735(257)	3.6(9)	1.1(4)
2	21.72(6)	4.088(11)	1090(68)	1.13(7)	1663(78)	1.53(17)	0.9(2)
3	25.1(2)	3.54(3)	758(57)	4.6(2)	3750(263)	4.9(7)	1.1(3)
4	28.213(14)	3.1606(15)	2351(100)	0.77(3)	2495(72)	1.06(8)	1.17(7)
5	31.47(3)	2.840(2)	2652(106)	1.73(7)	6340(278)	2.4(2)	1.17(7)
6	33.006(8)	2.7117(6)	10668(213)	0.681(16)	10041(465)	0.94(6)	1.17(7)
7	34.30(3)	2.612(2)	4371(136)	1.93(11)	11638(691)	2.7(2)	1.17(7)

8	36.104(11)	2.4858(8)	5490(153)	0.84(2)	6376(198)	1.16(7)	1.17(7)
9	40.16(15)	2.244(8)	404(41)	3.5(2)	1997(106)	4.9(8)	2.0(4)
10	47.56(3)	1.9102(11)	1099(68)	1.33(5)	2010(72)	1.83(18)	2.4(2)
11	55.22(18)	1.662(5)	489(46)	3.64(18)	1899(139)	3.9(6)	3.6(10)
12	56.469(10)	1.6282(3)	1449(78)	0.57(3)	1053(39)	0.73(7)	1.53(7)
13	59.391(17)	1.5549(4)	4843(143)	1.669(16)	10359(92)	2.14(8)	1.53(7)
14	62.764(15)	1.4792(3)	962(64)	0.71(4)	872(34)	0.91(10)	1.53(7)
15	67.86(8)	1.3801(14)	618(51)	0.53(6)	366(42)	0.59(12)	2.2(15)
16	69.21(5)	1.3564(8)	1069(67)	2.19(4)	2490(68)	2.3(2)	1.14(10)

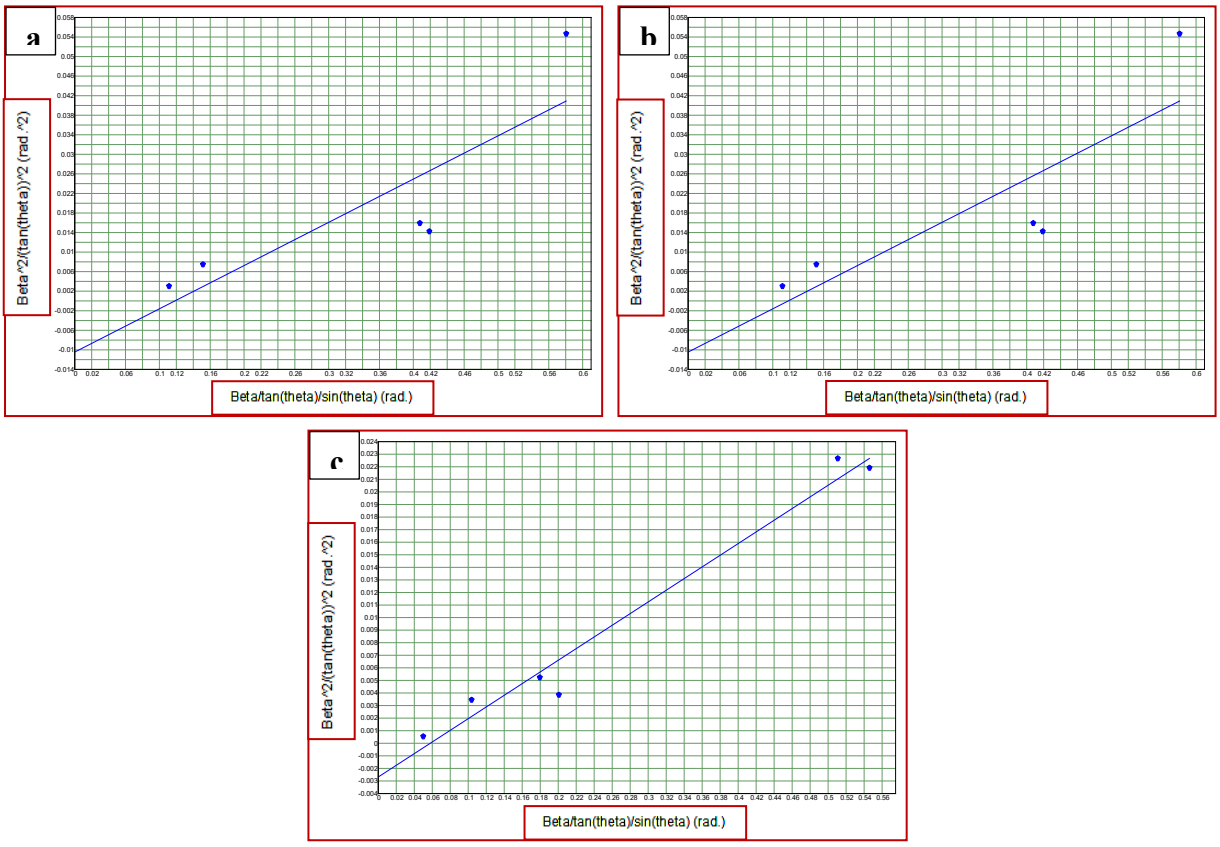

Figure 6.9.1: Crystalline size and lattice strain of a) ZnONP-Psc; b) ZnONP-Ab; and c) ZnONP-Le

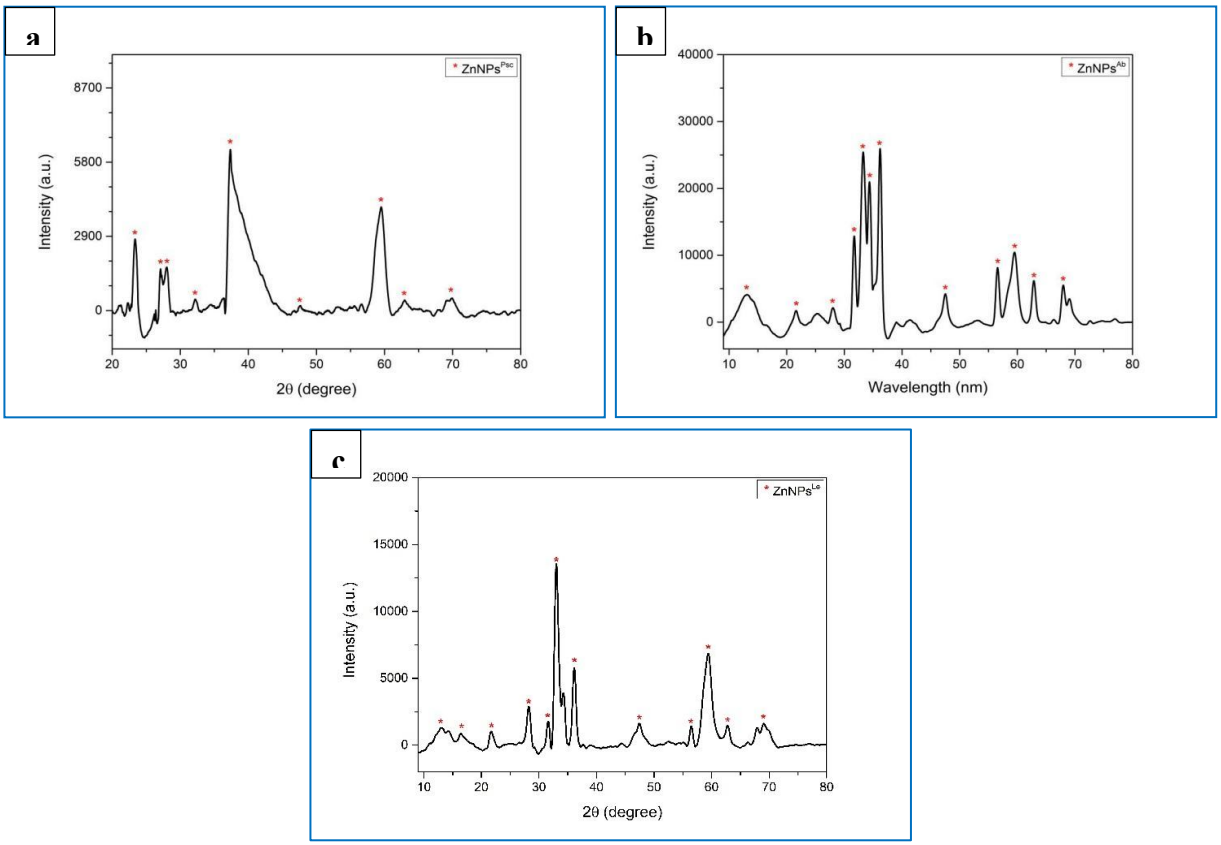

Figure 6.9.2: XRD Diffractograms for a) ZnONP-Psc; b) ZnONP-Ab; and c) ZnONP-Le

6.3.3.2. *XRD patterns of MgONPs*

XRD analysis was utilized to examine the crystalline state of myco-synthesized MgONPs. Data presented various sharp peaks in all three types of MgONPs (Table 6.3.1-6.3.3). In MgONP-Psc, the peaks were at 2θ of 7.29°, 18.12°, 18.38°, 19.48°, 20.11°, 21.08°, 22.12°, 22.39°, 24.69°, 26.05°, 26.63°, 27.12°, 29.82°, 30.32°, 30.71°, 31.78°, 32.19°, 32.79°, 33.59°, 33.89°, 34.46°, 35.45°, 36.88°, 37.33°, 38.41°, 40.53°, 41.30°, 43.45°, 45.32°, 46.99°, 48.72°, 50.07° and 54.53°. In MgONP-Ab, the peaks came out at 2θ of 19.04°, 26.21°, 27.18°, 29.42°, 33.11°, 36.14°, 38.03°, 41.16°, 42.90°, 45.85°, 48.31°, 50.52°, 58.74°, 61.94°, 68.56°, 72.15°, 75.25°, 76.81° and 77.00°. Similarly, MgONP-Le showed the peaks with 2θ of 18.54°, 26.59°, 29.37°, 31.83°, 33.42°, 34.39°, 35.36°, 36.22°, 37.97°, 38.95°, 42.51°, 47.92°, 48.35°, 50.75°, 56.45°, 58.82°, 62.21° and 68.05. This data verified that the MgONP-Psc were crystallographic structures conferring to the ICDD standard (ICDD no. 01-077-9812 for MgONP-Psc, ICDD no. 01-071-5972 for MgONP-Ab and ICDD no. 01-084-2163 for MgONP-Le)

(Safaei *et al.*, 2015). The occurrence of oxide in the sample, identified as MgO by XPS analysis, is indicated by the detected XRD peaks. It was reported that the diffraction peaks observed at 2θ of 42.6°, 62.2°, and 78.6° signified cubic MgONPs (Lekota *et al.*, 2019). The crystalline size and lattice strain of MgONPs are shown in Figure 6.10.1 while the diffractograms showing the absorption peaks of MgONPs are depicted in Figure 6.10.2.

Table 6.3.1: XRD data for the prediction of miller indices of MgONPs synthesized using *P. sajor caju*

S. No.	2-theta (deg)	d(ang.)	Height(cps)	FWHM (deg)	Int. I (cps deg)	Int. W (deg)	Asym. factor
1	7.287(4)	12.122(7)	7666(180)	0.106(6)	1268(44)	0.165(10)	0.99(18)
2	18.120(18)	4.892(5)	969(64)	0.15(4)	177(30)	0.18(4)	1.6(9)
3	18.383(18)	4.822(5)	2432(102)	0.144(16)	412(28)	0.169(19)	1.6(9)
4	19.482(4)	4.5528(10)	12812(233)	0.127(4)	2368(28)	0.185(6)	1.7(3)
5	20.110(3)	4.4120(7)	5735(156)	0.145(6)	1234(28)	0.215(11)	3.1(5)
6	21.079(11)	4.211(2)	4391(137)	0.233(10)	1268(45)	0.289(19)	0.60(15)
7	22.121(5)	4.0153(9)	14838(251)	0.138(5)	3050(82)	0.206(9)	1.8(3)
8	22.392(6)	3.9672(10)	4331(136)	0.127(17)	820(72)	0.19(2)	1.8(3)
9	24.69(2)	3.603(3)	2109(95)	0.188(16)	423(42)	0.20(3)	1.4(6)
10	26.050(7)	3.4178(9)	1551(81)	0.28(2)	458(45)	0.30(4)	5(3)
11	26.63(4)	3.344(5)	929(63)	0.13(5)	157(27)	0.17(4)	0.9(13)
12	27.118(11)	3.2856(13)	1275(74)	0.11(4)	154(39)	0.12(4)	2(2)
13	29.821(18)	2.9937(18)	2302(99)	0.147(16)	407(29)	0.18(2)	1.2(6)
14	30.325(8)	2.9451(7)	1128(69)	0.12(2)	145(26)	0.13(3)	0.6(5)
15	30.710(14)	2.9090(13)	1020(66)	0.05(4)	92(19)	0.09(2)	0.6(9)
16	31.78(2)	2.814(2)	2004(92)	0.46(2)	988(57)	0.49(5)	1.4(3)
17	32.186(9)	2.7789(8)	1016(66)	0.10(3)	108(22)	0.11(3)	1.4(3)
18	32.789(4)	2.7291(4)	3018(113)	0.257(19)	1394(37)	0.46(3)	0.63(16)
19	33.593(7)	2.6656(6)	2789(109)	0.134(19)	538(36)	0.19(2)	1.1(2)
20	33.895(6)	2.6426(4)	3670(125)	0.120(11)	637(36)	0.174(16)	1.1(2)
21	34.461(5)	2.6005(3)	4371(136)	0.111(7)	818(20)	0.187(10)	1.2(3)

22	35.45(6)	2.530(4)	398(41)	0.12(7)	50(24)	0.13(7)	0.9(18)
23	36.881(6)	2.4352(4)	1339(75)	0.103(16)	241(27)	0.18(3)	1.0(2)
24	37.332(11)	2.4068(7)	1716(85)	0.19(2)	555(32)	0.32(3)	1.0(2)
25	38.410(18)	2.3417(11)	1908(90)	0.24(3)	860(33)	0.45(4)	0.6(2)
26	40.526(15)	2.2242(8)	824(59)	0.091(15)	82(15)	0.10(3)	1.1(9)
27	41.297(10)	2.1844(5)	459(44)	0.10(3)	48(16)	0.10(4)	3(6)
28	43.452(16)	2.0809(7)	567(49)	0.26(4)	263(27)	0.46(9)	0.5(4)
29	45.32(4)	1.9996(19)	832(59)	0.22(3)	197(28)	0.24(5)	0.9(7)
30	46.99(2)	1.9323(9)	420(42)	0.22(6)	170(24)	0.40(10)	2(3)
31	48.72(4)	1.8676(16)	408(42)	0.11(4)	50(21)	0.12(6)	3(7)
32	50.07(5)	1.8204(17)	334(38)	0.13(5)	46(21)	0.14(8)	2(3)
33	54.534(9)	1.6814(3)	388(41)	0.07(3)	31(12)	0.08(4)	0.5(12)

Table 6.3.2: XRD data for the prediction of miller indices of MgONPs synthesized using *A. bisporus*

S. No.	**2-theta (deg)**	**d(ang.)**	**Height(cps)**	**FWHM (deg)**	**Int. I (cps deg)**	**Int. W (deg)**	**Asym. factor**
1	19.041(12)	4.657(3)	28209(346)	2.658(10)	83453(387)	2.96(5)	1.91(4)
2	26.209(7)	3.3975(9)	8708(192)	0.184(7)	2077(43)	0.238(10)	1.6(4)
3	27.182(12)	3.2780(15)	4528(139)	0.193(11)	1209(36)	0.267(16)	1.0(3)
4	29.425(8)	3.0330(9)	1157(70)	0.16(2)	253(26)	0.22(4)	2.7(16)
5	33.112(18)	2.7032(14)	3572(123)	0.455(19)	2171(58)	0.61(4)	2.6(7)
6	36.139(6)	2.4835(4)	2694(107)	0.337(17)	980(44)	0.36(3)	1.017(18)
7	38.033(7)	2.3641(4)	18849(283)	1.568(6)	31948(166)	1.69(3)	1.017(18)
8	41.16(10)	2.192(5)	501(46)	0.15(10)	79(46)	0.16(11)	1(2)
9	42.900(14)	2.1064(7)	2456(102)	0.186(18)	598(41)	0.24(3)	1.4(4)
10	45.852(6)	1.9774(2)	6848(171)	0.191(10)	2081(31)	0.304(12)	1.3(2)
11	48.308(7)	1.8825(3)	2833(110)	0.39(3)	1787(54)	0.63(4)	0.7(3)
12	50.523(18)	1.8050(6)	6612(168)	2.408(15)	16948(141)	2.56(9)	0.574(18)

13	58.738(13)	1.5706(3)	8559(191)	0.649(14)	8575(77)	1.00(3)	0.80(8)
14	61.94(2)	1.4970(5)	2505(103)	1.11(4)	4304(82)	1.72(10)	0.80(8)
15	68.56(5)	1.3677(9)	1559(81)	2.25(5)	3781(107)	2.4(2)	1.58(16)
16	72.15(4)	1.3082(7)	1008(65)	0.99(4)	1144(46)	1.13(12)	0.79(15)
17	75.25(14)	1.262(2)	275(34)	0.42(11)	124(30)	0.45(16)	0.8(10)
18	76.81(2)	1.2400(3)	438(43)	0.48(7)	234(32)	0.53(13)	0.5(4)
19	77.0(4)	1.237(5)	125(23)	2.1(4)	286(85)	2.3(11)	0.8(6)

Table 6.3.3: XRD data for the prediction of miller indices of MgONPs synthesized using *L. edodes*

S. No.	2-theta (deg)	d(ang.)	Height(cps)	FWHM (deg)	Int. I (cps deg)	Int. W (deg)	Asym. factor
1	18.539(12)	4.782(3)	2995(113)	0.409(16)	1379(60)	0.46(4)	1.6(2)
2	26.59(3)	3.349(3)	1098(68)	0.12(6)	239(35)	0.22(5)	2(3)
3	29.371(3)	3.0385(3)	18321(279)	0.124(3)	2665(49)	0.145(5)	2.1(2)
4	31.830(15)	2.8092(13)	2777(109)	0.390(18)	1167(46)	0.42(3)	2.2(4)
5	33.42(3)	2.679(2)	1701(85)	0.87(4)	1603(69)	0.94(9)	2.2(4)
6	34.386(18)	2.6060(13)	1661(84)	0.46(4)	830(56)	0.50(6)	2.2(4)
7	35.360(7)	2.5364(5)	2050(93)	0.094(16)	297(27)	0.14(2)	1.4(3)
8	36.22(2)	2.4783(14)	3191(116)	0.44(2)	2146(66)	0.67(5)	1.4(3)
9	37.970(18)	2.3678(11)	4429(137)	0.386(19)	2828(51)	0.64(3)	1.1(3)
10	38.949(5)	2.3105(3)	5599(154)	0.101(7)	829(31)	0.148(10)	1.9(6)
11	42.506(16)	2.1250(7)	1958(91)	0.11(2)	394(29)	0.20(2)	1.1(9)
12	47.918(8)	1.8969(3)	3216(117)	0.111(11)	541(40)	0.168(19)	1.4(5)
13	48.350(19)	1.8810(7)	1047(67)	0.18(5)	288(37)	0.27(5)	1.4(5)
14	50.752(12)	1.7974(4)	1197(71)	0.49(4)	856(44)	0.71(8)	0.8(4)
15	56.455(13)	1.6286(3)	1215(72)	0.38(5)	576(52)	0.47(7)	1.0(7)
16	58.818(12)	1.5687(3)	1629(83)	1.34(4)	2645(81)	1.62(13)	0.50(7)
17	62.21(3)	1.4910(7)	547(48)	1.44(11)	956(52)	1.7(2)	0.50(7)
18	68.05(3)	1.3767(6)	557(49)	1.39(11)	1001(68)	1.8(3)	0.50(19)

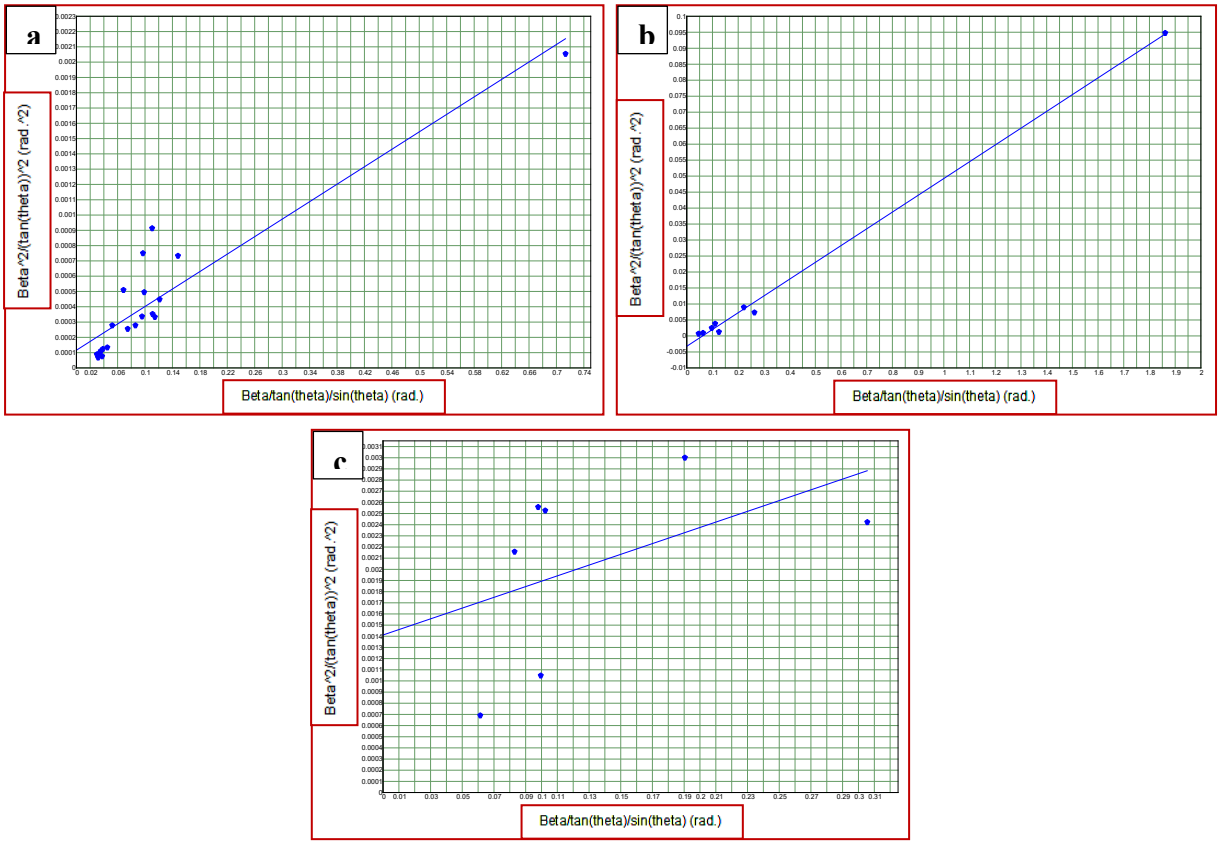

Figure 6.10.1: Crystalline size and lattice strain of a) MgONP-Psc; b) MgONP-Ab; and c) MgONP-Le

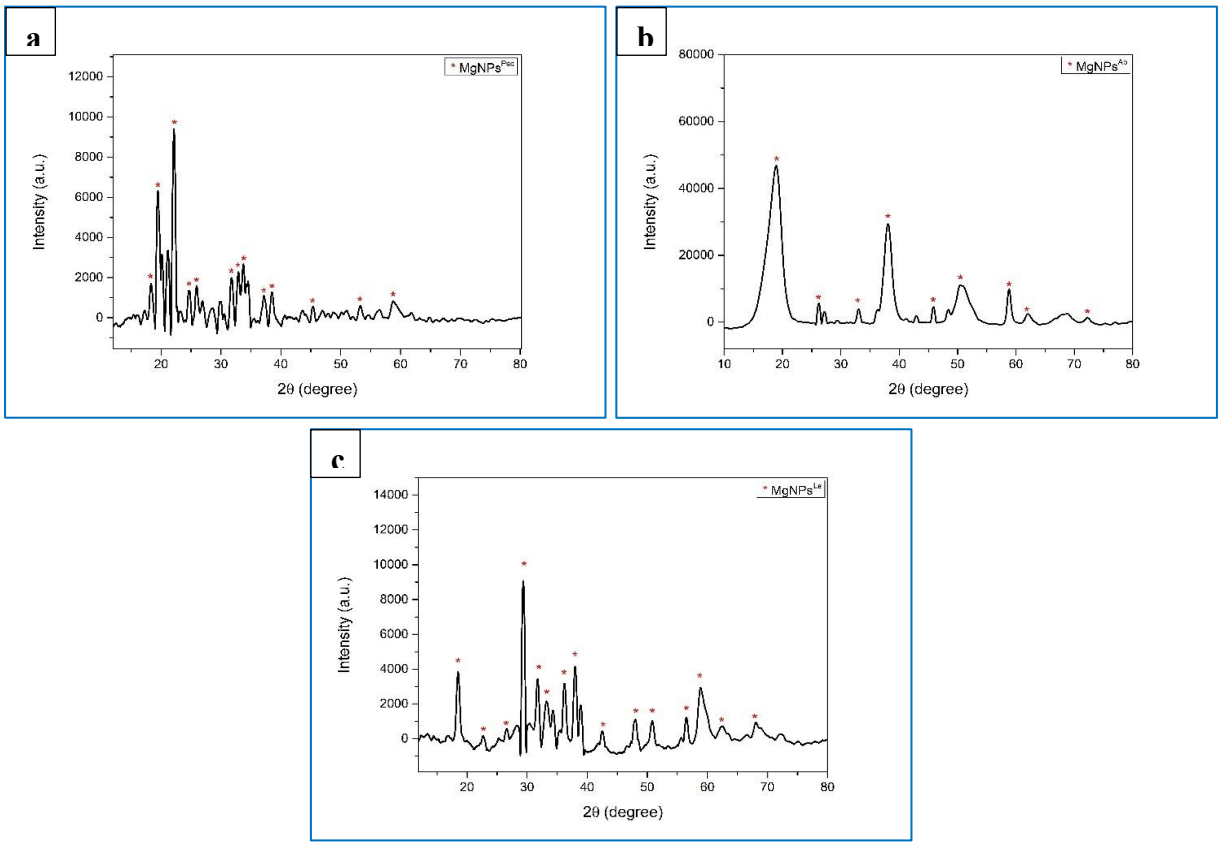

Figure 6.10.2: XRD Diffractograms for a) MgONP-Psc; b) MgONP-Ab; and c) MgONP-Le

6.3.3.3. *XRD patterns of MnO_2NPs*

The XRD patterns were employed to confirm the structure and phase purity of the synthesized samples. The crystallinity of the MnO_2NPs was assessed by the XRD pattern (Mahdavi *et al.*, 2020). As shown in Figure 6.11.2, the diffraction patterns of MnO_2NPs have good crystallinity with distinctive peaks of manganese. The XRD pattern of MnO_2NP-Psc showed peaks at 2θ with 18.33°, 26.67°, 28.58°, 37.33°, 42.68°, 55.33°, 56.60°, 60.02°, 65.49° and 72.30°. The XRD pattern showing distinct peaks at 2θ = 23.01°, 28.54°, 37.36°, 42.62°, 49.90°, 56.59°, 60.00°, 65.01°, 68.40° and 72.42° correspond to MnO_2NP-Ab, while the peaks at 2θ = 26.60°, 28.55°, 37.37°, 42.71°, 50.02°, 56.52°, 65.12°, 68.90° and 72.36° correspond to MnO_2NP-Le (Table 6.4.1-6.4.3). The data obtained matched with ICDD PDF card no. 00-044-0141 (MnO_2NP-Psc and MnO_2NP-Ab) and ICDD PDF card no. 01-081-2261 (MnO_2NP-Le), and the chief crystalline phase is that of manganese (Yulizar *et al.*, 2020a, 2020b). The crystalline size and lattice structure of MnO_2NPs is shown in Figure 6.11.1.

Table 6.4.1: XRD data for the prediction of miller indices of MnO_2NPs synthesized using *P. sajor caju*

S. No.	2-theta (deg)	d(ang.)	Height(cps)	FWHM (deg)	Int. I (cps deg)	Int. W (deg)	Asym. factor
1	18.33(15)	4.84(4)	596(50)	4.7(6)	4920(440)	8.2(14)	0.5(3)
2	26.667(4)	3.3401(5)	1465(79)	0.082(14)	143(21)	0.098(19)	4(6)
3	28.583(14)	3.1204(15)	4111(132)	0.294(13)	1665(47)	0.40(2)	1.3(3)
4	37.327(17)	2.4071(11)	3767(127)	0.48(2)	3276(57)	0.87(4)	0.95(19)
5	42.68(2)	2.1166(11)	728(56)	0.98(7)	782(79)	1.08(19)	3.2(14)
6	55.33(10)	1.659(3)	349(38)	1.18(17)	533(141)	1.5(6)	2.6(6)
7	56.60(3)	1.6249(9)	1957(91)	1.04(5)	2638(149)	1.35(14)	2.6(6)
8	60.02(7)	1.5401(17)	434(43)	1.79(15)	1005(71)	2.3(4)	2.6(6)
9	65.49(7)	1.4242(13)	402(41)	2.6(2)	1875(104)	4.7(7)	0.50(17)
10	72.30(14)	1.306(2)	429(43)	0.95(17)	579(64)	1.4(3)	1.0(7)

Table 6.4.2: XRD data for the prediction of miller indices of MnO_2NPs synthesized using *A. bisporus*

S. No.	2-theta (deg)	d(ang.)	Height(cps)	FWHM (deg)	Int. I (cps deg)	Int. W (deg)	Asym. factor
1	23.01(11)	3.862(17)	853(60)	3.9(3)	4264(366)	5.0(8)	2.6(13)
2	28.544(14)	3.1246(15)	3454(121)	0.337(13)	1695(38)	0.49(3)	0.80(16)
3	37.360(18)	2.4051(11)	3243(117)	0.62(2)	3163(55)	0.98(5)	1.5(2)
4	42.62(6)	2.120(3)	832(59)	1.05(5)	944(65)	1.13(16)	2.3(6)
5	49.9(2)	1.825(7)	252(33)	1.62(18)	433(71)	1.7(5)	1.5(9)
6	56.59(3)	1.6252(7)	2092(94)	1.31(4)	4491(64)	2.15(13)	2.8(3)
7	60.00(5)	1.5405(12)	553(48)	2.20(10)	1559(62)	2.8(4)	2.7(4)
8	65.01(17)	1.433(3)	276(34)	0.48(13)	142(43)	0.5(2)	0.5(8)
9	68.4(3)	1.371(5)	481(45)	8.7(2)	4826(176)	10.0(13)	1.9(3)
10	72.42(6)	1.3039(9)	473(45)	1.07(11)	831(51)	1.8(3)	1.3(4)

Table 6.4.3: XRD data for the prediction of miller indices of MnO_2NPs synthesized using *L. edodes*

S. No.	2-theta (deg)	d(ang.)	Height(cps)	FWHM (deg)	Int. I (cps deg)	Int. W (deg)	Asym. factor
1	26.598(7)	3.3486(8)	1246(73)	0.091(19)	180(20)	0.14(2)	0.7(6)
2	28.548(15)	3.1242(16)	3478(122)	0.351(15)	1923(39)	0.55(3)	1.0(2)
3	37.371(11)	2.4044(7)	3112(115)	0.643(17)	2839(63)	0.91(5)	2.02(15)
4	42.711(15)	2.1153(7)	972(64)	1.11(5)	1163(76)	1.20(16)	4.5(15)
5	50.02(12)	1.822(4)	348(38)	0.94(11)	355(58)	1.0(3)	2.1(13)
6	56.52(2)	1.6270(6)	1805(88)	1.33(4)	3209(86)	1.78(13)	2.32(18)
7	65.12(6)	1.4312(12)	231(31)	0.5(2)	126(52)	0.5(3)	1(2)
8	68.9(3)	1.362(5)	200(29)	12.8(9)	2839(274)	14(3)	3.6(14)
9	72.36(3)	1.3048(4)	684(54)	0.44(6)	640(35)	0.94(13)	1.0(3)

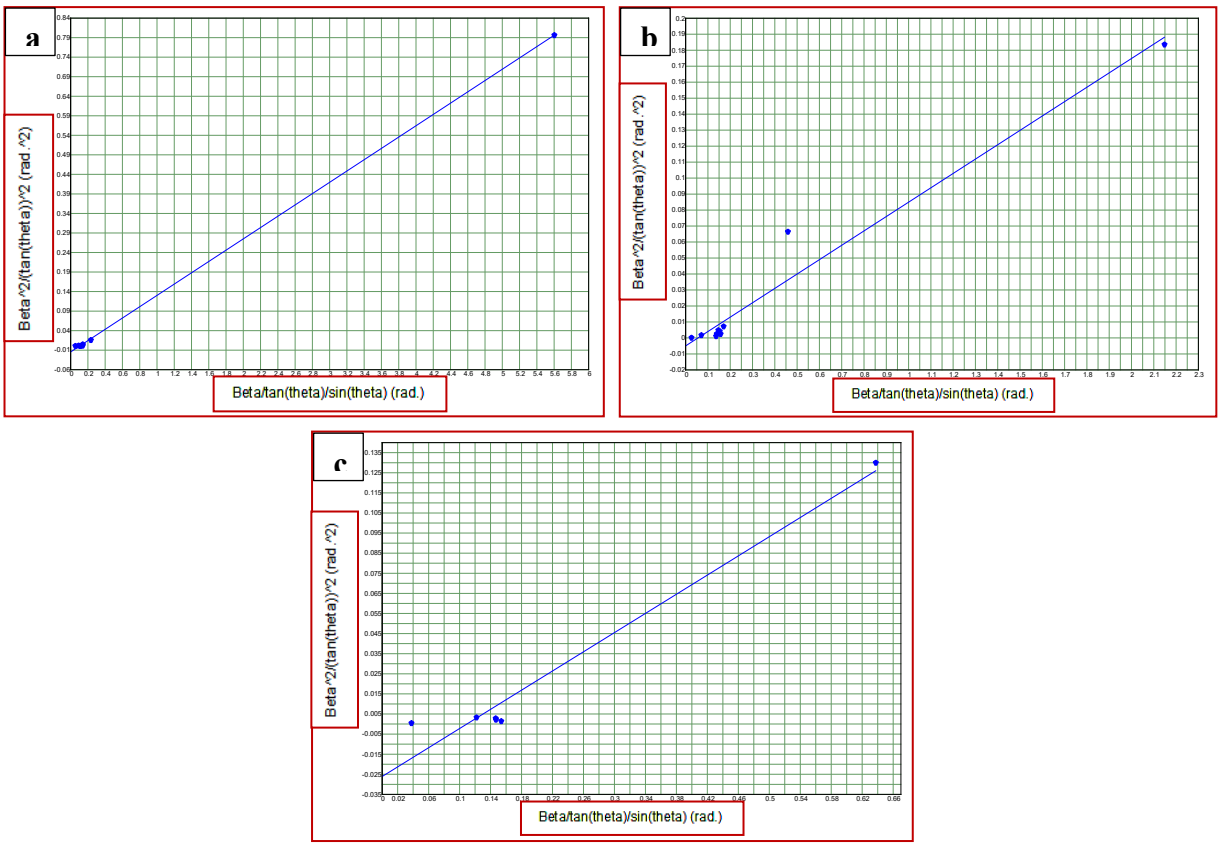

Figure 6.11.1: Crystalline size and lattice strain of a) MnO_2NP-Psc; b) MnO_2NP-Ab; and c) MnO_2NP-Le

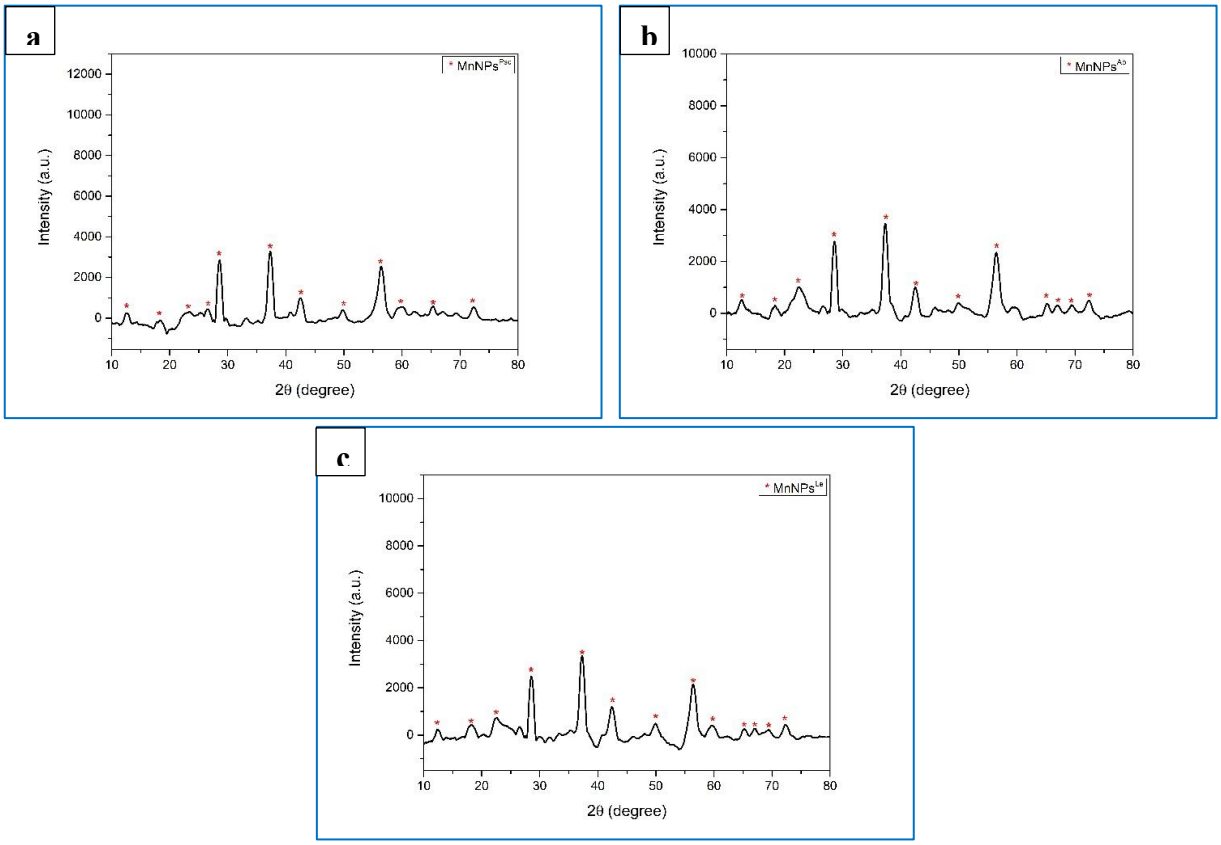

Figure 6.11.2: XRD Diffractograms for a) MnO_2NP-Psc; b) MnO_2NP-Ab; and c) MnO_2NP-Le

6.3.3.4. *XRD patterns of CNPs*

An XRD system was used to examine the crystallinity and phase orientation of the nanoparticles containing Zn, Mg and Mn in combination. In CNP-Psc, the absorption peaks were at 2θ of 12.71°, 18.13°, 22.10°, 28.61°, 33.23°, 37.51°, 42.51°, 49.88°, 56.64°, 60.04°, 65.14° and 72.49°. In CNP-Ab, the peaks were obtained at 2θ of 22.01°, 28.70°, 33.48°, 37.40°, 42.68°, 56.52°, 59.76°, 69.49° and 72.51°, while in CNP-Le, peaks at 2θ = 18.23°, 22.36°, 26.68°, 28.63°, 33.56°, 37.35°, 42.67°, 56.63°, 59.90° and 72.38°. The strength of peaks reflects the significant degree of crystallinity of the nanoparticles (Figure 6.12.2). The small crystallite size that was achieved, however, is consistent with the ICDD file no. 03-065-2880, 01-075-9568 and 00-044-0141 for CNP-Psc, ICDD file no. 01-077-8755, 00-004-0829 and 00-044-0141 for CNP-Ab, and ICDD file no. 01-083-5382, 01-077-2906 and 01-081-2261 for CNP-Le respectively, according to the broad diffraction peaks. The data obtained from XRD analysis of CNPs is shown in Tables 6.5.1, 6.5.2 and 6.5.3 while the crystalline size and lattice strain is shown in Figure 6.12.1.

Table 6.5.1: XRD data for the prediction of miller indices of CNPs synthesized using *P. sajor caju*

S. No.	2-theta (deg)	d(ang.)	Height(cps)	FWHM (deg)	Int. I (cps deg)	Int. W (deg)	Asym. factor
1	12.71(12)	6.96(7)	393(41)	0.69(11)	288(67)	0.7(2)	0.7(5)
2	18.13(14)	4.89(4)	501(46)	1.67(18)	1155(97)	2.3(4)	0.6(2)
3	22.1(3)	4.02(5)	288(35)	2.4(2)	739(110)	2.6(7)	1.0(5)
4	28.611(13)	3.1174(14)	3471(121)	0.326(15)	1678(41)	0.48(3)	0.67(14)
5	33.23(5)	2.694(4)	1185(71)	1.24(6)	2020(75)	1.71(17)	0.51(10)
6	37.512(7)	2.3957(4)	2133(95)	0.60(2)	1634(53)	0.77(6)	3.3(11)
7	42.51(5)	2.125(3)	924(63)	1.44(5)	1419(70)	1.54(18)	1.6(3)
8	49.88(4)	1.8269(15)	272(34)	0.91(13)	309(45)	1.1(3)	0.9(6)
9	56.64(4)	1.6237(9)	1104(68)	1.37(5)	1843(51)	1.67(15)	3.6(8)
10	60.04(5)	1.5397(11)	960(64)	1.79(6)	2096(64)	2.2(2)	3.6(8)
11	65.14(7)	1.4310(14)	225(31)	1.1(3)	420(56)	1.9(5)	0.5(5)
12	72.49(5)	1.3029(8)	220(31)	0.59(15)	137(42)	0.6(3)	2(3)

Table 6.5.2: XRD data for the prediction of miller indices of CNPs synthesized using *A. bisporus*

S. No.	2-theta (deg)	d(ang.)	Height(cps)	FWHM (deg)	Int. I (cps deg)	Int. W (deg)	Asym. factor
1	22.01(7)	4.036(13)	484(45)	2.7(3)	2311(124)	4.8(7)	0.50(16)
2	28.698(9)	3.1082(9)	3096(115)	0.309(18)	1603(40)	0.52(3)	2.1(3)
3	33.476(13)	2.6747(10)	1876(89)	1.32(5)	4442(84)	2.37(16)	0.51(7)
4	37.399(16)	2.4026(10)	2532(104)	0.46(3)	2291(47)	0.90(6)	0.76(14)
5	42.68(2)	2.1170(10)	717(55)	0.64(7)	753(50)	1.05(15)	1.3(5)
6	56.52(2)	1.6270(6)	1352(76)	1.07(5)	2150(67)	1.59(14)	1.53(16)
7	59.76(4)	1.5463(9)	1485(79)	1.86(5)	4109(88)	2.8(2)	1.53(16)
8	69.49(8)	1.3515(14)	393(41)	2.2(2)	1828(152)	4.7(9)	1.2(3)
9	72.51(4)	1.3026(7)	402(41)	0.68(13)	580(102)	1.4(4)	1.2(3)

Table 6.5.3: XRD data for the prediction of miller indices of CNPs synthesized using *L. edodes*

S. No.	2-theta (deg)	d(ang.)	Height(cps)	FWHM (deg)	Int. I (cps deg)	Int. W (deg)	Asym. factor
1	18.23(6)	4.861(16)	430(43)	1.6(2)	1112(96)	2.6(5)	0.5(3)
2	22.36(17)	3.97(3)	694(54)	3.64(17)	3101(152)	4.5(6)	0.66(17)
3	26.682(9)	3.3382(12)	1257(73)	0.095(17)	160(17)	0.13(2)	2.4(14)
4	28.627(13)	3.1158(14)	3660(125)	0.332(13)	1812(37)	0.50(3)	1.3(2)
5	33.56(18)	2.668(14)	282(35)	1.4(3)	632(87)	2.2(6)	0.8(5)
6	37.354(5)	2.4055(3)	3544(123)	0.50(2)	3492(56)	0.99(5)	0.80(12)
7	42.67(6)	2.117(3)	800(58)	1.03(7)	987(70)	1.23(18)	2.7(9)
8	56.625(11)	1.6241(3)	1723(86)	1.27(3)	2898(61)	1.68(12)	3.0(6)
9	59.90(3)	1.5429(7)	557(49)	1.46(10)	1081(56)	1.9(3)	3.0(6)
10	72.38(4)	1.3046(7)	355(39)	0.67(14)	319(47)	0.9(2)	1.0(13)

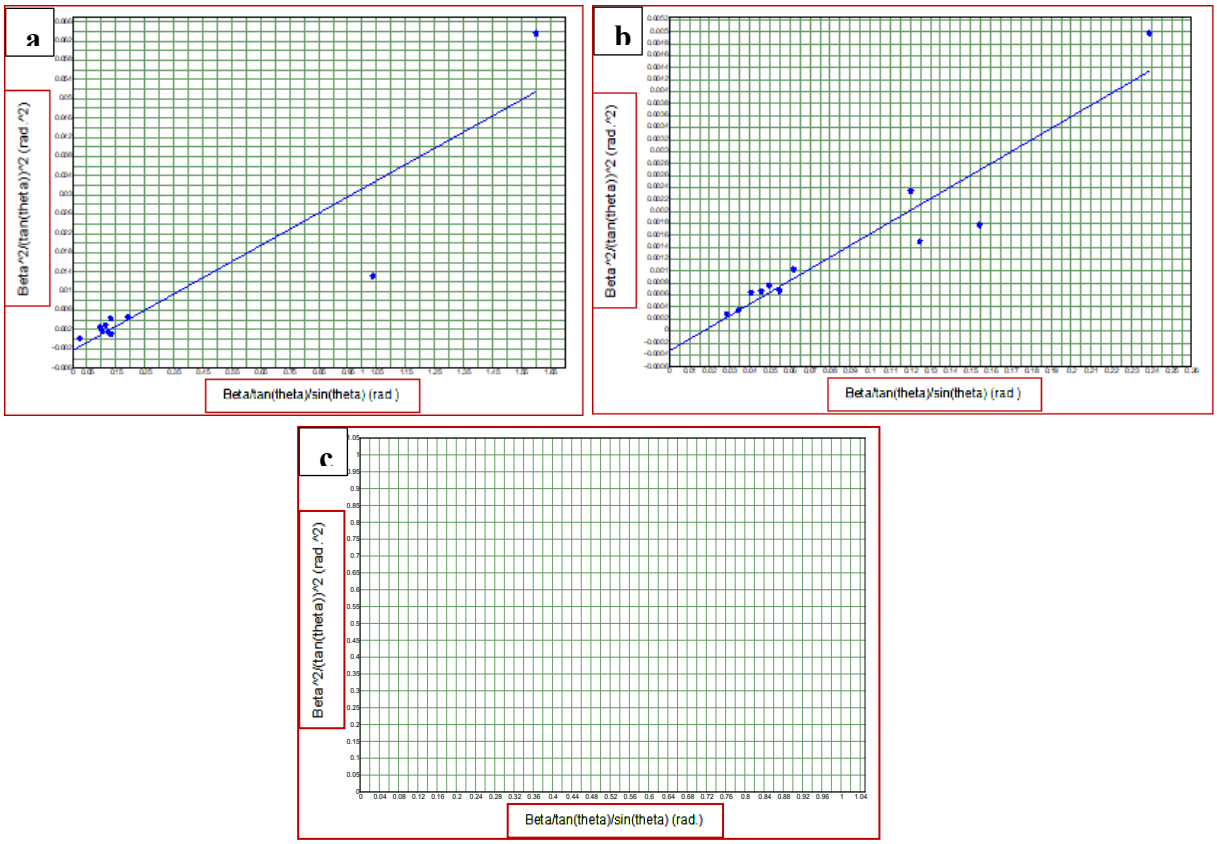

Figure 6.12.1: Crystalline size and lattice strain of a) CNP-Psc; b) CNP-Ab; and c) CNP-Le

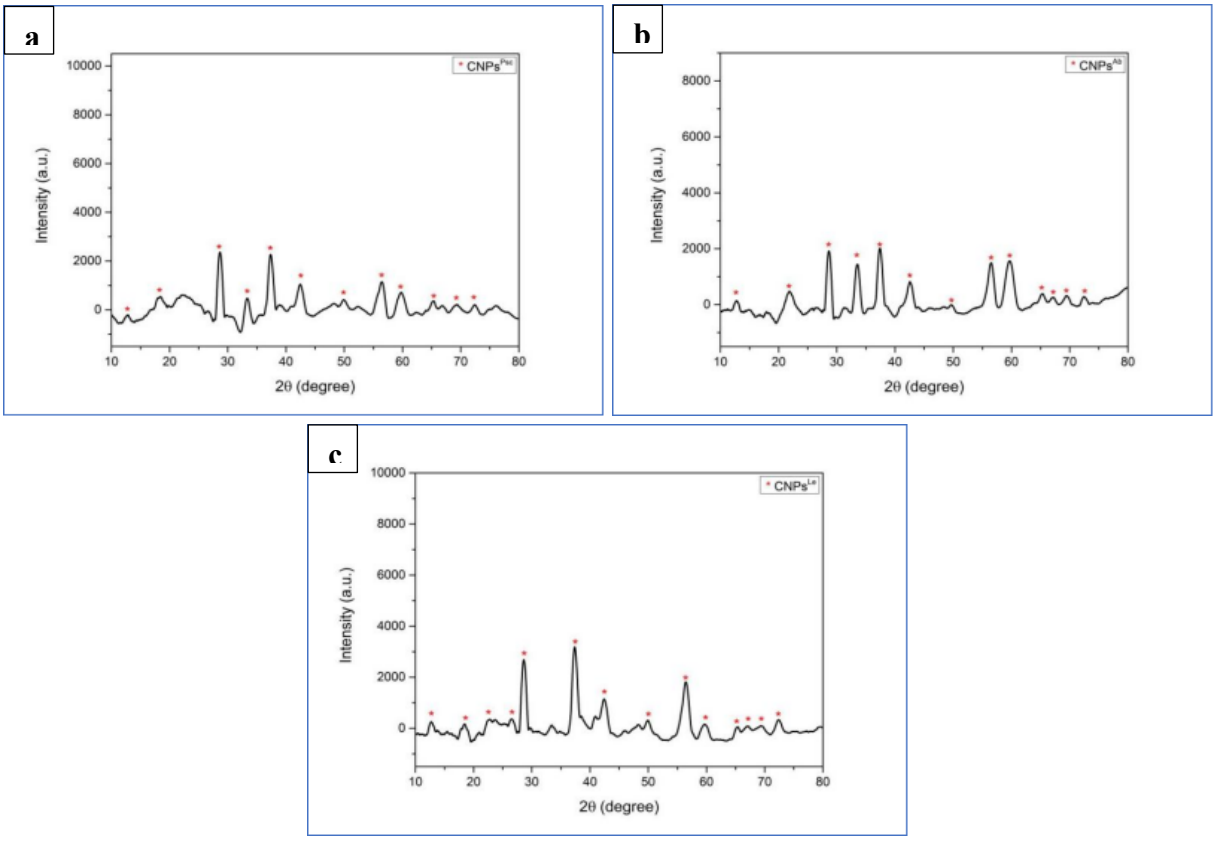

Figure 6.12.2: XRD Diffractograms for a) CNP-Psc; b) CNP-Ab; and c) CNP-Le

6.3.4. Scanning Electron Microscopy (SEM)

The morphology and particle size range obtained through the scanning electron micrographs of ZnONPs, MgONPs, MnO_2NPs and Combo NPs synthesized using *P. sajor caju*, *A. bisporus* and *L. edodes* are given in Tables 6.6.1 to 6.6.12. Due to presence of fungal debris in the nanoparticle mixtures, the surface of the nanoparticles is rough and most of the nanoparticles shown agglomeration (Naseer *et al.*, 2020). The SEM was carried out at two scales of 100 nm and 500 nm.

Table 6.6.1: Particle shape and average size of ZnONPs synthesized from *P. sajor caju*

S. No.	Shape of NPs	Scale	Particle size Range (nm)	Average particle size (nm)
1.	Rod-like; spherical;	100 nm	18-53	35.86
2.		500 nm	08-33	13.01

	irregular; agglomerated			

Table 6.6.2: Particle shape and average size of ZnONPs synthesized from *A. bisporus*

S. No.	Shape of NPs	Scale	Particle size Range (nm)	Average particle size (nm)
1.	Spherical; irregular; agglomerated	100 nm	17-42	29.68
2.		500 nm	62-112	80.16

Table 6.6.3: Particle shape and average size of ZnONPs synthesized from *L. edodes*

S. No.	Shape of NPs	Scale	Particle size Range (nm)	Average particle size (nm)
1.	Spherical; irregular; agglomerated	100 nm	08-19	13.98
2.		500 nm	52-94	72.92

Table 6.6.4: Particle shape and average size of MgONPs synthesized from *P. sajor caju*

S. No.	Shape of NPs	Scale	Particle size Range (nm)	Average particle size (nm)
1.	Spherical; irregular; agglomerated	100 nm	04-13	8.68
2.		500 nm	17-85	34.94

Table 6.6.5: Particle shape and average size of MgONPs synthesized from *A. bisporus*

S. No.	Shape of NPs	Scale	Particle size Range (nm)	Average particle size (nm)
1.	Spherical; agglomerated	100 nm	05-11	6.57
2.		500 nm	20-34	30.58

Table 6.6.6: Particle shape and average size of MgONPs synthesized from *L. edodes*

S. No.	Shape of NPs	Scale	Particle size Range (nm)	Average particle size (nm)
1.	Spherical; agglomerated	100 nm	05-17	13.80
2.		500 nm	34-76	46.80

Table 6.6.7: Particle shape and average size of MnO_2NPs synthesized from *P. sajor caju*

S. No.	Shape of NPs	Scale	Particle size Range (nm)	Average particle size (nm)
1.	Spherical; agglomerated	100 nm	10-17	12.89
2.		500 nm	17-69	38.52

Table 6.6.8: Particle shape and average size of MnO_2NPs synthesized from *A. bisporus*

S. No.	Shape of NPs	Scale	Particle size Range (nm)	Average particle size (nm)
1.	Spherical; agglomerated	100 nm	07-15	14.47
2.		500 nm	20-63	28.96

Table 6.6.9: Particle shape and average size of MnO_2NPs synthesized from *L. edodes*

S. No.	Shape of NPs	Scale	Particle size Range (nm)	Average particle size (nm)
1.	Spherical; agglomerated	100 nm	10-17	12.99
2.		500 nm	17-55	37.13

Table 6.6.10: Particle shape and average size of CNPs synthesized from *P. sajor caju*

S. No.	Shape of NPs	Scale	Particle size Range (nm)	Average particle size (nm)

1.	Angular; agglomerated	100 nm	04-16	9.24
2.		500 nm	34-73	46.53

Table 6.6.11: Particle shape and average size of CNPs synthesized from *A. bisporus*

S. No.	Shape of NPs	Scale	Particle size Range (nm)	Average particle size (nm)
1.	Angular; agglomerated	100 nm	08-16	13.53
2.		500 nm	37-80	51.56

Table 6.6.12: Particle shape and average size of CNPs synthesized from *L. edodes*

S. No.	Shape of NPs	Scale	Particle size Range (nm)	Average particle size (nm)
1.	Angular; agglomerated	100 nm	10-17	12.95
2.		500 nm	26-70	37.43

6.3.4.1. *SEM analysis of ZnONPs*

SEM examination was utilized to assess the morphology of myco-synthesized ZnONPs. In addition to individual particles with spherical and elongated structures, typical SEM micrographs of ZnONPs show many agglomerated particles with uneven shape. The particle sizes in ZnONP-Psc varied from 8 nm to 53 nm. The average size of these nanoparticles synthesized using *P. sajor caju* was 35.86 m at 100 nm scale and 13.01 nm at the scale of 500 nm (Table 6.6.1; Figure 6.13.2). The ZnONP-Ab showed the particle size range of 17-112 nm, and average particle size of 29.68 nm at 100 nm scale and 80.16 nm at 500 nm scale respectively (Table 6.6.2; Figure 6.13.4). In case of ZnONP-Le, particle size ranged from 08 nm to 94 nm. The average particle size was 13.98 nm, 72.92 nm at scales of 100 nm and 500 nm respectively (Table 6.6.3; Figure 6.13.6). The findings are consistent with those of several other researchers (Raut *et al.*, 2013; Rajendran and Sengodan, 2017; Suresh *et al.*, 2018). SEM micrographs of

ZnONP-Psc, ZnONP-Ab and ZnONP-Le are shown in Figures 6.13.1, 6.13.3 and 6.13.5 respectively.

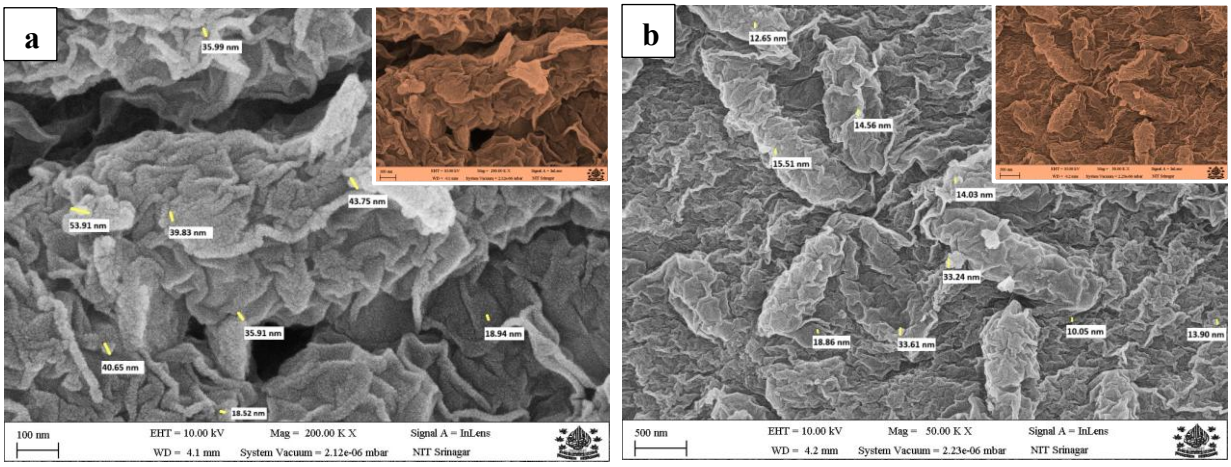

Figure 6.13.1: SEM micrographs of ZnONPs synthesized using *P. sajor caju*
a) 100 nm; b) 500 nm

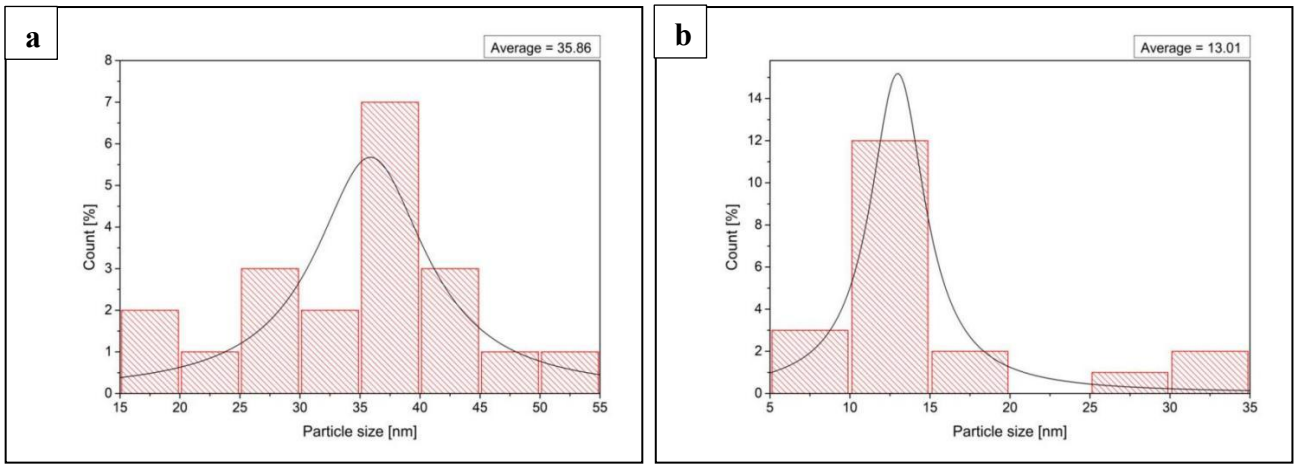

Figure 6.13.2: SEM histograms of ZnONPs synthesized using *P. sajor caju*
a) 100 nm; b) 500 nm

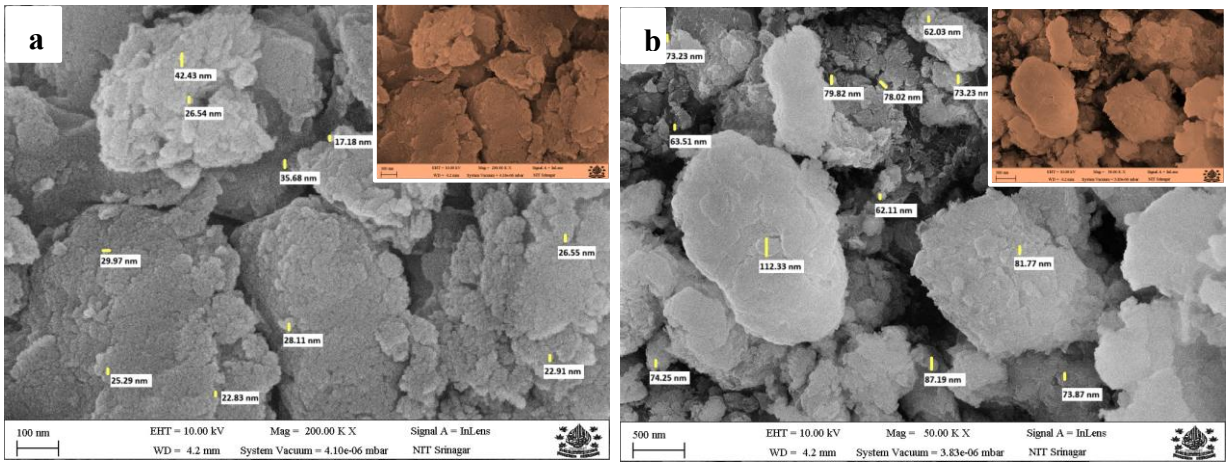

Figure 6.13.3: SEM micrographs of ZnONPs synthesized using *A. bisporus*
a) 100 nm; b) 500 nm

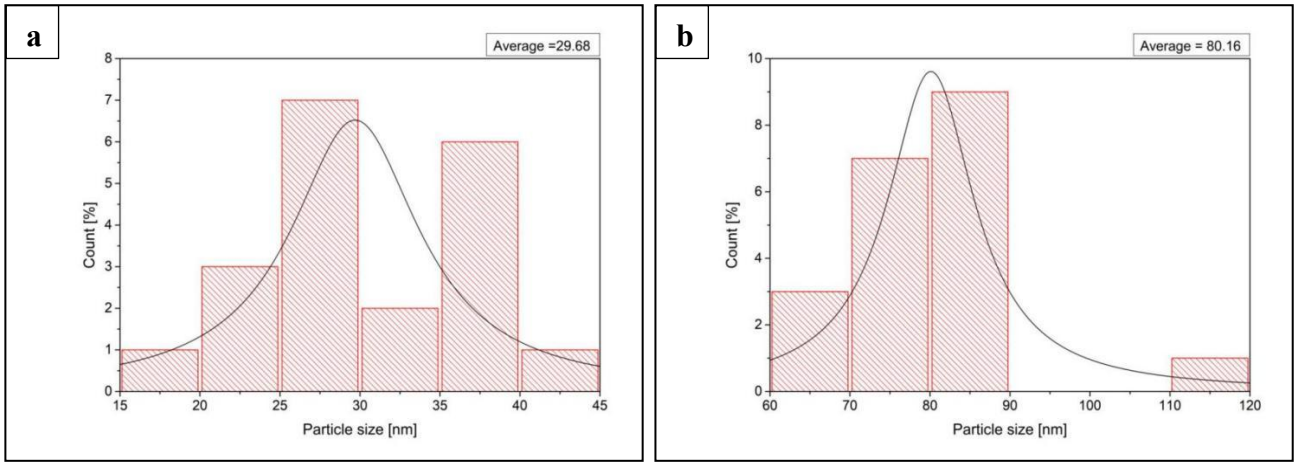

Figure 6.13.4: SEM histograms of ZnONPs synthesized using *A. bisporus*
a) 100 nm; b) 500 nm

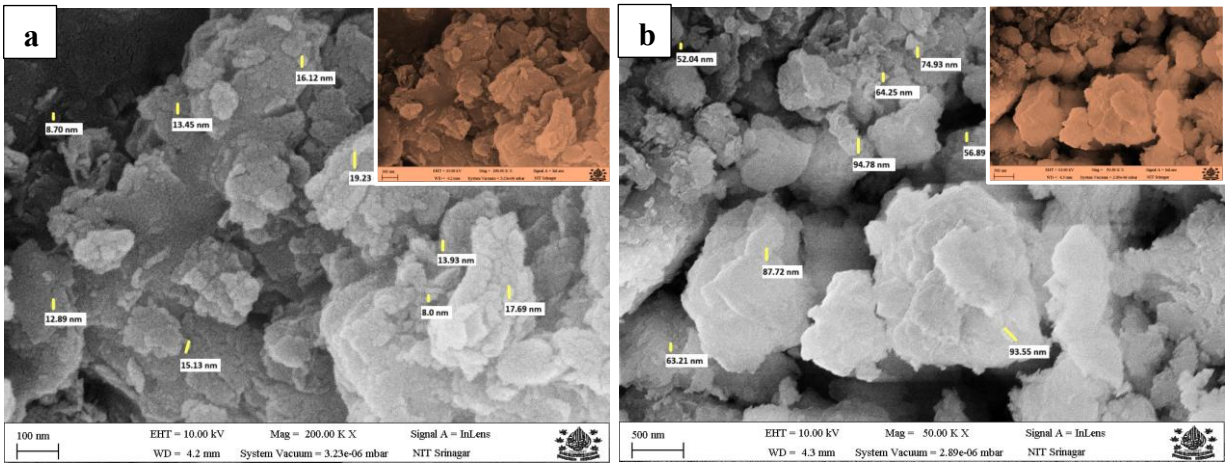

Figure 6.13.5: SEM micrographs of ZnONPs synthesized using *L. edodes*
a) 100 nm; b) 500 nm

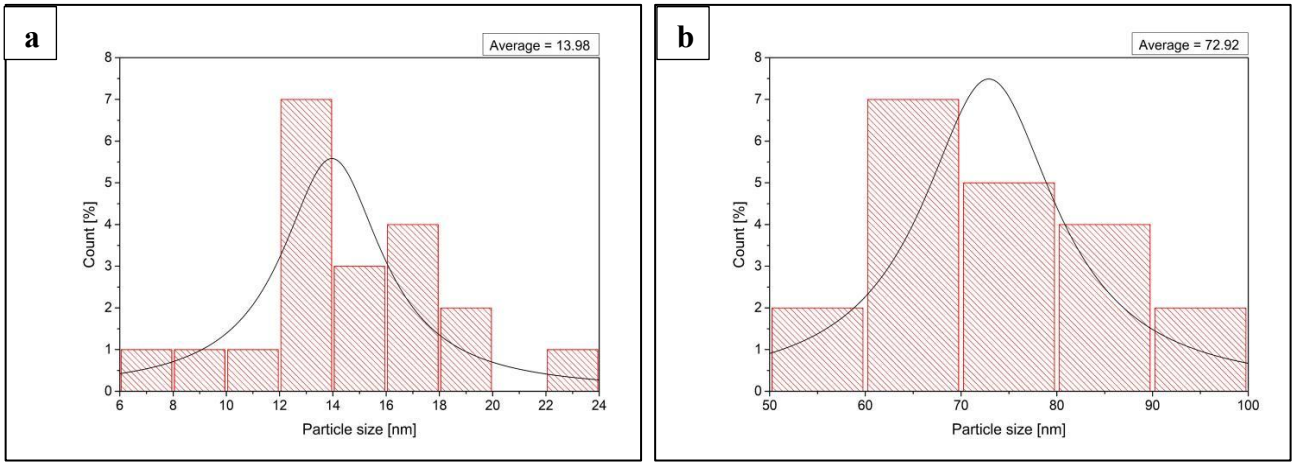

Figure 6.13.6: SEM histograms of ZnONPs synthesized using *L. edodes*
a) 100 nm; b) 500 nm

6.3.4.2. *SEM analysis of MgONPs*

SEM analysis was used to investigate the surface morphology, aggregation, and morphology of myco-synthesized MgONPs. Well-dispersed, spherical, somewhat irregular MgONPs with an aggregation were seen in the SEM micrographs (Figures 6.14.1, 6.14.3, 6.14.5). The MgONP-Psc showed the particle size range of 04-85 nm. The average size of these nanoparticles was 8.68 nm at 100 nm scale and 34.94 nm at 500 nm scale respectively (Table 6.6.4; Figure 6.14.2). In MgONP-Ab, the particle size range varied from 05-34 nm. An average size of 6.57 nm and 30.58 nm was shown by MgONP-Psc at 100 nm and 500 nm scales respectively. The particle size range of MgONP-Le was 05-76 nm (Table 6.6.6), and the average size was 13.80 nm and 46.80 nm at the scales of 100 nm and 500 nm respectively (Figure 6.14.6) (Fathy and Mahfouz, 2021).

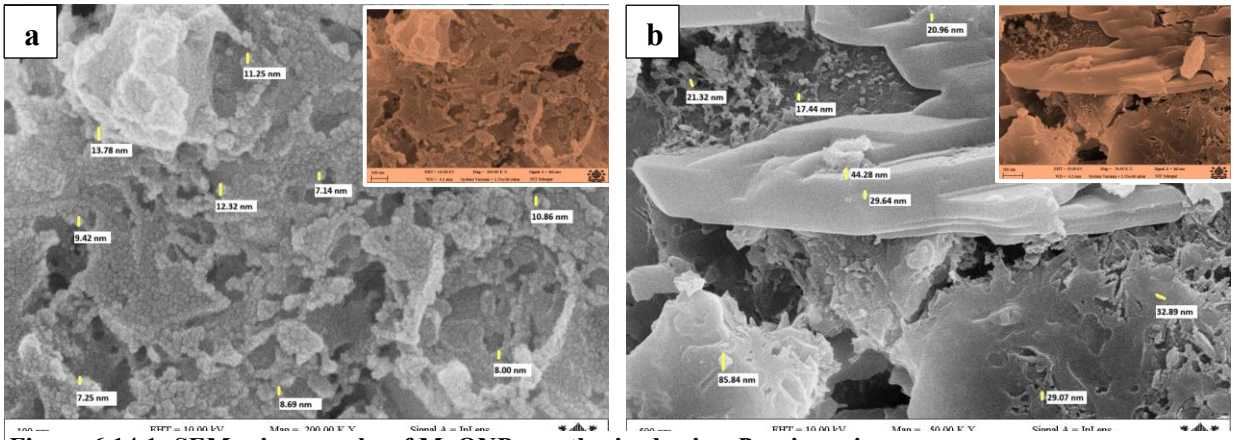

Figure 6.14.1: SEM micrographs of MgONPs synthesized using *P. sajor caju*
a) 100 nm; b) 500 nm

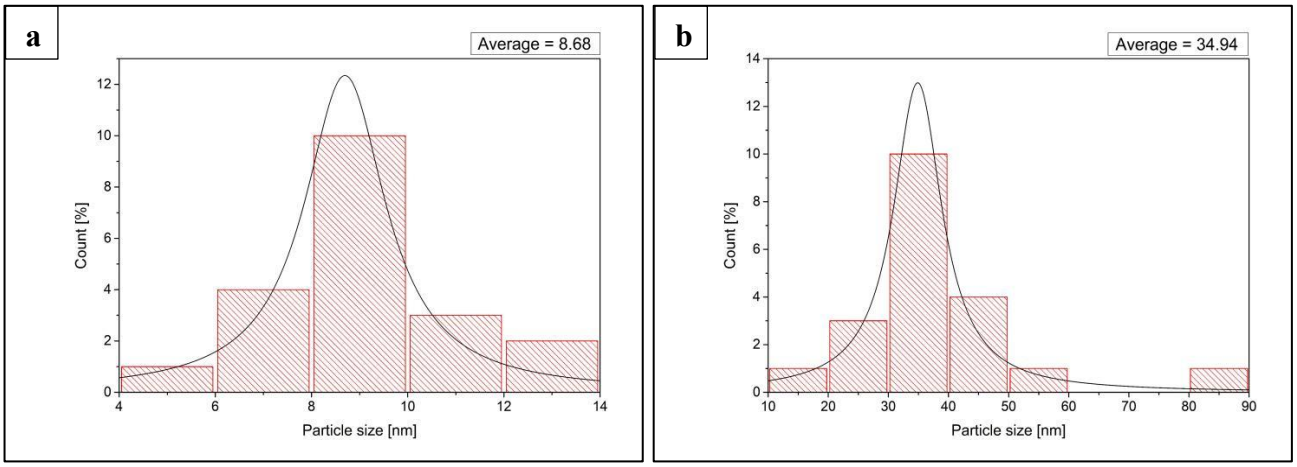

Figure 6.14.2: SEM histograms of MgONPs synthesized using *P. sajor caju*
a) 100 nm; b) 500 nm

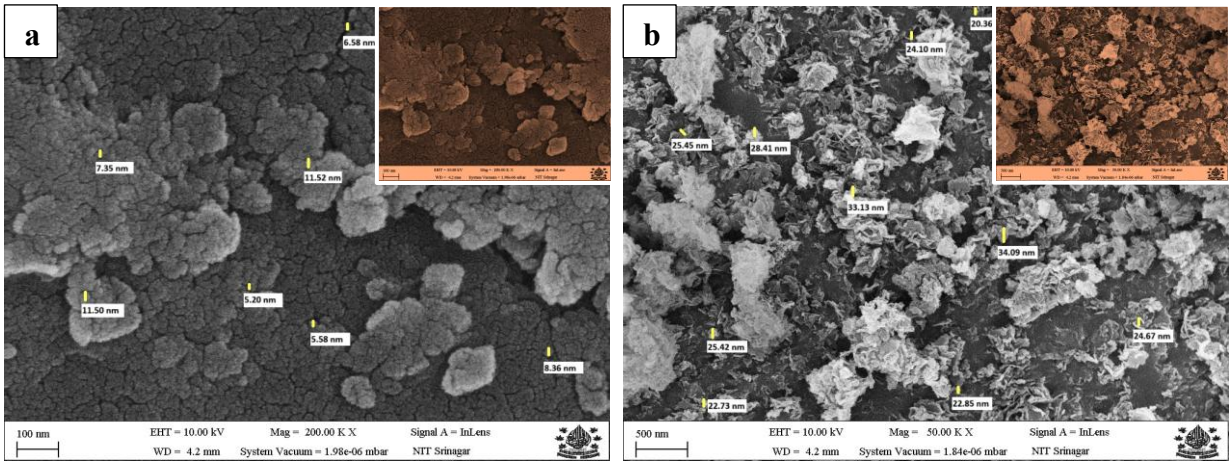

Figure 6.14.3: SEM micrographs of MgONPs synthesized using *A. bisporus*
a) 100 nm; b) 500 nm

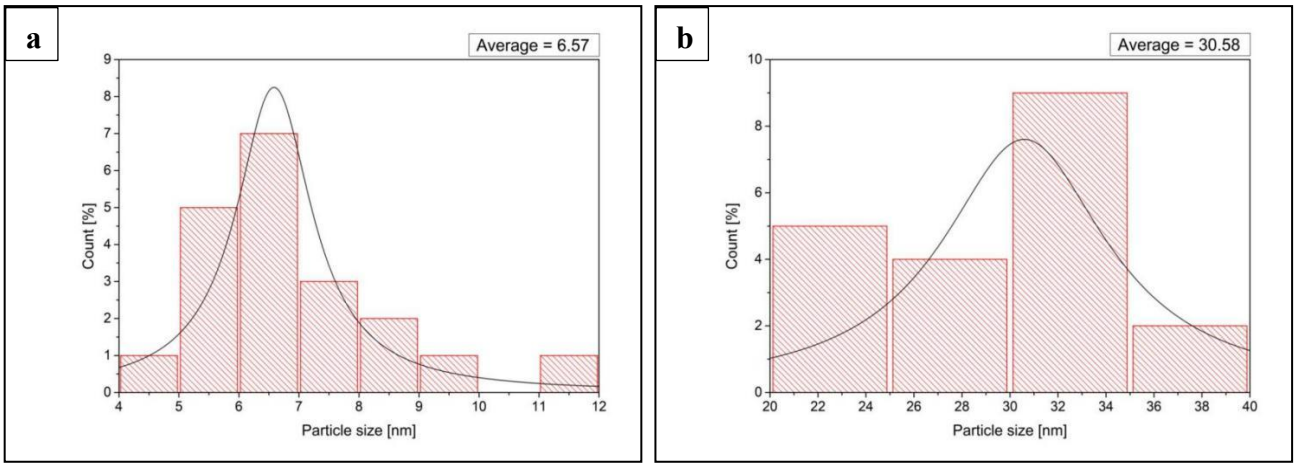

Figure 6.14.4: SEM histograms of MgONPs synthesized using *A. bisporus*
a) 100 nm; b) 500 nm

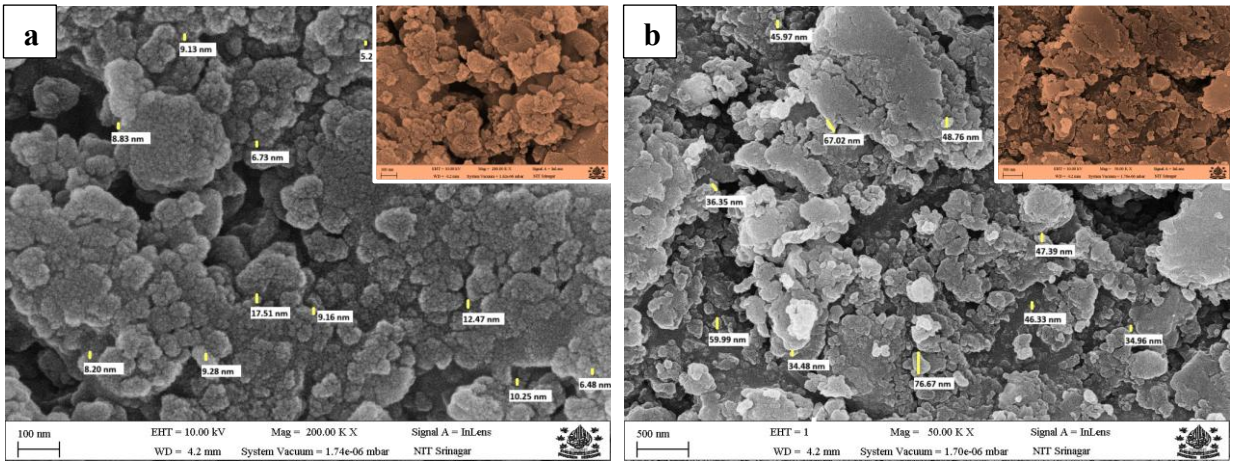

Figure 6.14.5: SEM micrographs of MgONPs synthesized using *L. edodes*
a) 100 nm; b) 500 nm

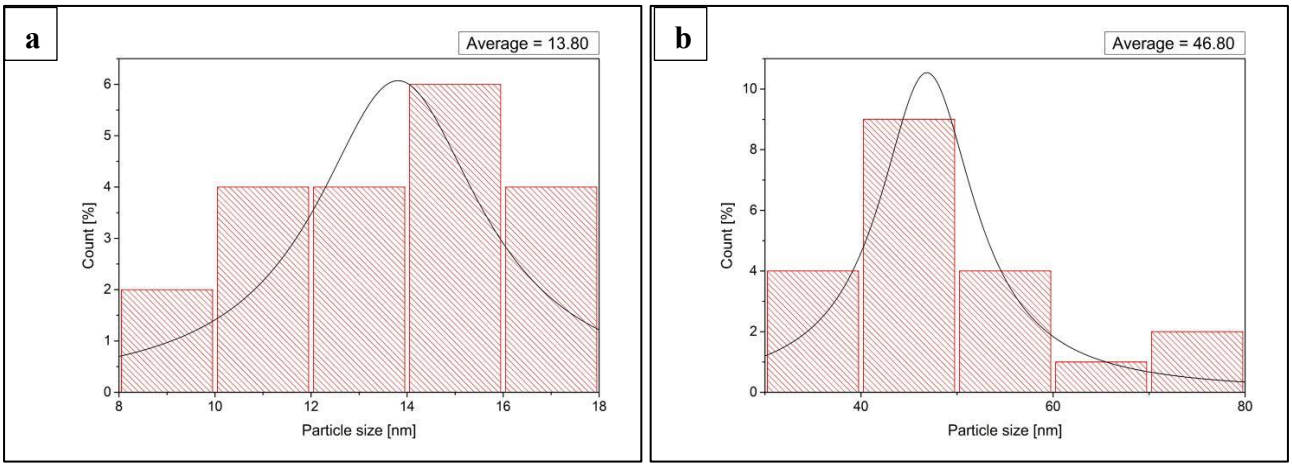

Figure 6.14.6: SEM histograms of MgONPs synthesized using *L. edodes*
a) 100 nm; b) 500 nm

6.3.4.3. *SEM analysis of MnO_2NPs*

SEM micrographs were used to investigate the morphological characteristics of the biosynthesized MnO_2NPs (Figures 6.15.1, 6.15.3, 6.15.5). The fungal biomass aqueous extract was used to create aggregations of roughly spherical, randomly oriented particles, as shown in the SEM pictures. The polarity, electrostatic attraction, high surface energy, and typically the process of nanoparticle production in water are the likely causes of nanoparticle aggregation (Madhumitha *et al.*, 2019). The MnO_2NPs synthesized using *P. sajor caju* showed the particle size range of 10-69 nm and average size of 12.89 nm and 38.52 nm in the scales of 100 nm and 500 nm respectively (Table

6.6.7; Figure 6.15.2). Similarly, MnO_2NP-Ab and MnO_2NP-Le showed the particle size range of 07-63 nm (Table 6.6.8) and 10-55 nm (Table 6.6.9) respectively. MnONP-Ab showed the average particle size of 14.47 nm (100 nm scale) and 28.96 nm (500 nm scale) (Figure 6.15.4). Moreover, in case of MnONP-Le, the average particle size at 100 nm and 500 nm scale came out to be 12.99 nm and 37.13 nm respectively (Figure 6.15.6) (Faisal *et al.*, 2022).

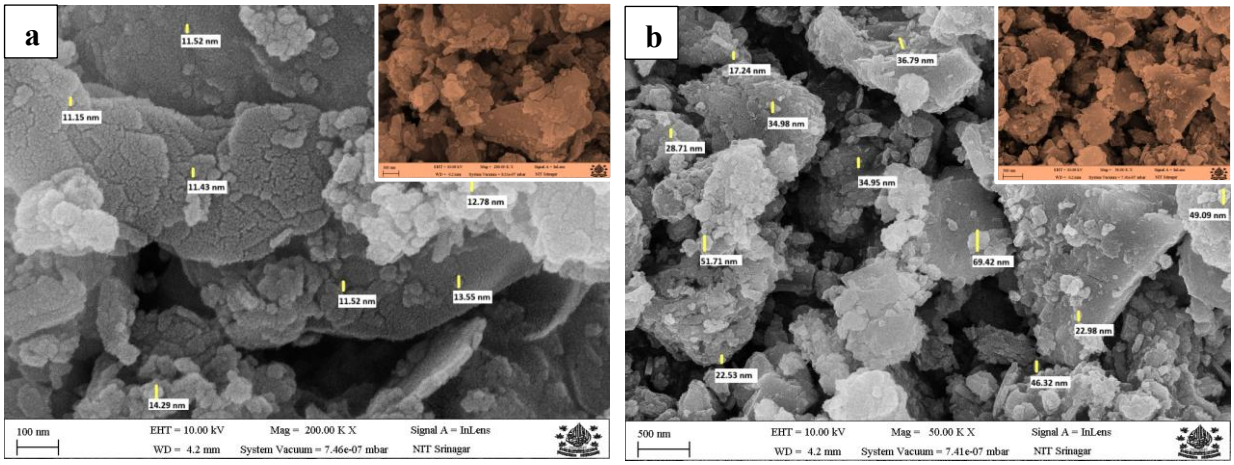

Figure 6.15.1: SEM micrographs of MnO_2NPs synthesized using *P. sajor caju*
a) 100 nm; b) 500 nm

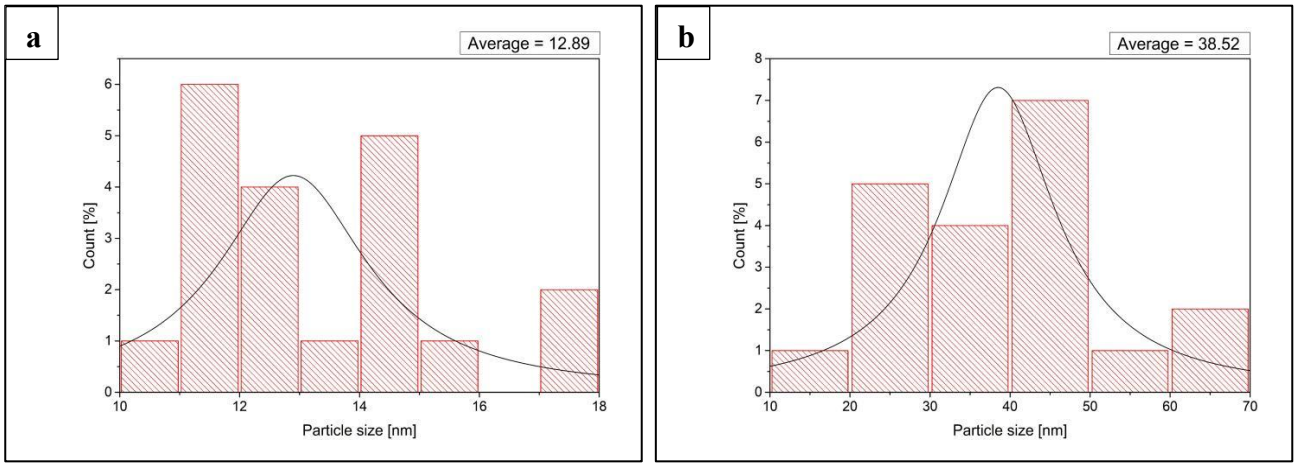

Figure 6.15.2: SEM histograms of MnO_2NPs synthesized using *P. sajor caju*
a) 100 nm; b) 500 nm

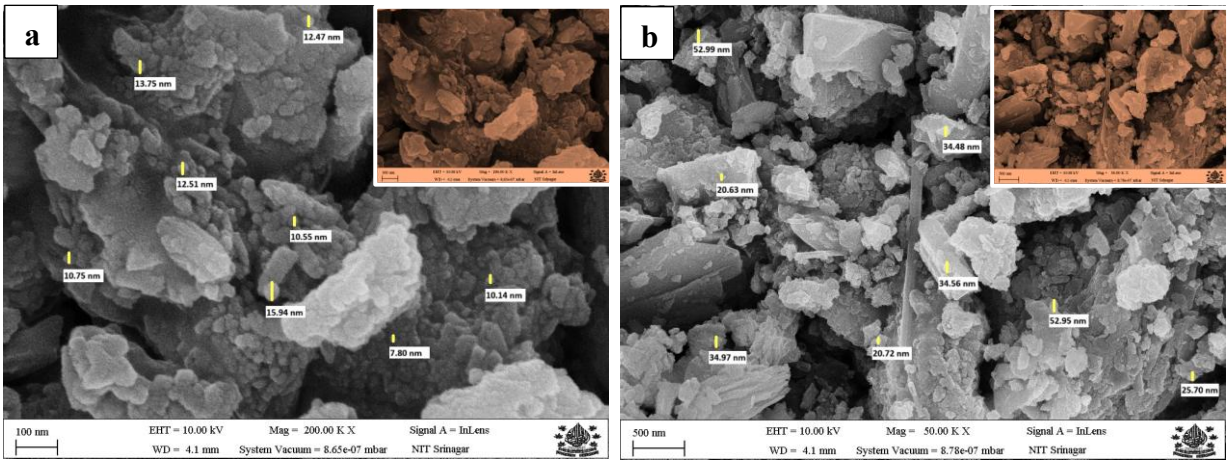

Figure 6.15.3: SEM micrographs of MnO_2NPs synthesized using *A. bisporus*
a) 100 nm; b) 500 nm

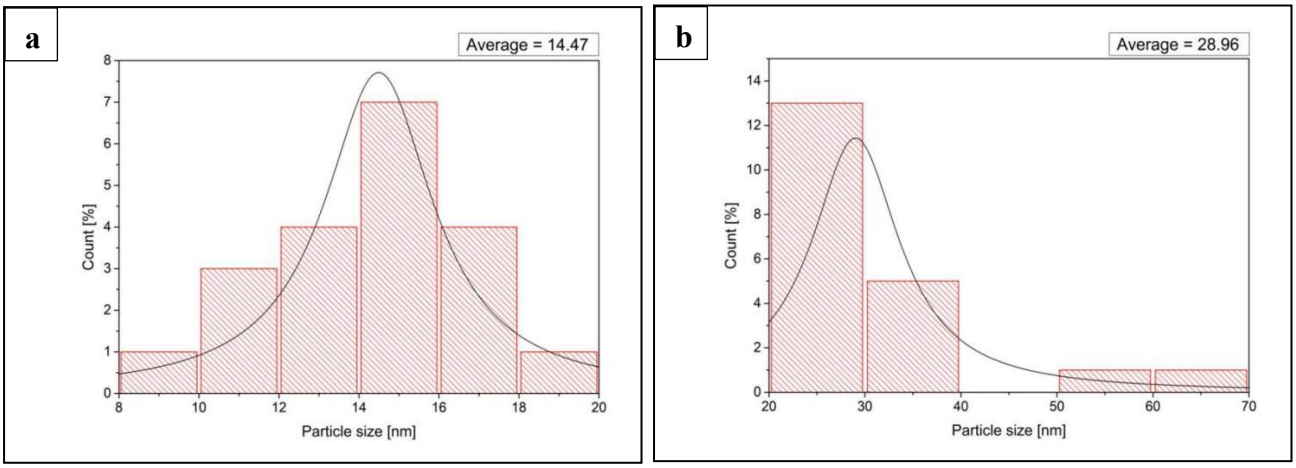

Figure 6.15.4: SEM histograms of MnO_2NPs synthesized using *A. bisporus*
a) 100 nm; b) 500 nm

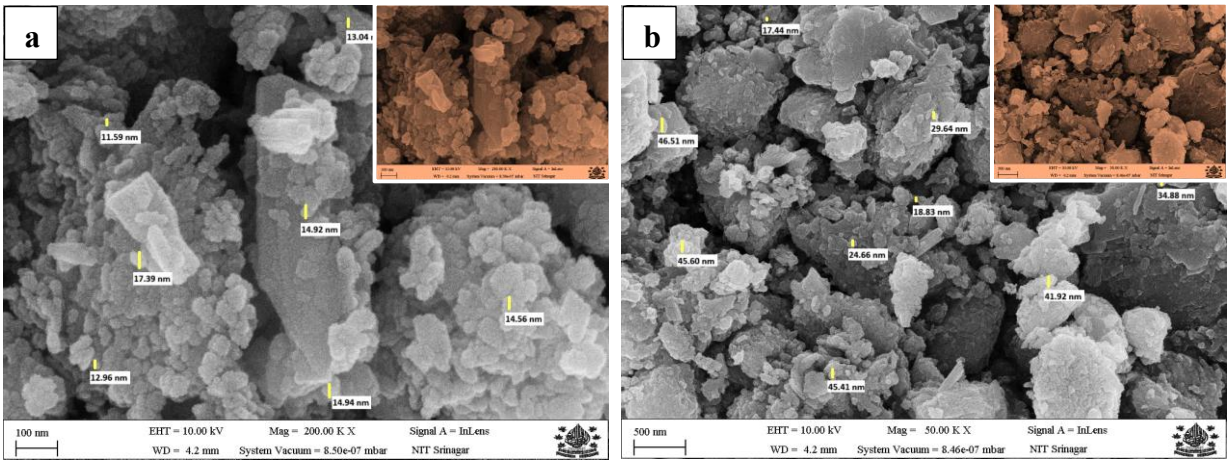

Figure 6.15.5: SEM micrographs of MnO_2NPs synthesized using *L. edodes*
a) 100 nm; b) 500 nm

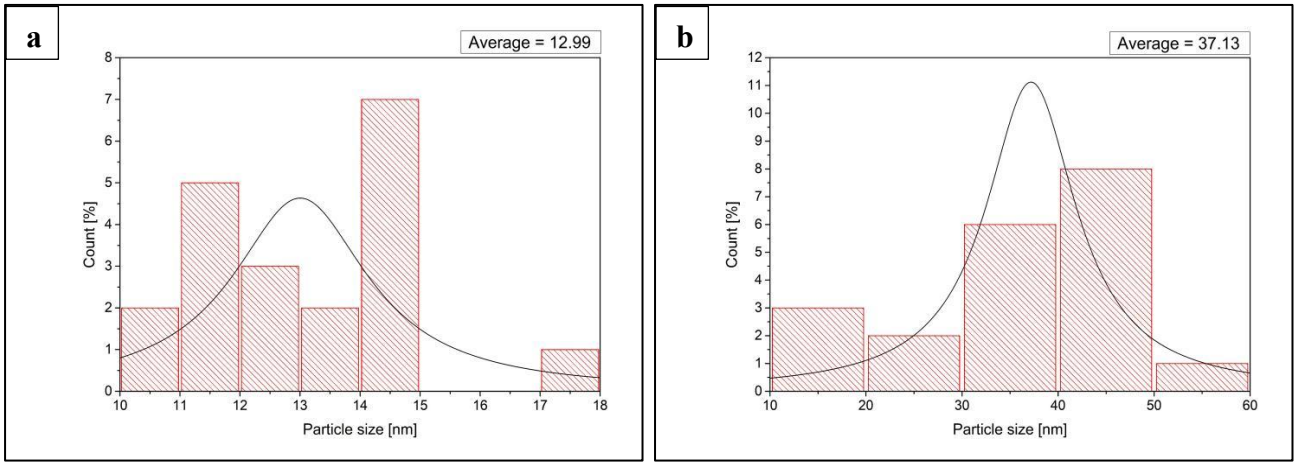

Figure 6.15.6: SEM histograms of MnO_2NPs synthesized using *L. edodes*
a) 100 nm; b) 500 nm

6.3.4.4. *SEM analysis of CNPs*

SEM was used to analyze the surface morphology of CNPs. One of the most widely utilized tools for studying the imaging of nanoparticles and characterizing solid materials is the SEM. The SEM micrographs of the combination of Zn, Mg and Mn nanoparticles are shown in Figures 6.16.1, 6.16.3 and 6.16.5 for CNP-Psc, CNP-Ab and CNP-Le respectively. The surface morphology of the CNPs synthesized from *P. sajor caju* was no different from that of the CNPs synthesized from *A. bisporus* and *L. edodes*, but varied with respect to the morphology of individual nanoparticles. All the nanoparticles were random, somewhat angular, and showed agglomeration. The CNPs showed a comparable particle size range of 04-73 nm, 08-80 nm and 10-70 nm in

CNPPsc (Table 6.6.10), CNPAb (Table 6.6.11) and CNPLe (Table 6.6.12) respectively. At the scales of 100 nm and 500 nm, the average particle size of the nanoparticles came out to be 9.24 nm and 46.53 nm in CNP-Psc (Figure 6.16.2); 13.53 nm and 51.56 nm in CNP-Ab (Figure 6.16.4); and, 12.95 nm and 37.43 nm in CNP-Le (Figure 6.16.6) respectively. It is important to note that certain evenly dispersed nanostructured grains may be observed as the concentration of each metal salt in the mixture increases, indicating the impact of increasing Mn and Mg doping on the ZnO matrix surface (Radhi Devi *et al.*, 2022).

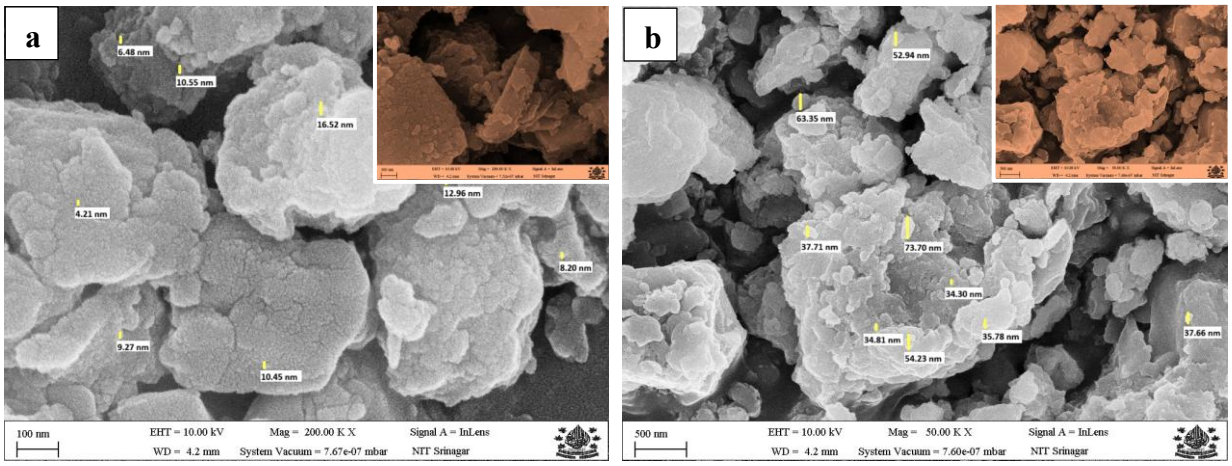

Figure 6.16.1: SEM micrographs of CNPs synthesized using *P. sajor caju*
a) 100 nm; b) 500 nm

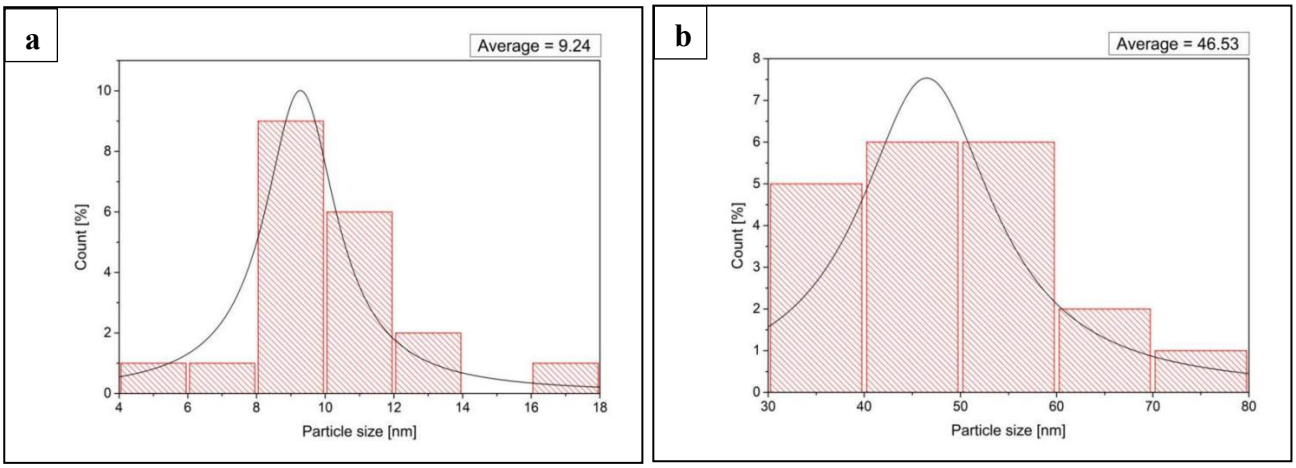

Figure 6.16.2: SEM histograms of CNPs synthesized using *P. sajor caju*
a) 100 nm; b) 500 nm

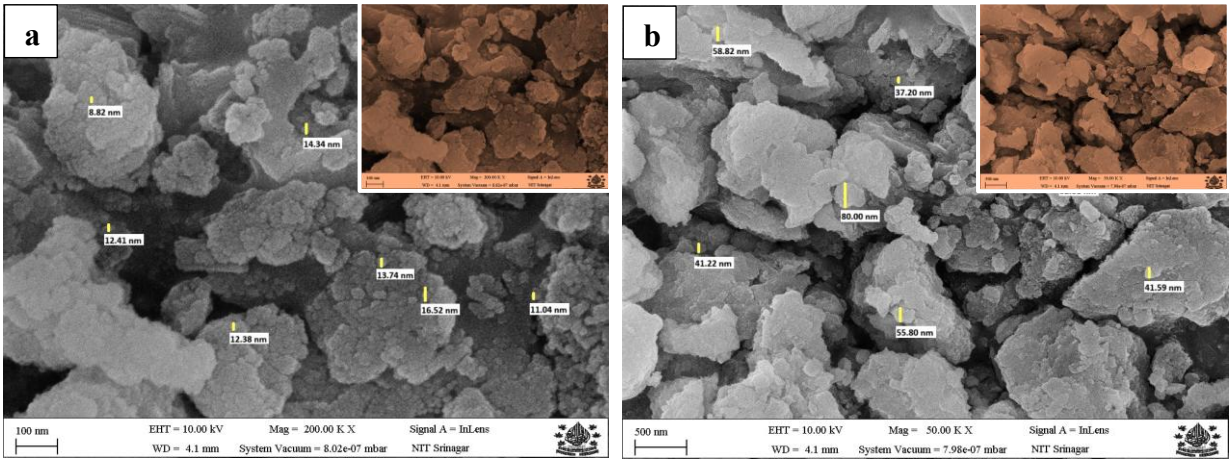

Figure 6.16.3: SEM micrographs of CNPs synthesized using *A. bisporus*
a) 100 nm; b) 500 nm

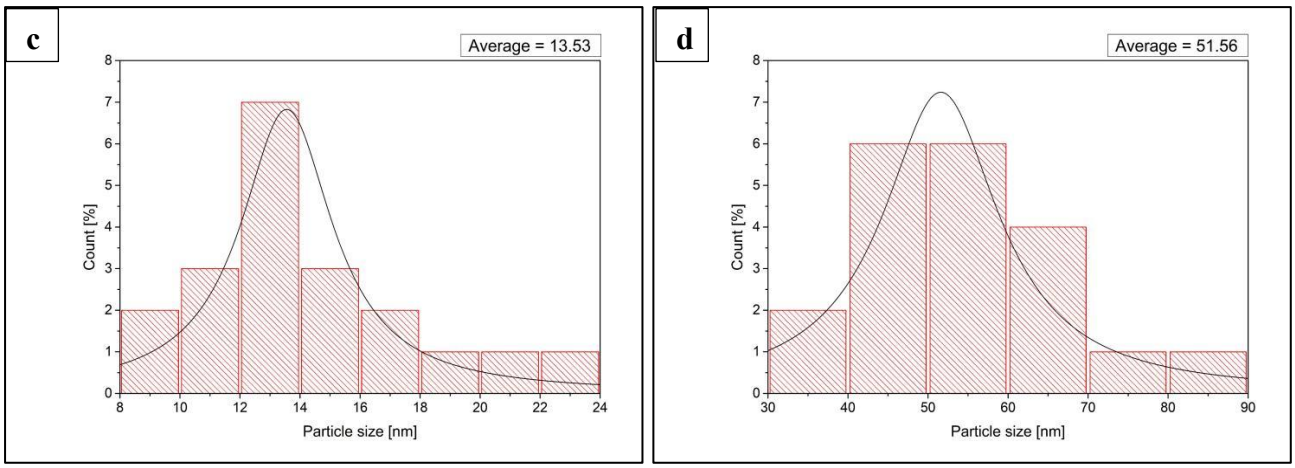

Figure 6.16.4: SEM histograms of CNPs synthesized using *A. bisporus*
a) 100 nm; b) 500 nm

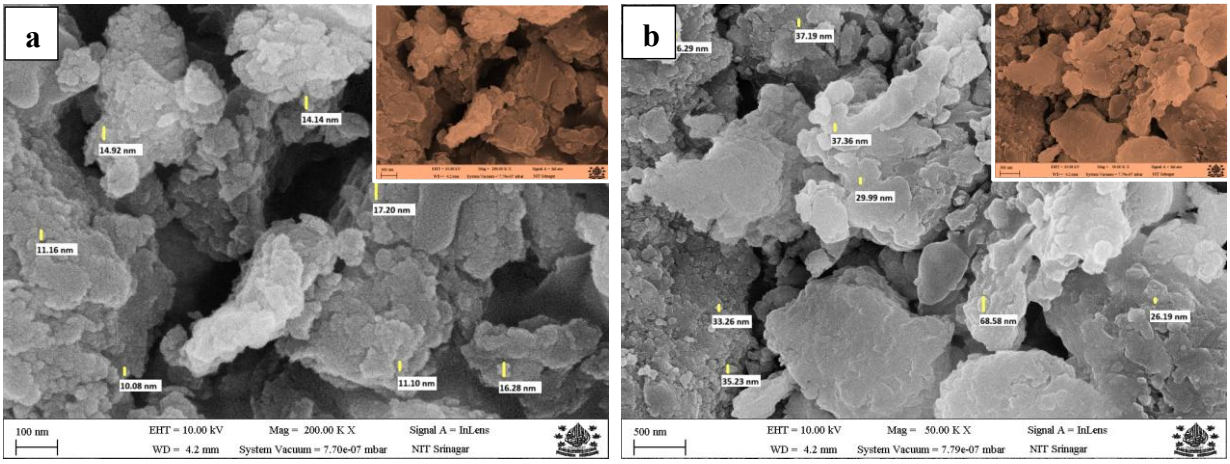

Figure 6.16.5: SEM micrographs of CNPs synthesized using *L. edodes*
a) 100 nm; b) 500 nm

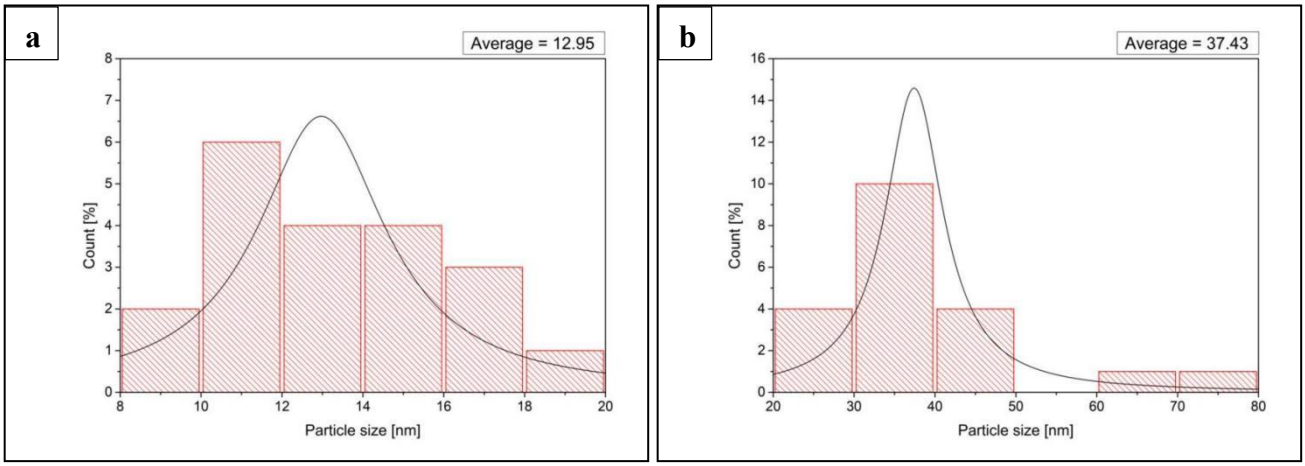

Figure 6.16.6: SEM histograms of CNPs synthesized using *L. edodes*
a) 100 nm; b) 500 nm

6.3.5. Energy dispersive X-ray (EDX) analysis

Energy dispersive X-ray analysis (EDX) was used to analyze the elemental makeup of the produced Zn-P, Zn-A, and Zn-L NPs. It is predicated on the fundamental idea that every element has a distinct atomic structure, which results in a distinct set of peaks in its spectrum of electromagnetic emission. The spectra's horizontal axis shows energy in keV, while the vertical axis shows the number of X-ray counts. The existence of elemental zinc, Magnesium and manganese was confirmed by the sharp signals of Energy Dispersive Spectra. Energy Dispersive spectra highlight the presence of signals that correlate to presence of specific elements present in sample. This further helps confirming the presence and strength of metallic particles in solution.

6.3.5.1. *EDX analysis of ZnONPs*

The EDX profile of ZnONP-Psc contains O and Zn with weight percentages of 23.2% and 76.8%, and atomic percentages of 55.2% and 44.8% respectively (Table 6.7.1). Similarly, the EDX patterns showed O and Zn in weight percentages of 36.8% and 63.3% in ZnONP-Ab and 38.5% and 61.5% in ZnONP-Le. Moreover, atomic percentages of 70.4% and 29.6% were present in ZnONP-Ab (Table 6.7.2) and 71.9% and 28.1% in ZnONP-Le (Table 6.7.3) respectively. These findings corroborate well with the results reported earlier (Mahobia *et al.*, 2016; Mohana and Sumathi, 2020).

Table 6.7.1: Quant results showing the elemental composition of ZnONP-Psc

Element	Weight %	MDL	Atomic %	Net Int.	Error %	R	A	F
O K	23.2	0.12	55.2	368.4	9.9	0.8188	0.1628	1.0000
Zn K	76.8	0.55	44.8	772.1	2.6	0.9322	0.9845	1.0470

Table 6.7.2: Quant results showing the elemental composition of ZnONP-Ab

Element	Weight %	MDL	Atomic %	Net Int.	Error %	R	A	F
O K	36.8	0.16	70.4	470.1	9.6	0.8409	0.1867	1.0000
Zn K	63.3	0.63	29.6	445.3	2.8	0.9443	0.9868	1.0497

Table 6.7.3: Quant results showing the elemental composition of ZnONP-Le

Element	Weight %	MDL	Atomic %	Net Int.	Error %	R	A	F
O K	38.5	0.14	71.9	640.7	9.5	0.8436	0.1907	1.0000
Zn K	61.5	0.52	28.1	551.7	2.7	0.9458	0.9871	1.0501

6.3.5.2. *EDX analysis of MgONPs*

The EDX profile of MgONPs contains O and Mg with weight percentages of 73.2% and 26.8% in MgONP-Psc, 59.1% and 40.9% in MgONP-Ab, and 64.8% and 35.2% in

MgONP-Le respectively. Furthermore, the EDX profiles displayed the atomic percentages of 80.6% and 19.4% in MgONP-Psc (Table 6.8.1), 68.7% and 31.3% in MgONP-Ab (Table 6.8.2), and 73.7% and 26.3% in MgONP-Le (Table 6.8.3) respectively. This investigation confirms that the effective synthesis of MgONPs is indicated by the appearance of peaks with an energy between 0.5 and 1.5 KeV (Dobrucka, 2018). The X-ray hydrolysis of the reducing, capping or stabilizing agents like proteins, polysaccharides, amino acids, and enzymes found in the fungal extracts may be the cause of the occurrence of peaks in addition to that of Mg and O (Alsharif *et al.*, 2020).

Table 6.8.1: Quant results showing the elemental composition of MgONP-Psc

Element	Weight %	MDL	Atomic %	Net Int.	Error %	R	A	F
O K	73.2	0.13	80.6	955.7	7.8	0.9265	0.3448	1.0000
Mg K	26.8	0.17	19.4	490.7	7.6	0.9408	0.3861	1.0012

Table 6.8.2: Quant results showing the elemental composition of MgONP-Ab

Element	Weight %	MDL	Atomic %	Net Int.	Error %	R	A	F
O K	59.1	0.05	68.7	1512.9	8.3	0.9220	0.2929	1.0000
Mg K	40.9	0.07	31.3	1949.1	6.9	0.9369	0.4337	1.0011

Table 6.8.3: Quant results showing the elemental composition of MgONP-Le

Element	Weight %	MDL	Atomic %	Net Int.	Error %	R	A	F
O K	64.8	0.10	73.7	1052.9	8.1	0.9238	0.3121	1.0000
Mg K	35.2	0.13	26.3	948.9	7.2	0.9385	0.4131	1.0012

6.3.5.3. *EDX analysis of MnO_2NPs*

The EDX method was used to determine the chemical makeup of MnO_2NPs. O and Mn have two prominent signals in the EDX profile, with weight percentages of 32.0% O and 68.0% Mn, and atomic percentage of 61.7% O and 38.3% Mn for MnO_2NP-Psc (Table 6.9.1). The EDX analysis of MnO_2NP-Ab and MnO_2NP-Le also showed the occurrence of oxygen and manganese as the key elements with the weight percentage 36.7% and 63.3% (MnO_2NP-Ab), 37.3% and 62.7% (MnO_2NP-Le) and atomic percentage of 66.6% and 33.4% (MnO_2NP-Ab) (Table 6.9.2), 67.1% and 32.9% (MnO_2NP-Le) (Table 6.9.3) respectively. This analysis is in line with the previous study (El-Moslamy *et al.*, 2023).

Table 6.9.1: Quant results showing the elemental composition of MnO_2NP-Psc

Element	Weight %	MDL	Atomic %	Net Int.	Error %	R	A	F
O K	32.0	0.12	61.7	909.4	8.2	0.8524	0.3103	1.0000
Mn K	68.0	0.32	38.3	1425.8	2.0	0.9296	0.9720	1.0235

Table 6.9.2: Quant results showing the elemental composition of MnO_2NP-Ab

Element	Weight %	MDL	Atomic %	Net Int.	Error %	R	A	F
O K	36.7	0.13	66.6	960.9	8.1	0.8585	0.3178	1.0000
Mn K	63.3	0.36	33.4	1192.7	2.0	0.9336	0.9730	1.0241

Table 6.9.3: Quant results showing the elemental composition of MnO_2NP-Le

Element	Weight %	MDL	Atomic %	Net Int.	Error %	R	A	F
O K	37.3	0.14	67.1	830.7	8.1	0.8592	0.3197	1.0000
Mn K	62.7	0.47	32.9	999.7	2.1	0.9341	0.9732	1.0241

6.3.5.4. *EDX analysis of CNPs*

An EDX spectroscopy was used to execute the existence of the compositional components. According to the EDX spectra, the material under analysis included oxygen, magnesium, manganese, and zinc in weight percentages of 45.3%, 4.4%, 25.2%, and 25.2% for the CNP-Psc, respectively. Also, the atomic percentage for these nanoparticles was 73.5%, 4.7%, 11.9% and 10.0% for O, Mg, Mn and Zn respectively (Table 6.10.1). In case of CNP-Ab, weight percentage of 40.9%, 2.60%, 24.9% and 31.5%, and atomic percentage of 71.0%, 3.0%, 12.6% and 13.4% was achieved for O, Mg, Mn and Zn respectively (Table 6.10.2). Similarly, the weight and atomic percentages for CNP-Le were obtained in the values of 45.0%, 3.6%, 26.6% and 24.8% (weight percentage) and 73.5%, 3.8%, 12.7% and 9.9% (atomic percentage) (Table 6.10.3). According to the EDX spectra, no additional foreign elements were observed in the synthesized nanoparticles. The results confirmed the presence of Zn, Mg and Mn in the samples successfully substituted as the combination materials.

Table 6.10.1: Quant results showing the elemental composition of CNP-Psc

Element	Weight %	MDL	Atomic %	Net Int.	Error %	R	A	F
O K	45.3	0.14	73.5	821.1	8.8	0.8665	0.2565	1.0000
Mg K	4.4	0.16	4.7	78.0	11.1	0.8876	0.2000	1.0024
Mn K	25.2	0.28	11.9	426.4	2.7	0.9387	0.9684	1.0799
Zn K	25.2	0.59	10.0	180.3	3.6	0.9571	0.9717	1.0602

Table 6.10.2: Quant results showing the elemental composition of CNP-Ab

Element	Weight %	MDL	Atomic %	Net Int.	Error %	R	A	F
O K	40.9	0.17	71.0	725.8	9.0	0.8576	0.2393	1.0000
Mg K	2.6	0.19	3.0	45.9	12.9	0.8794	0.1851	1.0024

Mn K	24.9	0.33	12.6	446.6	2.8	0.9330	0.9659	1.0902
Zn K	31.5	0.57	13.4	236.5	3.4	0.9528	0.9708	1.0570

Table 6.10.3: Quant results showing the elemental composition of CNP-Le

Element	Weight %	MDL	Atomic %	Net Int.	Error %	R	A	F
O K	45.0	0.15	73.5	764.1	8.8	0.8655	0.2582	1.0000
Mg K	3.6	0.17	3.8	59.1	11.4	0.8867	0.1990	1.0025
Mn K	26.6	0.29	12.7	419.0	2.7	0.9380	0.9686	1.0768
Zn K	24.8	0.63	9.9	165.2	3.8	0.9567	0.9706	1.0600

6.4. Evaluation of antifungal effect of myco-synthesized nanoparticles

A. mali and *V. inaequalis* are dominant phytopathogens of apple (*Malus domestica* Borkh.) in the Union Territory of Jammu and Kashmir situated in the north of India. While all foliar and fruit diseases in this area are being effectively managed by adhering to the recommended spray schedule which includes different chemical fungicides like Myclobutanil, Bitertinol, Difenconazole, Hexaconazole, Carbendazim, Captan, Mancozeb, Chlorothalonil, Copper oxychloride and others, however, no attention has been paid to exploit the fungicidal potential of botanicals extracted from various medicinal plants although the botanicals are eco-friendly in contrast to chemical pesticides.

Metal oxide nanoparticles have recently been investigated as a possible class of anti-microbial agents because of their possible uses in the field of food safety based on the stability, size, shape, and surface characteristics (Sardul *et al.*, 2017; Joshi *et al.*, 2020; Rajwade *et al.*, 2020). The primary benefit of metal oxide nanoparticles is their nanoscale range, which offers notably appropriate forms to join with biological folks like bacteria, yeast, and fungus (El-Batal *et al.*, 2018). This crucial difference between ordinary organic and synthetic antimicrobial treatments and metal oxide nanoparticles

may reduce the likelihood of developing antimicrobial resistance (El-Batal *et al.*, 2017a; 2017b). The ability of nanoparticles to generate highly reactive oxygen species (OH^-, H_2O_2, and O_2^{2-}) on their surface has been interpreted as an antifungal characteristic, and are linked to irreversible damage to fungus (Hoseinpour and Ghaemi, 2018).

The current study aims to assess the efficacy of ZnO, MgO, and MnO_2 and combination nanoparticles in order to create antifungal material with greater efficiency, and safe antimicrobial effectiveness and good compatibility. Since the presence of three lattices may induce point defects to form into the crystals, changing the antifungal characteristics, the notion of combining three different types of metal oxide nanoparticles (Zn+Mg+Mn) in combination nanoparticles is very intriguing. In this study, different concentrations of nanoparticles making nineteen treatments (T1=ZnONP-Psc; T2=ZnONP-Ab; T3=ZnONP-Le; T4=MgONP-Psc; T5=MgONP-Ab; T6=MgONP-Le; T7=MnO_2NP-Psc; T8=MnO_2NP-Ab; T9=MnO_2NP-Le; T10=CNP-Psc; T11=CNP-Ab; T12=CNP-Le; T13=Zn-MS; T14=Mg-MS; T15=Mn-MS; T16=C-MS; T17=Control; T18=Mancozeb; T19=Flusilazole) were examined in order to determine the optimal dose that would have the most antifungal potential against two fungal pathogens of apple plant- *Alternaria mali* and *Venturia inaequalis* using poison food technique and spore germination method respectively. Leaves showing Alternaria leaf blotch and apple scab prominently are displayed in Figures 6.21.1, 6.21.2. After subsequent growth of fungi on culture medium treated with different nanoparticles and other fractions, parameters like radial growth of fungal mycelium and inhibition in spore germination were recorded and it was determined that antifungal activity rose in tandem with an increase in metal salt concentration. Our results are in line with earlier research on the antifungal properties of nanoparticles (Hranisavljevic *et al.*, 2002). Oxygen-dehydrogenase enzyme interaction rises with doped metal content in culture media, boosting antimicrobial activity (Sikong *et al.*, 2010).

When compared to single or pure nanoparticles, combination nanoparticles have superior antifungal properties (Rekha *et al.*, 2010; Sharma *et al.*, 2010). When compared to single nanoparticles, the doped or combination metal oxide nanoparticles show superior antimicrobial activity against fungi (Pugazhendhi *et al.*, 2018). Only a limited number of studies have been undertaken on the antifungal impact of combination nanoparticles, and this area has gotten marginal attention.

Figure 6.21.1: Leaves of apple plant showing symptoms of Alternaria leaf blotch caused by *A. mali*

Figure 6.21.2: Leaves with apple scab caused by *V. inaequalis*

Figure 6.21.3: Inoculation of PDA plates with *A. mali* for PFT

Nanoparticles have demonstrated promising antifungal properties against a range of phytopathogens including *A. mali* and *V. inaequalis* due to their tiny size, vast surface area, and high reactivity. The loss of cell wall and membrane integrity is one of the main ways that these nanoparticles prevent fungal development. It has been shown that metal oxide nanoparticles, physically stick to the fungal cell surface, resulting in pore development, deformation, and eventually intracellular component leakage (Raghupathi et al., 2011). The osmotic balance and integrity of fungal cells is disrupted which inhibits growth and causes cell death. Significant morphological abnormalities, such as decreased germ tube production and sporulation, have been seen in *Alternaria*

spp. hyphae and spores treated with ZnO and MgO nanoparticles (Ali *et al*., 2018; Kumar *et al*., 2021). Comparable effects have been noted in other fungi, suggesting similar underlying processes, despite the fact that *V. inaequalis* has received little direct investigation. It is well known that nanoparticles, particularly those based on transition metals like Zn and Mn, can cause oxidative stress in fungal cells by producing reactive oxygen species (ROS) such as hydrogen peroxide, hydroxyl radicals, and superoxide anions. Fungal metabolism and replication may be hampered by the ability of ROS to harm cellular lipids, proteins, and nucleic acids (Sirelkhatim *et al*., 2015). The oxidative destruction of fungal membranes and intracellular organelles is facilitated by the strong ROS-generating potential of ZnO and manganese dioxide (MnO_2) nanoparticles. As seen in ZnO nanoparticle treatments against *A. mali* and other plant diseases, this oxidative stress mechanism inhibits spore germination in addition to affecting active fungal cells (Ghazal *et al*., 2020). In addition to membrane disruption and oxidative damage, nanoparticles disturb intracellular processes by releasing metal ions that interact with vital cellular components. It is known that Zn^{2+} ions produced from ZnO nanoparticles, interact with phosphate backbones in DNA to prevent transcription and replication and attach to thiol groups in fungal enzymes, causing enzymatic inactivation (Padmavathy and Vijayaraghavan, 2008). Similarly, Mn and Mg nanoparticles may cause energy deficits in the fungal cells by altering ATPase activity and disrupting the ionic balance (Ghotekar et al., 2020).

6.4.1. Antifungal activity of nanoparticles against *Alternaria mali* by poison food technique (PFT)

The metal ion-based nanoparticles have broad-spectrum biocidal capabilities against a variety of bacteria, fungi, and viruses (Raghupathi *et al.* (2011). Prior research on nanoparticles has demonstrated that the larger the particles in size, the more effective they are at preventing the development of pathogens, involving both ROS generation and nanoparticle accumulation (Jan *et al.*, 2013). The nanoparticles of Zn, Mg, Mn and combination of the three, synthesized using extracts of *P. sajor caju, A. bisporus* and *L. edodes* were evaluated against *A. mali* using poison food technique by inoculating the poisoned media containing the nanoparticles with *A. mali* (Figure 6.21.3). The data collected as mycelial growth and percent inhibition rate of nanoparticles against test

fungus is given as the mean value of three replications in Tables 6.11.1 and 6.11.2 respectively. According to results, all the nanoparticles synthesized using three test fungi showed a considerable inhibition rate against *A. mali* with every increase in the concentration of nanoparticles from 0.10% to 0.30% (Figure 6.22) (Ahmad *et al.*, 2020). Figures 6.23.2 to 6.23.13 show the visible difference in inhibition of mycelial growth with the change in concentration of nanoparticles. Figure 6.23.1 illustrates the boxplots showing the effect of each treatment at three different concentrations of ZnONPs. In metal salt concentrations, the inhibition rate increased with an increase in levels of the metal salt concentrations from 300 ppm to 700 ppm respectively.

Table 6.11.1: Comparison of means (Mycelial growth) for PFT using Duncan test

Treatments	Concentration		
	0.10%	**0.20%**	**0.30%**
T1	12.333^{ghi}	7.917^{f}	1.333^{j}
T2	14.500^{d}	9.917^{cd}	2.853^{gh}
T3	14.333^{de}	9.500^{de}	3.067^{gh}
T4	22.250^{a}	14.500^{a}	10.910^{a}
T5	14.113^{def}	10.053^{cd}	4.250^{ef}
T6	16.437^{c}	10.380^{cd}	3.840^{fg}
T7	15.610^{c}	10.777^{c}	4.917^{de}
T8	22.863^{a}	15.357^{a}	11.253^{a}
T9	11.473^{ij}	6.380^{h}	0.970^{j}
T10	13.360^{efg}	7.327^{fg}	3.837^{fg}
T11	13.200^{fg}	8.860^{e}	3.787^{fg}
T12	22.613^{a}	14.897^{a}	10.970^{a}

	300 ppm	**500 ppm**	**700 ppm**
T13	10.743^{j}	5.943^{h}	0.900^{j}
T14	11.730^{hij}	6.680^{gh}	1.693^{ij}
T15	12.680^{gh}	7.680^{f}	2.583^{hi}
T16	20.500^{b}	12.000^{b}	9.170^{b}

T17	24.500	24.500	24.500
T18	6.700^{k}	6.700^{gh}	6.700^{c}
T19	5.710^{k}	5.710^{h}	5.710^{d}

(T1=ZnONP-Psc; T2=ZnONP-Ab; T3=ZnONP-Le; T4=MgONP-Psc; T5=MgONP-Ab; T6=MgONP-Le; T7=MnO_2NP-Psc; T8=MnO_2NP-Ab; T9=MnO_2NP-Le; T10=CNP-Psc; T11=CNP-Ab; T12=CNP-Le; T13=Zn-MS; T14=Mg-MS; T15=Mn-MS; T16=C-MS; T17=Control; T18=Mancozeb; T19=Flusilazole)

Mean of three replicates; ** The figures in parenthesis are statistically identical and arc Sin √%age transformed values. The means with different Letters as superscripts are significant ($P < 0.05$). The means with same letters or having common letter(s) are not significantly different.

Table 6.11.2: Comparison of means (Inhibition %) for PFT using Duncan test

Treatments	Concentration		
	0.10%	**0.20%**	**0.30%**
T1	49.668 (44.810^{cde})	67.678 (55.391^{d})	94.568 (76.763^{ab})
T2	40.180 (39.326^{gh})	59.525 (50.500^{fg})	88.360 (70.076^{c})
T3	41.482 (40.091^{fg})	61.213 (51.482^{ef})	87.490 (69.291^{cd})
T4	9.190 (17.575^{k})	40.823 (39.707^{i})	49.933 (44.962^{k})
T5	42.373 (40.609^{fg})	58.953 (50.161^{fg})	82.647 (65.427^{ef})
T6	32.915 (34.983^{i})	57.631 (49.390^{fg})	84.313 (66.729^{de})
T7	36.293 (37.037^{hi})	56.008 (48.452^{g})	79.943 (63.433^{fg})
T8	6.670 (14.889^{l})	37.320 (37.650^{i})	54.083 (47.347^{jk})
T9	53.180 (46.824^{bc})	73.948 (59.319^{ab})	96.043 (78.564^{a})
T10	45.110 (42.193^{ef})	70.094 (56.855^{cd})	84.340 (66.691^{de})
T11	46.117 (42.773^{ef})	63.826 (53.029^{e})	84.535 (66.860^{de})
T12	7.703 (16.067^{kl})	39.182 (38.747^{i})	55.207 (47.992^{j})

	300 ppm	**500 ppm**	**700 ppm**
T13	56.132 (48.525^{b})	75.745 (60.502^{ab})	96.327 (78.996^{a})

T14	52.118 (46.214^{bcd})	72.733 (58.523^{bc})	93.093 (74.856^{b})
T15	48.230 (43.985^{de})	68.648 (55.951^{d})	89.460 (71.090^{c})
T16	16.334 (23.786^{j})	51.002 (45.575^{h})	62.560 (52.278^{i})

T17	0.000 (0.000^{m})	0.000 (0.000^{j})	0.000 (0.000^{l})
T18	72.643 (58.470^{a})	72.643 (58.470^{bc})	72.643 (58.470^{h})
T19	76.683 (61.140)	76.683 (61.140^{a})	76.683 (61.140^{gh})

Mean of three replicates; ** The figures in parenthesis are statistically identical and arc Sin √%age transformed values. The means with different Letters as superscripts are significant (P < 0.05). The means with same letters or having common letter(s) are not significantly different.

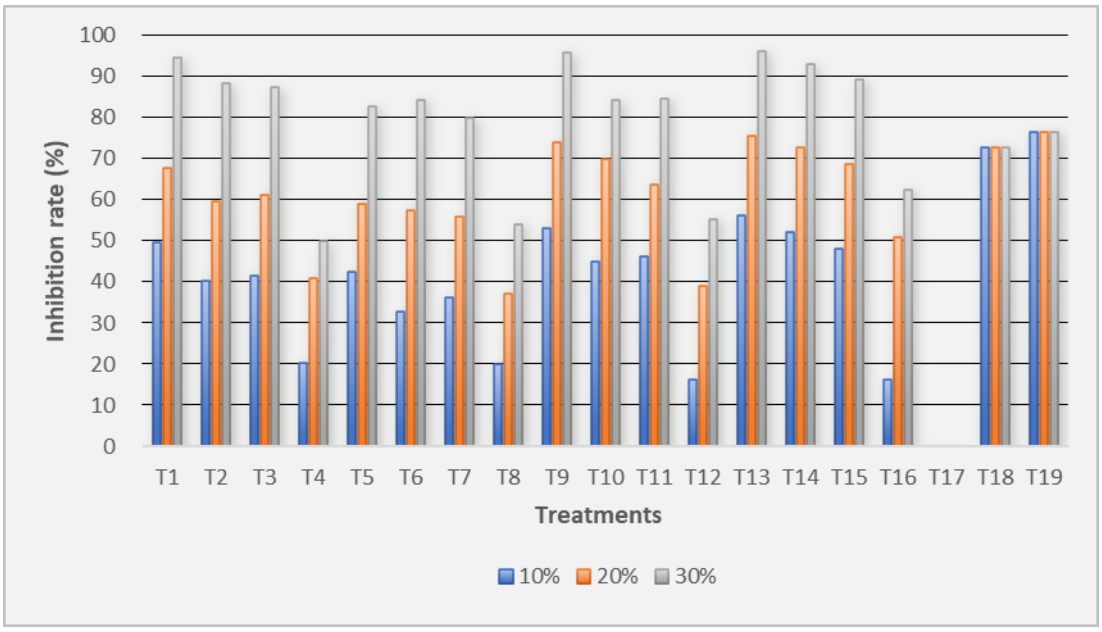

Figure 6.22: Percent inhibition rates of treatments against *A. mali* via PFT.

$$Inhibition\ rate\ (\%) = \frac{Mycelial\ growth\ in\ control - Mycelial\ growth\ in\ treatment}{Mycelial\ growth\ in\ control} \times 100$$

Colony diameters were assessed seven days post-inoculation. Three replicates of each experiment were used to determine the inhibition rates, which are shown as Means ± SD: For A. mali, inhibition rate of control = 0%.

Among the ZnONPs, maximum inhibition of 94.57% was shown by *ZnONP-Psc* at the highest concentration of 0.30% followed by ZnONPAb at 88.36% and ZnONPLe at 87.49% (minimum) at the same concentration. At 0.10%, inhibition was not much and maximum inhibition of 49.67% was shown by *ZnONP-Psc*. ZnONPs have been tested against *A. mali* (Ahmad *et al.*, 2020) and have shown considerable effects.

In MgONPs, comparatively lesser activity was seen and highest inhibition of 84.31% was shown by MgONPLe followed by MgONPAb (82.65%) and MgONPPsc (49.93%) at the highest concentration of 0.30%, while at 0.10%, the maximum inhibition of 42.37% was shown by MgONPAb. MgONPs have shown quite remarkable anti-microbial activity (though not better than the other nanoparticles) against *A. mali* (Immanuel and Iswareya, 2023).

In MnO_2NPs, MnO_2NP-Le was most active against the pathogenic fungus with 96.04% inhibition rate for *A. mali* at 0.30% concentration. This was followed by MnO_2NP-Psc with 79.94% inhibition rate at the same concentration. On the other hand, least effect was seen in case of MnO_2NP-Ab where inhibition rates ranged from 6.67-54.08% at 0.10% to 0.30% respectively. MnONPs have been evaluated on different species of *Alternaria* including *Alternaria solani* (Ingle and Gupta, 2021; Anar *et al.*, 2023), *Alternaria alternata* (Dhoble and Kulkarni, 2016), *Alternaria brassicae* (Gaba *et al.*, 2022), where they have shown considerable effects but have not been tested on *A. mali*.

CNP-Ab showed well-defined inhibition rate of 84.53% against *A. mali* at 0.30% as compared to CNP-Psc and CNP-Le with 84.34% and 55.21% inhibition rate respectively. At the lowest concentration of 0.10%, maximum inhibition was shown by CNP-Ab at 46.12% while the minimum inhibition came out in the treatment of CNP-Le at 7.70%. Ion solutions of Zn, Mg, Mn and combination were tested for their activity on the growth of mycelium of *A. mali*. The obtained results of CNPs are similar, and in some cases better, than previous results obtained with ZnO, MgO or MnO_2 nanoparticles individually. Some compounds found in most fungal materials have functional groups that are linked to their antimicrobial properties. These compounds

include primary metabolites like oxalic acid and secondary metabolites like anthraquinones, steroids, benzoic acid derivatives, quinolines, and sesquiterpenes and other terpenes (Alves *et al.*, 2012; Rahman *et al.*, 2021; Digra and Nonzom, 2023). In the metal ion solutions, at the lowest concentration (300 ppm), ZnMS showed 56.13% inhibition rate against *A. mali* which was the highest of all other metal salts at this concentration and increased as 96.33% in case of an increase in concentration to 700 ppm which was again the highest value at this concentration. On the other hand, the combination sample prepared by mixing Zn, Mg and Mn metal salts showed the minimum inhibition rate as compared to other metal salts which ranged from 16.33% at 300 ppm to 62.56% at 700 ppm. In case of the fungicides used, inhibition rate varied from 72.64% in mancozeb and 76.68% in flusilazole respectively. The control plates showed zero inhibition with the maximum growth of the pathogenic fungus (Kumar *et al.*, 2019).

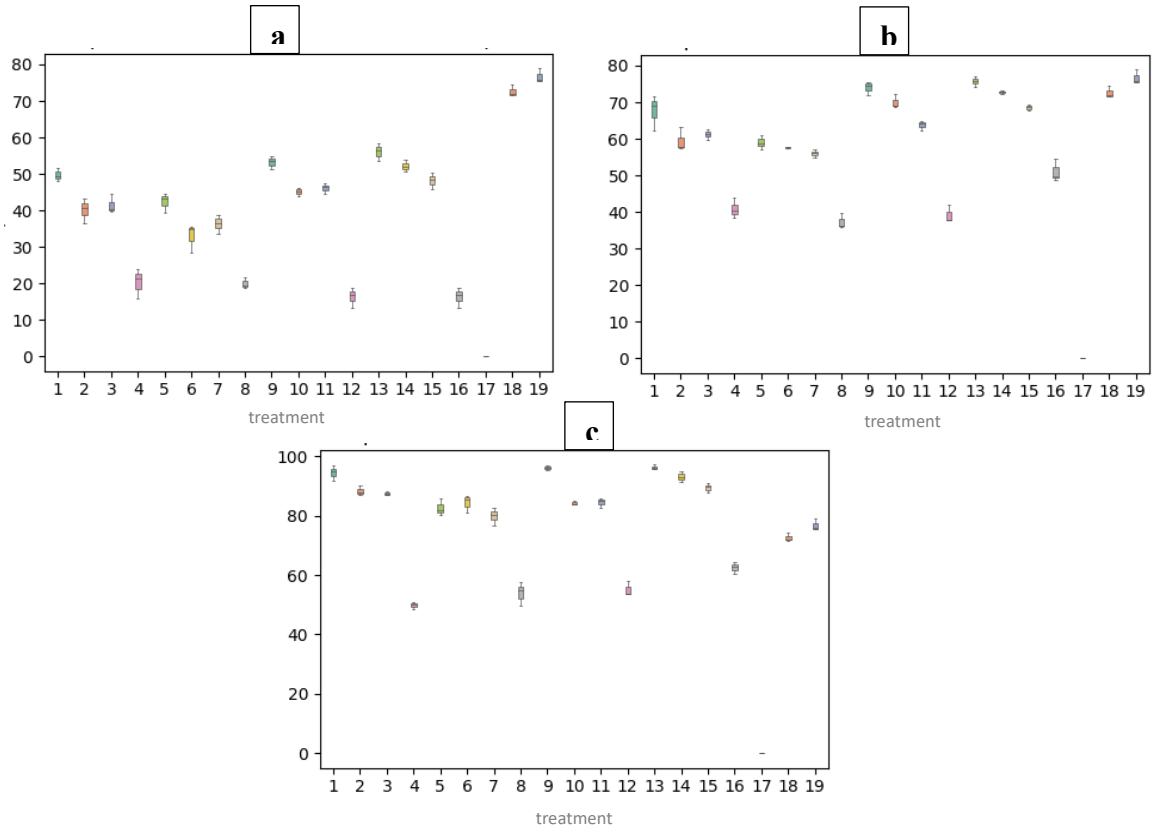

Figure 6.23.1: Boxplots showing effect of each treatment (against *A. mali*) at a) 0.10%; b) 0.20%; c) 0.30%

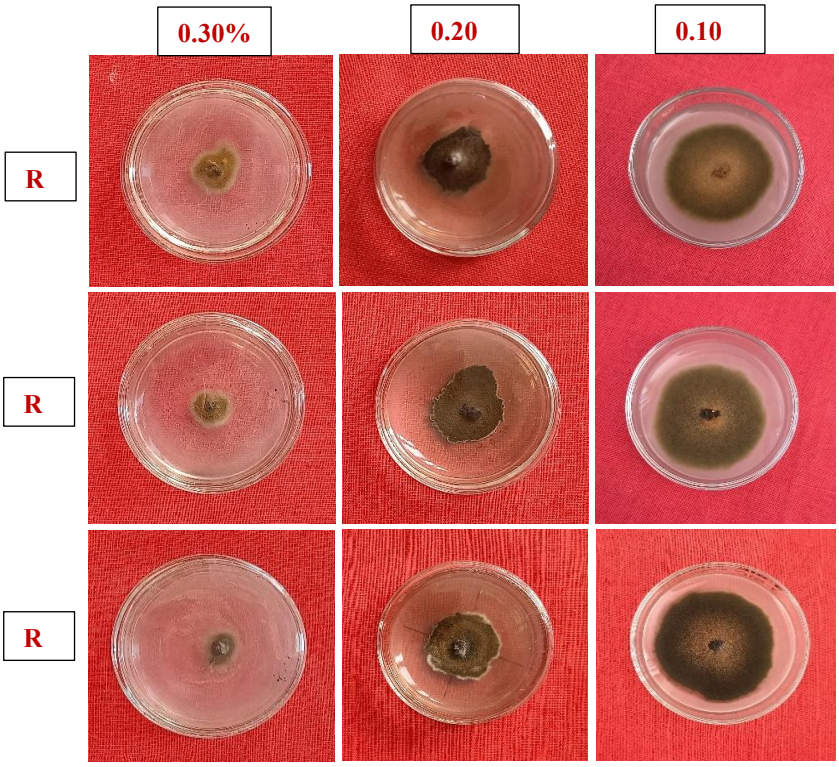

Figure 6.23.2: Assay of antifungal activity of ZnONP-Psc against *A. mali* at 0.30%; 0.20%; 0.10% (with 3 replicates)

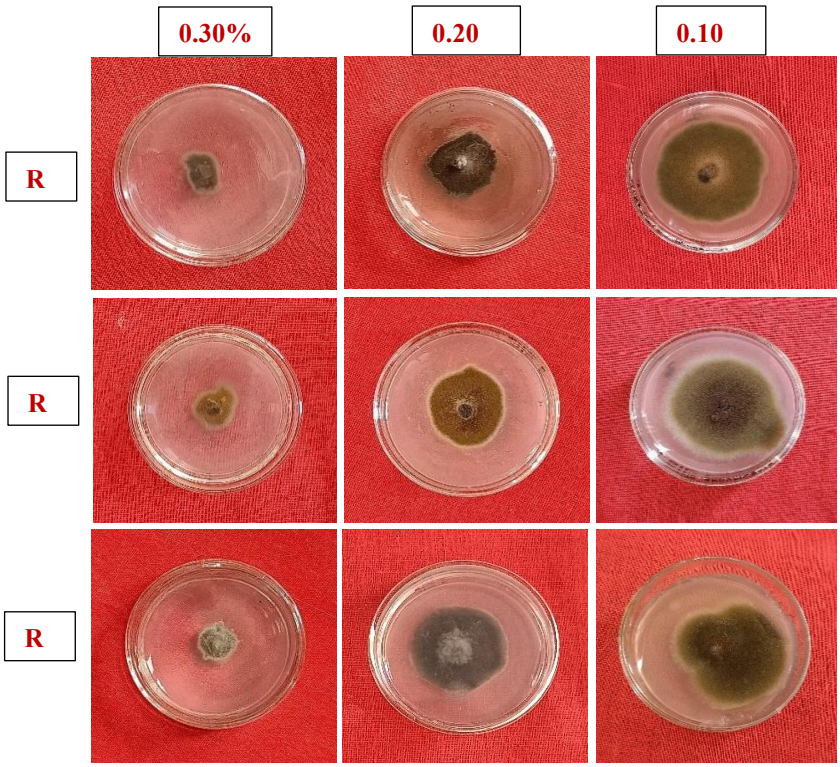

Figure 6.23.3: Assay of antifungal activity of ZnONP-Ab against *A. mali* at 0.30%; 0.20%; 0.10% (with 3 replicates)

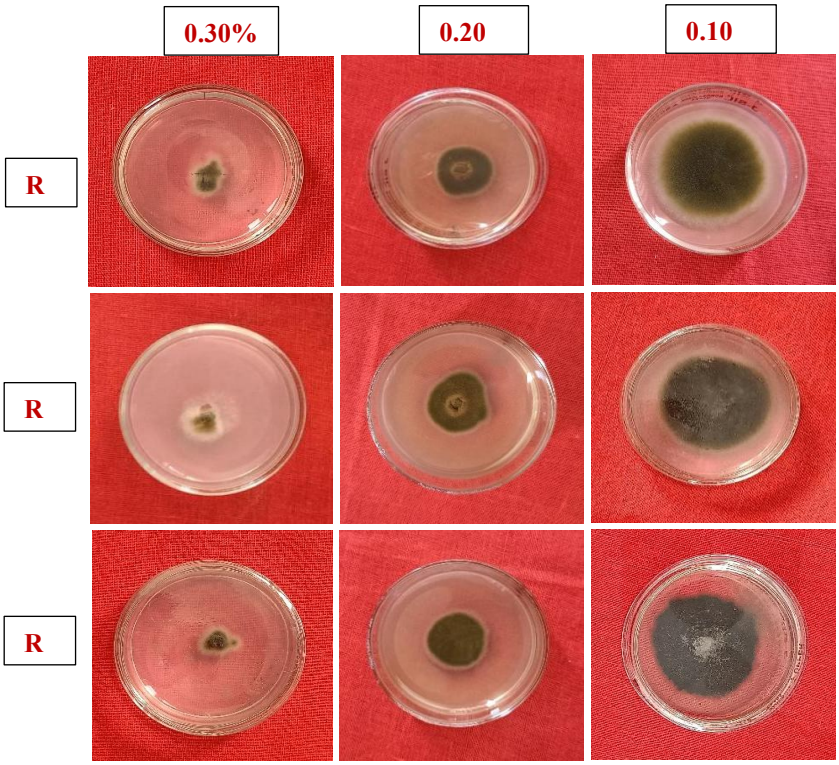

Figure 6.23.4: Assay of antifungal activity of ZnONP-Le against *A. mali* at 0.30%; 0.20%; 0.10% (with 3 replicates)

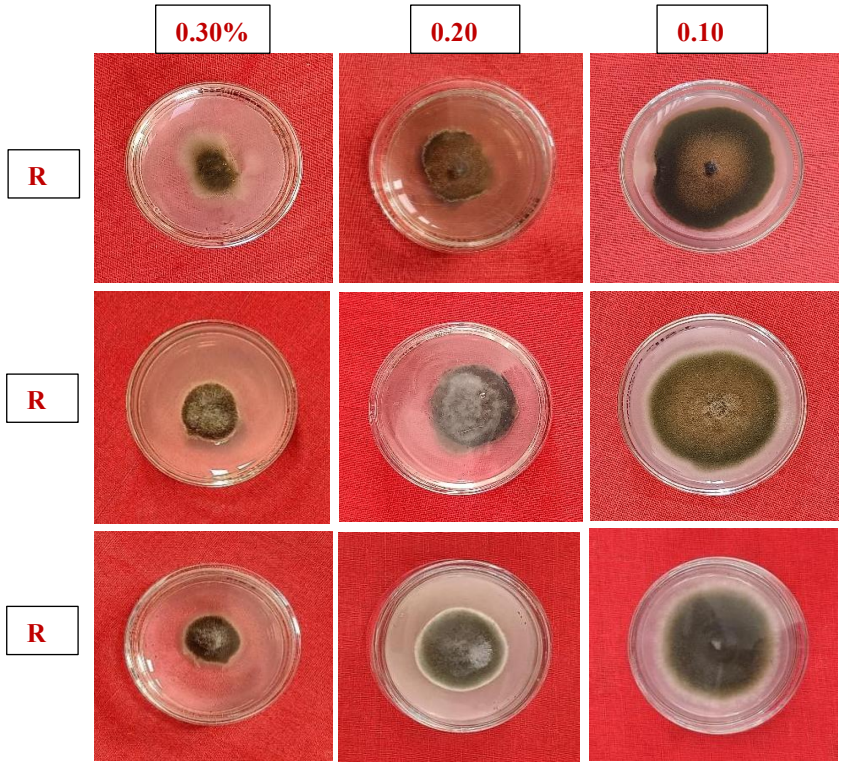

Figure 6.23.5: Assay of antifungal activity of MgONP-Psc against *A. mali* at 0.30%; 0.20%; 0.10% (with 3 replicates)

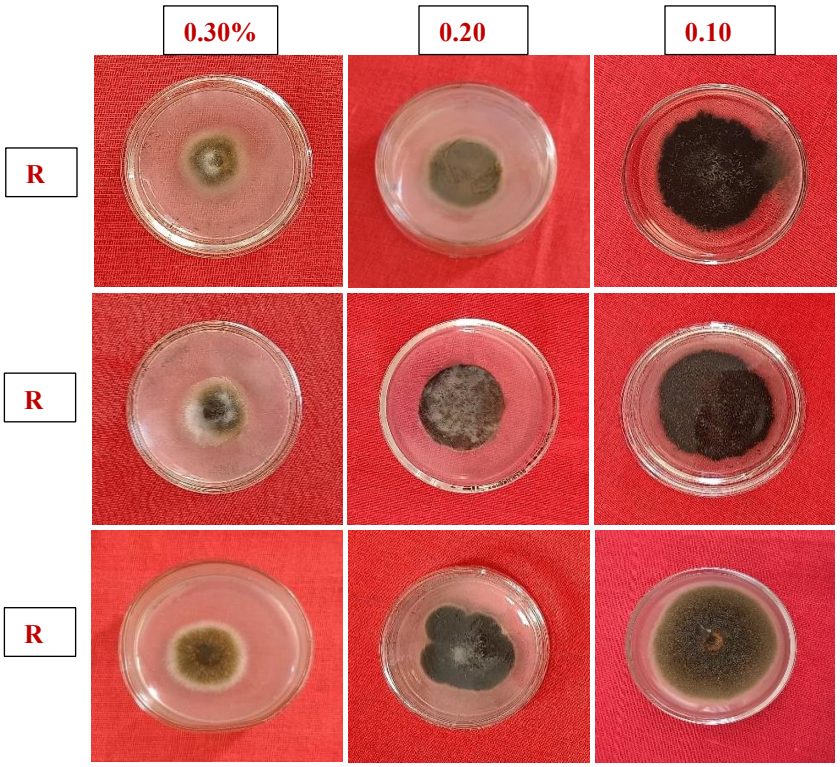

Figure 6.23.6: Assay of antifungal activity of MgONP-Ab against *A. mali* at 0.30%; 0.20%; 0.10% (with 3 replicates)

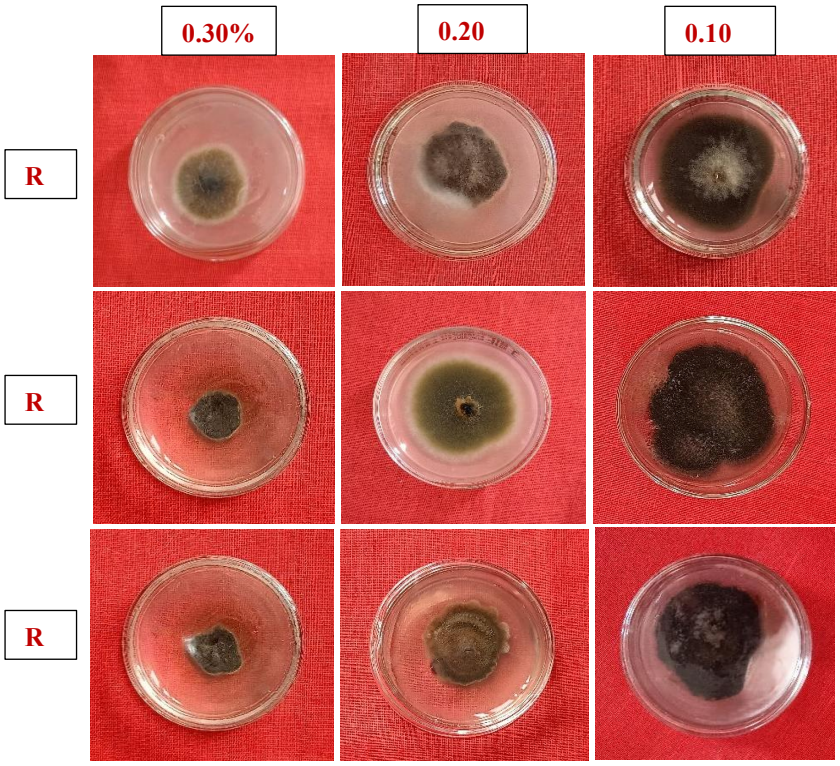

Figure 6.23.7: Assay of antifungal activity of MgONP-Le against *A. mali* at 0.30%; 0.20%; 0.10% (with 3 replicates)

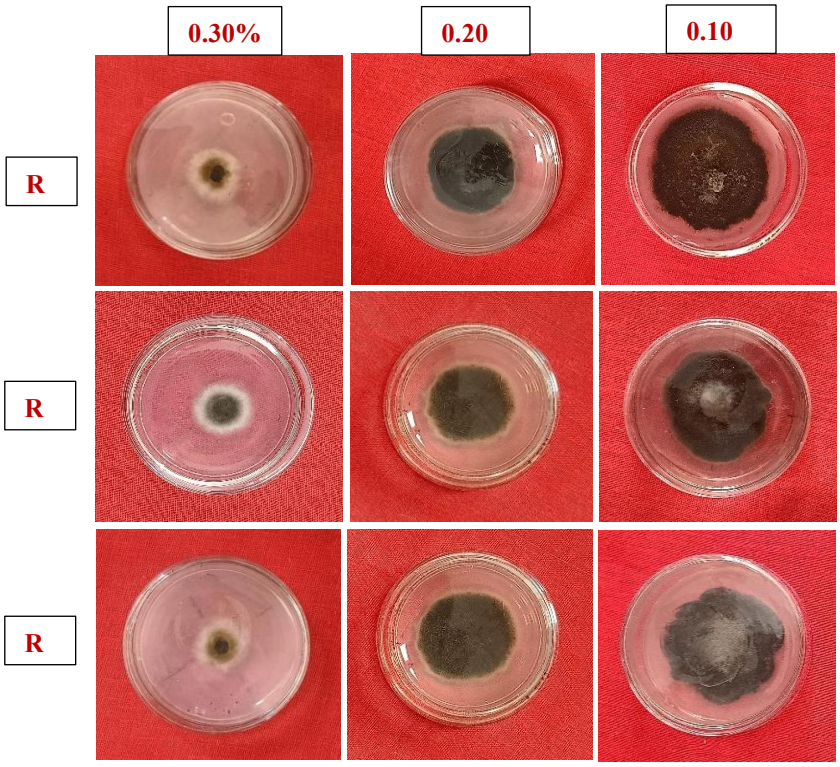

Figure 6.23.8: Assay of antifungal activity of MnO_2NP-Psc against *A. mali* at 0.30%; 0.20%; 0.10% (with 3 replicates)

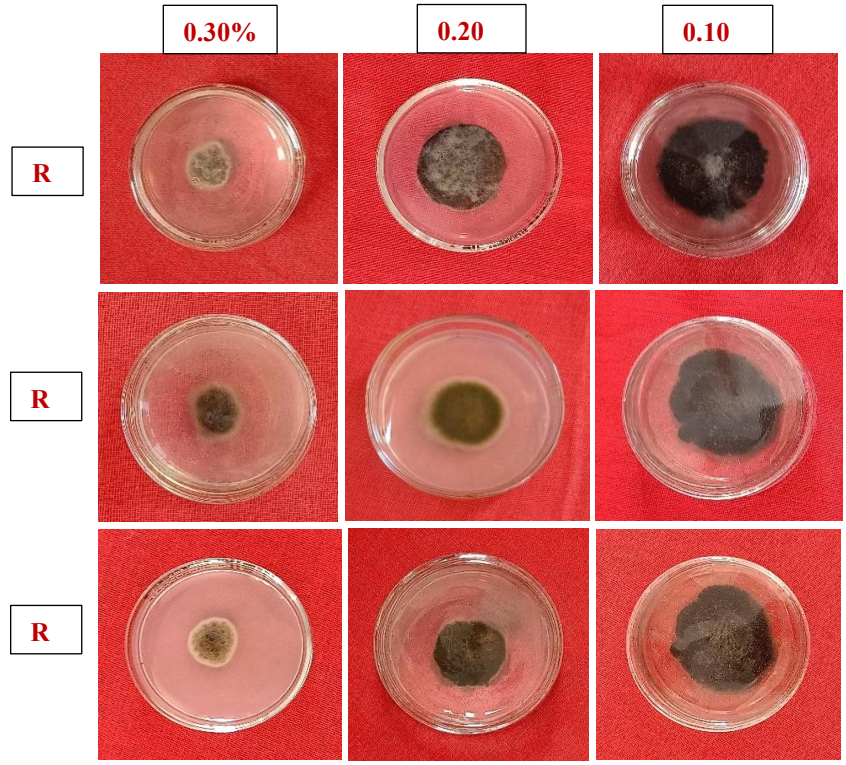

Figure 6.23.9: Assay of antifungal activity of MnO_2NP-Ab against *A. mali* at 0.30%; 0.20%; 0.10% (with 3 replicates)

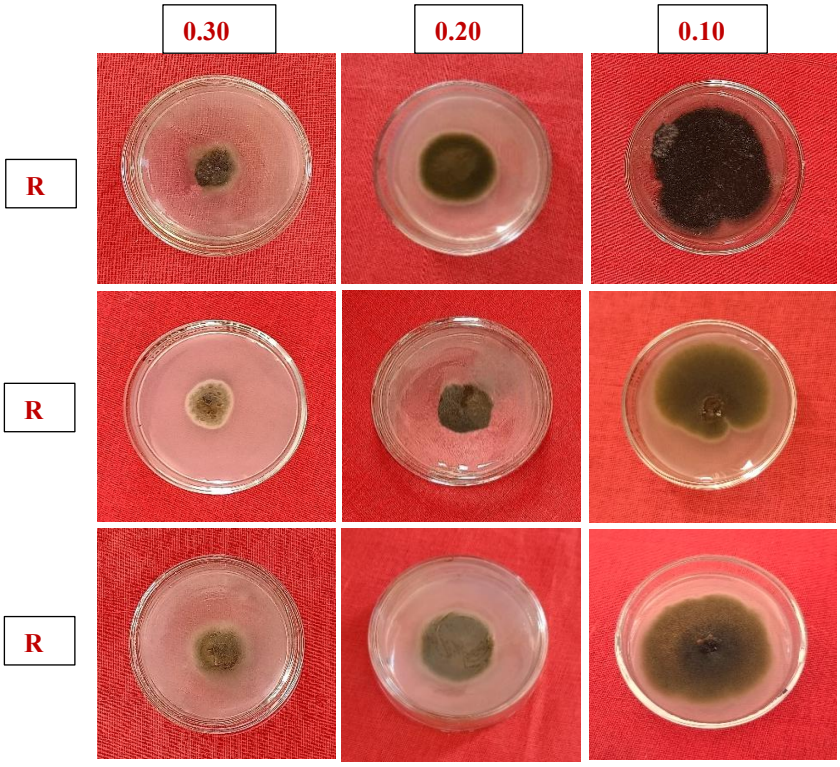

Figure 6.23.10: Assay of antifungal activity of MnO_2NP-Le against *A. mali* at 0.30%; 0.20%; 0.10% (with 3 replicates)

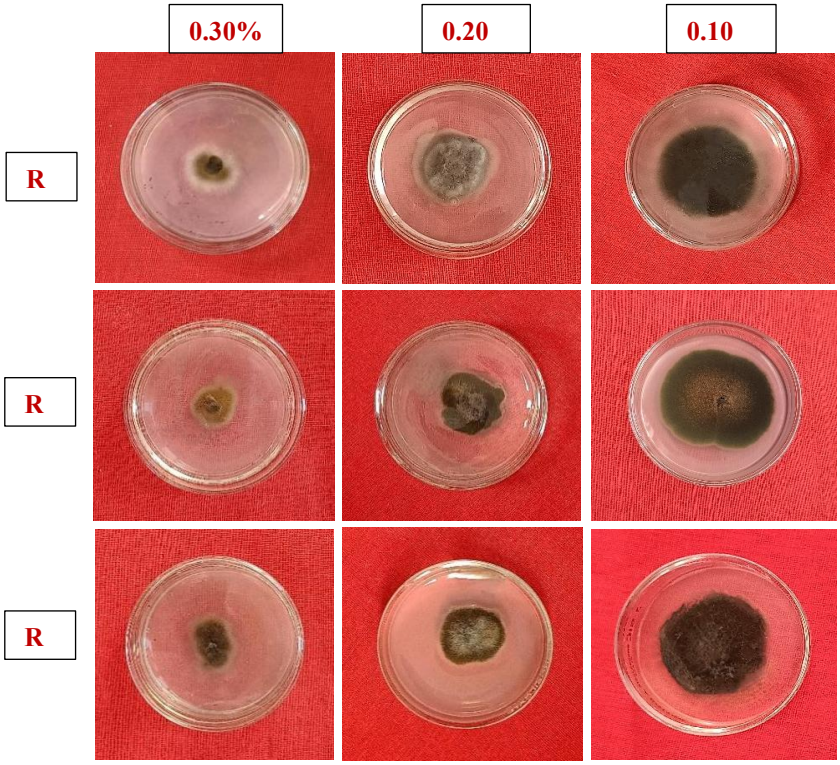

Figure 6.23.11: Assay of antifungal activity of CNP-Psc against *A. mali* at 0.30%; 0.20%; 0.10% (with 3 replicates)

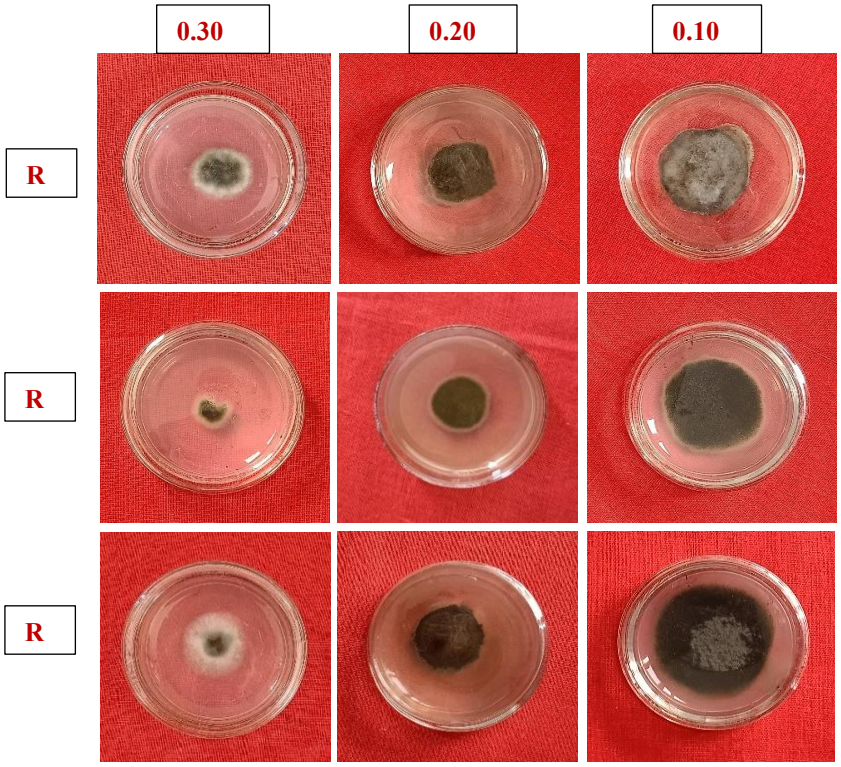

Figure 6.23.12: Assay of antifungal activity of CNP-Ab against *A. mali* at 0.30%; 0.20%; 0.10% (with 3 replicates)

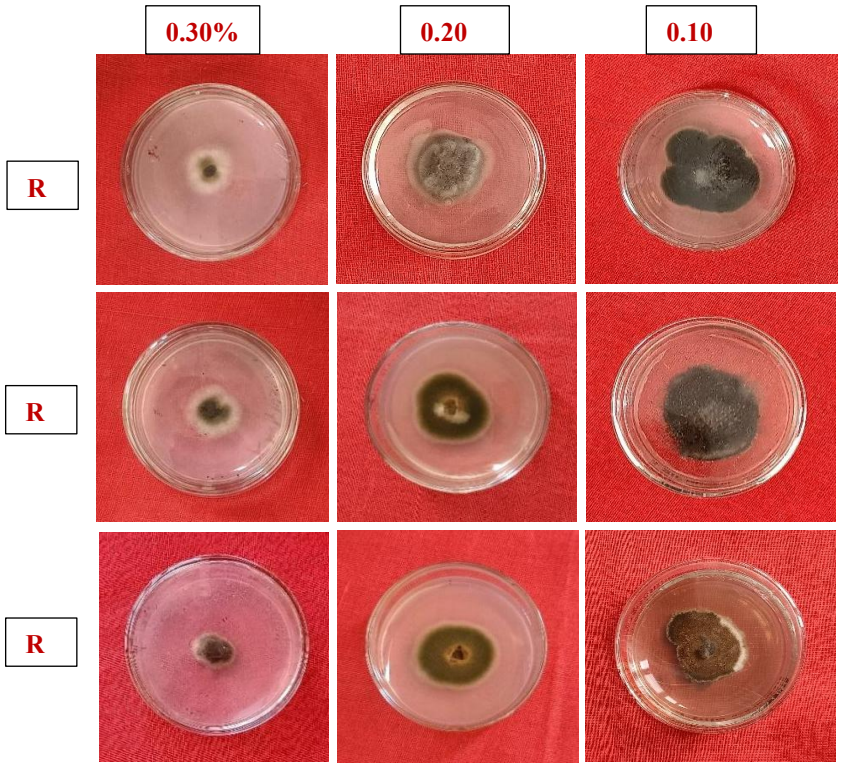

Figure 6.23.13: Assay of antifungal activity of CNP-Le against *A. mali* at 0.30%; 0.20%; 0.10% (with 3 replicates)

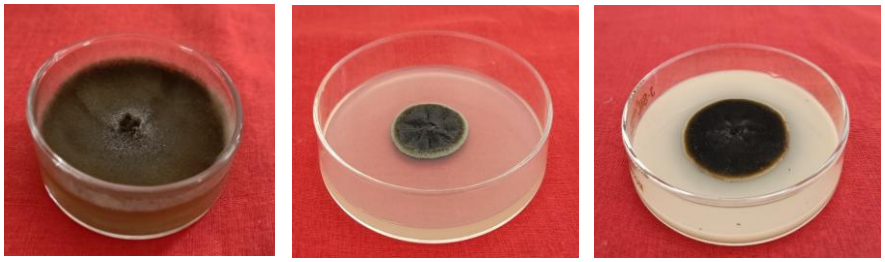

Figure 6.23.14: Assay of antifungal activity of a) Control b) Flusilazole–treated plate c) Mancozeb–treated plate

6.4.2. Antifungal activity against *Venturia inaequalis* by spore germination test (SGT)

The synthesized nanoparticles with considerable antifungal activity were further screened by estimating their spore germination inhibition activity after measuring their Percent Spore Germination Inhibition (PSGI) value against the isolated spores of *Venturia inaequalis* (Sutton *et al.*, 2000; dos Santos *et al*., 2024). The study conducted at different concentrations of 0.10%, 0.20% and 0.30% to check more accurate activity by measuring the germination and inhibition percentages of the pathogenic fungus (*V. inaequalis*) of apple plant is specified in Tables 6.12.1 and 6.12.2. The study found that spore germination was inhibited by varying concentrations of ZnO, MgO, MnO_2, and combination nanoparticles, but that the inhibition increased as the quantity of nanoparticles rose (Balint *et al.*, 2014; Talie *et al.*, 2020). However, the highest dose of 0.30% resulted in the greatest decrease in spore germination. It was followed by the nanoparticle concentrations of 0.20% and 0.10%. The CNPs at the highest concentration of 0.30% were shown to be the most efficient in suppressing spore germination, followed by ZnONPs, MnO_2NPs and MgONPs (Figures 6.24, 6.25).

Table 6.12.1: Comparison of means (Germination %) for SGT using Duncan test

Treatments	Concentration		
	0.10%	0.20%	0.30%
T1	68.500 (55.862^{b})	56.223 (48.575^{cd})	37.633 (37.839^{cd})
T2	67.413 (55.192^{bc})	54.423 (47.539^{d})	35.930 (36.827^{d})
T3	63.313 (52.723^{c})	59.147 (50.271^{b})	39.450 (38.909^{c})

T4	45.853 (42.619^{e})	38.467 (38.329^{h})	30.677 (33.632^{e})
T5	75.427 (60.293^{a})	58.447 (49.864^{bc})	49.563 (44.750^{a})
T6	72.947 (58.664^{a})	62.443 (52.209^{a})	44.660 (41.933^{b})
T7	75.280 (60.194^{a})	59.753 (50.624^{b})	49.253 (44.572^{a})
T8	63.837 (53.041^{c})	55.600 (48.216^{d})	37.947 (38.024^{cd})
T9	65.693 (54.147^{bc})	39.840 (39.137^{gh})	29.963 (33.187^{e})
T10	65.967 (54.319^{bc})	43.850 (41.466^{ef})	30.960 (33.808^{e})
T11	54.780 (47.745^{d})	34.613 (36.033^{i})	24.787 (29.855^{f})
T12	47.080 (43.326^{e})	30.540 (33.545^{j})	29.687 (33.010^{e})

	300 ppm	**500 ppm**	**700 ppm**
T13	65.280 (53.898^{bc})	45.323 (42.316^{e})	23.363 (28.877^{f})
T14	63.313 (52.721^{c})	41.503 (40.108^{fg})	23.577 (29.034^{f})
T15	67.040 (55.030^{bc})	45.533 (42.435^{e})	23.623 (29.041^{f})
T16	46.353 (42.908^{e})	30.190 (33.318^{j})	25.757 (30.492^{f})

T17	2.313 (8.735^{f})	79.510 (63.099)	79.510 (63.099)
T18	1.513 (7.004^{f})	2.313 (8.735^{k})	2.313 (8.735^{g})
T19	79.510 (63.099)	1.513 (7.004^{k})	1.513 (7.004^{g})

Mean of three replicates; ** The figures in parenthesis are statistically identical and arc Sin √%age transformed values. The means with different Letters as superscripts are significant ($P < 0.05$). The means with same letters or having common letter(s) are not significantly different.

Table 6.12.2: Comparison of means (Inhibition %) for SGT using Duncan test

Treatments	**Concentration**		
	0.10%	**0.20%**	**0.30%**

T1	13.813 (21.746^{e})	29.273 (32.751^{gh})	52.662 (46.526^{de})
T2	15.183 (22.898^{de})	31.543 (34.159^{g})	54.810 (47.761^{d})
T3	20.347 (26.790^{d})	25.570 (30.354^{i})	50.377 (45.216^{e})
T4	42.360 (40.603^{b})	51.607 (45.921^{d})	61.413 (51.598^{c})
T5	5.080 (12.231^{g})	26.447 (30.925^{hi})	37.637 (37.838^{g})
T6	8.240 (16.629^{f})	21.430 (27.533^{j})	43.843 (41.463^{f})
T7	5.299 (13.053^{fg})	24.830 (29.882^{i})	38.030 (38.071^{g})
T8	19.733 (26.358^{d})	30.027 (33.209^{gh})	52.253 (46.292^{de})
T9	17.353 (24.599^{de})	49.900 (44.943^{d})	62.297 (52.121^{c})
T10	17.023 (24.323^{de})	44.803 (42.012^{ef})	61.053 (51.386^{c})
T11	31.130 (33.907^{c})	56.463 (48.717^{c})	68.823 (56.061^{b})
T12	40.790 (39.693^{b})	61.567 (51.691^{b})	62.677 (52.345^{c})

	300 ppm	**500 ppm**	**700 ppm**
T13	17.877 (24.996^{de})	42.987 (40.967^{f})	70.553 (57.174^{b})
T14	20.350 (26.808^{d})	47.777 (43.725^{de})	70.363 (57.028^{b})
T15	15.737 (23.024^{de})	42.757 (40.833^{f})	70.267 (56.998^{b})
T16	41.690 (40.215^{b})	62.060 (51.984^{b})	67.623 (55.321^{b})

T17	0.000 (0.000^{h})	0.000 (0.000^{k})	0.000 (0.000^{h})
T18	97.096 (80.200^{a})	97.096 (80.200^{a})	97.096 (80.200^{a})
T19	98.097 (82.140^{a})	98.097 (82.140^{a})	98.097 (82.140^{a})

Mean of three replicates; ** The figures in parenthesis are statistically identical and arc Sin √%age transformed values. The means with different Letters as superscripts are significant ($P < 0.05$). The means with same letters or having common letter(s) are not significantly different.

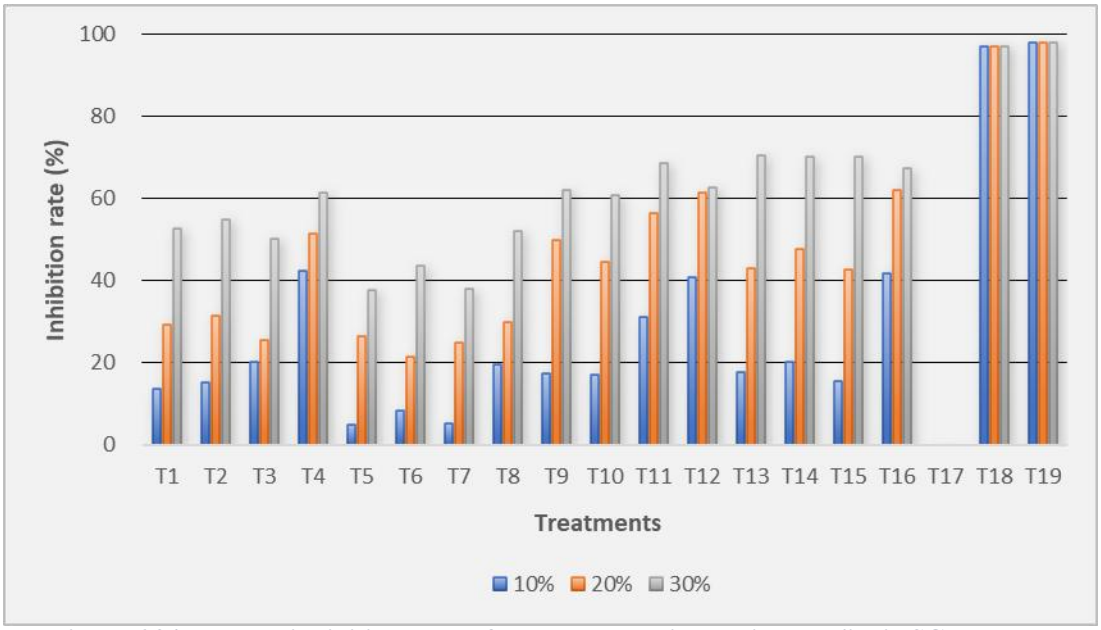

Figure 6.24: Percent inhibition rates of treatments against *V. inaequalis* via SGT.

$$Inhibition\ rate\ (\%) = \frac{Mycelial\ growth\ in\ control - Mycelial\ growth\ in\ treatment}{Mycelial\ growth\ in\ control} \times 100$$

Colony diameters were assessed seven days post-inoculation. Three replicates of each experiment were used to determine the inhibition rates, which are shown as Means ± SD: For A. mali, inhibition rate of control = 0%.

In ZnONPs, the decrease in spore germination varies from 13.81% in ZnONP-Psc (at 0.10%) to 54.81% in ZnONP-Ab (at 0.30%).

In case of MgONPs, spores of *V. inaequalis* were inhibited mostly by MgONP-Psc at 61.41% and MgONP-Le at 43.84%. Overall, MgONPs did not show any major suppression of spore germination when compared to the other nanoparticles.

The Percent Spore germination inhibition (PSGI) assessment report of MnO_2NPs further demonstrates that spores of *V. inaequalis* were inhibited mostly by MnO_2NP-Le (62.30%) followed by MnO_2NP-Ab (52.25%) and MnO_2NP-Psc (38.03%).

The highest inhibition appeared at the highest concentration of CNPs where CNP-Ab showed the maximum inhibition of 68.82% followed by CNP-Le (62.68%)

and CNP-Psc (61.05%). Additionally, there was a dose-dependent impact of metal salt concentrations on the inhibition of spore germination.

The maximum inhibition was shown by ZnMS (70.55%) at the highest concentraton of 700 ppm followed by MgMS (70.36%), MnMS (70.27%) and CMS (67.62%) at the same concentration. The fungicides suppressed the spore germination with higher percentages of 97.10% and 98.10% in mancozeb and flusilazole respectively. There was no or very little reduction in spore germination in the untreated control. This investigation has been conducted for the first time in Kashmir, India and suggests that the fungicidal impact of nanoparticle concentrations on *V. inaequalis* may be the cause of the influence on spore germination.

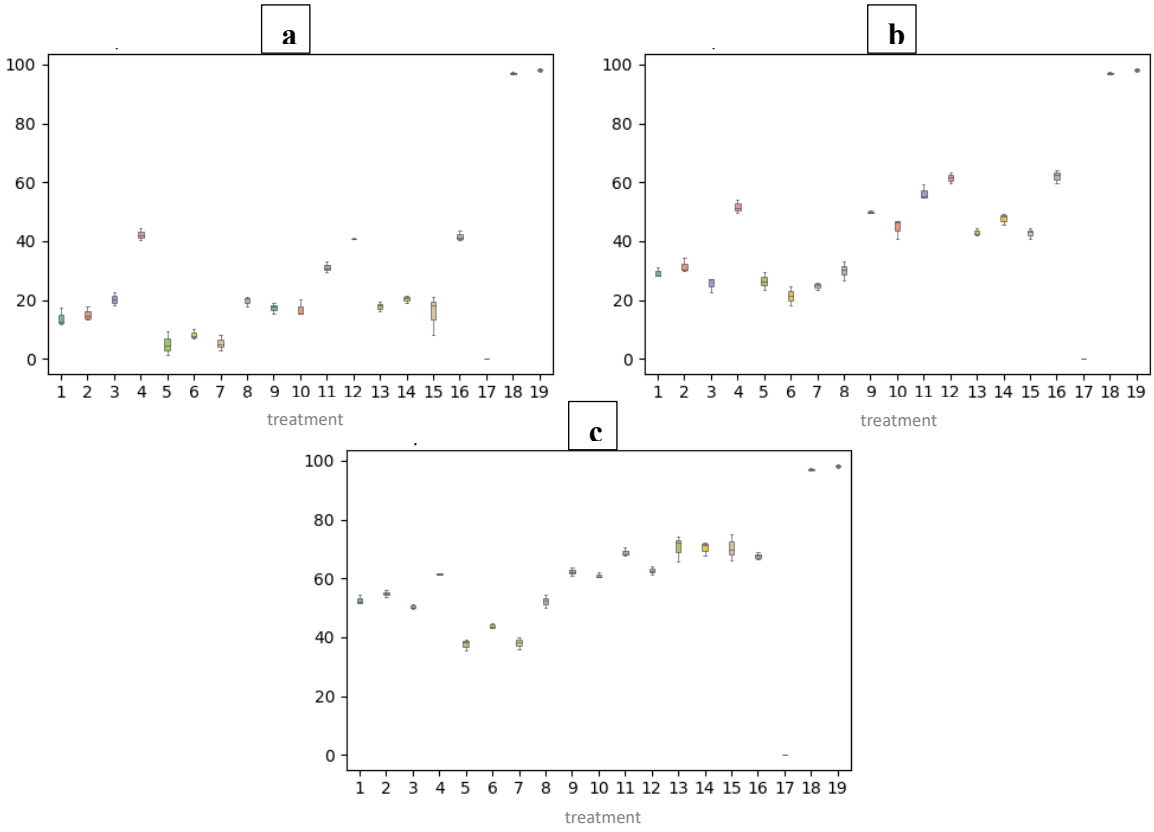

Figure 6.25: Boxplots showing effect of each treatment (against *V. inaequalis*) at a) 0.10%; b) 0.20%; c) 0.30%

6.5. Evaluation of nanoparticles against apple plant parameters

Nanoparticles have special physicochemical qualities that are not seen in bulk particles of the same material because of their incredibly tiny size, structure, and surface features (Prachi *et al.*, 2014). Moreover, nanoparticles enter and accumulate in plant tissues, but their penetration and accumulation is less than their ionic forms (Ebbs *et al.*, 2016; Zhang and Su, 2024). In this study, nanoparticles of ZnO, MgO, MnO_2 and Zn+Mg+Mn when sprayed on apple plants caused a considerable improvement in the gas exchange parameters as well as chlorophyll content of apple plant leaves (Elmer and White, 2016; Zaragosa *et al*., 2024). Figure 6.26.1 shows the working concentrations of nanoparticles, metal salts and controls ready prepared for spray, and Figure 6.26.2 shows the nanoparticles being sprayed on experimental plants in the field.

Figure 6.26.1: Concentrations of nanoparticles and metal salts prepared for spray

Figure 6.26.2: Working concentrations of the nanoparticles being sprayed onto the apple plants.

6.5.1. Gas exchange parameters

The nanoparticles prepared in the concentrations of 0.10%, 0.20% and 0.30%, when sprayed on apple plants (tagged accordingly) showed minimal or prominent effect on the plant parameters with a dose dependent response and the parameter being evaluated (Zhang *et al.*, 2015). In many plants, there has been decreased biomass, root tip shrinkage, and vacuolated or collapsed root epidermal and cortical cells, and nanoparticles have been evaluated (Lin and Xing, 2008). Figure 6.27 shows the ongoing evaluation of gas exchange parameters of apple plants in the experimental field using IRGA.

Figure 6.27: Measurement of gas exchange parameters using IRGA

6.5.1.1. Stomatal conductance (gs)

Stomatal conductance of the apple plants varied at a dose dependent response. With an upsurge in dosage from 0.10% to 0.30%, the value of gs increased significantly. Similarly, in case of metal salt applications, value of gs increased with each increase in metal salt concentration.

After 6 hours: After 6 hours of spray, stomatal conductance was significantly higher in plants sprayed with the highest concentration of 0.30%. The highest value of gs was shown by CNPs followed by MnO_2NPs and ZnONPs and the minimum in comparison was of MgONPs. Among CNPs, the highest value of gs was of CNP-Ab followed by CNP-Psc. In case of metal salt treated plants, gs was lower than the the nanoparticle-treated plants. With the increase in concentration of metal salts, the value of gs

decreased. The value of gs decreased with the increase in concentration from 300 ppm to 700 ppm in all four metal salt treatments of Zn, Mg, Mn and combination of the three respectively. In mancozeb and flusilazole treated plants, value of gs (0.055 mol m^{-2} s^{-1} and 0.050 mol m^{-2} s^{-1} respectively) was higher than concentration 1 (0.10%) treated plants but lesser that the concentration 3 (0.30%) treated plants but comparable with that of the concentration 2 (0.20%) treated plants, but lesser than the gs of plants treated with concentration 3. In control plant, value of gs came out to be 0.065 mol m^{-2} s^{-1} (Table 6.13) (Thomas *et al.*, 2008; Thunugunta *et al.*, 2018; Chachei *et al.*, 2025). The efficacy of three different concentrations of treatments is shown in Figures 6.28.1 and 6.28.2.

Table 6.13: Effect of different concentrations of treatments on stomatal conductance (mol m-2 s-1) of apple plant (6 hours)

Treatments	Concentration		
	0.10%	**0.20%**	**0.30%**
T1	0.005^{a}	0.050^{a}	0.135^{abc}
T2	0.015^{a}	0.035^{a}	0.140^{ab}
T3	0.050^{a}	0.040^{a}	0.140^{ab}
T4	0.015^{a}	0.035^{a}	0.130^{abc}
T5	0.005^{a}	0.035^{a}	0.095^{abcd}
T6	0.010^{a}	0.025^{a}	0.075^{bcde}
T7	0.010^{a}	0.045^{a}	0.125^{abc}
T8	0.020^{a}	0.065^{a}	0.140^{ab}
T9	0.020^{a}	0.070^{a}	0.155^{a}
T10	0.025^{a}	0.065^{a}	0.145^{ab}
T11	0.030^{a}	0.070^{a}	0.145^{ab}
T12	0.015^{a}	0.035^{a}	0.135^{abc}

	300 ppm	**500 ppm**	**700 ppm**
T13	0.050^{a}	0.035^{a}	0.015^{e}
T14	0.055^{a}	0.015^{a}	0.020^{e}

T15	0.050[a]	0.035[a]	0.015[e]
T16	0.040[a]	0.025[a]	0.015[e]
T17	**0.065[a]**	**0.065[a]**	**0.065[cde]**
T18	0.055[a]	0.055[a]	0.055[de]
T19	0.050[a]	0.050[a]	0.050[de]

Note: The means with different Letters as superscripts are significant (P < 0.05).

The means with same letters or having common letter(s) are not significantly different.

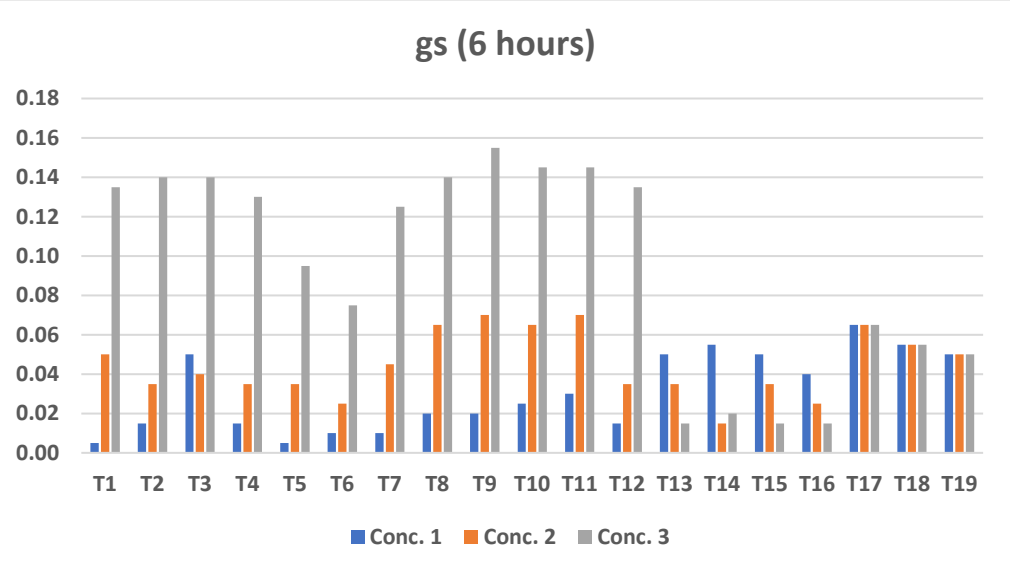

Figure 6.28.1: Graph showing the effect of three concentrations of treatments on stomatal conductance after 6 hours of spray

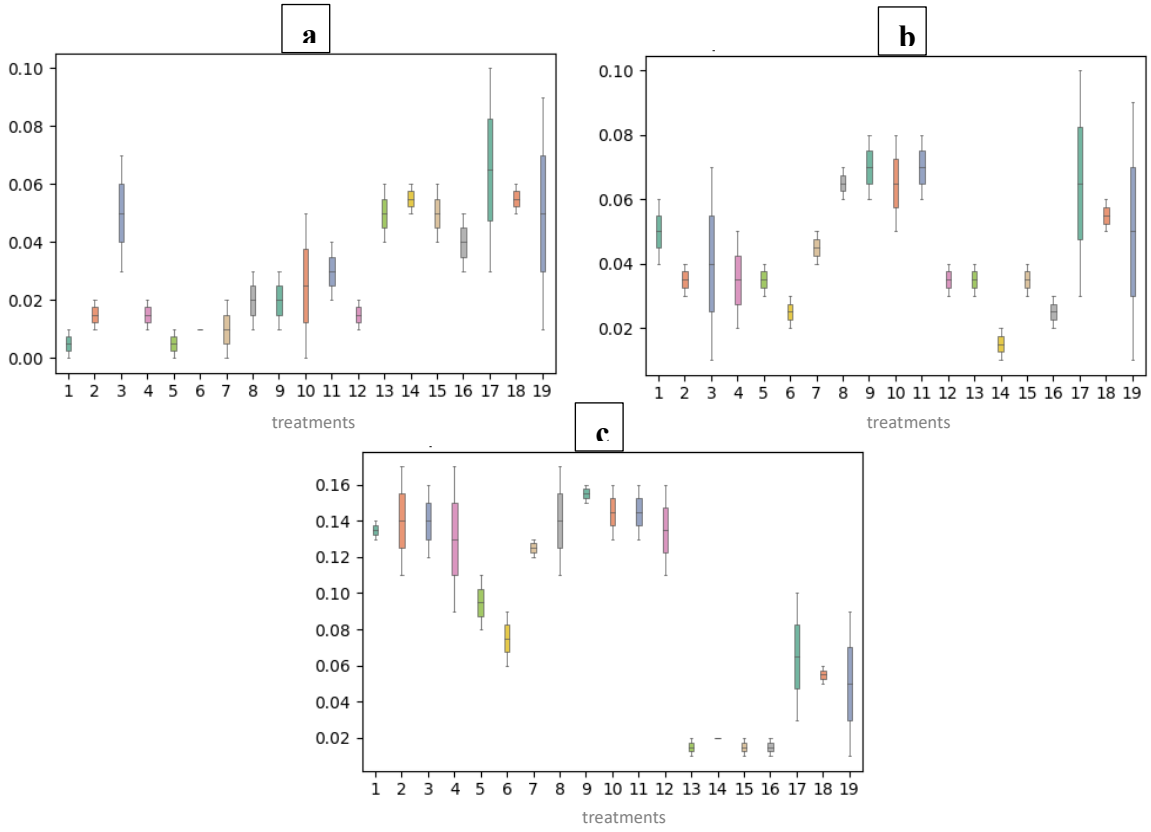

Figure 6.28.2: Boxplots showing the effect of three concentrations of treatments on stomatal conductance after 6 hours at: a) 0.10%; b) 0.20%; c) 0.30%

After 24 hours: After 24 hours of spray, the value of gs in the treated plants did not change much with the highest value in ZnONPs followed by MnO_2NPs, MgONPs and CNPs respectively. Among ZnONPs, highest value was shown by ZnONp-Ab treated plants. In treatments with metal salt concentrations, gs was lower as compared to the nanoparticle-treated plants. With the increase in concentration of metal salts, the value of gs decreased. In ZnMS, highest to lowest values of gs were achieved at 300 ppm, 500 ppm, and 700 ppm concentration respectively (Figure 6.29.1). Similar results were obtained in MgMS, MnMS and CMS where gs decreased with the increase in the ppm concentration of particular metal salts. In treatments of mancozeb and flusiazole, gs came out to be 0.010 mol m^{-2} s^{-1}. Plant kept as control showed the value of gs as 0.065 mol m^{-2} s^{-1} (Table 6.14; Figure 6.29.2) (Thomas *et al.*, 2008; Thunugunta *et al.*, 2018; Chachei *et al*., 2025).

Table 6.14: Effect of different concentrations of treatments on stomatal conductance (mol m-2 s-1) of apple plant (24 hours)

Treatments	Concentration		
	0.10%	**0.20%**	**0.30%**
T1	0.015^{b}	0.040^{cd}	0.130^{ab}
T2	0.015^{b}	0.040^{cd}	0.135^{a}
T3	0.030^{b}	0.065^{ab}	0.125^{abc}
T4	0.025^{b}	0.050^{bcd}	0.145^{a}
T5	0.020^{b}	0.045^{bcd}	0.110^{abc}
T6	0.025^{b}	0.045^{bcd}	0.090^{bcd}
T7	0.015^{b}	0.045^{bcd}	0.105^{abc}
T8	0.020^{b}	0.075^{a}	0.140^{a}
T9	0.020^{b}	0.060^{abc}	0.140^{a}
T10	0.020^{b}	0.075^{a}	0.125^{abc}
T11	0.015^{b}	0.060^{abc}	0.115^{abc}
T12	0.015^{b}	0.040^{cd}	0.085^{cd}
	300 ppm	**500 ppm**	**700 ppm**
T13	0.080^{a}	0.045^{bcd}	0.020^{e}
T14	0.070^{a}	0.050^{bcd}	0.020^{e}
T15	0.090^{a}	0.040^{cd}	0.020^{e}
T16	0.070^{a}	0.030^{de}	0.015^{e}
T17	**0.065^{a}**	**0.065^{ab}**	**0.065^{d}**
T18	0.010^{b}	0.010^{e}	0.010^{e}
T19	0.010^{b}	0.010^{e}	0.010^{e}

Note: The means with different Letters as superscripts are significant ($P < 0.05$). The means with same letters or having common letter(s) are not significantly different.

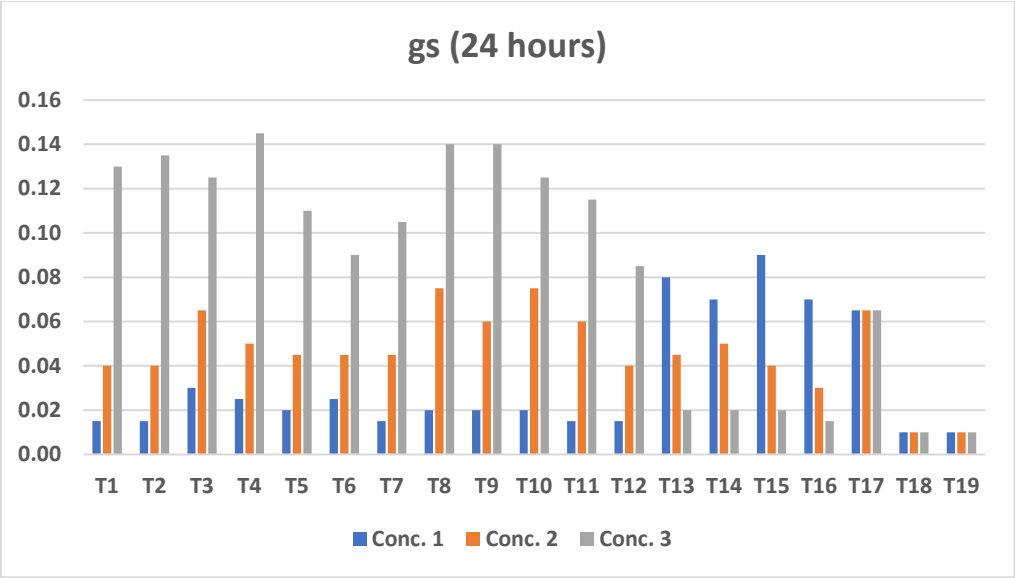

Figure 6.29.1: Graph showing the effect of three concentrations of treatments on stomatal conductance after 24 hours of spray

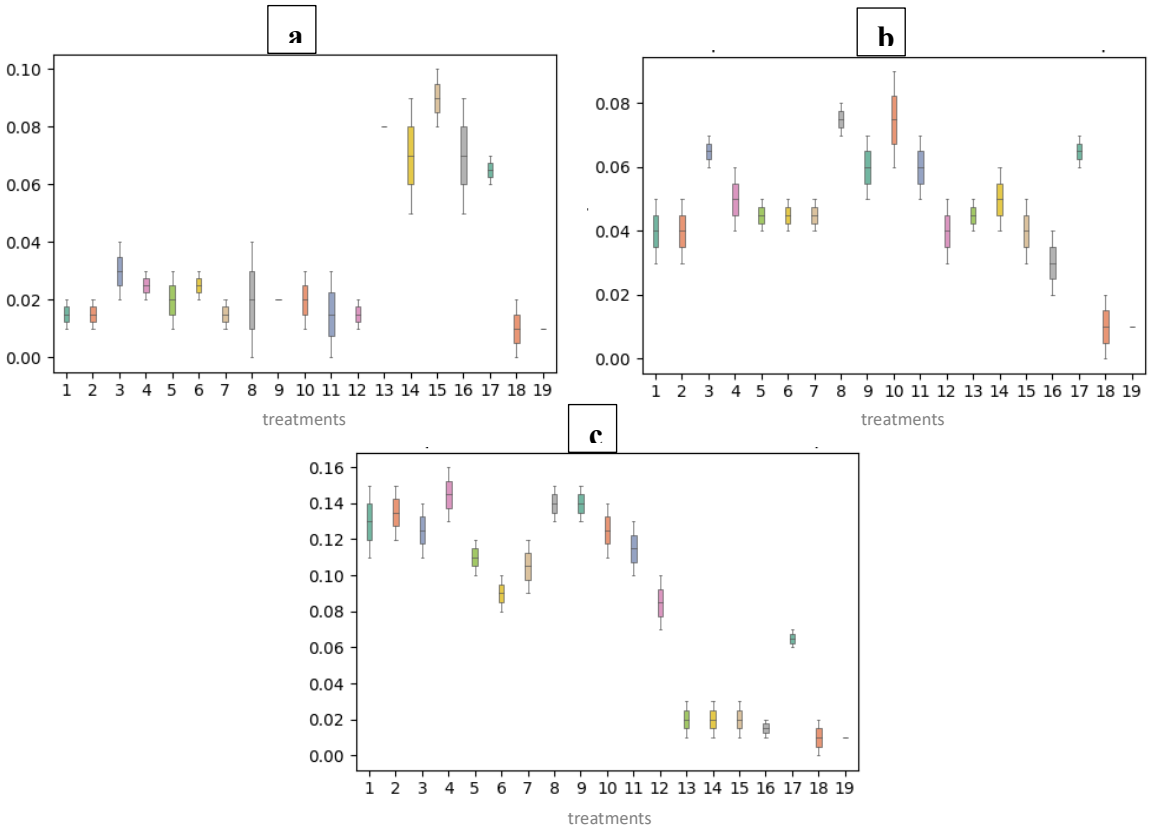

Figure 6.29.2: Boxplots showing the effect of three concentrations of treatments on stomatal conductance after 24 hours at: a) 0.10%; b) 0.20%; c) 0.30%

6.5.1.2. Net photosynthesis (Pn)

The nanoparticle concentrations sprayed exhibited variations in net photosynthetic rates. The overall Pn rates were significantly higher in CNP treated plants as compared to ZnONPs, MgONPs and MnO_2NPs, irrespective of the fungal extract used for synthesis. Also, with the increase in concentration in each of the treatments, Pn increased as well (Xu *et al.*, 2018).

After 6 hours: Among the nanoparticle concentrations sprayed, CNPs, ZnONPs had comparatively higher Pn rates than MnO_2NPs and MgONPs (Table 6.15). At 0.10%, higher Pn rate was shown by CNP-treated plants and among the CNPs, CNP-Ab (2020 µmol m^{-2} s^{-1}) showed the highest efficacy. From the assessment of 0.20% treated plants, it was depicted that CNPs at this concentration lead to an increase in Pn as compared to the other treatments of nanoparticles. Among CNPs, the highest value of Pn was shown by CNP-Ab (4.75 µmol m^{-2} s^{-1}) at this concentration. At the highest concentration of 0.30%, CNPs showed the highest value of Pn and among CNPs, CNP-Psc outstood the evaluation by showing the highest value of Pn (12.10 µmol m^{-2} s^{-1}) followed by ZnONP-Psc (13.25 µmol m^{-2} s^{-1}). In the metal salt treated plants, there was a reduction in the values of Pn with every increase in concentration from 300 ppm to 700 ppm. Among the metal salts, highest value of Pn was shown by MgMS, followed by MnMS and then ZnMS and CMS at lower doses. Plants treated with mancozeb and flusilazole showed Pn values at 5.00 µmol m^{-2} s^{-1} and 5.30 µmol m^{-2} s^{-1} respectively. In control, Pn came out to be 11.50 µmol m^{-2} s^{-1} (Figures 6.30.1 and 6.30.2) (Thunugunta *et al.*, 2018; Sharma *et al*., 2025).

Table 6.15: Effect of different concentrations of treatments on net photosynthesis (µmol m^{-2} s^{-1}) of apple plant (6 hours)

Treatments	Concentration		
	0.10%	**0.20%**	**0.30%**
T1	1.350^{def}	5.500^{a}	13.250^{a}
T2	0.900^{ef}	3.850^{abcde}	8.300^{cd}
T3	2.050^{def}	2.750^{def}	7.650^{cdef}
T4	2.500^{cd}	3.850^{abcde}	7.350^{cdef}
T5	2.200^{de}	2.350^{def}	6.850^{def}

T6	0.550^{f}	3.000^{cdef}	6.250^{def}
T7	2.550^{cd}	5.000^{ab}	10.000^{bc}
T8	1.800^{def}	3.600^{bcde}	8.200^{cd}
T9	1.600^{def}	2.850^{def}	6.350^{def}
T10	1.900^{def}	4.150^{abcd}	12.100^{ab}
T11	2.200^{de}	4.750^{abc}	11.150^{ab}
T12	2.150^{de}	4.050^{abcde}	7.900^{cde}

	300 ppm	**500 ppm**	**700 ppm**
T13	2.450^{cd}	1.150^{f}	0.800^{g}
T14	3.800^{bc}	2.250^{ef}	1.550^{g}
T15	2.500^{cd}	1.300^{f}	1.150^{g}
T16	2.450^{cd}	1.600^{f}	1.250^{g}

T17	11.500	11.500	11.500^{ab}
T18	5.000^{ab}	5.000^{ab}	5.000^{f}
T19	5.300^{a}	5.300^{ab}	5.300^{ef}

Note: The means with different Letters as superscripts are significant ($P < 0.05$). The means with same letters or having common letter(s) are not significantly different.

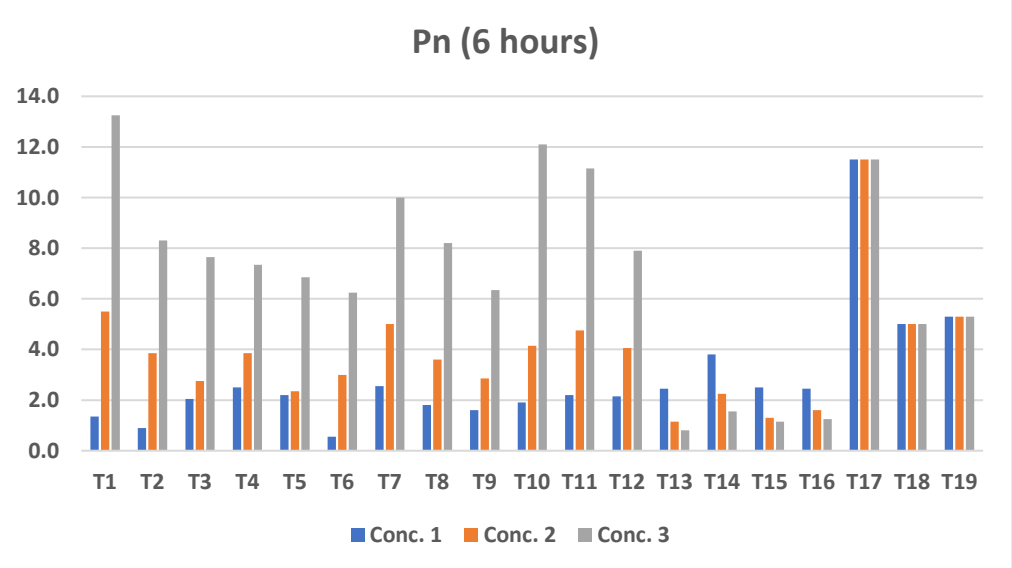

Figure 6.30.1: Graph showing the effect of three concentrations of treatments on net photosynthesis after 6 hours of spray

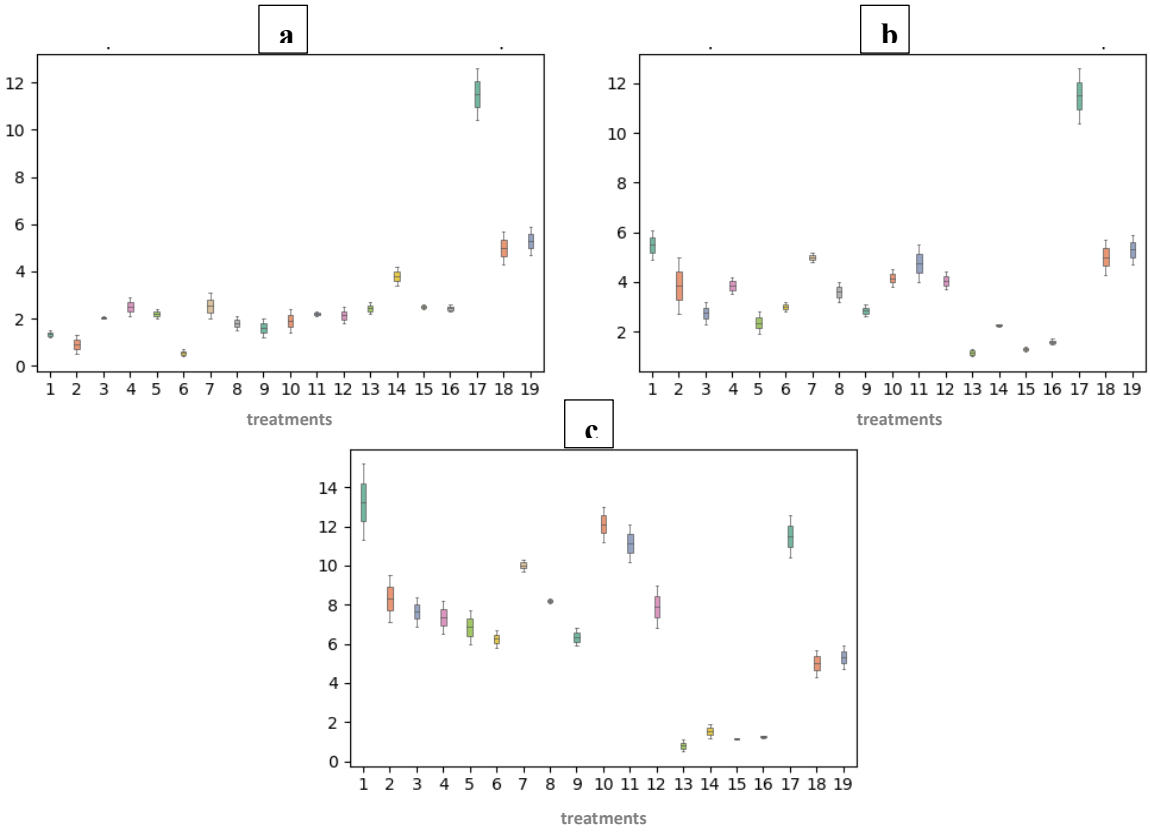

Figure 6.30.2: Boxplots showing the effect of three concentrations of treatments on net photosynthesis after 6 hours at: a) 0.10%; b) 0.20%; c) 0.30%

After 24 hours: There was not a prominent change in the values after 24 hours of spray. Again, the values of Pn came higher at highest concentration of the nanoparticles (0.30%). With an increase in concentration, the values of Pn increased accordingly. In ZnONPs, Pn was higher than that of MgONPs but lower than MnO_2NPs and CNP. Among ZnONPs, highest values were shown by ZnONP-Psc. In MgONPs, highest Pn was in MgONP-Psc treated plants. Similiarly, in case of MnO_2NPs, MnO_2NP-Psc had the highest Pn value. CNPs in general had a remarkable effect on the Pn of apple plant leaves. CNPPsc had the highest value of Pn (27.35 µmol m^{-2} s^{-1}) even higher than that of the control plant (11.10 µmol m^{-2} s^{-1}). Mancozeb and flusilazole treated plants showed Pn of 3.65 µmol m^{-2} s^{-1} and 3.95 µmol m^{-2} s^{-1} respectively (Table 6.16; Figures 6.31.1 and 6.31.2) (Thunugunta *et al.*, 2018; Khundi *et al.*, 2025).

Table 6.16: Effect of different concentrations of treatments on net photosynthesis (µmol m^{-2} s^{-1}) of apple plant (24 hours)

Treatments	Concentration		
	0.10%	0.20%	0.30%
T1	2.350^{cde}	6.250^{a}	13.100^{a}
T2	1.850^{e}	5.950^{ab}	11.200^{ab}
T3	2.350^{cde}	3.350^{ghi}	8.350^{ab}
T4	3.650^{a}	5.400^{abc}	9.900^{ab}
T5	2.900^{bc}	3.350^{ghi}	9.800^{ab}
T6	2.050^{de}	3.300^{ghi}	8.250^{ab}
T7	3.600^{a}	6.300^{a}	14.500^{a}
T8	2.500^{cde}	4.400^{cdefg}	11.950^{ab}
T9	2.900^{bc}	4.100^{defg}	10.200^{ab}
T10	2.800^{c}	4.900^{bcde}	27.350
T11	2.800^{c}	5.050^{bcd}	13.150^{a}
T12	2.550^{cd}	4.650^{cdef}	10.950^{ab}

	300 ppm	500 ppm	700 ppm
T13	2.950^{bc}	1.850^{j}	1.250^{b}
T14	3.800^{a}	2.700^{hij}	1.150^{b}
T15	2.800^{c}	2.350^{ij}	1.100^{b}
T16	3.500^{ab}	2.300^{ij}	1.150^{b}

T17	11.100	11.100	11.100^{ab}
T18	3.650^{a}	3.650^{fgh}	3.650^{ab}
T19	3.950^{a}	3.950^{efg}	3.950^{ab}

Note: The means with different Letters as superscripts are significant ($P < 0.05$).

The means with same letters or having common letter(s) are not significantly different.

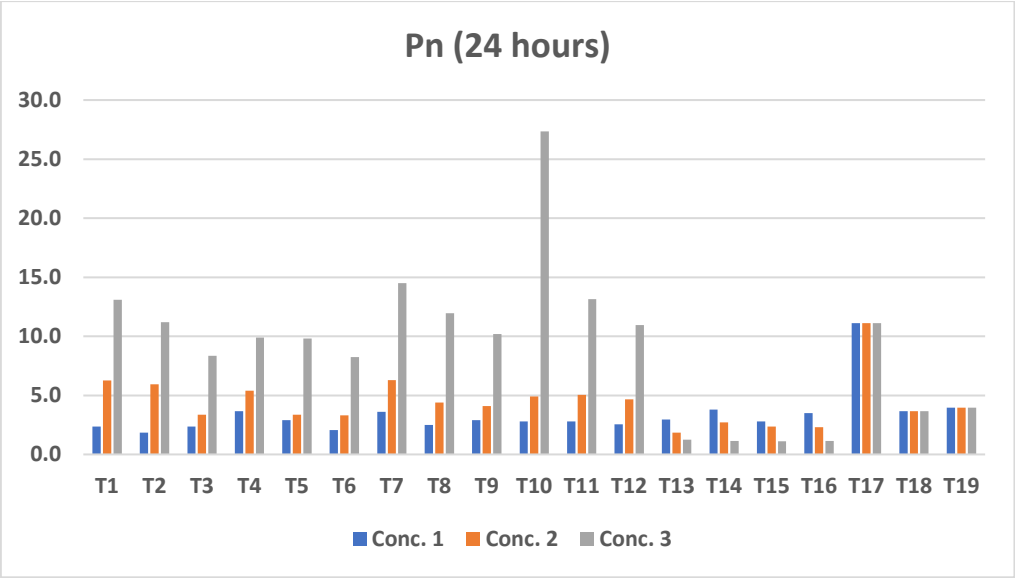

Figure 6.31.1: Graph showing the effect of three concentrations of treatments on net photosynthesis after 24 hours of spray

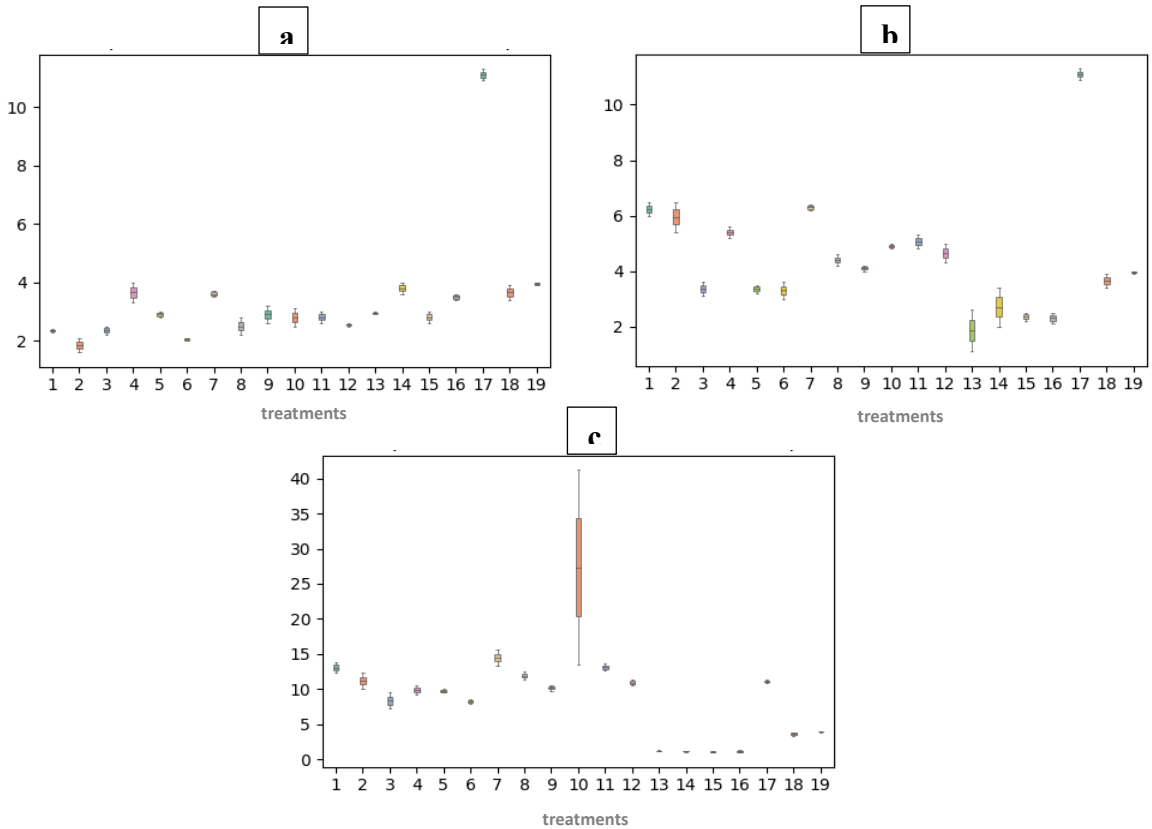

Figure 6.31.2: Boxplots showing the effect of three concentrations of treatments on net photosynthesis after 24 hours at: a) 0.10%; b) 0.20%; c) 0.30%

6.5.1.3. Intercellular CO_2 (Ci)

The intercellular CO_2 concentration varied between nanoparticle treatments. It also varied because of the fungal extract used. In general, significantly higher Ci was found in ZnONPs. As the concentration of nanoparticles augmented from 0.10% to 0.30%, the values of Ci decreased significantly. Similarly, in case of metal salts used, increase in concentration from 300 ppm to 700 ppm led to a decrease in Ci. Overall, all the nanoparticle treatments showed increased Ci as compared to the controls used.

After 6 hours:

ZnONPs showed the highest values of Ci among all the treatments used. At 0.10% of ZnONPs, ZnONP-Psc had the highest value of 9999.0 µmol mol^{-1}. MgONPs also showed higher values of Ci, highest being in MgONP-Psc in the value of 9498.50 µmol mol^{-1}. Similarly, MnO_2NPs and CNPs had positive impact on Ci in apple plants but at lower doses. At 0.10%, MnO_2NP-Le and CNP-Le showed the highest Ci values of 9999.0 µmol mol^{-1} and 9321.5 µmol mol^{-1} among MnO_2NPs and CNPs respectively. At highest concentration of 0.30%, higher values of Ci were achieved in ZnONP-Psc (1905.0 µmol mol^{-1}), MgONP-Psc (1153.5 µmol mol^{-1}), MnO_2NP-Psc (2028.0 µmol mol^{-1}), and CNP-Ab (2089.0 µmol mol^{-1}). In case of metal salts used, CMS showed the highest value of Ci (2311.0 µmol mol^{-1}) followed by MgMS (2209.0 µmol mol^{-1}), MnMS (2171.0 µmol mol^{-1}) and ZnMS (2112.0 µmol mol^{-1}) at lower dose of 300 ppm. With the increase in dosage/concentration, value of Ci decreased effectively. Mancozeb and flusilazole treated plants showed Ci in the range of 790.5 µmol mol^{-1} and 816.5 µmol mol^{-1} respectively. Control plant showed the value of Ci as 7709.5 µmol mol^{-1} (Table 6.17; Figure 6.32.1) (Thomas *et al.*, 2008). Figure 6.32.2 depicts the effect of three concentrations of treatments in the form of box plots.

Table 6.17: Effect of different concentrations of treatments on intercellular CO_2 (µmol.mol-1) of apple plant (6 hours)

Treatments	Concentration		
	0.10%	0.20%	0.30%
T1	9999.000[a]	2261.000[de]	1905.000[a]
T2	9467.500[a]	5140.500[ab]	1103.000[c]
T3	9155.000[a]	4179.500[bc]	1767.000[ab]
T4	9498.500[a]	4729.500[bc]	1153.500[c]
T5	8610.000[abcd]	2137.000[de]	1082.500[c]
T6	9096.000[abc]	4163.500[c]	1133.500[c]
T7	9101.500[ab]	5859.000[a]	2028.000[a]
T8	9482.500[a]	2661.500[d]	1689.500[ab]
T9	9999.000[a]	4952.500[bc]	1923.000[a]
T10	9267.500[a]	4326.500[bc]	2012.500[a]
T11	8878.000[abcd]	4808.500[bc]	2089.000[a]
T12	9321.500[a]	4280.500[bc]	2025.500[a]

	300 ppm	500 ppm	700 ppm
T13	2112.000[ef]	952.500[f]	790.500[c]
T14	2209.500[ef]	1609.000[ef]	1334.500[bc]
T15	2171.000[ef]	1091.000[f]	835.500[c]
T16	2311.000[e]	1118.500[f]	928.500[c]

T17	7709.500[b d]	7709.500	7709.500
T18	790.500[f]	790.500[f]	790.500[c]
T19	816.500[f]	816.500[f]	816.500[c]

Note: The means with different Letters as superscripts are significant (P < 0.05). The means with same letters or having common letter(s) are not significantly different

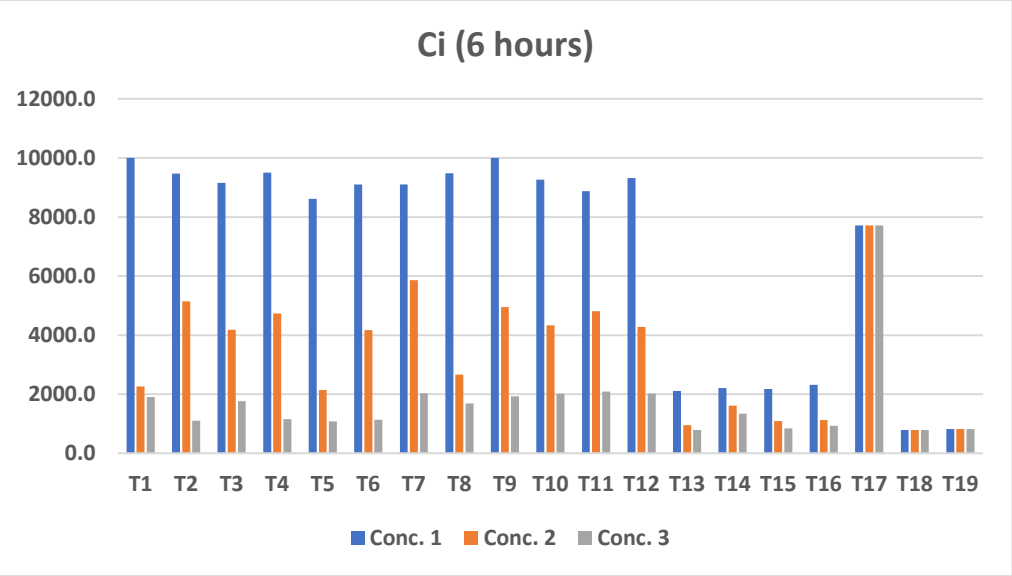

Figure 6.32.1: Graph showing the effect of three concentrations of treatments on intercellular CO_2 after 6 hours of spray

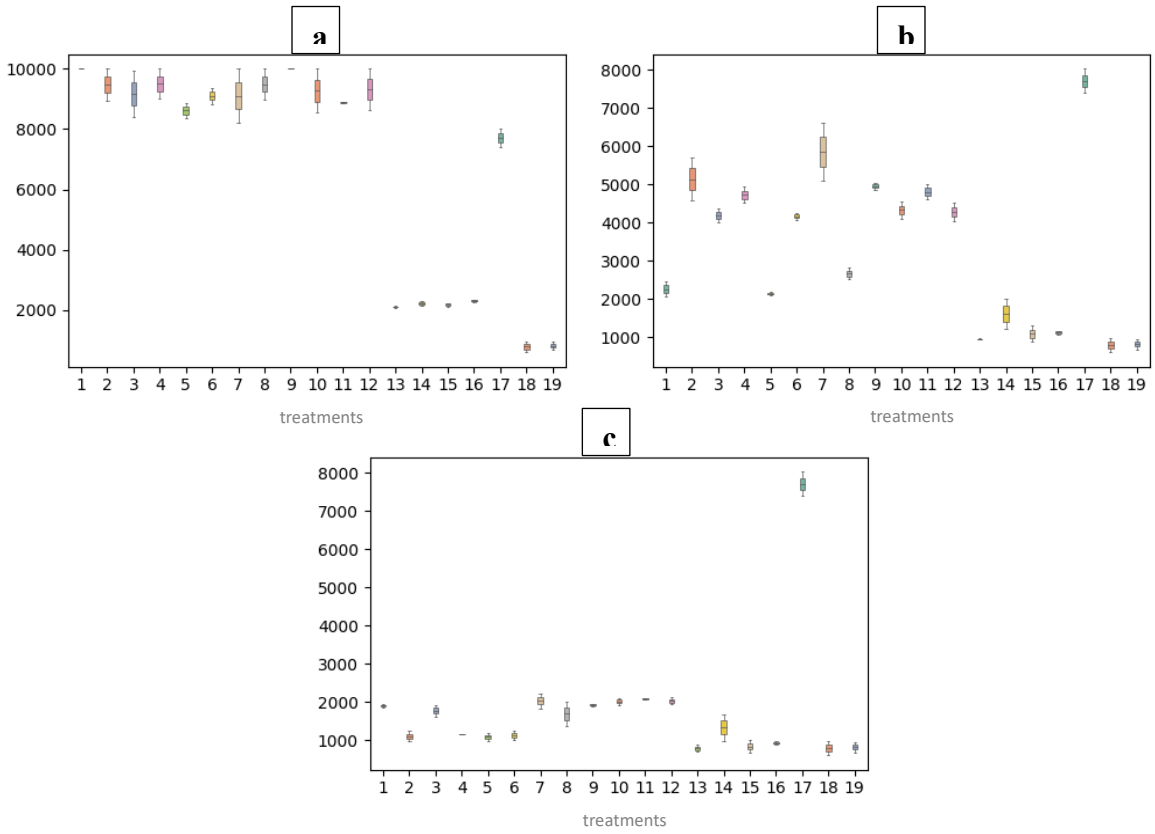

Figure 6.32.2: Boxplots showing the effect of three concentrations of treatments on intercellular CO_2 after 6 hours at: a) 0.10%; b) 0.20%; c) 0.30%

After 24 hours: In the second reading taken on the other day of spray, highest range of Ci was seen in CNPs, followed by MnO_2NPs, MgONPs and ZnONPs. At the concentration of 0.10%, on the basis of fungal extract used, the nanoparticles that gave the highest comparative values were ZnONP-Le (9604.5 µmol mol^{-1}), MgONP-Ab (9483.0 µmol mol^{-1}), MnO_2NP-Le (9933.0 µmol mol^{-1}) and CNP-Ab (9910.5 µmol mol^{-1}). Since increase in concentration lead to the decrease in Ci, therefore, at 0.30%, the values got decreased. At this concentration, the higher values of Ci were achieved in ZnONP-Le (2076.5 µmol mol^{-1}), MgONP-Le (1459.0 µmol mol^{-1}), MnO_2NP-Psc (2459.0 µmol mol^{-1}), CNP-Ab (2328.5 µmol mol^{-1}) respectively. In case of metal salt treatments, highest efficacy was seen at lowest concentration of 300 ppm in ZnMS (2484.5 µmol mol^{-1}). Fungicide treated plants showed Ci values of 719.5 µmol mol^{-1} and 826.0 µmol mol-1 in mancozeb and flusilazole respectively. Control plants showed the Ci value of 8466.0 µmol mol^{-1} (Table 6.18) (Thomas *et al.*, 2008). Figures 6.33.1

and 6.33.2 illustrate the effect of three different concentrations on Ci after 24 hours of application.

Table 6.18: Effect of different concentrations of treatments on intercellular CO_2 (µmol.mol-1) of apple plant (24 hours)

Treatments	Concentration		
	0.10%	**0.20%**	**0.30%**
T1	8765.500^{a}	2418.500^{e}	2036.500^{b}
T2	9487.500^{a}	5297.000^{b}	1322.500^{c}
T3	9604.500^{a}	4332.000^{c}	2076.500^{ab}
T4	8932.000^{a}	5087.000^{bc}	1326.000^{c}
T5	9483.000^{a}	2621.000^{e}	1262.500^{cd}
T6	9482.500^{a}	4721.000^{bc}	1459.000^{c}
T7	9447.500^{a}	6227.000^{a}	2459.000^{a}
T8	9488.000^{a}	3620.500^{d}	2085.000^{ab}
T9	9933.000^{a}	4770.000^{bc}	2101.500^{ab}
T10	9882.000^{a}	4409.500^{c}	2142.500^{ab}
T11	9910.500^{a}	4735.000^{bc}	2328.500^{ab}
T12	9880.500^{a}	4476.000^{c}	2177.500^{ab}
	300 ppm	**500 ppm**	**700 ppm**
T13	2484.500^{a}	1139.500^{f}	844.500^{e}
T14	2341.000^{a}	1366.000^{f}	1355.500^{c}
T15	2183.000^{a}	1163.000^{f}	951.000^{de}
T16	2116.000^{a}	1111.500^{f}	896.500^{e}
T17	8466.000^{a}	8466.000	8466.000
T18	719.500^{a}	719.500^{f}	719.500^{e}
T19	826.000^{a}	826.000^{f}	826.000^{e}

Note: The means with different Letters as superscripts are significant ($P < 0.05$).

The means with same letters or having common letter(s) are not significantly different.

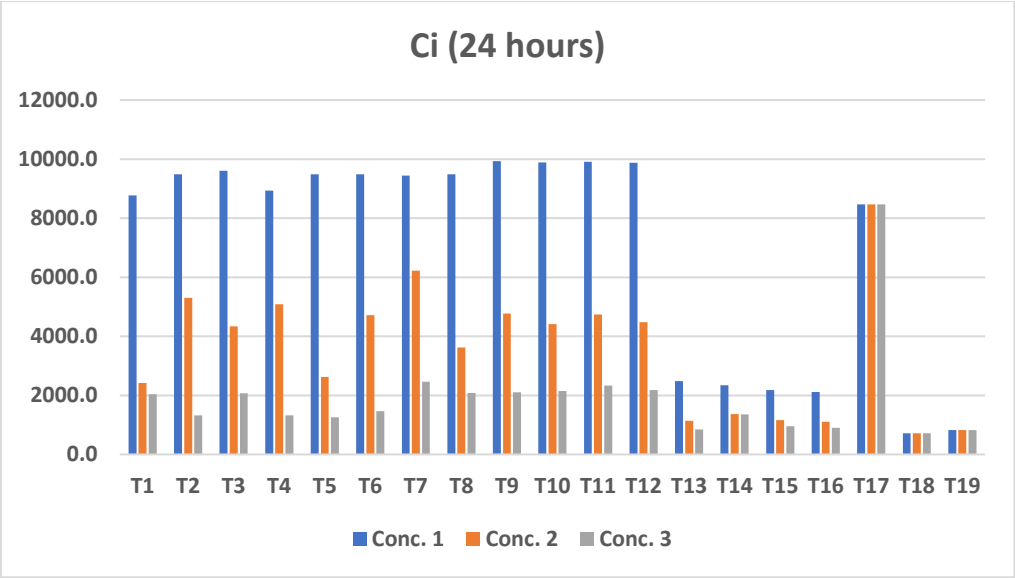

Figure 6.33.1: Graph showing the effect of three concentrations of treatments on intercellular CO_2 after 24 hours of spray

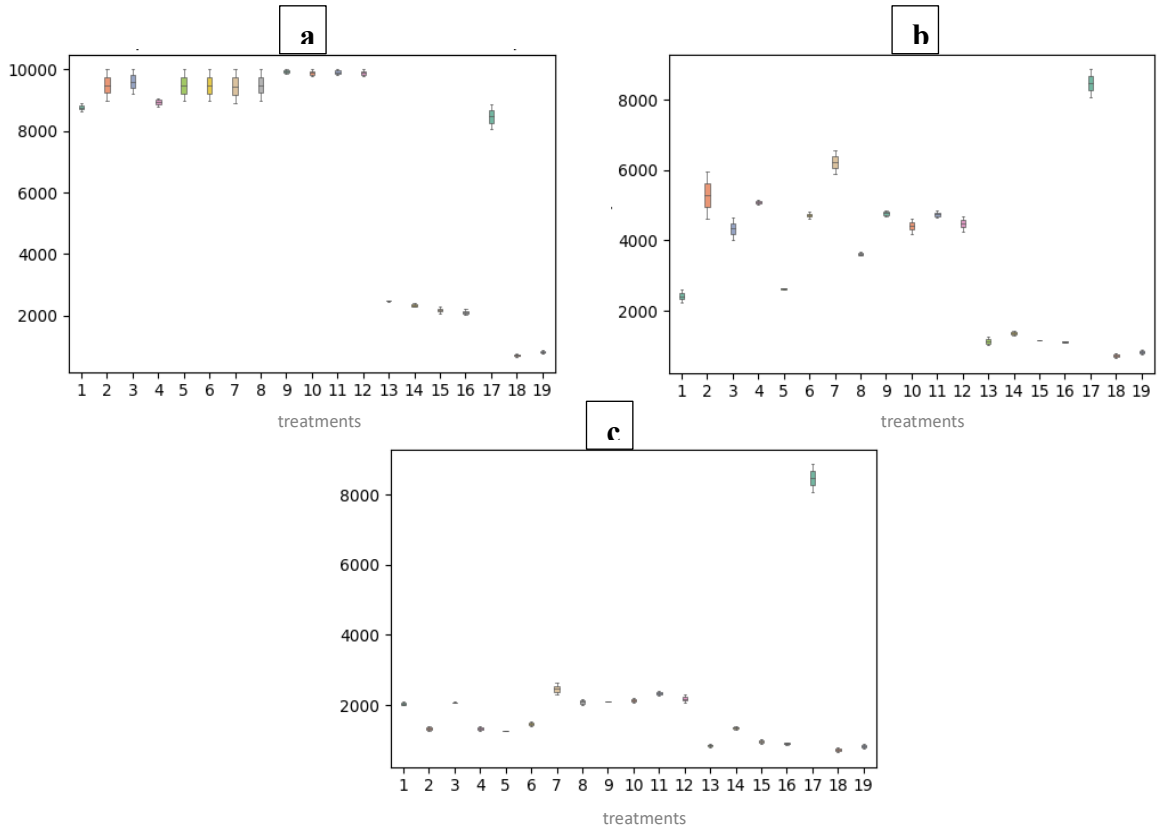

Figure 6.33.2: Boxplots showing the effect of three concentrations of treatments on intercellular CO_2 after 24 hours at: a) 0.10%; b) 0.20%; c) 0.30%

6.5.1.4. Transpiration rate (E)

Almost negligible variations were found in transpiration rate between treatments irrespective of the fungal extract and type of metal salt. Marginal increase and decrease in E with an increase in concentrations of the nanoparticles was noticed in some treatments. Similarly, the metal salt treated plants showed constant and increased E values depending upon the metal salt used. Fungicide treatments also resulted in both the increase and decrease in E values.

After 6 hours:

At the concentration of 0.10%, CNPs showed the highest E rate of 2.50 mmol m^{-2} s^{-1} followed by ZnONPs (ZnONP-Le - 2.00 mmol m^{-2} s^{-1}), MnO_2NPs (all three - 1.50 mmol m^{-2} s^{-1}), MgONPs (MgONP-Psc - mmol m^{-2} s^{-1}). At 0.20%, highest E rate was seen in ZnONPs where both ZnONP-Psc and ZnONP-Ab gave the value of 2.00 mmol m^{-2} s^{-1}. MnO_2NPs followed the ZnONPs at the same concentration with the highest value (1.00 mmol m^{-2} s^{-1}) in both MnO_2NP-Psc and MnO2NP-Le treated plants. MgONPs and CNPs showed almost same results with the highest values of 1.00 mmol m^{-2} s^{-1} at this concentration. The highest concentration of 0.30% was not any different to the plants as there was an unnoticeable change in the E rate. MgONPs showed the highest range in MgONP-Psc (3.00 mmol m^{-2} s^{-1}) followed by ZnONPs where the highest value was shown by ZnONP-Ab (2.50 mmol m^{-2} s^{-1}). In MnO_2NPs, highest value of E rate was achieved in MnO_2NP-Le (1.00 mmol m^{-2} s^{-1}). In CNPs, highest rate of E was achieved in CNP-Psc (1.50 mmol m^{-2} s^{-1}). Similarly, in the metals salt treated plants, there was no such change in E rate. Mancozeb and flusilazole showed almost same effects as that of the nanoparticle concentrations with the values of 1.50 mmol m^{-2} s^{-1} and 1.00 mmol m^{-2} s^{-1} respectively. The control plant gave the E rate in the value of 0.50 mmol m^{-2} s^{-1} (Table 6.19; Figures 6.34.1 and 6.34.2) (Thunugunta *et al.*, 2018; Sharma *et al*., 2025).

Table 6.19: Effect of different concentrations of treatments on transpiration rate (mmol m-2 s-1) of apple plant (6 hours)

Treatments	Concentration		
	0.10%	0.20%	0.30%
T1	1.500[a]	2.000[a]	1.500[a]
T2	1.000[a]	2.000[a]	2.500[a]
T3	2.000[a]	0.500[a]	1.000[a]
T4	1.500[a]	0.500[a]	3.000[a]
T5	1.000[a]	1.000[a]	1.000[a]
T6	1.000[a]	0.500[a]	1.000[a]
T7	1.500[a]	1.000[a]	1.000[a]
T8	1.500[a]	0.500[a]	1.000[a]
T9	1.500[a]	1.000[a]	2.000[a]
T10	1.500[a]	1.500[a]	1.500[a]
T11	2.500[a]	0.500[a]	1.000[a]
T12	1.500[a]	0.500[a]	0.500[a]

	300 ppm	500 ppm	700 ppm
T13	0.500[a]	0.500[a]	1.000[a]
T14	0.000[a]	1.000[a]	0.000[a]
T15	0.500[a]	1.000[a]	0.500[a]
T16	0.500[a]	0.000[a]	0.500[a]

T17	0.500[a]	0.500[a]	0.500[a]
T18	1.500[a]	1.500[a]	1.500[a]
T19	1.000[a]	1.000[a]	1.000[a]

Note: The means with different Letters as superscripts are significant ($P < 0.05$).

The means with same letters or having common letter(s) are not significantly different.

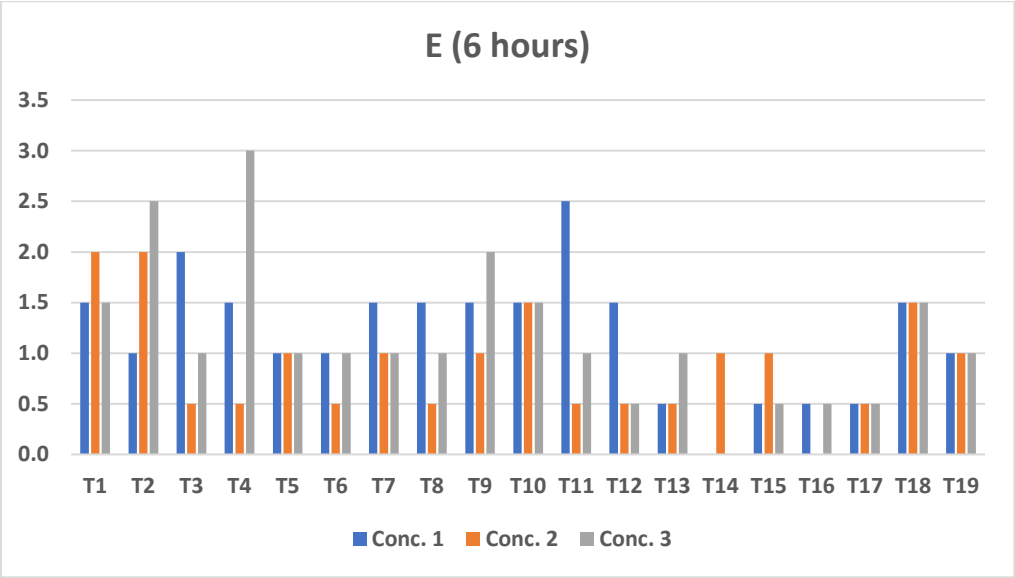

Figure 6.34.1: Graph showing the effect of three concentrations of treatments on transpiration rate after 6 hours of spray

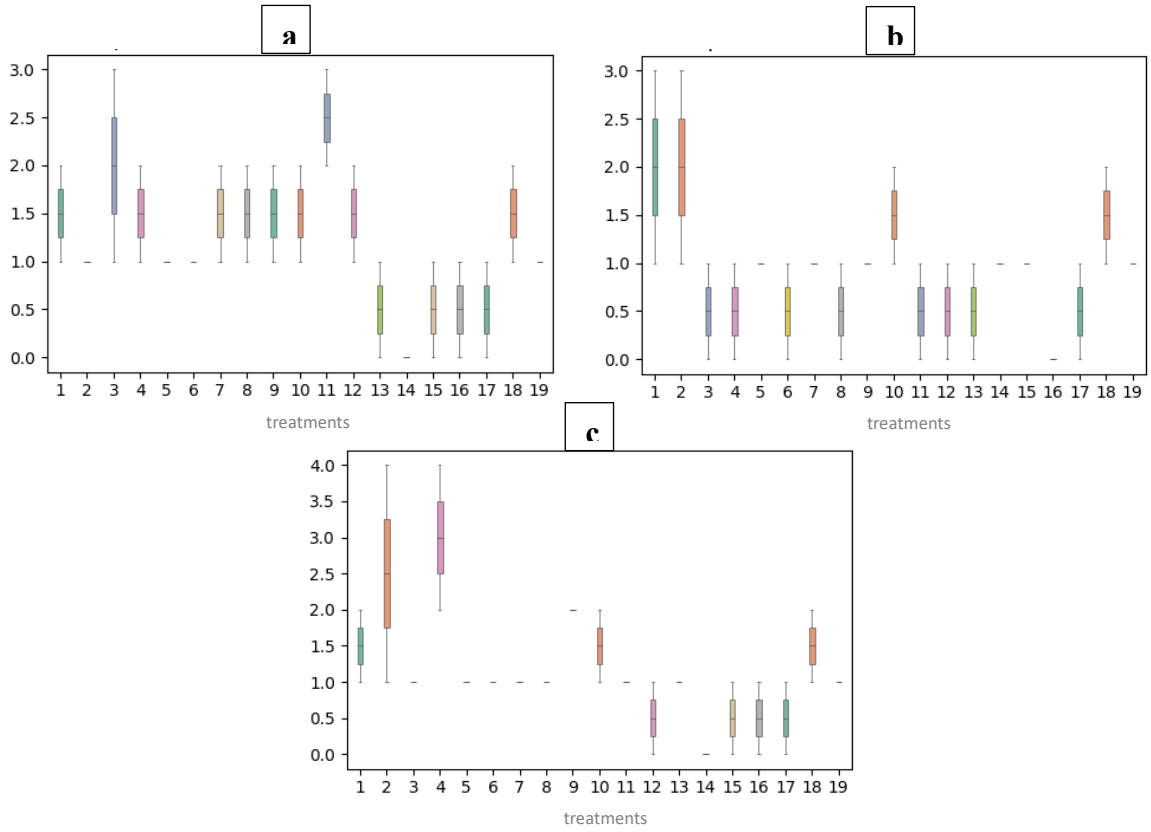

Figure 6.34.2: Boxplots showing the effect of three concentrations of treatments on transpiration rate after 6 hours at: a) 0.10%; b) 0.20%; c) 0.30%

After 24 hours:

On the next day of spray, reading was taken again after the completion of 24 hours where a slight increase in the E rate of apple plant leaves was noticed. Figure 6.35.1 shows the effect of treatments on E rate after 24 hours of application. At the first concentration of 0.10%, highest values were shown by ZnONP and MnO_2NP treated plants, followed by CNPs and MgONPs respectively. In ZnONPs, highest values were seen in first two types – ZnONP-Psc and ZnONP-Ab (1.50 mmol m^{-2} s^{-1}). In MgONPs, all three types of nanoparticles gave the same value of E rate (0.50 mmol m^{-2} s^{-1}). Similarly, MnO_2NPs showed higher values in last two nanoparticles - MnO_2NP-Ab and MnO_2NP-Le (1.50 mmol m^{-2} s^{-1}). CNP-Ab had the highest values of 1.50 mmol m^{-2} s^{-1} among CNPs. Metal salt treatments gave almost unaltered values in all three concentrations. Fungicide treated plant showed the E rates of 1.00 mmol m^{-2} s^{-1} and 1.50 mmol m^{-2} s^{-1} respectively. Control plant showed the E rate of 0.50 mmol m^{-2} s^{-1} (Table 6.20; Figure 6.35.2) (Thunugunta *et al.*, 2018; Chachei *et al*., 2025; Tari *et al*., 2025).

Table 6.20: Effect of different concentrations of treatments on transpiration rate (mmol m-2 s-1) of apple plant (24 hours)

Treatments	Concentration		
	0.10%	**0.20%**	**0.30%**
T1	1.500^{a}	2.500^{a}	1.500^{bcde}
T2	1.500^{a}	1.000^{bcd}	2.500^{abc}
T3	1.000^{a}	1.500^{abc}	3.500^{a}
T4	0.500^{a}	1.500^{abc}	1.500^{bcde}
T5	0.500^{a}	1.500^{abc}	2.000^{abcd}
T6	0.500^{a}	1.500^{abc}	2.500^{abc}
T7	1.000^{a}	2.000^{ab}	3.000^{ab}
T8	1.500^{a}	2.500^{a}	3.000^{ab}
T9	1.500^{a}	2.500^{a}	3.000^{ab}
T10	1.000^{a}	1.500^{abc}	3.000^{ab}
T11	1.500^{a}	1.000^{bcd}	2.500^{abc}
T12	1.000^{a}	1.500^{abc}	2.500^{abc}

	300 ppm	500 ppm	700 ppm
T13	1.000^{a}	0.500^{cd}	0.000^{e}
T14	1.000^{a}	0.000^{d}	1.000^{cde}
T15	1.000^{a}	1.000^{bcd}	0.000^{e}
T16	0.500^{a}	0.500^{cd}	0.000^{e}
T17	0.500^{a}	0.500^{cd}	0.500^{de}
T18	1.000^{a}	1.000^{bcd}	1.000^{cde}
T19	0.500^{a}	0.500^{cd}	0.500^{de}

Note: The means with different Letters as superscripts are significant ($P < 0.05$).

The means with same letters or having common letter(s) are not significantly different.

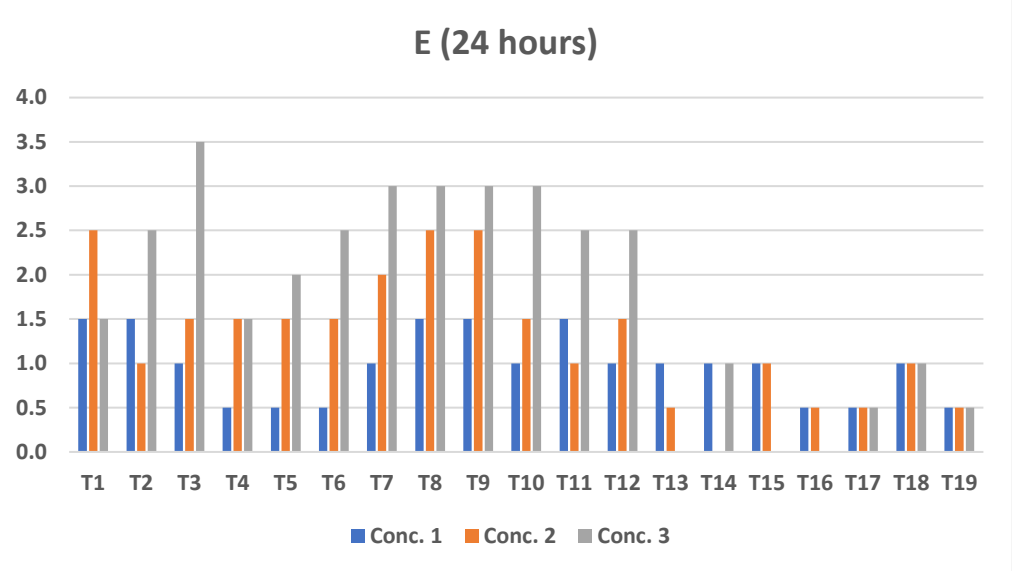

Figure 6.35.1: Graph showing the effect of three concentrations of treatments on transpiration rate after 24 hours of spray

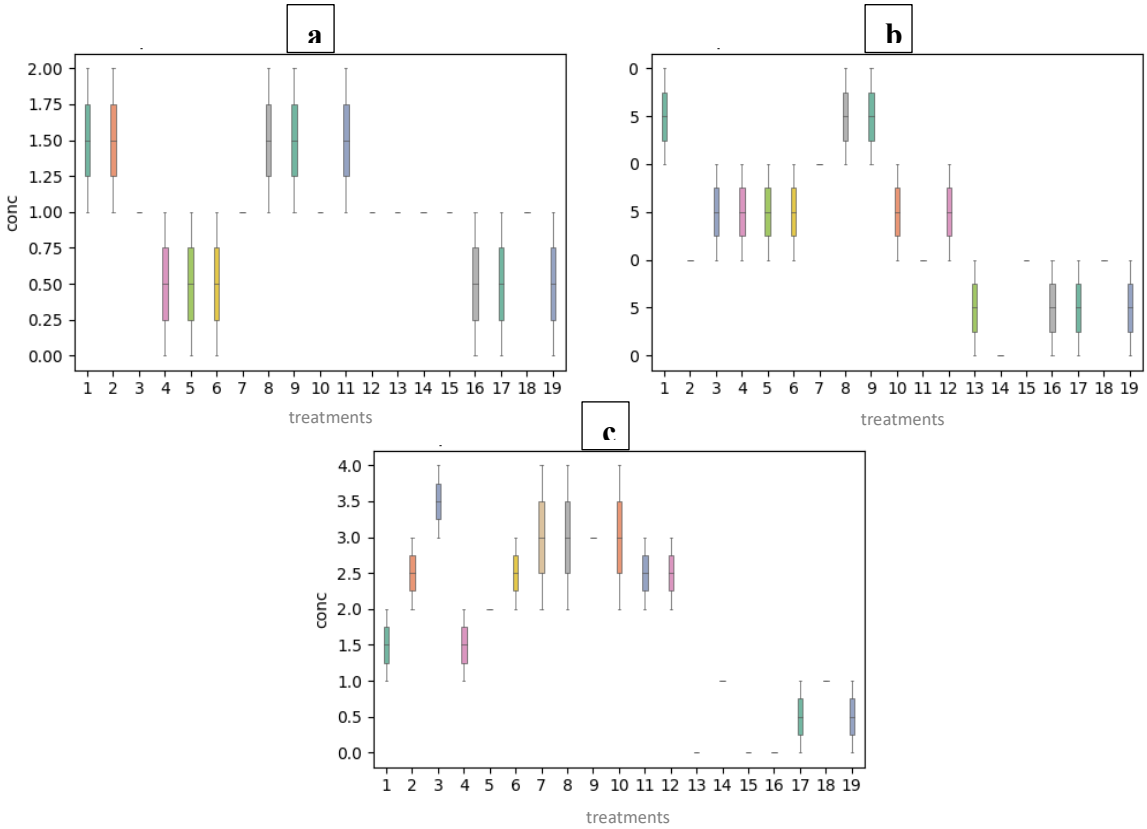

Figure 6.35.2: Boxplots showing the effect of three concentrations of treatments on transpiration rate after 24 hours at: a) 0.10%; b) 0.20%; c) 0.30%

6.5.1.5. Total chlorophyll content

Chlorophyll content was measured using SPAD after controlled and dose dependent application of the nanoparticle concentrations, metal salt concentrations and control formulations on the apple plants (Figure 6.36). There was not any prominent change in the chlorophyll content of apple plant leaves after the application of nanoparticles, metal salts and fungicides in any concentration.

Figure 6.36: Measurement of chlorophyll content of apple leaves using SPAD

After 6 hours:

At the first concentration of 0.10%, it was observed that out of the four types of nanoparticles, ZnONPs enhanced chlorophyll content the most as compared to other nanoparticles with the highest value of 42.867 µmol m^{-2} in ZnONP-Ab followed by MnO_2NPs where highest value was shown by MnO_2NP-Psc (40.633 µmol m^{-2}). In MgONPs, highest value of chlorophyll content was achieved in MgONP-Psc (40.700 µmol m^{-2}), while in CNPs, CNP-Le showed the highest value of chlorophyll content (42.667 µmol m^{-2}). Similarly, at 0.20%, ZnONPs showed the highest range of chlorophyll content followed by CNPs, MgONPs and MnO_2NPs. At the highest concentration of 0.30%, there was a marginal change in the chlorophyll content in nanoparticle treated plants. ZnONPs again showed the highest value in ZnONP-Psc (41.200 µmol m^{-2}) out of all other treatments, followed by CNP where highest value was shown by CNP-Psc (38.267 µmol m^{-2}). In MgONPs and CNPs, highest chlorophyll content values came out in MgONP-Le (38.300 µmol m^{-2}) and CNP-Psc (38.267 µmol m^{-2}) treated plants respectively (Thunugunta *et al.*, 2018; Samsoon *et al*., 2024; Sharma *et al*., 2025). In contrast, metal salts of Zn, Mg, Mn and the combination of three showed a slight reduction in chlorophyll content at the highest concentration (Table 6.21). Mancozeb and flusilazole treated plants showed the chlorophyll content in the range of 38.467 µmol m^{-2} and 40.400 µmol m^{-2} respectively. The chlorophyll content equal to 42.133 µmol m^{-2} was achieved in the control plant as illustrated in Figures 6.37.1 and 6.37.2.

Table 6.21: Effect of different concentrations of treatments on chlorophyll content (µmol m-2) of apple plant (6 hours)

Treatments	Concentration		
	0.10%	**0.20%**	**0.30%**
T1	45.533^{a}	40.367^{a}	41.200^{a}
T2	42.867^{ab}	39.500^{a}	40.367^{a}
T3	39.900^{bcd}	40.200^{a}	38.000^{a}
T4	40.700^{abcd}	40.933^{a}	35.000^{a}
T5	39.167^{bcd}	41.900^{a}	36.467^{a}
T6	39.233^{bcd}	36.267^{a}	38.300^{a}
T7	40.633^{abcd}	38.933^{a}	34.800^{a}

T8	40.367^{abcd}	41.033^{a}	37.400^{a}
T9	40.567^{abcd}	37.733^{a}	37.833^{a}
T10	39.567^{bcd}	40.067^{a}	38.267^{a}
T11	39.900^{bcd}	40.367^{a}	36.767^{a}
T12	42.667^{abc}	38.100^{a}	37.067^{a}

	300 ppm	**500 ppm**	**700 ppm**
T13	40.833^{abcd}	41.767^{a}	36.300^{a}
T14	37.367^{cd}	40.200^{a}	37.700^{a}
T15	36.600^{d}	40.833^{a}	38.500^{a}
T16	36.133^{d}	36.373^{a}	37.604^{a}

T17	42.133^{abc}	42.133^{a}	42.133^{a}
T18	38.467^{bcd}	38.467^{a}	38.467^{a}
T19	40.400^{abcd}	40.400^{a}	40.400^{a}

Note: Different alphabets represent significant differences among treatments. The means with different Letters as superscripts are significant ($P < 0.05$). The means with same letters or having common letter(s) are not significantly different.

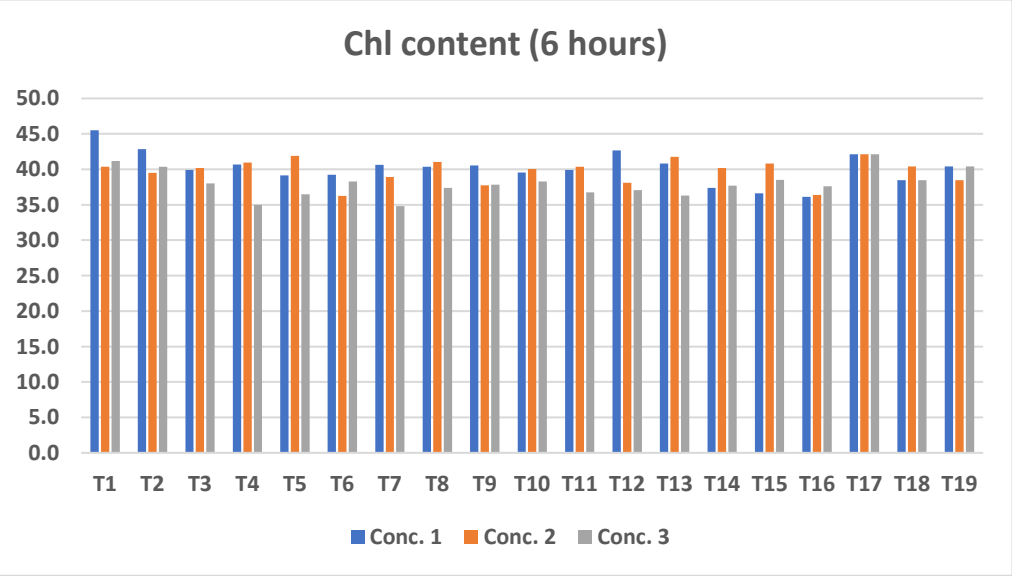

Figure 6.37.1: Graph showing the effect of three concentrations of treatments on chlorophyll content after 6 hours of spray

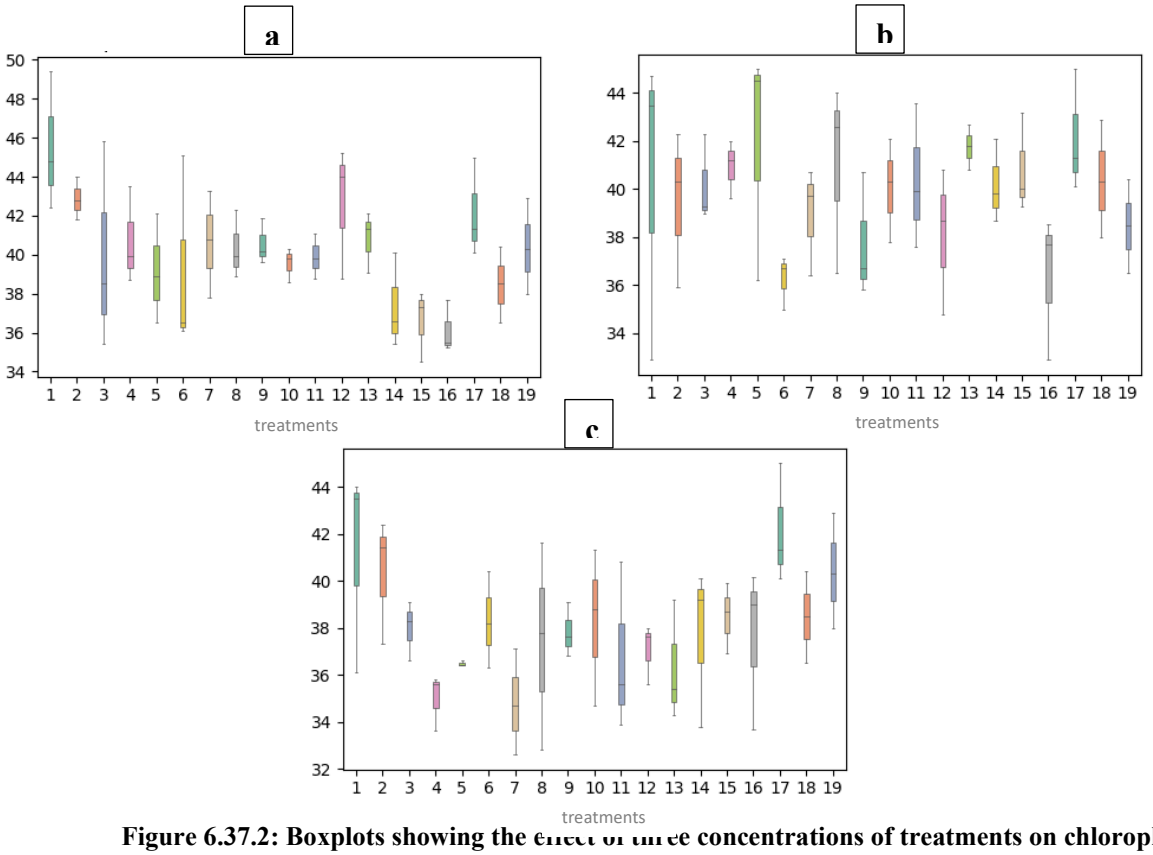

Figure 6.37.2: Boxplots showing the effect of three concentrations of treatments on chlorophyll content after 6 hours at: a) 0.10%; b) 0.20%; c) 0.30%

After 24 hours:

On the other day of evaluation, the treated plants showed the chlorophyll content in almost same range without much alterations (Table 6.22). At 0.10%, MgONPs showed the highest range of chlorophyll content in MgONP-Le (40.667 µmol m^{-2}) followed by MnO_2NPs, CNPs and ZnONPs respectively. At the concentration of 0.20%, ZnONPs showed the highest value in ZnONP-Psc (42.633 µmol m^{-2}) followed by MgONPs, CNPs and MnO_2NPs. Similarly, at the maximum concentration of 0.30%, ZnONP treated plants showed the highest value of chlorophyll content out of all other treatments higher being in ZnONP-Ab (42.033 µmol m^{-2}) followed by MnO_2NPs, CNPs and MgONPs respectively (Thunugunta *et al.*, 2018; Tahir *et al.*, 2024). Metal salt treated plants did not show any noticeable variation with the change in concentration from 300 ppm to 700 ppm. Fungicide treated plants showed chlorophyll content in the range of

37.267 µmol m^{-2} and 37.533 µmol m^{-2} while the control plant showed the value of 40.567 µmol m^{-2} (Figures 6.38.1 and 6.38.2).

Table 6.22: Effect of different concentrations of treatments on chlorophyll content (µmol m-2) of apple plant (24 hours)

Treatments	Concentration		
	0.10%	**0.20%**	**0.30%**
T1	35.567^{a}	42.633^{a}	38.800^{abc}
T2	40.600^{a}	37.267^{a}	42.033^{a}
T3	40.400^{a}	37.900^{a}	36.200^{bcde}
T4	40.500^{a}	40.100^{a}	37.133^{bcd}
T5	37.800^{a}	37.567^{a}	33.067^{de}
T6	40.667^{a}	38.733^{a}	34.167^{cde}
T7	40.633^{a}	38.800^{a}	34.800^{cde}
T8	39.667^{a}	35.400^{a}	35.567^{cde}
T9	39.633^{a}	35.700^{a}	38.667^{abc}
T10	40.667^{a}	38.400^{a}	37.100^{bcd}
T11	39.733^{a}	38.533^{a}	34.200^{cde}
T12	38.800^{a}	37.700^{a}	37.833^{abcd}
	300 ppm	**500 ppm**	**700 ppm**
T13	39.600^{a}	39.667^{a}	31.867^{e}
T14	38.100^{a}	37.633^{a}	37.133^{bcd}
T15	36.533^{a}	35.767^{a}	37.967^{abcd}
T16	37.083^{a}	36.543^{a}	37.590^{abcd}
T17	40.567^{a}	40.567^{a}	40.567^{ab}
T18	37.267^{a}	37.267^{a}	37.267^{abcd}
T19	37.533^{a}	37.533^{a}	37.533^{abcd}

Note: Different alphabets represent significant differences among treatments. The means with different Letters as superscripts are significant ($P < 0.05$). The means with same letters or having common letter(s) are not significantly different.

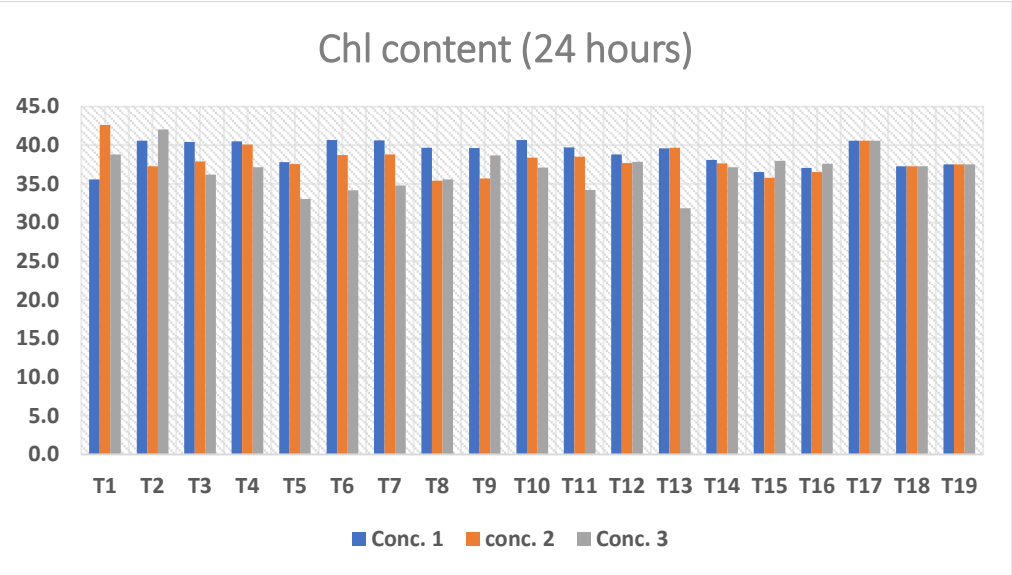

Figure 6.38.1: Graph showing the effect of three concentrations of treatments on chlorophyll content after 24 hours of spray

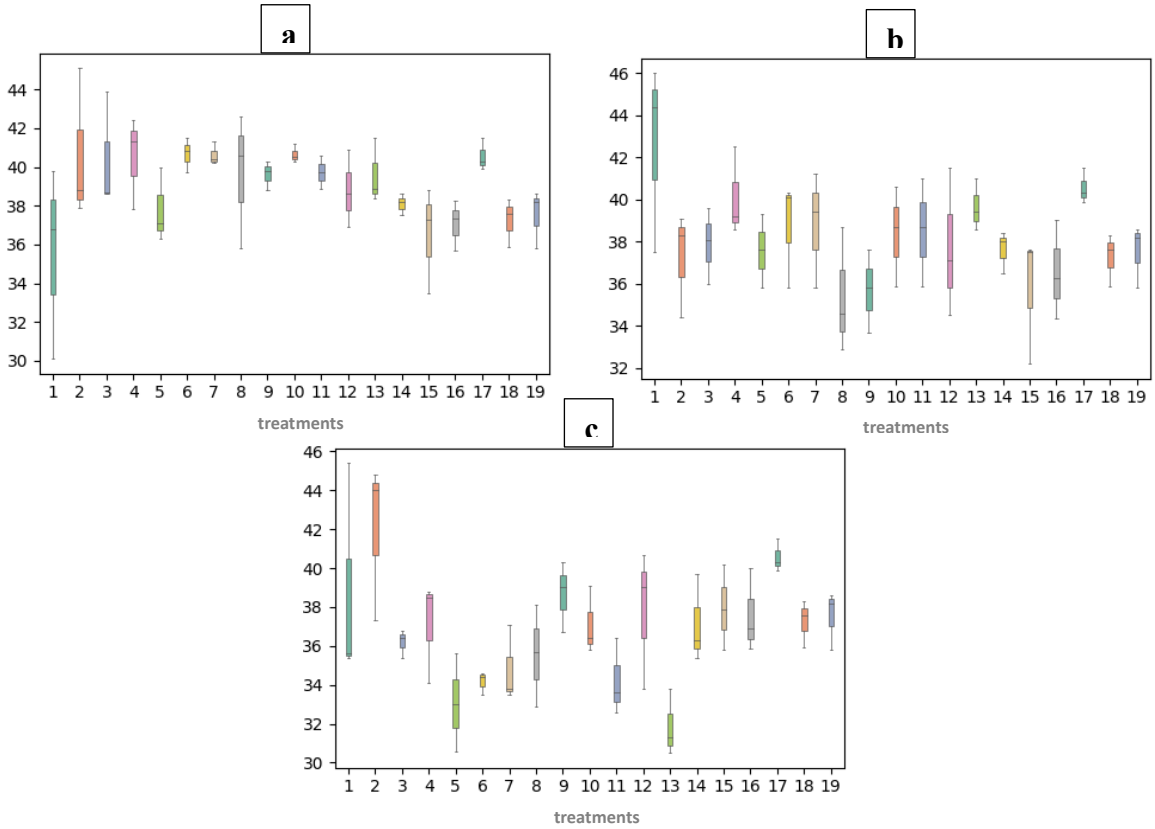

Figure 6.38.2: Boxplots showing the effect of three concentrations of treatments on chlorophyll content after 24 hours at: a) 0.10%; b) 0.20%; c) 0.30%

Chapter 7

Summary and Conclusions

The chronology of work done in the present effort has been summarized besides being correspondingly concluded which goes as follows:

7.1. Collection, preservation and preparation of cell-free fungal extracts

Three fungal cultures of *P. sajor caju*, *A. bisporus* and *L. edodes* were collected from MRTC, SKUAST-Kashmir. The cultures were sub-cultured so as to preserve them for further use. The cultures were then independently grown in PDB and the respective flasks were transferred to incubator at 26 ± 1°C and left for 6-7 days till the appearance of mycelial mats in the flasks. The mycelia were separated by filtration, transferred to sterile de-ionized water and again left for incubation in dark conditions for 3 days. Using second filtration, individual cell-free extracts of the fungal cultures were obtained from the fermented broth of the mycelial mats separated. These extracts were used further for metal salt reduction in nanoparticles.

7.2. Mycogenic synthesis and characterization of nanoparticles

The extracts prepared from the fungal cultures were used for the synthesis of ZnO, MgO, MnO_2 and Combination nanoparticles. The mycogenic synthesis of nanoparticles was supported by mixing 5 mM metal salts of zinc, magnesium and manganese with the fungal extracts individually for the single nanoparticles and in combination for the Combination nanoparticles. Each resultant solution was agitated continuously on the magnetic stirrer at 60°C for 1 hour till the reaction mixture showed color change and nanoparticle synthesis became visible. The solutions were centrifuged at 10,000 rpm for 15-20 minutes. The process of centrifugation was repeated thrice along with washing and decantation so as the nanoparticles in pellet are free from any macromolecules or foreign particles. The latter was oven-dried overnight at 60°C, ground, and stored under -4°C for further use. Hence, a total of twelve samples of nanoparticles (four from each fungal extract) were obtained.

The physicochemical characterization of the synthesized nanoparticles was carried out through an alliance of spectroscopic and microscopic analytical techniques. The preliminary physicochemical characterization was done to evaluate the potential synthesis of ZnO, MgO, MnO_2 and Combination nanoparticles and comprised of a basic technique of UV-Vis Spectroscopy. This process was utilized to have an elementary

screening of all the twelve myco-synthesized nanoparticles, to initially filter out the most desirable nanoparticle sample chiefly in terms of SPR positioned within the range of 200-800 nm. Twelve samples of nanoparticles were seen to yield satisfactory results. After successfully screening the potentially synthesized nanoparticles via UV-visible spectroscopy, the nanoparticles were sought for a detailed physicochemical characterization using analytical techniques such as FT-IR Spectroscopy, XRD, and SEM with EDX Spectroscopy. The XRD diffractograms presented typical sharp diffraction peaks agreeing to the presence of ZnO, MgO, MnO_2 and the Combination nanoparticles. Furthermore, the FT-IR bands of the nanoparticles confirmed the existence of various functional assemblies as contributed by the extracellular or intracellular fraction of the respective fungi used. These functional groups represented as natural reducing as well as capping agents consequently, assisting in the bio-amalgamation of ZnONPs, MgONPs, MnO_2NPs and CNPs respectively. The SEM micrographs showed the presence of irregular, spherical and angular aggregates comprising of hexagonal to quasi-spheroidal nanoforms. The EDX spectrum for all twelve nanoparticles was seen to display basic emission peaks conforming to O, Zn, Mg and Mn establishing the formation of ZnO, MgO, MnO_2 and their combination nanoparticles.

7.3. Evaluation of antifungal activity of the nanoparticles

The *in vitro* antifungal activities of the nanoparticles of ZnO, MgO, MnO_2 and their combination were assessed against two fungal pathogens of Apple plant namely *A. mali* and *V. inaequalis* using two techniques- poison food technique and spore germination test respectively. Three concentrations (0.10%, 0.20% and 0.30%) were prepared from each of the nanoparticles and were applied to the media (PDA in case of PFT and water agar in case of SGT). Metal salts of zinc, magnesium and manganese were selected as positive controls while two fungicides- mancozeb and flusilazole were selected as standard controls. Furthermore, all the nanoparticles showed a broad-spectrum and appreciable dose-dependent antifungal potential. In case of *A. mali*, maximum inhibition of 96.04% was shown by MnO_2NP-Le at the highest concentration used (0.30%) compared to no inhibition in the control (0%), indicating a maximal inhibitory effect. The antifungal activity of the comparative controls i.e., metals salts and

fungicides, was seen to be comparatively less or equal, than that shown by these mycogenic nanoparticles at lower doses. Among the metal salts used, maximum inhibition was shown by Zn-Ms at 96.33% at the highest concentration of 700 ppm. Similarly, in case of *V. inaequalis*, CNP-Ab showed the inhibition percentage of 68.823%, meaning only 31.177% of spores germinated in the treated group at the highest concentration of 0.30%, and caused a 3.21fold decrease in spore germination compared to the control. Among the metal salts, maximum inhibition in spore germination was caused by Zn-MS (70.553%).

Nanotechnology, therefore, provides highly efficient ways to manage plant diseases. ZnO, MgO, MnO_2, and combination nanoparticles exhibit extremely strong antifungal potential, according to a critical review of the research conducted thus far in the area of using nanoparticles to manage plant diseases. These nanoparticles are also significantly more potent than traditional insecticides and work well at lower concentrations. Higher concentrations of metal ions of the Zn, Mg, and Mn combination require more research since it is evident from the data that an increase in nanoparticle concentration significantly increases antifungal potential. However, given the results of current research, it is certain that combination nanoparticles have a great deal of promise as antifungal agents and may thus be investigated further.

7.4. Evaluation of the effect of nanoparticles on apple plant parameters

The efficacy of synthesized nanoparticles in changing the gas exchange parameters and chlorophyll content of the apple plants was appraised on the trial maintained at experimental field in SKUAST, Kashmir employing IRGA and SPAD analysers. Three concentrations (0.10%, 0.20% and 0.30%) were prepared from each of the nanoparticles and were applied to the Apple plants. Readings were taken after 6 hours and 24 hours of spray. Among the gas exchange parameters evaluated, stomatal conductance showed an increase with the increase in concentration of nanoparticles, while in metal salt treated plants, values decreased with an increase in concentration of metal salts from 300 ppm to 700 ppm. The values shown by metal salt concentrations (at 300 ppm) were in accordance with 0.20% concentration of the nanoparticles. The nanoparticle treated plants showed better stomatal conductance than the standard and normal control. Among all the nanoparticles tested, at 0.30% concentration, MnO_2NP-Le and MgONP-

Psc resulted in a 2.38 and 2.23 fold increase in stomatal conductance compared to the control after 6 hours and 24 hours respectively. Similarly, all the nanoparticles were observed to present a promising efficacy for net photosynthesis which was seen to be dose-dependent (increasing with an increase in concentration) in comparison to the comparative controls i.e., fungicides, being seen to hold a value of net photosynthesis equivalent to that of the net photosynthesis in nanoparticle treated plants at concentration for 0.20%. ZnONP-Psc at 0.30% showed the highest net photosynthesis value after 6 hours, representing a 1.15 fold increase compared to the control. Similarly, at the same concentration, CNP-Psc showed the highest value after 24 hours, indicating a 2.46 fold increase in net photosynthesis compared to the control. The values decreased in plants sprayed with metal salts with highest values shown at lower concentration of 300 ppm. In case of intercellular CO_2 of the plants, the values decreased with the increase in concentration of the nanoparticles. At the highest concentration of 0.30%, the lowest decrease was recorded with CNP-Ab and MnO_2NP-Psc, showing the values of 2089 μmol.mol-1 and 2459 μmol.mol-1, compared to the controls (7709 μmol.mol-1 and 8466 μmol.mol-1) after 6 hours and 24 hours respectively. These values indicated the fold decrease of 4.05 and 3.44. Furthermore, the highest decrease was shown by MgONP-Ab with the values of 1082.500 μmol.mol-1 and 1262.500 μmol.mol-1 (after 6 hours and 24 hours respectively) compared to the controls - 7709 μmol.mol-1 (after 6 hours) and 8466 (after 24 hours) indicating the fold decrease of 7.12 and 6.71 respectively. Likewise, in metal salts, with an increase in concentration form 300 ppm to 700 pm, a decrease in the values of intercellular CO_2 was observed. The transpiration rate of treated plants showed a net increase in values as compared to the control plants. After 6 hours, MgONP-Psc showed the highest value at 0.30% concentration indicating a 6 fold increase, while after 24 hours, the highest value was shown by ZnONP-Le at the same concentration with a 7 fold increase. In case of chlorophyll content, change/increase in nanoparticle concentration did not result in any increase in the values. There were minimal variations in the chlorophyll content of apple plants treated with nanoparticles with the maximum values shown by ZnONP-Psc (after 6 hours) and ZnONP-Ab (after 24 hours) at the highest concentration of 0.30% indicating 1.02 fold decrease and 1.04 fold increase respectively.

Metal nanoparticles have been thoroughly researched due of their unique physical and biological characteristics, which allow them to perform a variety of tasks not seen in the bulk phase. The myco-synthesized nanoparticles showed effective antifungal activity against phyto-pathogens of apple orchards – *Alternaria mali* and *Venturia inaequalis*. The biological source of nanoparticle synthesis influences the activity of corresponding nanoparticles. The extracellular and intracellular components of all three fungal cultures- *P. sajor caju, A. bisporus and L. edodes* were seen to yield nanoparticles that demonstrated significant properties. As it has already been cited that fungi are mostly known to synthesize nanoforms extracellularly. Hence, this work certainly gave us an edge over the aforementioned notion and garnered that the fungi could efficiently synthesize ZnO, MgO, MnO_2 and combination nanoparticles. The resulting nanoparticles synthesized gave satisfactory efficacy under the tested parameters as antifungal, besides their dose dependent effects on the physiological gas exchange parameters and chlorophyll content. Therefore, nanotechnology can offer a sustainable crop protection alternative, but it must be handled cautiously because of the toxicity of the related nanoparticles. Henceforward, in-depth work must be undertaken to fully exploit the worth of these mycogenic nanoparticles in other areas of research.

7.5. Future Prospects

Nanotechnology is often referred to as "the future technology" that can solve many problems. The accelerated advance in the knowledge of nanoparticle synthesis and application is not synchronous with the advance of knowledge about their assimilation in the environment. The forthcoming set-ups of this current effort embraces an extensive probability to additionally comprehend ZnO, MgO, MnO_2 and combination nanoparticles for their supplementary yet unexplored domains in addition to their other latent activities besides safety. Several factors also need to be considered for better and safer utilization of these nanoparticles in various applications. Henceforth, it broadly includes the following-

1. According to this study, the impact of nanoparticles on plants varies depending on their type and concentration. To assess the toxicity at greater concentrations, further research must be done on the impact of nanoparticles in open fields.

2. These nanoparticles should be assessed for their distinctive antimicrobial potential adopting additional *in vitro* and *in vivo* parameters and that too against an extensive range of microbes.

3. In addition to the use of nanoparticles in agriculture, nanomaterials in various forms are being utilized in many other diverse fields. Since nano-fertilizer technology is highly creative and there is a dearth of published information in scientific publications, nanoparticles can be employed to formulate nano-fertilizers if the aforementioned difficulties are resolved. Nonetheless, a number of papers and patented technologies indicate that there is a great deal of room for developing nano-fertilizers.

4. The active components of insecticides and substances that boost host defence can be delivered to the target pathogens via nanoparticles. Nano-pesticides have improved penetration, enhanced effective duration and decreased the entry of chemicals into the ecosystem. They also require fewer amounts of active ingredients to control pest. But

their higher penetration capacity is the major concern as there is a high chance of their entry into the human body through skin or inhalation which has to be taken care.

5. The nanoparticles could be tried out for functionalization in combination with existing conventional drugs as antimicrobials, antioxidants, immunomodulators, chemotherapeutic drugs, or routinely used medications against various other aetiologies, etc., or with certain natural surface-active agents so as to boost the corresponding pharmacological activity and possibly minimizing the toxic side effects.

6. Additional studies might be steered to assess the antioxidant capacity of these mycogenic nanoparticles via employing spare *in vitro* as well as *in vivo* models in addition to determining their underlying antioxidant mechanisms.

7. The nanoparticles ought to undergo a thorough in-depth assessment of their anticancer efficacy via utilizing an array of more sophisticated *in vitro* tests and additional cell lines as well as *in vivo* assessments. The appraisal of the basic mechanisms for the same should also be undertaken.

8. As kingdom fungi is diversified, still more fungal species are in the way to be used in the fabrication of zinc, magnesium or manganese nanoparticles where the fungal extracts act as reducing, stabilizing or capping agents.

9. The bioaccumulation of mycogenic nanoparticles in the plant system is normally low when compared to their corresponding ionic form and, therefore, cause less damage to the metabolism, antioxidant system, morphological and anatomical features of the plants. Still, toxicity studies on experimental apple plants treated with various concentrations of mycogenic nanoparticles and corresponding bulk materials need to be undertaken.

10. Moreover, the nanoparticle accumulation in plants that have the chances to pass these nanoparticles to animal and human consumers has to be considered as an important issue to address.

Chapter 8

Bibliography

Abbas, Z.; Hassan, M. A.; Huang, W.; Yu, H.; Xu, M.; Chang, X.; Fang, X.; Liu, L. Influence of Magnesium Oxide (MgO) Nanoparticles on Maize (*Zea mays* L.). *Agronomy* **2024**, *14* (3), 617. https://doi.org/10.3390/agronomy14030617

Abdallah, Y.; Ogunyemi, S. O.; Abdelazez, A.; Zhang, M.; Hong, X.; Ibrahim, E.; Hossain, A.; Fouad, H.; Li, B.; Chen, J. The Green Synthesis of MgO Nano-Flowers Using *Rosmarinus officinalis* L. (Rosemary) and the Antibacterial Activities Against *Xanthomonas oryzae* pv. *oryzae*. *Biomed. Res. Int.* **2019,** *2019*, 5620989. https://doi.org/10.1155/2019/5620989

Abdel-Aziz, H. M.; Farag, R. S.; Abdel-Gawad, S. A. Removal of Caffeine from Aqueous Solution by Green Approach Using *Ficus benjamina* Zero-Valent Iron/Copper Nanoparticles. *Adsorp. Sci. Technol.* **2020**, *38*, 325–343. https://doi.org/10.1177/0263617420947495

Abdelhady, M. A.; Abdelghany, T. M.; Mohamed, S. H.; Abdelbary, S. A. Impact of Green Synthesized Zinc Oxide Nanoparticles for Treating Dry Rot in Potato Tubers. *BioResources* **2024**, *19* (2). https://doi.org/10.15376/biores.19.2.2106-2119

Abdelkader, D. H.; Negm, W. A.; Elekhnawy, E.; Eliwa, D.; Aldosari, B. N.; Almurshedi, A. S. Zinc Oxide Nanoparticles as Potential Delivery Carrier: Green Synthesis by *Aspergillus niger* Endophytic Fungus, Characterization, and In Vitro/In Vivo Antibacterial Activity. *Pharmaceuticals* **2022,** *15* (9), 1057. https://doi.org/10.3390/ph15091057

Abdelraheem, W. M.; Khairy, R. M.; Zaki, A. I.; Zaki, S. H. Effect of ZnO nanoparticles on Methicillin, Vancomycin, Linezolid Resistance and Biofilm Formation in *Staphylococcus aureus* isolates. *Ann. Clin. Microbiol. Antimicrob.* **2021**, *20* (1), 54. https://doi.org/10.1186/s12941-021-00459-2

Abou El-Nour, K. M. M.; Eftaiha, A.; Al-Warthan, A.; Ammar, R. A. A. Synthesis and Applications of Silver Nanoparticles. *Arab. J. Chem.* **2010**, *3* (3), 135–140. https://doi.org/10.1016/j.arabjc.2010.04.008

Absar, A.; Satyajyoti, S.; Khan, M. I.; Rajiv, K.; Sastry, M. Extracellular/Intracellular Biosynthesis of Gold Nanoparticles by an Alkalo-tolerant Fungus *Trichothecium* sp. *J. Biomed. Nanotechnol.* **2005**, *1*, 47–53. https://doi.org/10.1166/jbn.2005.012

Adeli, M.; Hosainzadegan, H.; Pakzad, I.; Zabihi, F.; Alizadeh, M.; Karimi, F. Preparation of Silver Nanoparticle Containing Starch Foods and Evaluation of Antimicrobial Activity. *Jundishapur J. Microbiol.* **2013**, *6* (4), e5075. https://doi.org/10.5812/jjm.5075

Agarwal, H.; Kumar, S. V.; Rajeshkumar, S. A Review on Green Synthesis of Zinc Oxide Nanoparticles—An Eco-Friendly Approach. *Resour.-Efficient Technol.* **2017**, *3* (4), 406–413. https://doi.org/10.1016/j.reffit.2017.03.002

Agarwal, H.; Kumar, S. V.; Rajeshkumar, S. A Review on Green Synthesis of Zinc Oxide Nanoparticles–An Eco-Friendly Approach. *Resour.-Efficient Technol.* **2017,** *3* (4), 406-413. https://doi.org/10.1016/j.reffit.2017.03.002

Ahmad, A.; Senapati, S.; Khan, M. I.; Kumar, R.; Ramani, R.; Srinivas, V.; Sastry, M. Intracellular Synthesis of Gold Nanoparticles by a Novel Alkalotolerant Actinomycete, *Rhodococcus* Species. *Nanotechnology* **2003**, *14* (7), 824. https://doi.org/10.1088/0957-4484/14/7/323

Ahmad, H.; Venugopal, K.; Rajagopal, K.; De Britto, S.; Nandini, B.; Pushpalatha, H. G.; Konappa, N.; Udayashankar, A. C.; Geetha, N.; Jogaiah, S. Green Synthesis and Characterization of Zinc Oxide Nanoparticles Using *Eucalyptus globulus* and Their Fungicidal Ability Against Pathogenic Fungi of Apple Orchards. *Biomolecules* **2020**, *10* (3), 425. https://doi.org/10.3390/biom10030425

Ahmed, S.; Chaudhry, S. A.; Ikram, S. A Review on Biogenic Synthesis of ZnO Nanoparticles Using Plant Extracts and Microbes: A Prospect Towards Green Chemistry. *J. Photochem. Photobiol. B Biol.* **2017,** *166*, 272-284. https://doi.org/10.1016/j.jphotobiol.2016.12.003

Ahmed, S.; Khan, M. T.; Abbasi, A.; Haq, I. U.; Hina, A.; Mohiuddin, M.; Li, Y. Characterizing Stomatal Attributes and Photosynthetic Induction in Relation to Biochemical Changes in *Coriandrum sativum* L. by Foliar-Applied Zinc Oxide

Nanoparticles under Drought Conditions. *Front. Plant Sci.* **2023**, *13*, 1079283. https://doi.org/10.3389/fpls.2023.1079283

Ahmed, S.; Saifullah, S.; Ahmad, M.; Swami, B. L.; Ikram, S. Green Synthesis of Silver Nanoparticles Using *Azadirachta indica* Aqueous Leaf Extract. *J. Radiat. Res. Appl. Sci.* **2016**, *9* (1), 1–7. https://doi.org/10.1016/j.jrras.2015.06.006

Ainsworth, E. A.; Serbin, S. P.; Skoneczka, J. A.; Townsend, P. A. Using Leaf Optical Properties to Detect Ozone Effects on Foliar Biochemistry. *Photosynth. Res.* **2014**, *119* (1), 65–76. https://doi.org/10.1007/s11120-013-9800-2

Al Musayeib, N. M.; Amina, M.; Maqsood, F.; Bokhary, K. A.; Alrashidi, N. S. Biogenic Synthesis of Photosensitive Magnesium Oxide Nanoparticles Using Citron Waste Peel Extract and Evaluation of Their Antibacterial and Anticarcinogenic Potential. *Bioinorg. Chem. Appl.* **2024**, *2024* (1), 8180102. https://doi.org/10.1155/2024/8180102

Alaniz, S.; Leoni, C.; Bentancur, O.; Mondino, P. Elimination of Summer Fungicide Sprays for Apple Scab (*Venturia inaequalis*) Management in Uruguay. *Scientia Horticulturae* **2014**, *165*, 331–335, ISSN 0304-4238. https://doi.org/10.1016/j.scienta.2013.11.016

Al-Darwesh, M. Y.; Ibrahim, S. S.; Mohammed, M. A. A Review on Plant Extract Mediated Green Synthesis of Zinc Oxide Nanoparticles and Their Biomedical Applications. *Results Chem.* **2024**, 101368. https://doi.org/10.1016/j.rechem.2023.101368

Al-Dbass, A. M., Al Daihan, S., Al-Nasser, A. A., Al-Suhaibani, L. S., Almusallam, J., Alnwisser, B. I., & Bhat, R. S. Biogenic Silver Nanoparticles from Two Varieties of *Agaricus bisporus* and Their Antibacterial Activity. *Molecules* **2022**, *27* (21), 7656. https://doi.org/10.3390/molecules27217656

Alexopoulos, C. J.; Mims, C. W.; Blackwell, M. *Introductory Mycology*; John Wiley & Sons: New York, **1996**; pp. 869.

Alghuthaymi, M. A.; Almoammar, H.; Rai, M.; Said-Galiev, E.; Abd-Elsalam, K. A. Myconanoparticles: Synthesis and Their Role in Phytopathogens Management. *Biotechnol. Biotechnol. Equip.* **2015**, *29*, 221–236. https://doi.org/10.1080/13102818.2015.1008194

Ali, A. T.; Karem, L. K. A. Biosynthesis, Characterization, Adsorption and Antimicrobial Studies of Manganese Oxide Nanoparticles Using *Punica granatum* Extract. *Baghdad Sci. J.* **2024**, *21* (3), 0952-0952. https://doi.org/10.21123/bsj.2024.21.3.0952

Ali, J.; Irshad, R.; Li, B.; Tahir, K.; Ahmad, A.; Shakeel, M.; Khan, N. U.; Khan, Z. U. H. Synthesis and Characterization of Phytochemical Fabricated Zinc Oxide Nanoparticles with Enhanced Antibacterial and Catalytic Applications. *J. Photochem. Photobiol. B* **2018**, *183*, 349–356. https://doi.org/10.1016/j.jphotobiol.2018.05.006

Ali, K.; Dwivedi, S.; Azam, A.; Saquib, Q.; Al-Said, M. S.; Alkhedhairy, A. A.; Musarrat, J. *Aloe vera* Extract Functionalized Zinc Oxide Nanoparticles as Nanoantibiotics Against Multidrug-Resistant Clinical Bacterial Isolates. *J. Colloid Interface Sci.* **2016,** *472*, 145–156. https://doi.org/10.1016/j.jcis.2016.03.021

Ali, M. A.; Ahmed, T.; Wu, W.; Hossain, A.; Hafeez, R.; Islam Masum, M. M.; Wang, Y.; An, Q.; Sun, G.; Li, B. Advancements in Plant and Microbe-Based Synthesis of Metallic Nanoparticles and Their Antimicrobial Activity Against Plant Pathogens. *Nanomaterials* **2020**, *10* (6), 1146. https://doi.org/10.3390/nano10061146

Ali, M. I.; Sharma, G.; Kumar, M.; Jasuja, N. D. Biological Approach of Magnesium Oxide Nanoparticles Synthesize by *Spirulina platensis*. *World J. Pharm. Res.* **2015**, *4* (7), 1234–1241.

Ali, S.; Fatima, L.; Ahmad, M. U.; Khan, Q. F.; Hayyat, M. U.; Siddiq, Z.; Bourhia, M. Green Synthesis of *Agaricus avensis*-Mediated Silver Nanoparticles for Improved Catalytic Efficiency of Tyrosine Hydroxylase Towards Potential Biomedical

Implications. *Discover Life* **2024a**, *54* (1), 4. https://doi.org/10.1007/s11084-024-09647-4

Ali, S.; Ulhassan, Z.; Ali, S.; Kaleem, Z.; Yousaf, M. A.; Sheteiwy, M. S.; Zhou, W. Differential Responses of *Brassica napus* Cultivars to Dual Effects of Magnesium Oxide Nanoparticles. *Environ. Sci. Pollut. Res.* **2024b**, *31* (8), 12446–12466. https://doi.org/10.1007/s11356-023-25533-9

Alizadeh, S.; Dumanoğlu, H. The Effects of Zinc Oxide Nanoparticles Loaded with IAA and IBA on In Vitro Rooting of Apple Microcuttings. *Turkish J. Agric. For.* **2022**, *46* (3), 306–317. https://doi.org/10.55730/1300-011x.3004

Al-Mohaimeed, A. M.; Al-Onazi, W. A.; El-Tohamy, M. F. Multifunctional Eco-Friendly Synthesis of ZnO Nanoparticles in Biomedical Applications. *Molecules* **2022**, *27* (2), 579. https://doi.org/10.3390/molecules27020579

Alsharif, S. M.; Salem, S. S.; Abdel-Rahman, M. A.; Fouda, A.; Eid, A. M.; Hassan, S. E.-D.; Awad, M. A.; Mohamed, A. A. Multifunctional Properties of Spherical Silver Nanoparticles Fabricated by Different Microbial Taxa. *Heliyon* **2020**, *6*, e03943. https://doi.org/10.1016/j.heliyon.2020.e03943

Alves, M. J.; Ferreira, I. C.; Dias, J.; Teixeira, V.; Martins, A.; Pintado, M. A Review on Antimicrobial Activity of Mushroom (Basidiomycetes) Extracts and Isolated Compounds. *Planta Med.* **2012**, *78* (16), 1707–1718. https://doi.org/10.1055/s-0032-1329460

Amatya, S.P.; Shrestha, S.; Aryal, Y. Green Approach for Synthesis of Manganese Nanoparticle using Banana Peel (*Musa paradiasca*) and Its Characterization. *Environment* **2021**, *2*, 1-6.

Amin, M. A. A.; Abu-Elsaoud, A. M.; Nowwar, A. I.; Abdelwahab, A. T.; Awad, M. A.; Hassan, S. E. D.; Elkelish, A. Green Synthesis of Magnesium Oxide Nanoparticles Using Endophytic Fungal Strain to Improve the Growth, Metabolic Activities, Yield Traits, and Phenolic Compounds Content of *Nigella sativa* L.

Green Process. Synth. **2024,** *13* (1), 20230215. https://doi.org/10.1515/gps-2023-0215

Ammar, H. A.; Alghazaly, M. S.; Assem, Y.; Abou Zeid, A. A. Bioengineering and Optimization of PEGylated Zinc Nanoparticles by Simple Green Method Using *Monascus purpureus*, and Their Powerful Antifungal Activity Against the Most Famous Plant Pathogenic Fungi, Causing Food Spoilage. *Environ. Nanotechnol. Monit. Manage.* **2021**, *16*, 100543. https://doi.org/10.1016/j.enmm.2021.100543

Ammulu, M. A.; Viswanath, K. V.; Giduturi, A. K.; Vemuri, P. K.; Mangamuri, U.; Poda, S. Phytoassisted Synthesis of Magnesium Oxide Nanoparticles from *Pterocarpus marsupium* Rox.b Heartwood Extract and Its Biomedical Applications. *J. Genet. Eng. Biotechnol.* **2021**, *19*, 21. https://doi.org/10.1186/s43141-021-00109-4

Anar, M.; Akbar, M.; Tahir, K.; Chaudhary, H. J.; Munis, M. F. H. Biosynthesized Manganese Oxide Nanoparticles Maintain Firmness of Tomato Fruit by Modulating Soluble Solids and Reducing Sugars Under Biotic Stress. *Physiol. Mol. Plant Pathol.* **2023**, *127*, 102126. https://doi.org/10.1016/j.pmpp.2023.102126

Anil Kumar, S. A.; Abyaneh, M. K.; Gosavi, S. W.; Kulkarni, S. K.; Pasricha, R.; Ahmad, A.; Khan, M. I. Nitrate Reductase-Mediated Synthesis of Silver Nanoparticles from AgNO3. *Biotechnol. Lett.* **2007**, *29* (3), 439–445. https://doi.org/10.1007/s10529-006-9256-7

Anjum, S.; Vyas, A.; Sofi, T. A. Mycogenic Fabrication of Zinc Nanoparticles for Their Antifungal Activity Against *Alternaria mali*. *Indian J. Microbiol.* **2024**, *1–19*. https://doi.org/10.1007/s12088-024-01363-x

Anonymous. *Annual Report 1999–2000*; Sher-e-Kashmir University of Agricultural Sciences and Technology (Kashmir): Shalimar, Srinagar, **2000**; pp. 74.

Anonymous. *Digest of Statistics 2012–13*; Directorate of Economics and Statistics, Government of Jammu and Kashmir: Srinagar, J & K, India, 2013.

Aryal, S.; Park, H.; Leary, J. F.; Key, J. Top-Down Fabrication-Based Nano/Microparticles for Molecular Imaging and Drug Delivery. *Int. J. Nanomed.* **2019**, *14*, 6631–6644. https://doi.org/10.2147/IJN.S212037

Asaikkutti, A.; Bhavan, P. S.; Vimala, K.; Karthik, M.; Cheruparambath, P. Dietary Supplementation of Green Synthesized Manganese-Oxide Nanoparticles and Its Effect on Growth Performance, Muscle Composition, and Digestive Enzyme Activities of the Giant Freshwater Prawn *Macrobrachium rosenbergii*. *J. Trace Elem. Med. Biol.* **2016**, *35*, 7–17. https://doi.org/10.1016/j.jtemb.2016.01.007

Ashrafi, A. A.; Jagadish, C. Review of Zincblende ZnO: Stability of Metastable ZnO Phases. *J. Appl. Phys.* **2007**, *102* (7), 071101–071101-12. https://doi.org/10.1063/1.2787957

Aung, Y. M.; Than, Y. M.; Khin, J. J.; Kyaw, M. T.; Kyaw, N. E. E. Green Synthesis and Characterization of Magnesium Oxide Nanoparticles Using Aqueous Leaf Extract of *Moringa oleifera* Lam. Doctoral Dissertation, MERAL Portal, **2023**.

Azhar, B. J.; Noor, A.; Zulfiqar, A.; Zeenat, A.; Ahmad, S.; Chishti, I.; Shakeel, S. N. Effect of ZnO, SiO2 and Composite Nanoparticles on Arabidopsis thaliana and Involvement of Ethylene and Cytokinin Signaling Pathways. *Pak. J. Bot.* **2021**, *53* (2), 437-446. http://dx.doi.org/10.30848/PJB2021-2(40)

Aziz, N.; Faraz, M.; Pandey, R.; Shakir, M.; Fatma, T.; Varma, A.; Barman, I.; Prasad, R. Facile Algae derived Route to Biogenic Silver Nanoparticles: Synthesis, Antibacterial and Photocatalytic Properties. *Langmuir* **2015**, *31* (42), 11605–11612. https://doi.org/10.1021/acs.langmuir.5b03081

Baig, N.; Kammakakam, I.; Falath, W. Nanomaterials: A Review of Synthesis Methods, Properties, Recent Progress, and Challenges. *Mater. Adv.* **2021**, *2*, 182. https://doi.org/10.1039/d0ma00807a

Balint, J.; Nagy, S.; Thiesz, R.; Nyaradi, I. I.; Balog, A. Using Plant Extracts to Reduce Asexual Reproduction of Apple Scab (*Venturia inaequalis*). *Turk. J. Agric. For.* **2014**, *38* (1), 91–98. https://doi.org/10.3906/tar-1309-98

Banerjee, S.; Islam, J.; Mondal, S.; Saha, A.; Saha, B.; Sen, A. Proactive Attenuation of Arsenic-Stress by Nano-Priming: Zinc Oxide Nanoparticles in *Vigna Mungo* (L.) Hepper Trigger Antioxidant Defense Response and Reduce Root-Shoot Arsenic Translocation. *J. Hazard. Mater.* **2023**, *446*, 130735. https://doi.org/10.1016/j.jhazmat.2023.130735

Bano, Z.; Rajarathnam, S. Pleurotus Mushrooms. II. Chemical Composition, Nutritional Value, Post-Harvest Physiology, Preservation and Role as Human Food. *CRC Crit. Rev. Food Sci. Nutr.* **1988**, *27*, 87–102. https://doi.org/10.1080/10408398809527480

Barabadi, H.; Tajani, B.; Moradi, M.; Damavandi Kamali, K.; Meena, R.; Honary, S.; Mahjoub, M. A.; Saravanan, M. *Penicillium* Family as Emerging Nanofactory for Biosynthesis of Green Nanomaterials: A Journey into the World of Microorganisms. *J. Cluster Sci.* **2019**, *30*, 843–856. https://doi.org/10.1007/s10876-019-01554-3

Bayda, S.; Adeel, M.; Tucumcari, T.; Cordani, M.; Rizzolio, F. The History of Nanoscience and Nanotechnology: From Chemical-Physical Applications to Nanomedicine. *Molecules* **2019**, *25*, 112. https://doi.org/10.3390/molecules25010112

Bekele, S. G.; Ganta, D. D.; Endashaw, M. Green Synthesis and Characterization of Zinc Oxide Nanoparticles Using *Monoon longifolium* Leaf Extract for Biological Applications. *Discover Chem.* **2024**, *1* (1), 1–17. https://doi.org/10.1007/s44371-024-00007-9

Bénaouf, G.; Parisi, L. Genetics of Host-Pathogen Relationships Between *Venturia inaequalis* Races 6 and 7 and *Malus* Species. *Phytopathology* **2000**, *90*, 236–242. https://doi.org/10.1094/PHYTO.2000.90.3.236

Bernaś, E.; Jaworska, G.; Kmiecik, W. Storage and Processing of Edible Mushrooms. *Acta Sci. Pol. Technol. Aliment.* **2006a**, *5*, 5–23.

Bernaś, E.; Jaworska, G.; Lisiewska, Z. Edible Mushrooms as a Source of Valuable Nutritive Constituents. *Acta Sci. Pol. Technol. Aliment.* **2006b**, *5*, 5–20.

Berrie, A. M.; Xu, X. M. Managing Apple Scab (*Venturia inaequalis*) and Powdery Mildew (*Podosphaera leucotricha*) Using Adem. *Int. J. Pest Manag.* **2003**, *49*, 243–249. https://doi.org/10.1080/0967087031000123938

Bhardwaj, K.; Dhanjal, D. S.; Sharma, A.; Thakur, M. S.; Khan, Y.; Kumar, S.; Prasad, J.; Singh, R. Conifer-Derived Metallic Nanoparticles: Green Synthesis and Biological Applications. *Int. J. Mol. Sci.* **2020**, *21* (23), 9028. https://doi.org/10.3390/ijms21239028

Bhardwaj, K.; Sharma, A.; Tejwan, N.; Bhardwaj, S.; Bhardwaj, P.; Nepovimova, E.; Shami, A.; Kalia, A.; Kumar, A.; Abd-Elsalam, K. A.; Kuca, K. *Pleurotus* Macrofungi-Assisted Nanoparticle Synthesis and Its Potential Applications: A Review. *J. Fungi* **2020**, *6*, 351. https://doi.org/10.3390/jof6040351

Bharose, A. A.; Hajare, S. T.; HP, G.; Soni, M.; Prajapati, K. K.; Singh, S. C.; Upadhye, V. Bacteria-Mediated Green Synthesis of Silver Nanoparticles and Their Antifungal Potentials against *Aspergillus flavus*. *PLoS One* **2024**, *19* (3), e0297870. https://doi.org/10.1371/journal.pone.0297870

Bhat, K. A.; Peerzada, S. H.; Anwar, A. *Alternaria* Epidemic of Apple in Kashmir Valley. *Afr. J. Microbiol. Res.* **2015**, *9* (12), 831–837. https://doi.org/10.5897/AJMR2015.7397

Bhushan, A.; Kulshreshtha, M. The Medicinal Mushroom *Agaricus bisporus*: Review of Phytopharmacology and Potential Role in the Treatment of Various Diseases. *J. Nat. Sci. Med.* **2018**, *1* (1), 4–9. https://doi.org/10.4103/JNSM.JNSM_1_18

Birla, S. S.; Tiwari, V. V.; Gade, A. K.; Ingle, A. P.; Yadav, A. P.; Rai, M. K. Fabrication of Silver Nanoparticles by *Phoma glomerata* and Its Combined Effect Against *Escherichia coli, Pseudomonas aeruginosa* and *Staphylococcus aureus*. *Lett. Appl. Microbiol.* **2009**, *48* (2), 173–179. https://doi.org/10.1111/j.1472-765X.2008.02510.x

Biswas, P.; Wu, C.-Y. Nanoparticles and the Environment. *J. Air Waste Manag. Assoc.* **2005**, *55* (6), 708–746. https://doi.org/10.1080/10473289.2005.10464656

Bloom, A. J.; Mooney, H. A.; Björkman, O.; Berry, J. Materials and Methods for Carbon Dioxide and Water Exchange Analysis. *Plant, Cell Environ.* **1980**, *3* (5), 371–376. https://doi.org/10.1111/j.1365-3040.1980.tb00835.x

Bodke, M. R.; Purushotham, Y.; Dole, B. N. Comparative Study on Zinc Oxide Nanocrystals Synthesized by Two Precipitation Methods. *Cerâmica* **2018**, *64* (369), 91–96. https://doi.org/10.1590/0366-69132018643691102

Bouqellah, N. A.; El-Sayyad, G. S.; Attia, M. S. Induction of Tomato Plant Biochemical Immune Responses by the Synthesized Zinc Oxide Nanoparticles Against Wilt-Induced *Fusarium oxysporum*. *Int. Microbiol.* **2024**, *27* (2), 435–448. https://doi.org/10.1007/s10123-023-00404-7

Boutchuen, A.; Zimmerman, D.; Aich, N.; Masud, A. M.; Arabshahi, A.; Palchoudhury, S. Increased Plant Growth with Hematite Nanoparticle Fertilizer Drop and Determining Nanoparticle Uptake in Plants Using Multimodal Approach. *J. Nanomater.* **2019**, *2019*, 6890572. https://doi.org/10.1155/2019/6890572

Bulajic, A.; Babovic, M. *Alternaria mali*, a New Pathogen of Apple in Yugoslavia. *Jugoslovensko Vocarstvo* **1997**, *31*, 21–25.

Burni, T.; Iftikhar, S.; Jabeen, M.; Zainab, S. B. Diversity of VA (Vesicular Arbuscular) Fungi in Some Weeds of Cauliflower Fields of Peshawar, Pakistan. *Pak. J. Plant Sci.* **2009**, *15*, 59–67.

Caglar, N. The Nutrients of Exotic Mushrooms (*Lentinula edodes* and *Pleurotus* Species) and an Estimated Approach to the Volatile Compounds. *Food Chem.* **2007**, *105*, 1188–1194. https://doi.org/10.1016/j.foodchem.2007.02.021

Cai, L.; Liu, M.; Liu, Z.; Yang, H.; Sun, X.; Chen, J.; Xiang, S.; Ding, W. MgONPs Can Boost Plant Growth: Evidence from Increased Seedling Growth, Morpho-Physiological Activities, and Mg Uptake in Tobacco (*Nicotiana tabacum* L.). *Molecules* **2018**, *23* (12), 3375. DOI: 10.3390/molecules23123375. https://doi.org/10.3390/molecules23123375

Cai, Y.; Li, C.; Wu, D.; Wang, W.; Tan, F.; Wang, X.; Wong, P. K.; Qiao, X. Highly Active MgO Nanoparticles for Simultaneous Bacterial Inactivation and Heavy Metal Removal from Aqueous Solution. *Chem. Eng. J.* **2017**, *312*, 158–166. https://doi.org/10.1016/j.cej.2016.11.120

Cao, Y.; Zhou, G.; Zhou, R.; Zhao, Y.; Liu, Y.; Zhang, J.; Xu, Y.; Zhang, J.; Zhang, J. Green Synthesis of Reusable Multifunctional γ-Fe_2O_3/Bentonite Modified by Doped TiO_2 Hollow Spherical Nanocomposite for Removal of BPA. *Sci. Total Environ.* **2020**, *708*, 134669. https://doi.org/10.1016/j.scitotenv.2019.134669

Cavalu, S.; Fritea, L.; Brocks, M.; Barbaro, K.; Murvai, G.; Costea, T. O.; Antoniac, I.; Verona, C.; Romani, M.; Latini, A.; Zilli, R.; Rau, J. V. Novel Hybrid Composites Based on PVA/SeTiO_2 Nanoparticles and Natural Hydroxyapatite for Orthopaedic Applications: Correlations between Structural, Morphological and Biocompatibility Properties. *Materials* **2020**, *13* (9), 2077. https://doi.org/10.3390/ma13092077

Chachei, K.; Ranjan, S.; Ram, K.; Singh, R. S. Effect of Nanocomposites on Sustainable Growth of Crop Plants and Productivity. *Nanotechnol.-Based Sustainable Agric.* **2025**, *47–76*. https://doi.org/10.1002/9783527849949.ch02

Chang, H. W.; Tsai, Y. C.; Cheng, C. W.; Lin, C. Y.; Wu, P. H. Preparation of Graphene-Supported Platinum Nanoparticles in Aqueous Solution by Femtosecond Laser Pulses for Methanol Oxidation. *J. Power Sources* **2013**, *239*, 164–168. https://doi.org/10.1016/j.jpowsour.2013.03.119

Chang, S. T.; Miles, P. G. *Mushroom Biology: A New Discipline.* The Mycologist, 1993.

Chang, S. T.; Miles, P. G. *Mushrooms: Cultivation, Nutritional Value, Medicinal Effect, and Environmental Impact*; CRC Press: Boca Raton, **2004**; pp. 451.

Chang, S. T.; Miles, P. G. Recent Trends in World Production of Cultivated Edible Mushrooms. *Mushroom J.* **1991**, *504*, 15–18.

Chatterjee, S.; Ja, A.; Subramanian, A.; Subramanian, S. Synthesis and Characterization of Manganese Dioxide Using *Brassica oleracea* (Cabbage). *J. Ind. Pollut. Control* **2017,** *33* (2), 1627-1632.

Chaudhuri, S. K.; Malodia, L. Biosynthesis of Zinc Oxide Nanoparticles Using Leaf Extract of *Calotropis gigantea*: Characterization and Its Evaluation on Tree Seedling Growth in Nursery Stage. *Appl. Nanosci.* **2017**, *7*, 501–512. https://doi.org/10.1007/s13204-017-0586-7

Chen, H.; Song, Y.; Wang, Y.; Wang, H.; Ding, Z.; Fan, K. ZnO Nanoparticles: Improving Photosynthesis, Shoot Development, and Phyllosphere Microbiome Composition in Tea Plants. *J. Nanobiotechnol.* **2024,** *22* (1), 389. https://doi.org/10.1186/s12951-024-02667-2

Chen, S.; Zhu, J.; Wu, X.; Han, Q.; Wang, X. Graphene Oxide−MnO_2 Nanocomposites for Supercapacitors. *ACS Nano* **2010,** *4* (5), 2822-2830. https://doi.org/10.1021/nn901531n

Chen, Y.-H.; Yeh, C.-S. Laser Ablation Method: Use of Surfactants to Form the Dispersed Ag Nanoparticles. *Colloids Surf. A Physicochem. Eng. Asp.* **2002**, *197* (1–3), 133–139. https://doi.org/10.1016/S0927-7757(01)00854-8

Cheung, P. C. K. Mini-Review on Edible Mushrooms as Source of Dietary Fiber: Preparation and Health Benefits. *Food Sci. Human Wellness* **2013**, *2*, 162–166. https://doi.org/10.1016/j.fshw.2013.08.001

Chokriwal, A.; Sharma, M. M.; Singh, A. Biological Synthesis of Nanoparticles Using Bacteria and Their Applications. *Am. J. Pharm. Tech. Res.* **2014**, *4* (6), 38–61.

Cioffi, N.; Torsi, L.; Ditaranto, N.; Tantillo, G.; Ghibelli, L.; Sabbatini, L. Copper Nanoparticle/Polymer Composites with Antifungal and Bacteriostatic Properties. *Chem. Mater.* **2005**, *17*, 5255–5262. https://doi.org/10.1021/cm0505244

Cioffi, N.; Torsi, L.; Ditaranto, N.; Tantillo, G.; Ghibelli, L.; Sabbatini, L. Copper nanoparticle/polymer composites with antifungal and bacteriostatic properties. *Chem. Mater.* **2005**, *17*, 5255-5262. https://doi.org/10.1021/cm0481693

Clarance, P.; Luvankar, B.; Sales, J.; Khusro, A.; Agastian, P.; Tack, J. C.; Al Khulaifi, M. M.; Al-Shwaiman, H. A.; Elgorban, A. M.; Syed, A.; Kim, H. J. Green Synthesis and Characterization of Gold Nanoparticles Using Endophytic Fungi *Fusarium solani* and Its In-Vitro Anticancer and Biomedical Applications. *Saudi J. Biol. Sci.* **2020**, *27*, 706–712. https://doi.org/10.1016/j.sjbs.2019.12.026

Coates, J. Interpretation of Infrared Spectra, a Practical Approach. *Encycl. Anal. Chem. Appl. Theory Instrum.* **2006**, 1–23.

Colak, M.; Baysal, E.; Simsek, H.; Toker, H.; Yilmaz, F. Cultivation of Agaricus bisporus on Wheat Straw and Waste Tea Leaves Based Composts and Locally Available Casing Materials Part III: Dry Matter, Protein, and Carbohydrate Contents of Agaricus bisporus. *Afr. J. Biotechnol.* **2007**, *6* (24), 2855–2859. https://doi.org/10.5897/AJB2007.000-2455

Crisian, E. V.; Sands, A. The Biology and Cultivation of Edible Fungi; Academic Press: New York, **1978**.

da Silva Magalhães, A. A.; de Amorim Silva, T.; da Silva, S. D.; Teixeira, M. F. S.; Seabra, A. B.; de Magalhães Junior, P. F. C.; Pereira, J. O. Biosynthesis of Silver Nanoparticles by *Lentinus crinitus*: Characterization and Antimicrobial Activity. *Res. Soc. Dev.* **2022**, *11* (14), e429111436261. https://doi.org/10.33448/rsd-v11i14.436261

Dang, K.; Wang, Y.; Tian, H.; Bai, J.; Cheng, X.; Guo, L.; Shao, X. Impact of ZnO NPs on Photosynthesis in Rice Leaves Plants Grown in Saline-Sodic Soil. *Sci. Rep.* **2024**, *14* (1), 16233.

Das, B.; Moumita, S.; Ghosh, S.; Khan, M. I.; Indira, D.; Jayabalan, R.; Tripathy, S. K.; Mishra, A.; Balasubramanian, P. Biosynthesis of Magnesium Oxide (MgO) Nanoflakes by Using Leaf Extract of *Bauhinia purpurea* and Evaluation of Its

Antibacterial Property Against *Staphylococcus aureus*. *Mater. Sci. Eng. C* **2018,** *91*, 436-444. https://doi.org/10.1016/j.msec.2018.05.047.

Das, R. K.; Pachapur, V. L.; Lonappan, L.; Naghdi, M.; Pulicharla, R.; Maiti, S.; Cledon, M.; Dalila, L. M.; Sarma, S. J.; Brar, S. K. Biological Synthesis of Metallic Nanoparticles: Plants, Animals and Microbial Aspects. *Nanotechnol. Environ. Eng.* **2017**, *2*, 1–21. https://doi.org/10.1007/s41204-017-0029-4

Das, S. K.; Das, A. R.; Guha, A. K. Microbial Synthesis of Multishaped Gold Nanostructures. *Small* **2010**, *6* (9), 1012–1021. https://doi.org/10.1002/smll.200902367

Debbarma, S.; Sharma, S.; Kalia, A. Pleurotus Extract–Mediated Selenium and Zinc Nanoparticles Exhibited Improved Yield of Biofortified Fruit Bodies. *International Microbiology* **2024**, 1–12. https://doi.org/10.1007/s10123-023-00283-4

Dėnė, L.; Chrapačienė, S.; Laurinaitytė, G.; Rudinskaitė, A.; Viškelis, J.; Viškelis, P.; Balčiūnaitienė, A. Green Synthesis of Silver Nanoparticles with *Hyssopus officinalis* and *Salvia officinalis* Extracts, Their Properties, and Antifungal Activity on *Fusarium* spp. *Plants* **2024**, *13* (12), 1611. https://doi.org/10.3390/plants13121611

Dessie, Y.; Tadesse, S.; Eswaramoorthy, R. Physicochemical Parameter Influences and Their Optimization on the Biosynthesis of MnO_2 Nanoparticles Using *Vernonia amygdalina* Leaf Extract. *Arab J. Chem.* **2020**, *13*, 6472–6492. https://doi.org/10.1016/j.arabjc.2020.06.006

Dhanalakshmi, M.; Losetty, V. Investigation of Antibacterial, Antioxidant, Cytotoxicity, and Photocatalytic Dye Degradation Activity of Green Synthesized Copper Oxide Nanoparticles Using *Ceropegia debilis* Plant Extract. *Clean Technol. Environ. Policy* **2024**, *1*–16. https://doi.org/10.1007/s10098-023-02627-1

Dhillon, G. S.; Brar, S. K.; Kaur, S.; Verma, M. Green Approach for Nanoparticle Biosynthesis by Fungi: Current Trends and Applications. *Crit. Rev. Biotechnol.* **2012**, *32* (1), 49–73. https://doi.org/10.3109/07388551.2010.550568

Dhoble, S. M.; Kulkarni, N. S. Antimycotic Activity of Zinc and Manganese Nanoparticles on Commercially Important Phytopathogens of Soybean (*Glycine max* (L.) Merril). *Sch. Acad. J. Biosci.* **2016**, *4* (11), 1032–1037. https://doi.org/10.36347/sajb.2016.v04i11.010

Dhoble, S. M.; Kulkarni, N. S. Biosynthesis and Characterization of Different Metal Nanoparticles Using Fungi. *Sch. Acad. J. Biosci.* **2016,** *4* (11), 1022-1031. https://doi.org/10.36347/sajb.2016.v04i11.009

Dias, C.; Ayyanar, M.; Amalraj, S.; Khanal, P.; Subramaniyan, V.; Das, S.; Gurav, S. Biogenic Synthesis of Zinc Oxide Nanoparticles Using Mushroom Fungus *Cordyceps militaris*: Characterization and Mechanistic Insights of Therapeutic Investigation. *J. Drug Deliv. Sci. Technol.* **2022,** *73*, 103444. https://doi.org/10.1016/j.jddst.2022.103444

Digra, S.; Nonzom, S. An Insight into Endophytic Antimicrobial Compounds: An Updated Analysis. *Plant Biotechnol. Rep.* **2023**, *17* (4), 427–457. https://doi.org/10.1007/s11816-023-00958-x

Dimkpa, C. O.; Bindraban, P. S. Nanofertilizers: New Products for the Industry? *J. Agric. Food Chem.* **2017**, *66* (26), 6462–6473.

Din, M. I.; Najeeb, J.; Ahmad, G. Recent Advancements in the Architecting Schemes of Zinc Oxide-Based Photocatalytic Assemblies. *Sep. Purif. Rev.* **2018**, *47*, 267–287. https://doi.org/10.1080/15422119.2017.1405737

Dobrucka, R. Synthesis of MgO Nanoparticles Using *Artemisia abrotanum* Herba Extract and Their Antioxidant and Photocatalytic Properties. *Iran. J. Sci. Technol. Trans. A Sci.* **2018**, *42*, 547–555. https://doi.org/10.1007/s40940-018-0051-5

dos Santos, O. A. L.; dos Santos, M. S.; Antunes Filho, S.; Backx, B. P. Nanotechnology for the Control of Plant Pathogens and Pests. *Plant Nano Biol.* **2024**, *100080*. https://doi.org/10.1016/j.plana.2024.100080

Doughari, J. H.; Nuya, S. P. In Vitro Antifungal Activity of *Deteriummicrocarpum*. *Pak. J. Med. Sci.* **2008**, *24* (1), 91–95.

Doughari, J. H.; Nuya, S. P. In vitro antifungal activity of Deteriummicrocarpum. *Pak . J. Med. Sci.* **2008**, *24*, 91-955. https://doi.org/10.3923/pjms.2008.91.95

Drexler, E. K.; Peterson, C. L.; Pergamit, G. *Unbounding the Future: The Nanotechnology Revolution*; William Morrow and Company, Inc.: New York, NY, USA, **1991**.

Duncan, T. V. Applications of Nanotechnology in Food Packaging and Food Safety: Barrier Materials, Antimicrobials and Sensors. *J. Colloid Interface Sci.* **2011**, *363* (1), 1–24. https://doi.org/10.1016/j.jcis.2011.07.017

Duong, T. H. Y.; Nguyen, T. N.; Oanh, H. T.; Dang Thi, T. A.; Giang, L. N. T.; Phuong, H. T.; Anh, N. T.; Nguyen, B. M.; Tran Quang, V.; Le, G. T.; Nguyen, T. V. Synthesis of Magnesium Oxide Nanoplates and Their Application in Nitrogen Dioxide and Sulfur Dioxide Adsorption. *J. Chem.* **2019**, *2019*, 4376429. https://doi.org/10.1155/2019/4376429

Durán, A.; Nombela, C. Fungal Cell Wall Biogenesis: Building a Dynamic Interface with the Environment. *Microbiology (Reading)* **2004**, *150* (10), 3099–3103. https://doi.org/10.1099/mic.0.27551-0

Durán, N.; Marcato, P. D.; Alves, O. L.; De Souza, G. I.; Esposito, E. Mechanistic Aspects of Biosynthesis of Silver Nanoparticles by Several *Fusarium oxysporum* Strains. *J. Nanobiotechnol.* **2005**, *3* (1), 1-7. https://doi.org/10.1186/1477-3155-3-7

Durán, N.; Seabra, A. B. Metallic Oxide Nanoparticles: State of the Art in Biogenic Syntheses and Their Mechanisms. *Appl. Microbiol. Biotechnol.* **2012**, *95* (2), 275–288. https://doi.org/10.1007/s00253-012-4118-9

Durán, N.; Seabra, A. B. Metallic Oxide Nanoparticles: State of the Art in Biogenic Syntheses and Their Mechanisms. *Appl. Microbiol. Biotechnol.* **2012**, *95*, 275–288. https://doi.org/10.1007/s00253-012-4010-2

Ebbs, S. D.; Bradfield, S. J.; Kumar, P.; White, J. C.; Musante, C.; Ma, X. Accumulation of Zinc, Copper, or Cerium in Carrot (*Daucus carota*) Exposed to Metal Oxide Nanoparticles and Metal Ions. *Environ. Sci. Nano* **2016**, *3* (1), 114–126. https://doi.org/10.1039/C5EN00146A

El Messaoudi, N.; Ciğeroğlu, Z.; Şenol, Z. M.; Bouich, A.; Kazan-Kaya, E. S.; Noureen, L.; Américo-Pinheiro, J. H. P. Green Synthesis of Nanoparticles for Remediation of Organic Pollutants in Wastewater by Adsorption. **In** *Advances in Chemical Pollution, Environmental Management and Protection*; Elsevier: **2024**; Vol. 10, pp. 305–345.

El-Abeid, S. E.; Mosa, M. A.; El-Tabakh, M. A.; Saleh, A. M.; El-Khateeb, M. A.; Haridy, M. S. Antifungal Activity of Copper Oxide Nanoparticles Derived from *Zizyphus spina* Leaf Extract Against Fusarium Root Rot Disease in Tomato Plants. *J. Nanobiotechnol.* **2024**, *22* (1), 28. https://doi.org/10.1186/s12951-023-02102-7

El-Batal, A. I.; Al-Hazmi, N. E.; Mosallam, F. M.; El-Sayyad, G. S. Biogenic Synthesis of Copper Nanoparticles by Natural Polysaccharides and *Pleurotus ostreatus* Fermented Fenugreek Using Gamma Rays with Antioxidant and Antimicrobial Potential Towards Some Wound Pathogens. *Microb. Pathog.* **2018,** *118*, 1–8. https://doi.org/10.1016/j.micpath.2018.03.013

El-Batal, A. I.; El-Sayyad, G. S.; El-Ghamery, A.; Gobara, M. Response Surface Methodology Optimization of Melanin Production by *Streptomyces cyaneus* and Synthesis of Copper Oxide Nanoparticles Using Gamma Radiation. *J. Clust. Sci.* **2017a,** *28* (3), 1083–1112.

El-Batal, A. I.; El-Sayyad, G. S.; El-Ghamery, A.; Gobara, M. Response Surface Methodology Optimization of Melanin Production by *Streptomyces cyaneus* and Synthesis of Copper Oxide Nanoparticles Using Gamma Radiation. *J. Clust. Sci.* **2017a,** *28* (3), 1083–1112. https://doi.org/10.1007/s10876-016-1101-0

El-Batal, A. I.; El-Sayyad, G. S.; El-Ghamry, A.; Agaypi, K. M.; Elsayed, M. A.; Gobara, M. Melanin-Gamma Rays Assistants for Bismuth Oxide Nanoparticles

Synthesis at Room Temperature for Enhancing Antimicrobial, and Photocatalytic Activity. *J. Photochem. Photobiol. B* **2017b,** *173*, 120–139.

El-Batal, A. I.; El-Sayyad, G. S.; El-Ghamry, A.; Agaypi, K. M.; Elsayed, M. A.; Gobara, M. Melanin-Gamma Rays Assistants for Bismuth Oxide Nanoparticles Synthesis at Room Temperature for Enhancing Antimicrobial, and Photocatalytic Activity. *J. Photochem. Photobiol. B* **2017b,** *173*, 120–139. https://doi.org/10.1016/j.jphotobiol.2017.05.030

Elkhateeb, O.; Atta, M. B.; Mahmoud, E. Biosynthesis of Iron Oxide Nanoparticles Using Plant Extracts and Evaluation of Their Antibacterial Activity. *AMB Express* **2024**, *14* (1), 92. https://doi.org/10.1186/s13568-024-01598-7

Elmastas, M.; Isildak, O.; Turkekul, I.; Temur, N. Determination of Antioxidant Activity and Antioxidant Compounds in Wild Edible Mushrooms. *J. Food Compos. Anal.* **2007**, *20*, 337–345. https://doi.org/10.1016/j.jfca.2006.07.003

Elmer, W. H.; White, J. C. The Use of Metallic Oxide Nanoparticles To Enhance Growth of Tomatoes and Eggplants in Disease-Infested Soil or Soilless Medium. *Environ. Sci.: Nano* **2018**, *5* (6), 1300-1310. https://doi.org/10.1039/C8EN00279A

Elmer, W. H.; White, J. C. The Use of Metallic Oxide Nanoparticles to Enhance Growth of Tomatoes and Eggplants in Disease Infested Soil or Soilless Medium. *Environ. Sci.: Nano* **2016,** *3* (5), 1072–1079. https://doi.org/10.1039/C6EN00146G

El-Moslamy, S. H.; Yahia, I. S.; Zahran, H. Y.; Kamoun, E. A. Novel Biosynthesis of MnO NPs Using Mycoendophyte: Industrial Bioprocessing Strategies and Scaling-Up Production with Its Evaluation as Anti-Phytopathogenic Agents. *Sci. Rep.* **2023**, *13* (1), 2052. https://doi.org/10.1038/s41598-023-28788-0

El-Naggar, N. E. A.; Shiha, A. M.; Mahrous, H.; Mohammed, A. A. A Sustainable Green Approach for Biofabrication of Chitosan Nanoparticles: Optimization, Characterization, Antifungal Activity Against Phytopathogenic *Fusarium culmorum*, and Antitumor Activity. *Sci. Rep.* **2024**, *14* (1), 11336. https://doi.org/10.1038/s41598-024-71024-4

El-Saadony, M. T.; Alkhatib, F. M.; Alzahrani, S. O.; Shafi, M. E.; Abdel-Hamid, S. E.; Taha, T. F.; Aboelenin, S. M.; Soliman, M. M.; Ahmed, N. H. Impact of Mycogenic Zinc Nanoparticles on Performance, Behavior, Immune Response, and Microbial Load in *Oreochromis niloticus*. *Saudi J. Biol. Sci.* **2021**, *28* (8), 4592–4604. https://doi.org/10.1016/j.sjbs.2021.04.066

El-Sayyad, G. S.; Mosallam, F. M.; El-Batal, A. I. One-Pot Green Synthesis of Magnesium Oxide Nanoparticles Using *Penicillium chrysogenum* Melanin Pigment and Gamma Rays with Antimicrobial Activity Against Multidrug-Resistant Microbes. *Adv. Powder Technol.* **2018**, *29* (11), 2616–2625. https://doi.org/10.1016/j.apt.2018.07.009

El-Sayyad, G. S.; Mosallam, F. M.; El-Batal, A. I. One-Pot Green Synthesis of Magnesium Oxide Nanoparticles Using *Penicillium chrysogenum* Melanin Pigment and Gamma Rays with Antimicrobial Activity Against Multidrug-Resistant Microbes. *Adv. Powder Technol.* **2018,** *29* (11), 2616-2625. https://doi.org/10.1016/j.apt.2018.07.009

Escalona, J.; Flexas, J.; Medrano, H. Stomatal and Nonstomatal Limitations of Photosynthesis Under Water Stress in Field-Grown Grapevines. *Funct. Plant Biol.* **2000**, *127*, 87–87. https://doi.org/10.1071/PP99209

Essien, E. R.; Atasie, V. N.; Okeafor, A. O.; Nwude, D. O. Biogenic Synthesis of Magnesium Oxide Nanoparticles Using *Manihot esculenta* (Crantz) Leaf Extract. *Int. Nano Lett.* **2020**, *10* (1), 43–48. https://doi.org/10.1007/s40089-019-00296-7

Faisal, S.; Khan, S.; Abdullah, Z.; Zafar, S.; Rizwan, M.; Ali, M.; Akbar, F. Fagonia cretica-Mediated Synthesis of Manganese Oxide (MnO_2) Nanomaterials: Their Characterization and Evaluation of Their Bio-Catalytic and Enzyme Inhibition Potential for Maintaining Flavor and Texture in Apples. *Catalysts* **2022**, *12* (5), 558. https://doi.org/10.3390/catal12050558

Faizan, M.; Bhat, J. A.; El-Serehy, H. A.; Moustakas, M.; Ahmad, P. Magnesium Oxide Nanoparticles (MgO-NPs) Alleviate Arsenic Toxicity in Soybean by Modulating

Photosynthetic Function, Nutrient Uptake, and Antioxidant Potential. *Metals* **2022**, *12* (12), 2030. https://doi.org/10.3390/met12122030

Faizan, M.; Faraz, A.; Yusuf, M.; Khan, S.; Hayat, S. Zinc Oxide Nanoparticle-Mediated Changes in Photosynthetic Efficiency and Antioxidant System of Tomato Plants. *Photosynthetica* **2017**, *56*, 678–686. https://doi.org/10.1007/s11099-018-0794-5

Fakhari, S.; Jamzad, M.; Kabiri Fard, H. Green Synthesis of Zinc Oxide Nanoparticles: A Comparison. *Green Chem. Lett. Rev.* **2019**, *12* (1), 19-24. https://doi.org/10.1080/17518253.2018.1547925

FAO. *FAOSTAT* | © FAO Statistics Division; Vol. 2012 | 13 January 2012, 2012. http://www.faostat.fao.org

FAOSTAT. http://www.fao.org/faostat/en/#data/QC (accessed February 23 2021)

Fatemi, A.; Moaveni, P.; Daneshian, J.; Mozafari, H.; Ghaffari, M. Magnesium Nanoparticles Improve Grain Yield, Oil Percentage, Physiological, and Biochemical Traits of Sunflower (*Helianthus annuus* L.) under Drought Stress. *J. Agric. Sci. Technol.* **2022**, *24* (3), 665–678. https://doi.org/10.1080/10643389.2020.1818461

Fathy, R. M.; Mahfouz, A. Y. Eco-Friendly Graphene Oxide-Based Magnesium Oxide Nanocomposite Synthesis Using Fungal Fermented By-Products and Gamma Rays for Outstanding Antimicrobial, Antioxidant, and Anticancer Activities. *J. Nanostruct. Chem.* **2021,** *11*, 301-321. https://doi.org/10.1007/s40097-020-00369-3

Fathy, R. M.; Mahfouz, A. Y. Eco-Friendly Graphene Oxide-Based Magnesium Oxide Nanocomposite Synthesis Using Fungal Fermented By-Products and Gamma Rays for Outstanding Antimicrobial, Antioxidant, and Anticancer Activities. *J. Nanostruct. Chem.* **2021**, *11*, 301–321. https://doi.org/10.1007/s40097-021-00365-x

Fedlheim, D. L.; Foss, C. A. *Metal Nanoparticles: Synthesis, Characterization, and Applications*; CRC Press: Boca Raton, FL, USA, 2001.

Fei, J. B.; Cui, Y.; Yan, X. H.; Qi, W.; Yang, Y.; Wang, K. W.; He, Q.; Li, J. B. Controlled Preparation of MnO_2 Hierarchical Hollow Nanostructures and Their Application in Water Treatment. *Adv. Mater.* **2008,** *20* (3), 452-456. https://doi.org/10.1002/adma.200701666

Fernandez, V.; Sotiropoulos, T.; Brown, P. H. *Foliar Fertilization: Scientific Principles and Field Practices*, 1st ed.; International Fertilizer Industry Association (IFA): Paris, France, **2013**; pp. 140.

Fifere, N.; Ardeleanu, R.; Doroftei, F.; Dobromir, M.; Airinei, A. Tailoring the Structural and Optical Properties of Cerium Oxide Nanoparticles Prepared by an Ecofriendly Green Route Using Plant Extracts. *Int. J. Mol. Sci.* **2024**, *25* (1), 681. https://doi.org/10.3390/ijms25010681

Filipponi, L.; Sutherland, D. Overview of Nanomaterials. *NANOYOU Teach. Train. Kit Nanosci. Nanotechnol.* **2010**, 18–46.

Fouda, A.; Hassan, S. E.-D.; Saied, E.; Hamza, M. F. Photocatalytic Degradation of Real Textile and Tannery Effluent Using Biosynthesized Magnesium Oxide Nanoparticles (MgO-NPs), Heavy Metal Adsorption, Phytotoxicity, and Antimicrobial Activity. *J. Environ. Chem. Eng.* **2021**, *9*, 105346. https://doi.org/10.1016/j.jece.2021.105346

Fouda, A.; Saad, E.; Elgamal, M. S.; Mohmed, A. A.; Salem, S. S. Optimal Factors for Biosynthesis of Silver Nanoparticles by *Aspergillus* sp. *Al Azhar Bull. Sci.*, **2017**, Conf., 9th, pp. 161–172.

Foulongne-Orio, M.; Murat, C.; Castanera, R.; Ramírez, L.; Sonnenberg, A. D. W. Genome-Wide Survey of Repetitive DNA Elements in the Button Mushroom *Agaricus bisporus*. *Fungal Genet. Biol.* **2013**, *55*, 6–21. https://doi.org/10.1016/j.fgb.2013.07.005

Gaba, S.; Varma, A.; Goel, A. Protective and Curative Activity of Biogenic Copper Oxide Nanoparticles Against *Alternaria* Blight Disease in Oilseed Crops: A Review. *J. Plant Dis. Protect.* **2022**, *129* (2), 215–229. https://doi.org/10.1007/s41348-021-00486-7

Gade, A. K.; Bonde, P.; Ingle, A. P.; Marcato, P. D.; Duran, N.; Rai, M. K. Exploitation of *Aspergillus niger* for Synthesis of Silver Nanoparticles. *J. Biobased Mater. Bioenergy* **2008**, *2*, 243–247. https://doi.org/10.1166/jbmb.2008.200

Gade, A. K.; Bonde, P.; Ingle, A. P.; Marcato, P. D.; Durán, N.; Rai, M. K. Exploitation of Aspergillus niger for Synthesis of Silver Nanoparticles. *J. Biobased Mat. Bioenergy* **2008**, *2* (3), 243–247. https://doi.org/10.1166/jbmb.2008.401

Gade, A.; Ingle, A.; Whiteley, C.; Rai, M. Mycogenic Metal Nanoparticles: Progress and Applications. *Biotechnol. Lett.* **2010**, *32*, 593–600. https://doi.org/10.1007/s10529-010-0302-y

Gade, A.; Ingle, A.; Whiteley, C.; Rai, M. Mycogenic metal nanoparticles: progress a nd applications. *Biotechnol. Lett.* **2010**, *32*, 593-6003. https://doi.org/10.1007/s10529-010-0311-3

Gaikwad, S. C.; Birla, S.; Ingle, A.; Gade, A. K.; Marcato, P. D.; Rai, M.; Duran, N. Screening of Different *Fusarium* Species to Select Potential Species for the Synthesis of Silver Nanoparticles. *J. Braz. Chem. Soc.* **2013**, *24* (12), 1974–1982. https://doi.org/10.5935/0103-5053.20130247

Garibo, D.; Khan, M. Fungi-Assisted Biosynthesis of Nanoparticles and Their Effect on Plant Pests and Pathogens. In *Nanoparticles in Plant Biotic Stress Management*; Springer Nature Singapore: Singapore, 2024; pp. 231–245. https://doi.org/10.1007/978-981-15-7856-5_12

Gehrke, I.; Geiser, A.; Somborn-Schulz, A. Innovations in Nanotechnology for Water Treatment. *Nanotechnol. Sci. Appl.* **2015,** *8*, 1-7. https://doi.org/10.2147/NSA.S43773

Gericke, M.; Pinches, A. Biological Synthesis of Metal Nanoparticles. *Hydrometallurgy* **2006**, *83* (1–4), 132–140. https://doi.org/10.1016/j.hydromet.2006.03.019

Ghazal, S.; Akbari, A.; Hosseini, H. A.; Sabouri, Z.; Forouzanfar, F.; Khatami, M.; Darroudi, M. Sol-gel Biosynthesis of Nickel Oxide Nanoparticles Using *Cydonia oblonga* Extract and Evaluation of Their Cytotoxicity and Photocatalytic Activities. *J. Mol. Struct.* **2020**, *1217*, 128378. https://doi.org/10.1016/j.molstruc.2020.128378

Ghotekar, S.; Pagar, T.; Pansambal, S.; Oza, R. A Review on Green Synthesis of Sulfur Nanoparticles via Plant Extract, Characterization and its Applications. *Adv. J. Chem. B* **2020**, *2* (3), 128–143.

Goswami, A.; Roy, I.; SenGupta, S.; Debnath, N. Novel Applications of Solid and Liquid Formulations of Nanoparticles Against Insect Pests and Pathogens. *Thin Solid Films* **2010**, *519* (3), 1252–1257. https://doi.org/10.1016/j.tsf.2010.08.079

Goyal, S.; Pawar, S. A Review on Green Synthesis of Zinc Oxide Nanoparticles from Plant Extract. *JIER* **2018**, *1* (2), 25–29.

Greenwood, N. N.; Earnshaw, A. *Chemistry of the Elements*, 2nd ed.; Butterworth-Heinemann: Oxford, UK, **1997**; pp. 1340.

Gu, H.; Ho, P. L.; Tong, E.; Wang, L.; Xu, B. Presenting Vancomycin on Nanoparticles to Enhance Antimicrobial Activities. *Nano Lett.* **2003**, *3*, 1261–1263. https://doi.org/10.1021/nl034396c

Gu, H.; Ho, P. L.; Tong, E.; Wang, L.; Xu, B. Presenting vancomycin on nanoparticle s to enhance antimicrobial activities. *Nano Lett.* **2003**, *3*, 1261-1263. https://doi.org/10.1021/nl0340742

Guilger-Casagrande, M.; Lima, R. Synthesis of Silver Nanoparticles Mediated by Fungi: A Review. *Front. Bioeng. Biotechnol.* **2019**, *7*, 287. https://doi.org/10.3389/fbioe.2019.00287

Guo, J.; Li, S.; Brestic, M.; Li, N.; Zhang, P.; Liu, L.; Li, X. Modulations in Protein Phosphorylation Explain the Physiological Responses of Barley (*Hordeum*

vulgare) to Nanoplastics and ZnO Nanoparticles. *J. Hazard. Mater.* **2023**, *443*, 130196. https://doi.org/10.1016/j.jhazmat.2022.130196

Gupta, G. K.; Agarwala, R. K. *Alternaria* Blight of Apple. *FAO Plant Prot. Bull.* **1968**, *16*, 32.

Gupta, K.; Chundawat, T. S. Zinc Oxide Nanoparticles Synthesized Using *Fusarium oxysporum* to Enhance Bioethanol Production from Rice-Straw. *Biomass Bioenergy* **2020**, *143*, 105840. https://doi.org/10.1016/j.biombioe.2020.105840

Hamad, M. T. Biosynthesis of Silver Nanoparticles by Fungi and Their Antibacterial Activity. *Int. J. Environ. Sci. Technol.* **2019**, *16*, 1015–1024. https://doi.org/10.1007/s13762-018-1814-8 .

Hammad, S. E.; El-Rouby, M. N.; Abdel-Aziz, M. M.; El-Sayyad, G. S.; Elshikh, H. H. Endophytic Fungi–Assisted Biomass Synthesis of Gold and Zinc Oxide Nanoparticles for Increasing Antibacterial and Anticancer Activities. *Biomass Convers. Biorefin.* **2023,** 1-18. https://doi.org/10.1007/s13399-023-04954-8

Hamza, M. F.; Salih, K. A. M.; Abdel-Rahman, A. A. H.; Zayed, Y. E.; Wei, Y.; Liang, J.; Guibal, E. Sulfonic-Functionalized Algal/PEI Beads for Scandium, Cerium and Holmium Sorption from Aqueous Solutions (Synthetic and Industrial Samples). *Chem. Eng. J.* **2021**, *403*, 126399. https://doi.org/10.1016/j.cej.2020.126399

Han, Y. F.; Chen, F.; Zhong, Z.; Ramesh, K.; Chen, L.; Widjaja, E. Controlled synthe sis, characterization, and catalytic properties of Mn2O3 and Mn3O4 nanoparticles supported on mesoporous silica SBA15. *J. Phys. Chem. B* **2006**, *110* (48), 24450-24456. https://doi.org/10.1021/jp064941v

Hanafy, M. H. Myconanotechnology in Veterinary Sector: Status Quo and Future Perspectives. *Int. J. Vet. Sci. Med.* **2018**, *6* (2), 270–273. https://doi.org/10.1016/j.ijvsm.2018.11.003

Harish, K.; Manisha; Poonam, S. Synthesis and Characterization of MnO_2 Nanoparticl es using co-precipitation technique. *Inter. J. Chem. Chem. Eng.* **2013**, *3* (3), 155-160.

Harley, P. C.; Loreto, F.; Di Marco, G.; Sharkey, T. D. Theoretical considerations when estimating the mesophyll conductance to CO_2 flux by analysis of the response of photosynthesis to CO_2. *Plant physiology* **1992**, *98* (4), 1429-1436.

Hassan, S. E. D.; Fouda, A.; Saied, E.; Farag, M. M.; Eid, A. M.; Barghoth, M. G.; Awad, M. F. *Rhizopus oryzae*-Mediated Green Synthesis of Magnesium Oxide Nanoparticles (MgO-NPs): A Promising Tool for Antimicrobial, Mosquitocidal Action, and Tanning Effluent Treatment. *J. Fungi* **2021,** *7* (5), 372. https://doi.org/10.3390/jof7050372

Hatamie, A.; Khan, A.; Golabi, M.; Turner, A. P.; Beni, V.; Mak, W. C.; Sadollahkhani, A.; Alnoor, H.; Zargar, B.; Bano, S.; Nur, O.; Willander, M. Zinc Oxide Nanostructure-Modified Textile and Its Application to Biosensing, Photocatalysis, and as Antibacterial Material. *Langmuir* **2015**, *31* (39), 10913–10921. https://doi.org/10.1021/acs.langmuir.5b02341

Hayat, K.; Din, I. U.; Alam, K.; Khan, F. U.; Khan, M.; Mohamed, H. I. Green Synthesis of Zinc Oxide Nanoparticles Using Plant Extracts of *Fumaria officinalis* and *Peganum harmala* and Their Antioxidant and Antibacterial Activities. *Biomass Convers. Biorefin.* **2024**, *1*–15. https://doi.org/10.1007/s13399-023-04589-5

Hayles, J.; Johnson, L.; Worthley, C.; Losic, D. *Nanopesticides: A Review of Current Research and Perspectives, New Pesticides and Soil Sensors*; Elsevier, 2017, pp 193–225.

He, L.; Liu, Y.; Mustapha, A.; Lin, M. Antifungal Activity of Zinc Oxide Nanoparticles Against *Botrytis cinerea* and *Penicillium expansum*. *Microbiol. Res.* **2011,** *166* (3), 207–215. https://doi.org/10.1016/j.micres.2010.03.003

He, Y.; Ingudam, S.; Reed, S.; Gehring, A.; Strobaugh, T. P.; Irwin, P. Study on the Mechanism of Antibacterial Action of Magnesium Oxide Nanoparticles Against Foodborne Pathogens. *J. Nanobiotechnol.* **2016,** *14* (1), 54. https://doi.org/10.1186/s12951-016-0202-0

Healy, P. C.; Hocking, A.; Tran-Dinh, N.; Pitt, J. I.; Shivas, R. G.; Mitchell, J. K.; Davis, R. A. Xanthones from a Microfungus of the Genus *Xylaria*. *Phytochemistry* **2004,** *65* (16), 2373–2378. https://doi.org/10.1016/j.phytochem.2004.07.019

Heinicke, A. J.; Hoffman, M. B. An Apparatus for Determining the Absorption of Carbon Dioxide by Leaves Under Natural Conditions. *Science* **1933**, *77* (1985), 55–58. https://doi.org/10.1126/science.77.1985.55

Helaly, M. N.; El-Hoseiny, H.; El-Sheery, N. I.; Rastogi, A.; Kalaji, H. M. Regulation and Physiological Role of Silicon in Alleviating Drought Stress of Mango. *Plant Physiol. Biochem.* **2017**, *118*, 31–44. https://doi.org/10.1016/j.plaphy.2017.06.010

Henini, M. Nanotechnology—Growing in a Shrinking World. *III-Vs Rev.* **1998**, *11* (4), 30–34. https://doi.org/10.1016/S0961-1290(98)80118-X

Hernandez-Viezcas, J. A.; Castillo-Michel, H.; Andrews, J. C.; Cotte, M.; Rico, C.; Peralta-Videa, J. R.; Gardea-Torresdey, J. L. In Situ Synchrotron X-ray Fluorescence Mapping and Speciation of CeO2 and ZnO Nanoparticles in Soil Cultivated Soybean (*Glycine max*). *ACS Nano* **2013**, *7* (2), 1415–1423. https://doi.org/10.1021/nn305196q

Hobbs, C. *Medicinal Mushrooms: An Exploration of Tradition, Healing and Culture*; Botanica Press: Santa Cruz, CA, **1995**.

Hobbs, C. Medicinal Value of *Lentinus edodes* (Berk.) Sing.: A Literature Review. *Int. J. Med. Mushr.* **2000**, *2*, 287–302. https://doi.org/10.1615/IntJMedMushr.v2.i3.20

Holb, I. J.; Heijne, B.; Withagen, J. C.; Gáll, J. M.; Jeger, M. J. Analysis of Summer Epidemic Progress of Apple Scab at Different Apple Production Systems in the Netherlands and Hungary. *Phytopathology* **2005**, *95*, 1001–1020. https://doi.org/10.1094/PHYTO-95-1001

Honary, S.; Barabadi, H.; Gharaei-Fathabad, E.; Naghibi, F. Green Synthesis of Silver Nanoparticles Induced by the Fungus Penicillium citrinum. *Trop. J. Pharm. Res.* **2013a**, *12* (1), 7–11. https://doi.org/10.4314/tjpr.v12i1.2

Honary, S.; Gharaei-Fathabad, E.; Barabadi, H.; Naghibi, F. Fungus-Mediated Synthesis of Gold Nanoparticles: A Novel Biological Approach to Nanoparticle Synthesis. *J. Nanosci. Nanotechnol.* **2013b**, *13* (2), 1427–1430. https://doi.org/10.1166/jnn.2013.5989

Hoseinpour, V.; Ghaemi, N. Green Synthesis of Manganese Nanoparticles: Applications and Future Perspective – A Review. *J. Photochem. Photobiol. B* **2018**, *189*, 234–243. https://doi.org/10.1016/j.jphotobiol.2018.10.005

Hoseinpour, V.; Souri, M.; Ghaemi, N. Green Synthesis, Characterisation, and Photocatalytic Activity of Manganese Dioxide Nanoparticles. *Micro Nano Lett.* **2018**, *13* (11), 1560–1563. https://doi.org/10.1049/mnl.2018.5334

Hranisavljevic, J.; Dimitrijevic, N.; Wurtz, G.; Wiederrecht, G. Photoinduced Charge Separation Reactions of J-Aggregates Coated on Silver Nanoparticles. *J. Am. Chem. Soc.* **2002,** *124*, 4536–4537. https://doi.org/10.1021/ja012263e

Hsu, C. H.; Chen, L. C.; Lin, Y. F. Preparation and Optoelectronic Characteristics of ZnO/CuO-Cu2O Complex Inverse Heterostructure with GaP Buffer for Solar Cell Applications. *Materials* **2013,** *6* (10), 4479-4488. https://doi.org/10.3390/ma6104479

Huang, X.; Wang, X.; Liu, X.; Cheng, L.; Pan, J.; Yang, X. Nanotechnology in Agriculture: Manganese Ferrite Nanoparticles as a Micronutrient Fertilizer for Wheat. *Plants* **2024**, *13* (10), 1395. https://doi.org/10.3390/plants13101395

Iablokov, V.; Frey, K.; Geszti, O.; Kruse, N. High catalytic activity in CO oxidation o ver MnOx nanocrystals. *Catal. Lett.* **2010**, *134* (3-4), 210-216. https://doi.org/10.1007/s10562-009-0244-0

Ibrahem, E. J.; Thalij, K. M.; Badawy, A. S. Antibacterial Potential of Magnesium Oxide Nanoparticles Synthesized by *Aspergillus niger*. *Biotechnol. J. Int.* **2017,** *18* (1), 1-7. https://doi.org/10.9734/BJI/2017/29534

Ibrahim, E.; Ahmad, A. A.; Abdo, E. S.; Bakr, M. A.; Khalil, M. A.; Abdallah, Y.; Ogunyemi, S. O.; Mohany, M.; Al-Rejaie, S. S.; Shou, L.; Li, B. Suppression of Root Rot Fungal Diseases in Common Beans (*Phaseolus vulgaris* L.) Through the Application of Biologically Synthesized Silver Nanoparticles. *Nanomaterials* **2024**, *14* (8), 710. https://doi.org/10.3390/nano14080710

Ibrahim, M.; Oyebanji, E.; Fowora, M.; Aiyeolemi, A.; Orabuchi, C.; Akinnawo, B.; Adekunle, A. A. Extracts of Endophytic Fungi from Leaves of Selected Nigerian Ethnomedicinal Plants Exhibited Antioxidant Activity. *BMC Complement. Med. Ther.* **2021**, *21* (1), 98. https://doi.org/10.1186/s12906-021-03269-3

Immanuel, S. J.; Iswareya, L. V. Nanoparticles: Plant Protective Agents Against Pathogenic Microbes and Pests. **In** *Nanotechnology for Sustainable Agriculture*; Apple Academic Press: **2023**; pp. 129–162.

Ingle, A. P.; Gupta, I. Role of Metal-Based Nanoparticles in Plant Protection. **In** *Nanotechnology in Plant Growth Promotion and Protection: Recent Advances and Impacts*; Elsevier: **2021**; pp. 220–238.

Ingle, A.; Gade, A.; Pierrat, S.; Sonnichsen, C.; Rai, M. K. Mycosynthesis of Silver Nanoparticles Using the Fungus Fusarium acuminatum and Its Activity Against Some Human Pathogenic Bacteria. *Curr. Nanosci.* **2008**, *4* (2), 141–144. https://doi.org/10.2174/157341308784340804

Ingle, A.; Gade, A.; Pierrat, S.; Sonnichsen, C.; Rai, M. K. Mycosynthesis of Silver Nanoparticles Using the Fungus *Fusarium acuminatum* and Its Activity Against Some Human Pathogenic Bacteria. *Curr. Nanosci.* **2008**, *4*, 141–144. https://doi.org/10.2174/157341308784191683

Ingle, A.; Gade, A.; Pierrat, S.; Sonnichsen, C.; Rai, M. Mycosynthesis of Silver Nanoparticles Using the Fungus *Fusarium acuminatum* and Its Activity Against Some Human Pathogenic Bacteria. *Curr. Nanosci.* **2008**, *4* (2), 141–144. https://doi.org/10.2174/157341308784340804

Ingle, P. U.; Shende, S. S.; Hande, D.; Rai, M.; Golinska, P.; Gade, A. K. Mycogenic Copper Oxide Nanoparticles for Fungal Infection Management in Agricultural Crop Plants. *BioNanoScience* **2024**, *14* (1), 359–367. https://doi.org/10.1007/s12951-023-01649-y

Jadhav, A. H.; Lim, A. C.; Thorat, G. M.; Jadhav, H. S.; Seo, J. G. Green Solvent Ionic Liquids: Structural Directing Pioneers for Microwave-Assisted Synthesis of Controlled MgO Nanostructures. *RSC Adv.* **2016,** *6* (38), 31675-31686. https://doi.org/10.1039/C5RA26399E

Jagadish, L. K.; Krishnan, V. V.; Shenbhagaraman, R.; Kaviyarasan, V. Comparative Study on the Antioxidant, Anticancer and Antimicrobial Property of Agaricus Bisporus (JE Lange) Imbach Before and After Boiling. *Afr. J. Biotechnol.* **2009**, *8* (4).

Jahan, Q. S. A.; Sultana, Z.; Ud-Daula, M. A.; Ashikuzzaman, M.; Reja, M. S.; Rahman, M. M.; Khaton, A.; Tang, M. A. K.; Rahman, M. S.; Faruquee, H. M.; Lee, S. J. Optimization of Green Silver Nanoparticles as Nanofungicides for Management of Rice Bakanae Disease. *Heliyon* **2024**, *10* (6). https://doi.org/10.1016/j.heliyon.2024.e16777

Jain, D.; Kachhwaha, S.; Jain, R.; Srivastava, G.; Kothari, S. L. Novel Microbial Route to Synthesize Silver Nanoparticles Using Spore Crystal Mixture of *Bacillus thuringiensis*. *Indian J. Exp. Biol.* **2010**, *48*, 1152–1156.

Jain, N.; Bhargava, A.; Tarafdar, J. C.; Singh, S. K.; Panwar, J. A Biomimetic Approach Towards Synthesis of Zinc Oxide Nanoparticles. *Appl. Microbiol. Biotechnol.* **2013**, *97*, 859–869. https://doi.org/10.1007/s00253-012-3934-2

James, J.; Sutton, I. A Model for Predicting Ascospores Maturation of *V. inaequalis*. *Phytopathology* **1982**, *72*, 1081–1085. https://doi.org/10.1094/PHYTO-72-1081

Jan, T.; Iqbal, J.; Ismail, M.; Zakaullah, M.; Naqvi, S. H.; Badshah, N. Sn Doping Induced Enhancement in the Activity of ZnO Nanostructures Against Antibiotic Resistant *S. aureus* Bacteria. *Int. J. Nanomed.* **2013,** *8*, 3679–3687.

Janaki, A. C.; Sailatha, E.; Gunasekaran, S. Synthesis, Characteristics and Antimicrobial Activity of ZnO Nanoparticles. *Spectrochim. Acta A Mol. Biomol. Spectrosc.* **2015,** *144*, 17–22. https://doi.org/10.1016/j.saa.2015.02.041

Jandail, C. L. Artificial Cultivation of *Pleurotus sajor-caju* (Fr.) Singer. *Mushroom J.* 1974, *22*, 405.

Jandail, C. L.; Kapoor, J. N. Studies on Cultivation of *Pleurotus sajor-caju* (Fr.) Singer. *Mushroom Sci.* **1976**, *9*, 667–672.

Jayandran, M.; Haneefa, M. M.; Balasubramanian, V. Green Synthesis and Characterization of Manganese Nanoparticles Using Natural Plant Extracts and Its Evaluation of Antimicrobial Activity. *J. Appl. Pharm. Sci.* **2015,** *5* (12), 105-110. https://doi.org/10.7324/JAPS.2015.51215

Jeevanandam, J.; Chan, Y. S.; Danquah, M. K. Biosynthesis and Characterization of MgO Nanoparticles from Plant Extracts via Induced Molecular Nucleation. *New J. Chem.* **2017,** *41*, 2800–2814. https://doi.org/10.1039/C6NJ03176E

Jeevanandam, J.; Chan, Y. S.; Danquah, M. K. Evaluating the Antibacterial Activity of MgO Nanoparticles Synthesized from Aqueous Leaf Extract. *Med. One* **2019**, *4*, e190011. https://doi.org/10.20900/mo.20190011

Jha, A. K.; Prasad, K. Chap. 1. Understanding Mechanism of Fungus Mediated Nanosynthesis: A Molecular Approach. **In** *Adv App Through Fungal Nanobiotechnol*; Prasad, R., Ed., **2016**, pp. 1–23. https://doi.org/10.1007/978-3-319-42990-8_1

Jha, A. K.; Prasad, K.; Kulkarni, A. R. Synthesis of Gd2O3 Nanoparticles Using Lactobacillus sp.: A Novel Green Approach. *Int. J. Green Nanotechnol. Phys. Chem.* **2010**, *2* (2), 31-38. https://doi.org/10.1080/19430876.2010.532411

Jha, A. K.; Prasad, K.; Kulkarni, A. R. Synthesis of TiO2 nanoparticles using microor ganisms. *Colloids Surf. B Biointerfaces* **2009**, *71*, 226-2292. https://doi.org/10.1016/j.colsurfb.2008.11.002

Jha, A. K.; Prasad, K.; Kulkarni, A. R. Yeast mediated synthesis of silver nanoparticle s. *Int. J. Nanosci. Nanotechnol.* **2008**, *4*, 17-21. https://doi.org/10.1007/s11671-007-9060-x

Jia, X.; Wu, Y.; Liu, Z.; Dai, Y.; Li, T.; Gao, M.; Xu, C. Coating Effect of Renatured Triple-Helix Lentinan on the Morphology and Antimicrobial Activity of ZnO Synthesized by Hydrothermal Method. *RSC Adv.* **2024**, *14* (25), 17814-17823. https://doi.org/10.1039/D4RA01590H

Jiang, W.; Mashayekhi, H.; Xing, B. Bacterial Toxicity Comparison Between Nano- and Micro-Scaled Oxide Particles. *Environ. Pollut.* **2009**, *157* (5), 1619–1625. https://doi.org/10.1016/j.envpol.2008.12.025

Johnson, J.; Shanmugam, R.; Manigandan, P. Characterization and Biomedical Applications of Green-Synthesized Selenium Nanoparticles Using *Tridax procumbens* Stem Extract. *Cureus* **2024**, *16* (6). https://doi.org/10.7759/cureus.63535

Jomeyazdian, A.; Pirnia, M.; Alaei, H.; Taheri, A.; Sarani, S. Control of Fusarium Wilt Disease of Tomato and Improvement of Some Growth Factors Through Green Synthesized Zinc Oxide Nanoparticles. *Eur. J. Plant Pathol.* **2024**, *1*–13. https://doi.org/10.1007/s10658-024-02717-0

Joshi, N. C.; Joshi, E.; Singh, A. Biological Synthesis, Characterisations and Antimicrobial Activities of Manganese Dioxide (MnO_2) Nanoparticles. *Res. J. Pharm. Technol.* **2020,** *13* (1), 135. https://doi.org/10.5958/0974-360x.2020.00027.x

Kadam, V. V.; Ettiyappan, J. P.; Balakrishnan, R. M. Mechanistic Insight into the Endophytic Fungus-Mediated Synthesis of Protein-Capped ZnO Nanoparticles. *Mater. Sci. Eng. B* **2019**, *243*, 214–221. https://doi.org/10.1016/j.mseb.2019.04.032

Kairyte, K.; Kadys, A.; Luksiene, Z. Antibacterial and Antifungal Activity of Photoactivated ZnO Nanoparticles in Suspension. *J. Photochem. Photobiol. B: Biol.* **2013,** *128*, 78–84. https://doi.org/10.1016/j.jphotobiol.2013.07.017

Kaler, A.; Patel, N.; Banerjee, U. C. Green Synthesis of Silver Nanoparticles. *Curr. Res. Inf. Pharm. Sci.* **2010**, *11*, 68–71.

Kamran, U.; Bhatti, H.N.; Iqbal, M.; Jamil, S.; Zahid, M. Biogenic Synthesis, Characterization and Investigation of Photocatalytic and Antimicrobial Activity of Manganese Nanoparticles Synthesized from *Cinnamomum verum* Bark Extract. *J. Mol. Struct.* **2019**, *1179*, 532-539. https://doi.org/10.1016/j.molstruc.2019.03.086

Kang, M.; Liu, Y.; Weng, Y.; Wang, H.; Bai, X. A Critical Review on the Toxicity Regulation and Ecological Risks of Zinc Oxide Nanoparticles to Plants. *Environ. Sci.: Nano* **2024**, *11* (1), 14–35. https://doi.org/10.1039/D3EN00625E

Kaningini, A. G.; Motlhalamme, T.; More, G. K.; Azizi, S.; Mohale, K. C.; Maaza, M. Evaluation of the Antimicrobial Activity and Chickpea Growth Stimulation Effects of Green Synthesized Zinc Oxide Nanoparticles. *Plant Stress* **2024**, *12*, 100442. https://doi.org/10.1016/j.stress.2024.100442

Karthik, K.; Dhanuskodi, S.; Gobinath, C.; Prabukumar, S.; Sivaramakrishnan, S. Fabrication of MgO Nanostructures and Its Efficient Photocatalytic, Antibacterial and Anticancer Performance. *J. Photochem. Photobiol. B Biol.* **2019**, *190*, 8–20. https://doi.org/10.1016/j.jphotobiol.2018.10.008

Kashyap, P. L.; Kumar, S.; Srivastava, A. K.; Sharma, A. K. Myconanotechnology in Agriculture: A Perspective. *World J. Microbiol. Biotechnol.* **2013**, *29* (2), 191–207. https://doi.org/10.1007/s11274-012-1171-6

Kashyap, P. L.; Kumar, S.; Srivastava, A. K.; Sharma, A. K. Myconanotechnology in Agriculture: A Perspective. *World J. Microbiol. Biotechnol.* **2012**, *29*, 191–207. https://doi.org/10.1007/s11274-012-0913-4

Katz, M. The Heterogeneous Oxidation of Carbon Monoxide. **In** *Advances in Catalysis*; Frankenburg, W. G.; Komarewsky, V. I., Eds.; Academic Press: New York, **1953**; Vol. *5*, pp. 177-216.

Khalid, M.F.; Iqbal Khan, R.; Jawaid, M.Z.; Shafqat, W.; Hussain, S.; Ahmed, T.; Rizwan, M.; Ercisli, S.; Pop, O.L.; Alina Marc, R. Nanoparticles: the plant saviour

under abiotic stresses. *Nanomaterials* **2022**, *12* (21), 3915. https://doi.org/10.3390/nano12213915

Khan, A.; Shabbier, D.; Ahmad, P.; Khandaker, M. U.; Faruque, M. R. I.; Din, I. Biosynthesis and Antibacterial Activity of MgO-NPs Produced from *Camellia-sinensis* Leaves Extract. *Mater. Res. Express* **2020**, *8*, 015402. https://doi.org/10.1088/2053-1591/abcee0

Khan, M. R.; Adam, V.; Rizvi, T. F.; Zhang, B.; Ahamad, F.; Josko, I.; Zhu, Y.; Yang, M.; Mao, C. Nanoparticle-Plant Interactions: Two-Way Traffic. *Small* **2019**, *15*, e1901794. https://doi.org/10.1002/smll.201901794

Khan, S.; Rizvi, S. M. D.; Saeed, M.; Srivastava, A. K.; Khan, M. S. A Novel Approach for the Synthesis of Gold Nanoparticles Using Trypsin. *Adv. Sci. Lett.* **2014**, *20* (5), 1061–1065. https://doi.org/10.1166/asl.2014.5481

Khandel, P.; Shahi, S. K. Mycogenic Nanoparticles and Their Bio-Prospective Applications: Current Status and Future Challenges. *J. Nanostruct. Chem.* **2018**, *8*, 369–391. https://doi.org/10.1007/s40097-018-0285-2

Khanra, K.; Panja, S.; Choudhuri, I.; Bhattacharyya, N. Evaluation of Antibacterial Activity and Cytotoxicity of Green Synthesized Silver Nanoparticles Using *Scoparia dulcis*. *Nano Biomed. Eng.* **2015,** *7*, 128–133. https://doi.org/10.5101/nbe.v7i3.p128-133

Khataee, A.; Sheydaei, M.; Hassani, A.; Taseidifar, M.; Karaca, S. Sonocatalytic Removal of an Organic Dye Using TiO2/Montmorillonite Nanocomposite. *Ultrason. Sonochem.* **2015**, *22*, 404–411. https://doi.org/10.1016/j.ultsonch.2014.07.002

Khundi, Q.; Jiang, Y.; Sun, Y.; Rui, Y. Nanofertilizers for Sustainable African Agriculture: A Global Review of Agronomic Efficiency and Environmental Sustainability. *Nanomaterials* **2025**, *15* (5), 390. https://doi.org/10.3390/nano15050390

Kirubakaran, D.; Wahid, J. B. A.; Karmegam, N.; Jeevika, R.; Sellapillai, L.; Rajkumar, M.; SenthilKumar, K. J. A Comprehensive Review on the Green Synthesis of

Nanoparticles: Advancements in Biomedical and Environmental Applications. *Biomed. Mater. Devices* **2025**, *1*, 1–26.

Klemm, R. D. W. Supplementation: Programmatic Issues. **In** *Encyclopedia of Human Nutrition*, 3rd ed.; Caballero, B., Ed.; Academic Press, **2013**; pp. 251–259. https://doi.org/10.1016/B978-0-12-375083-9.00259-2

Konappa, N.; Joshi, S. M.; Dhamodaran, N.; Krishnamurthy, S.; Basavaraju, S.; Chowdappa, S.; Jogaiah, S. Green Synthesis of *Callicarpa tomentosa*-Routed Zinc Oxide Nanoparticles and Their Bactericidal Action Against Diverse Phytopathogens. *Biomass Convers. Biorefin.* **2024**, *14* (13), 13821–13832. https://doi.org/10.1007/s13399-023-04676-7

Korbekandi, H.; Iravani, S. *Silver Nanoparticles.* **In** *The Delivery of Nanoparticles*; Informational Technology, **2012**; pp. 3.

Korbekandi, H.; Jouneghani, R. M.; Mohseni, S.; Pourhossein, M.; Iravani, S. Synthesis of Silver Nanoparticles Using Biotransformations by Saccharomyces boulardii. *Green Process. Synth.* **2014**, *3* (4), 271–277. https://doi.org/10.1515/gps-2014-0035

Kruis, F. E.; Fissan, H.; Peled, A. Synthesis of Nanoparticles in the Gas Phase for Electronic, Optical and Magnetic Applications. *J. Aerosol Sci.* **1998**, *29*, 511–535. https://doi.org/10.1016/S0021-8502(97)10032-5

Kumar, C.; Akhtar, M. N. S.; Chand, P.; Choudhary, C. S. Efficacy of Newer Fungicides Against Maydis Leaf Blight Disease of Maize Caused by *Helminthosporium maydis*. *J. Pharm. Phytochem.* **2019**, *8* (6), 1553–1559.

Kumar, R. V.; Vinoth, S.; Baskar, V.; Arun, M.; Gurusaravanan, P. Synthesis of Zinc Oxide Nanoparticles Mediated by *Dictyota dichotoma* Endophytic Fungi and Its Photocatalytic Degradation of Fast Green Dye and Antibacterial Applications. *S. Afr. J. Bot.* **2022,** *151*, 337-344. https://doi.org/10.1016/j.sajb.2022.03.016

Kumar, S. A.; Abyaneh, M. K.; Gosavi, S. W.; Kulkarni, S. K.; Pasricha, R.; Ahmad, A.; Khan, M. I. Nitrate Reductase-Mediated Synthesis of Silver Nanoparticles from

AgNO3. *Biotechnol. Lett.* **2007**, *29*, 439–445. https://doi.org/10.1007/s10529-006-9197-5

Kumar, S. A.; Jarvin, M.; Sharma, S.; Umar, A.; Inbanathan, S. S. R.; Lalla, N. P. Facile and Green Synthesis of Mgo Nanoparticles for the Degradation of Victoria Blue Dye Under UV Irradiation and their Antibacterial Activity. *ES Food Agrofor.* **2021**, *5* (12), 14–19. http://dx.doi.org/10.30919/esfaf519

Laane, H.-M. The Effects of Foliar Sprays with Different Silicon Compounds. *Plants* **2018**, *7*, 45. https://doi.org/10.3390/plants7020045

Lateef, A.; Adeeyo, A. O. Green Synthesis and Antibacterial Activities of Silver Nanoparticles Using Extracellular Laccase of *Lentinus edodes*. *Not. Sci. Biol.* **2015**, *7* (4), 405–411. https://doi.org/10.15835/nsb745686

Lekota, M. W.; Dimpe, K. M.; Nomngongo, P. N. MgO-ZnO/Carbon Nanofiber Nanocomposite as an Adsorbent for Ultrasound-Assisted Dispersive Solid-Phase Microextraction of Carbamazepine from Wastewater Prior to High-Performance Liquid Chromatographic Detection. *J. Anal. Sci. Technol.* **2019**, *10*, 25. https://doi.org/10.1186/s40543-019-0189-9

Li, Q.; Feng, T.; Li, H.; Wang, Z.; Wei, X.; Liu, J. Green Synthesis of Silver Nanoparticles Using Endophytic Bacterium *Bacillus zanthoxyli* GBE11 and Their Antimicrobial Activity. *Biomass Conversion and Biorefinery* **2024**, *14* (12), 13173–13185. https://doi.org/10.1007/s13399-023-04673-w

Lin, D.; Xing, B. Root Uptake and Phytotoxicity of ZnO Nanoparticles. *Environ. Sci. Technol.* **2008,** *42* (15), 5580–5585. https://doi.org/10.1021/es800422x

Liu, J.; Jia, L.; Kan, J.; Jin, C. H. In Vitro and In Vivo Antioxidant Activity of Ethanolic Extract of White Button Mushroom (Agaricus bisporus). *Food Chem. Toxicol.* **2013**, *51*, 310–316. https://doi.org/10.1016/j.fct.2012.10.014

Liu, R.; Zhang, H.; Lal, R. Effects of Stabilized Nanoparticles of Copper, Zinc, Manganese, and Iron Oxides in Low Concentrations on Lettuce (*Lactuca sativa*)

Seed Germination: Nanotoxicants or Nanonutrients? *Water Air Soil Pollut.* **2016,** *227* (1), 42. https://doi.org/10.1007/s11270-016-2697-5

Liu, Y.; Kang, M.; Weng, Y.; Ding, Y.; Bai, X. Toxicity and Tolerance Mechanism of Binary Zinc Oxide Nanoparticles and Tetrabromobisphenol Regulated by Humic Acid in *Chlorella vulgaris*. *Environ. Sci.: Processes Impacts* **2023**, *25*, 1615–1625. https://doi.org/10.1039/D3EM00136F

Liu, Y.; Yang, Y.; Yuhan, E.; Pang, C.; Cui, D.; Li, A. Insight into Microbial Synthesis of Metal Nanomaterials and Their Environmental Applications: Exploration for Enhanced Controllable Synthesis. *Chinese Chemical Letters* **2024**, 109651. https://doi.org/10.1016/j.cclet.2024.109651

Lohiya, G.; Tamta, A.; Chandra, B.; Kandpal, N. D.; Joshi, R. Green Route Synthesis of Manganese Oxide Nanoparticles by Using Methanolic Extract of *Sapindus mukorossi* (Reetha). *J. Water Environ. Nanotechnol.* **2024**, *9* (2), 211-222. https://doi.org/10.22090/jwent.2024.143471.1818

Long, S. P.; Bernacchi, C. J. Gas Exchange Measurements, What Can They Tell Us About the Underlying Limitations to Photosynthesis? Procedures and Sources of Error. *J. Exp. Bot.* **2003**, *54* (392), 2393–2401. https://doi.org/10.1093/jxb/erg262

Long, S. P.; Farage, P. K.; Garcia, R. L. Measurement of Leaf and Canopy Photosynthetic CO2 Exchange in the Field. *J. Exp. Bot.* **1996**, *47* (11), 1629–1642. https://doi.org/10.1093/jxb/47.11.1629

Long, S. P.; Hällgren, J.-E. Measurement of CO2 Assimilation by Plants in the Field and the Laboratory. **In** *Photosynthesis and Production in a Changing Environment*; Hall, D. O., Scurlock, J. M. O., Bolhar-Nordenkampf, H. R., Leegood, R. C., Long, S. P., Eds.; Chapman & Hall: New York, NY, **1993**; pp. 129–167.

Long, S. P.; Ireland, C. R. The Measurement and Control of Air and Gas Flow Rates for the Determination of Gaseous Exchanges of Living Organisms. **In** *Instrumentation for Environmental Physiology*; Marshall, B., Woodward, F. I., Eds.; Cambridge University Press: Cambridge, England, **1985**; pp. 123–137.

Longvah, T.; Dosthale, Y. G. Compositional and Nutritional Studies on Edible Wild Mushroom from Northeast India. *Food Chem.* **1998**, *63*, 331–334. https://doi.org/10.1016/S0308-8146(98)00033-0

MacHardy, W. E. *Apple Scab: Biology, Epidemiology and Management*; American Phytopathological Society: St. Paul, MN, **1996**.

Machardy, W. E. *Apple Scab: Biology, Epidemiology and Management*; The America n Phytopathological Society: St. Paul, MN, **1996**.

Madhavi, A.; Srinivasulu, M.; Shankar, P. C.; Rangaswamy, V. Synthesis and Applications of Fungal-Mediated Nanoparticles. **In** *Microbial Processes for Synthesizing Nanomaterials*; Springer: Singapore, **2023**; pp. 113–131.

Madhumitha, G.; Fowsiya, J.; Gupta, N.; Kumar, A.; Singh, M. Green Synthesis, Characterization, and Antifungal and Photocatalytic Activity of *Pithecellobium dulce* Peel–Mediated ZnO Nanoparticles. *J. Phys. Chem. Solids* **2019**, *127*, 43–51. https://doi.org/10.1016/j.jpcs.2018.12.005

Mahawar, L.; Živčák, M.; Barboricova, M.; Kovár, M.; Filaček, A.; Ferencova, J.; Vysoká, D. M.; Brestič, M. Effect of Copper Oxide and Zinc Oxide Nanoparticles on Photosynthesis and Physiology of *Raphanus sativus* L. Under Salinity Stress. *Plant Physiol. Biochem.* **2024**, *206*, 108281. https://doi.org/10.1016/j.plaphy.2023.108281

Mahdavi, B.; Paydarfard, S.; Zangeneh, M. M.; Goorani, S.; Seydi, N.; Zangeneh, A. Assessment of Antioxidant, Cytotoxicity, Antibacterial, Antifungal, and Cutaneous Wound Healing Activities of Green Synthesized Manganese Nanoparticles Using *Ziziphora clinopodioides* Lam Leaves Under In Vitro and In Vivo Conditions. *Appl. Organomet. Chem.* **2020**, *34* (1). https://doi.org/10.1002/aoc.5248

Mahobia, S.; Bajpai, J.; Bajpai, A. K. An In-Vitro Investigation of Swelling Controlled Delivery of Insulin from Egg Albumin Nanocarriers. *Iran. J. Pharm. Res.* **2016**, *15*, 695–711.

Majumder, D. R. Waste to health: Bioleaching of nanoparticles from e-waste and their medical applications. *Indian J. Appl. Res.* **2013**, *3* (2), 277-286.

Makvandi, P.; Wang, C.; Zare, E. N.; Borzacchiello, A.; Niu, L.; Tay, F. R. Metal-Based Nanomaterials in Biomedical Applications: Antimicrobial Activity and Cytotoxicity Aspects. *Adv. Funct. Mater.* **2020,** *30* (22), 1910021. https://doi.org/10.1002/adfm.201910021

Mallikarjuna, K.; Narasimha, G.; Dillip, G. R.; Praveen, B.; Shreedhar, B.; Sree Lakshmi, C.; Reddy, B. V. S.; Deva Prasad Raju, B. Green Synthesis of Silver Nanoparticles Using Ocimum Leaf Extract and Their Characterization. *Dig. J. Nanomater. Bios.* **2011,** *6* (1), 181–186. https://doi.org/10.2174/1994589621106010181

Mandal, D.; Bolander, M. E.; Mukhopadhyay, D.; Sarkar, G.; Mukherjee, P. The Use of Microorganisms for the Formation of Metal Nanoparticles and Their Application. *Applied Microbiology and Biotechnology* **2006**, *69*, 485–492. https://doi.org/10.1007/s00253-005-0179-3

Mandal, M.; Sarkar, A. Green Syntheses of Nanoparticles from Plant Growth–Promoting Microorganisms and Their Application in the Agri-Food Industries. **In** *Nanotechnology and Nanomaterials in the Agri-Food Industries*; Elsevier: **2024**; pp. 185–204.

Manimaran, K.; Balasubramani, G.; Ragavendran, C.; Natarajan, D.; Murugesan, S. Biological Applications of Synthesized ZnO Nanoparticles Using *Pleurotus djamor* Against Mosquito Larvicidal, Histopathology, Antibacterial, Antioxidant and Anticancer Effect. *J. Cluster Sci.* **2021**, *32*, 1635–1647. https://doi.org/10.1007/s10876-021-01961-0

Manjula, R.; Thenmozhi, M.; Thilagavathi, S.; Srinivasan, R.; Kathirvel, A. Green Synthesis and Characterization of Manganese Oxide Nanoparticles from *Gardenia resinifera* Leaves. *Mater. Today: Proc.* **2020**, *26*, 3559-3563. https://doi.org/10.1016/j.matpr.2020.02.774

Mariappan, A.; Harikrishnan, L.; Eswaran, J.; Arumugham, N.; Balasubramaniam, Y.; Daniel, S.; Kanthapazham, R. Green Synthesis of Metal-Doped ZnO Nanoparticles Using *Bauhinia racemosa* Lam. Extract and Evaluation of Their Photocatalysis and Biomedical Applications. *ACS Appl. Bio Mater.* **2024**, *7* (4), 2519–2532. https://doi.org/10.1021/acsabm.4c00117

Marques da Silva, J.; Arrabac, M. C. Photosynthesis in the Water-Stressed C4 Grass *Setaria Sphacelata* Is Mainly Limited by Stomata with Both Rapidly and Slowly Imposed Water Deficits. *Physiol. Plant.* **2004**, *121*, 409–420. https://doi.org/10.1111/j.1399-3054.2004.00232.x

Mattila, P.; Konko, K.; Eurola, M.; Pihlava, J. M.; Astola, J.; Vahteristo, L.; Hietaniemi, V.; Kumpulainen, J.; Valtonen, M.; Piironen, V. Contents of Vitamins, Mineral Elements, and Some Phenolic Compounds in Cultivated Mushrooms. *J. Agric. Food Chem.* **2001**, *49*, 2343–2348. https://doi.org/10.1021/jf0011998

Mattila, P.; Salo-Vaananen, P.; Konko, K.; Aro, H.; Jalava, T. Basic Composition and Amino Acid Contents of Mushrooms Cultivated in Finland. *J. Agric. Food Chem.* **2002**, *50*, 6419–6422. https://doi.org/10.1021/jf020221c

Mazari, S. A.; Ali, E.; Abro, R.; Khan, F. S. A.; Ahmed, I.; Ahmed, M.; Nizamuddin, S.; Siddiqui, T. H.; Hossain, N.; Mubarak, N. M.; Shah, A. Nanomaterials: Applications, Waste-Handling, Environmental Toxicities, and Future Challenges—A Review. *J. Environ. Chem. Eng.* **2021**, *9* (2), 105028. https://doi.org/10.1016/j.jece.2021.105028

McLean, F. T. Field Studies of the Carbon Dioxide Absorption of Coconut Leaves. *Ann. Bot.* **1920**, *34* (3), 367–389.

Mehmood, S.; Ahmed, W.; Rizwan, M.; Bundschuh, J.; Elnahal, A. S.; Li, W. Green Synthesized Zinc Oxide Nanoparticles for Removal of Carbamazepine in Water and Soil Systems. *Separation Purif. Technol.* **2024**, *334*, 125988. https://doi.org/10.1016/j.seppur.2023.125988

Mejía-Méndez, J. L.; Sánchez-Ante, G.; Cerro-López, M.; Minutti-Calva, Y.; Navarro-López, D. E.; Lozada-Ramírez, J. D.; Sánchez-Arreola, E. Green Synthesis of Silver Nanoparticles with Extracts from *Kalanchoe fedtschenkoi*: Characterization and Bioactivities. *Biomolecules* **2024**, *14* (7), 782. https://doi.org/10.3390/biom14070782

Mekky, A. E.; Farrag, A. A.; Hmed, A. A.; Sofy, A. R. Preparation of Zinc Oxide Nanoparticles Using *Aspergillus niger* as Antimicrobial and Anticancer Agents. *J. Pure Appl. Microbiol.* **2021**, *15* (3), 1547–1566. https://doi.org/10.22207/JPAM.15.3.49

Messaoudi, O.; Bendahou, M. Biological Synthesis of Nanoparticles Using Endophytic Microorganisms: Current Development, Nanotechnology and the Environment. *IntechOpen* **2020**. https://doi.org/10.5772/intechopen.93734

Mills, W. D.; LaPlante, A. A. *Diseases and Insects in the Orchard*; Cornell University Agricultural Experimental Station Bulletin No. 711, **1951**; pp. 21–27.

Mills, W. D.; Laplante, A. A. Diseases and insects in the orchard. *Cornell Univ. Agric . Exp. Stn. Bull.* **1951**, *711*, 21-27.

Miralles, P.; Church, T. L.; Harris, A. T. Toxicity, Uptake, and Translocation of Engineered Nanomaterials in Vascular Plants. *Environ. Sci. Technol.* **2012**, *46*, 9224–9239. https://doi.org/10.1021/es301250j

Miri, A.; Khatami, M.; Ebrahimy, O.; Sarani, M. Cytotoxic and Antifungal Studies of Biosynthesized Zinc Oxide Nanoparticles Using Extract of *Prosopis farcta* Fruit. *Green Chem. Lett. Rev.* **2020,** *13* (1), 27–33. https://doi.org/10.1080/17518253.2020.1717005

Mistry, H.; Thakor, R.; Patil, C.; Trivedi, J.; Bariya, H. Biogenically Proficient Synthesis and Characterization of Silver Nanoparticles Employing Marine Procured Fungi *Aspergillus brunneoviolaceus* Along with Their Antibacterial and Antioxidative Potency. *Biotechnol. Lett.* **2020,** https://doi.org/10.1007/s10529-020-03008-7

Mittal, A. K.; Chisti, Y.; Banerjee, U. C. Synthesis of Metallic Nanoparticles Using Plant Extracts. *Biotechnol. Adv.* **2013**, *31* (2), 346–356. https://doi.org/10.1016/j.biotechadv.2013.01.003

Mizuno, T. *Shiitake, Lentinus edodes*: Functional Properties for Medicinal and Food Purposes. *Food Rev. Int.* **1995**, *11*, 7–21. https://doi.org/10.1080/87559129509541027

Mkhize, S. S.; Pooe, O. J.; Khoza, S.; Mongalo, I. N.; Khan, R.; Simelane, M. B. C. Characterization and Biological Evaluation of Zinc Oxide Nanoparticles Synthesized from *Pleurotus ostreatus* Mushroom. *Appl. Sci.* **2022**, *12* (17), 8563. https://doi.org/10.3390/app12178563

Mohamed, A. A.; Fouda, A.; Abdel-Rahman, M. A.; Hassan, S. E. D.; El-Gamal, M. S.; Salem, S. S.; Shaheen, T. I. Fungal Strain Impacts the Shape, Bioactivity and Multifunctional Properties of Green Synthesized Zinc Oxide Nanoparticles. *Biocatal. Agric. Biotechnol.* **2019**, *19*, 101103. https://doi.org/10.1016/j.bcab.2019.101103

Mohana, S.; Sumathi, S. *Agaricus bisporus* Mediated Synthesis of Cobalt Ferrite, Copper Ferrite, and Zinc Ferrite Nanoparticles for Hyperthermia Treatment and Drug Delivery. *J. Clust. Sci.* **2024**, *35* (1), 129–142. https://doi.org/10.1007/s10876-023-02472-4

Mohana, S.; Sumathi, S. Synthesis of Zinc Oxide Using *Agaricus bisporus* and Its In-Vitro Biological Activities. *J. Environ. Chem. Eng.* **2020**, *8* (5), 104192. https://doi.org/10.1016/j.jece.2020.104192

Mohanpuria, P.; Rana, N. K.; Yadav, S. K. Biosynthesis of Nanoparticles: Technological Concepts and Future Applications. *J. Nanopart. Res.* **2008**, *10*, 507–517. https://doi.org/10.1007/s11051-007-9275-x

Mohiudden, A. S.; Mohammed, M. J.; Jassim, M. A. Biosynthesis of Manganese Nanoparticle Mn-NPs by the Fungus *Aspergillus niger*. *IOP Conf. Ser.: Earth*

Environ. Sci. **2023,** *1214* (1), 012009. https://doi.org/10.1088/1755-1315/1214/1/012009

Mohmed, A. A.; Saad, E. D.; Hassan, S. E. D.; Fouda, A.; Elgamal, M. S.; Salem, S. S. Extracellular Biosynthesis of Silver Nanoparticles Using *Aspergillus* sp. and Evaluation of Their Antibacterial and Cytotoxicity. *J. Appl. Life Sci. Int.* **2017**, *11* (2), 1–1233491. https://doi.org/10.9734/JALSI/2017/33491

Montaño-Herrera, A.; Santiago-Saenz, Y. O.; López-Palestina, C. U.; Cadenas-Pliego, G.; Pinedo-Guerrero, Z. H.; Hernández-Fuentes, A. D.; Pinedo-Espinoza, J. M. Effects of Edaphic Fertilization and Foliar Application of Se and Zn Nanoparticles on Yield and Bioactive Compounds in *Malus domestica* L. *Horticulturae* **2022**, *8* (6), 542. https://doi.org/10.3390/horticulturae8060542

Moon, J. W.; Roh, Y.; Lauf, R. J.; Vali, H.; Yeary, L. W.; Phelps, T. J. Microbial Preparation of Metal-Substituted Magnetite Nanoparticles. *J. Microbiol. Methods* **2007,** *70* (1), 150-158. https://doi.org/10.1016/j.mimet.2007.04.006

Mooney, H. A. Carbon Dioxide Exchange of Plants in Natural Environments. *Bot. Rev.* **1972**, *38* (3), 455–469. https://doi.org/10.1007/BF02859104

Mooney, H. A.; Dunn, E. L.; Harrison, A. T.; Morrow, P. A.; Bartholomew, B.; Hays, R. L. A Mobile Laboratory for Gas Exchange Measurements. *Photosynthetica* **1971**, *5* (2), 128–132.

Morachevskii, A. G.; Beloglazov, I. N.; Poole, C. P., Jr.; Owens, F. J. Introduction to Nanotechnology. *Russ. J. Appl. Chem.* **2006**, *79*, 1213–1214. https://doi.org/10.1134/S1070427206070366

Moradnia, F.; Fardood, S. T.; Zarei, A.; Heidarzadeh, S.; Ramazani, A.; Sillanpää, M. Green Synthesis of Nickel Oxide Nanoparticles Using Plant Extracts: An Overview of Their Antibacterial, Catalytic, and Photocatalytic Efficiency in the Degradation of Organic Pollutants. *Iran. J. Catal.* **2024**, *14* (1), 1–24. https://doi.org/10.57647/j.ijc.2024.1401.01

Mosanna, R.; Khalilvand, B. E. Morpho-physiological Response of Maize (*Zea mays* L.) to Zinc Nano-chelate Foliar and Soil Application at Different Growth Stages. *J. New Biol. Rep.* **2015**, *4*, 46–50.

Moshfegh, M.; Forootanfar, H.; Zare, B.; Shahverdi, A. R.; Zarrini, G.; Faramarzi, M. A. Biological Synthesis of Au, Ag, and Au-Ag Bimetallic Nanoparticles by α-Amylase. *J. Nanomater. Biostruct.* **2011**, *6*, 1419–1426.

Mourdikoudis, S.; Pallares, R. M.; Thanh, N. T. K. Characterization techniques for nanoparticles: comparison and complementarity upon studying nanoparticle properties. *Nanoscale* **2018**, *10* (27), 12871-12934.

Mousa, S. A.; Wissa, D. A.; Hassan, H. H.; Ebnalwaled, A. A.; Khairy, S. A. Enhanced Photocatalytic Activity of Green Synthesized Zinc Oxide Nanoparticles Using Low-Cost Plant Extracts. *Sci. Rep.* **2024**, *14* (1), 16713. https://doi.org/10.1038/s41598-024-66975-1

Muhaymin, A.; Mohamed, H.E.A.; Hkiri, K.; Safdar, A.; Azizi, S.; Maaza, M. Green Synthesis of Magnesium Oxide Nanoparticles Using *Hyphaene thebaica* Extract and Their Photocatalytic Activities. *Sci. Rep.* **2024**, *14* (1), 20135. https://doi.org/10.1038/s41598-024-71149-0

Mukherjee, P.; Ahmad, A.; Mandal, D.; Senapati, S.; Sainkar, S. R.; Khan, M. I.; Parishcha, R.; Ajaykumar, P. V.; Alam, M.; Kumar, R.; Sastry, M. Fungus-Mediated Synthesis of Silver Nanoparticles and Their Immobilization in the Mycelial Matrix: A Novel Biological Approach to Nanoparticle Synthesis. *Nano Lett.* **2001**, *1* (10), 515–519. https://doi.org/10.1021/nl0155274

Mukherji, S.; Bharti, S.; Shukla, G. M.; Mukherji, S. Synthesis and Characterization of Size and Shape-Controlled Silver Nanoparticles. *Phys. Sci. Rev.* **2018**, *4*. https://doi.org/10.1515/PSR-2017-0082

Musarrat, J.; Dwivedi, S.; Singh, B. R.; Saquib, Q.; Abdulaziz, A.; Al Khedhair. Microbially Synthesized Nanoparticles, Scope, and Applications. *Microbes Microb. Technol.* **2011**, 101–126. https://doi.org/10.1007/978-1-4419-7931-5_5

Muszyńska, B.; Sułkowska-Ziaja, K.; Łojewski, M.; Opoka, W.; Zając, M.; Rojowski, J. Edible Mushrooms in Prophylaxis and Treatment of Human Diseases. *Med. Inter. Rev.* **2013**, *101*, 170–183.

Nagarajan, S.; Kuppusamy, K. A. Extracellular Synthesis of Zinc Oxide Nanoparticle Using Seaweeds of Gulf of Mannar, India. *J. Nanobiotechnol.* **2013**, *11*, 1–11. https://doi.org/10.1186/1477-3155-11-39

Nair, R.; Varghese, S. H.; Nair, B. G.; Maekawa, T.; Yoshida, Y.; Kumar, D. S. Nanoparticulate Material Delivery to Plants. *Plant Sci.* **2010**, *179*(3), 154-163. https://doi.org/10.1016/j.plantsci.2010.04.012

Narayan, T. C.; Hayee, F.; Baldi, A.; Koh, A. L.; Sinclair, R.; Dionne, J. A. Direct Visualization of Hydrogen Absorption Dynamics in Individual Palladium Nanoparticles. *Nat. Commun.* **2017,** *8* (1), 14020. https://doi.org/10.1038/ncomms14020

Narayanan, K. B.; Sakthivel, N. Biological Synthesis of Metal Nanoparticles by Microbes. *Advances in Colloid and Interface Science* **2010**, *156* (1–2), 1–13. https://doi.org/10.1016/j.cis.2010.02.001

Narware, J.; Singh, S. P.; Ranjan, P.; Behera, L.; Das, P.; Manzar, N.; Kashyap, A. S. Enhancing Tomato Growth and Early Blight Disease Resistance Through Green-Synthesized Silver Nanoparticles: Insights into Plant Physiology. *South Afr. J. Bot.* **2024**, *166*, 676–689. https://doi.org/10.1016/j.sajb.2024.01.059

Naseer, M.; Aslam, U.; Khalid, B.; Chen, B. Green Route to Synthesize Zinc Oxide Nanoparticles Using Leaf Extracts of *Cassia fistula* and *Melia azadarach* and Their Antibacterial Potential. *Sci. Rep.* **2020**, *10* (1), 9055. https://doi.org/10.1038/s41598-020-65949-3

Nassar, M. Y.; Amin, A. S.; Ahmed, I. S.; Abdallah, S. Spherelike Mn2O3 Nanoparticles: Facile Hydrothermal Synthesis and Adsorption Properties. *J. Taiwan Inst. Chem. Eng.* **2016**, *64*, 79–88. https://doi.org/10.1016/j.jtice.2016.03.041

Natarajan, K.; Selvaraj, S.; Murty, V. R. Microbial Production of Silver Nanoparticles. *Dig. J. Nanomater. Bios.* **2010**, *5*, 135–140.

Naveed Ul Haq, A.; Nadhman, A.; Ullah, I.; Mustafa, G.; Yasinzai, M.; Khan, I. Synthesis Approaches of Zinc Oxide Nanoparticles: The Dilemma of Ecotoxicity. *J. Nanomater.* **2017**, *2017*, 8510342. https://doi.org/10.1155/2017/8510342

Nekoukhou, M.; Fallah, S.; Abbasi-Surki, A.; Pokhrel, L. R.; Rostamnejadi, A. Improved Efficacy of Foliar Application of Zinc Oxide Nanoparticles on Zinc Biofortification, Primary Productivity and Secondary Metabolite Production in Dragonhead. *J. Cleaner Prod.* **2022**, *379*, 134803. https://doi.org/10.1016/j.jclepro.2022.134803

Netala, V. R.; Hou, T.; Sana, S. S.; Li, H.; Zhang, Z. Rosmarinic Acid-Rich *Perilla frutescens* Extract-Derived Silver Nanoparticles: A Green Synthesis Approach for Multifunctional Biomedical Applications Including Antibacterial, Antioxidant, and Anticancer Activities. *Molecules* **2024**, *29* (6), 1250. https://doi.org/10.3390/molecules29061250

Netala, V. R.; Kotakadi, V. S.; Bobbu, P.; Gaddam, S. A.; Tartte, V. Endophytic Fungal Isolate-Mediated Biosynthesis of Silver Nanoparticles and Their Free Radical Scavenging Activity and Antimicrobial Studies. *3 Biotech* **2016**, *6*, 1–9. https://doi.org/10.1007/s13205-016-0480-2

Nguyen, D. T. C.; Dang, H. H.; Vo, D.-V. N.; Bach, L. G.; Nguyen, T. D.; Tran, T. V. Biogenic Synthesis of MgO Nanoparticles from Different Extracts (Flower, Bark, Leaf) of *Tecoma stans* (L.) and Their Utilization in Selected Organic Dyes Treatment. *J. Hazard. Mater.* **2021,** *404*, 124146. https://doi.org/10.1016/j.jhazmat.2020.124146

Nithya, R.; Premalatha, R.; Ananthi, V.; Arun, A. Microbial Sources and Applications of Enzyme-Incorporated Nanoparticles. **In** *Nano-Enzyme Incorporated Particles*; Academic Press: **2024**; pp. 159–174. https://doi.org/10.1016/B978-0-443-18810-7.00006-5

Ogunyemi, S. O.; Abdallah, Y.; Zhang, M.; Fouad, H.; Hong, X.; Ibrahim, E.; Masum, M. M. I.; Hossain, A.; Mo, J.; Li, B. Green Synthesis of Zinc Oxide Nanoparticles Using Different Plant Extracts and Their Antibacterial Activity Against *Xanthomonas oryzae* pv. *oryzae*. *Artif. Cells Nanomed. Biotechnol.* **2019**, *47* (1), 341–352. https://doi.org/10.1080/21691401.2018.1517651

Osei, P. Mushroom Cultivation with Special Emphasis on Appropriate Techniques for Developing Countries. *Backhuys Publishers*: The Netherlands, **1996**; pp. 2–21.

Owolade, O. F.; Ogunleti, D. O.; Adenekan, M. O. Titanium Dioxide Affects Disease Development and Yield of Edible Cowpea. *Electron. J. Environ. Agric. Food Chem.* **2008**, *7* (50), 2942–2947.

Oyefusi, A.; Olanipekun, O.; Neelgund, G. M.; Peterson, D.; Stone, J. M.; Williams, E.; Oki, A. Hydroxyapatite Grafted Carbon Nanotubes and Graphene Nanosheets: Promising Bone Implant Materials. *Spectrochim. Acta A Mol. Biomol. Spectrosc.* **2014,** *132*, 410–416. https://doi.org/10.1016/j.saa.2014.04.004

Ozdal, O. G. Green Synthesis of Ag, Se, and Ag_2Se Nanoparticles by *Pseudomonas aeruginosa*: Characterization and Their Biological and Photocatalytic Applications. *Folia Microbiologica* **2024**, *69* (3), 625–638. https://doi.org/10.1007/s12223-023-01100-9

Padmavathy, N.; Vijayaraghavan, R. Enhanced Bioactivity of ZnO Nanoparticles – An Antimicrobial Study. *Sci. Technol. Adv. Mater.* **2008**, *9*, 1–7. https://doi.org/10.1088/1468-6996/9/3/035004

Pahuja, P.; Ahlawat, S.; Singh, M.; Ghosal, A.; Gupta, S. K. Green Synthesis of Metal Nanoparticles Using Essential Oils and Plant Extracts. **In** *Vegetable Oil-Based Polymers and Their Surface Applications*; Elsevier: Amsterdam, **2024**; pp. 201–218. https://doi.org/10.1016/B978-0-12-822189-1.00018-0

Pal, R.; Kumar, L.; Anand, S.; Bharadvaja, N. Environmental Pollutants Remediation Using Phyto-Nanoparticles: An Overview on Synthesis, Characterization, and Remediation Potential. **In** *Biogenic Nanomaterials for Environmental*

Sustainability: Principles, Practices, and Opportunities; **2024**; pp 111–145. https://doi.org/10.1007/978-3-031-45956-6_5

Palanikumar, L.; Ramasamy, S. N.; Balachandran, C. Size-dependent antimicrobial response of zinc oxide nanoparticles. *IET Nanobiotechnol.* **2014**, *8* (2), 111-117. https://doi.org/10.1049/iet-nbt.2012.00081

Pandit, C.; Roy, A.; Ghotekar, S.; Khusro, A.; Islam, M. N.; Emran, T. B.; Lam, S. E.; Khandaker, M. U.; Bradley, D. A. Biological Agents for Synthesis of Nanoparticles and Their Applications. *J. King Saud Univ. Sci.* **2022**, *34*, 101869. https://doi.org/10.1016/j.jksus.2022.101869

Parada, J.; Tortella, G.; Seabra, A. B.; Fincheira, P.; Rubilar, O. Potential Antifungal Effect of Copper Oxide Nanoparticles Combined with Fungicides Against *Botrytis cinerea* and *Fusarium oxysporum*. *Antibiotics* **2024**, *13* (3), 215. https://doi.org/10.3390/antibiotics13030215

Perdomo, J. A.; Sales, C. R. G.; Carmo-Silva, E. Quantification of Photosynthetic Enzymes in Leaf Extracts by Immunoblotting. **In** *Photosynthesis Methods and Protocols*; Covshoff, S., Ed.; Humana Press: Totowa, NJ, **2018**; pp. 215–227. https://doi.org/10.1007/978-1-4939-7389-8_14

Persley, D.; Horlock, C. M. *Alternaria* Leaf Blotch and Fruit Spot of Apple. **In** *Diseases of Fruit Crops in Australia*; Cooke, T., Persley, D., House, S., Eds.; CSIRO Publishing: Collingwood, Victoria, Australia, **2009**; pp. 31–39.

Piccinno, F.; Gottschalk, F.; Seeger, S.; Nowack, B. Industrial Production Quantities and Uses of Ten Engineered Nanomaterials in Europe and the World. *J. Nanopart. Res.* **2012**, *14*, 1109. https://doi.org/10.1007/s11051-012-1109-9

Pimentel, D.; McLaughlin, L.; Zepp, A.; Lakitan, B.; Kraus, T.; Kleinman P, Vancini F, Roach WJ, Graap E, Keeton WS, Selig G. Environmental and Economic Effects of Reducing Pesticide Use in Agriculture. *Agric. Ecosyst. Environ.* **1993**, *46*, 273–288. https://doi.org/10.1016/0167-8809(93)90030-S

Pons, T. L.; Flexas, J.; Von Caemmerer, S.; Evans, J. R.; Genty, B.; Ribas-Carbo, M.; Brugnoli, E. Estimating mesophyll conductance to CO2: methodology, potential errors, and recommendations. *Journal of Experimental Botany*, **2009**, *60* (8), 2217-2234.

Prachi, A. M.; Patel, R.; Singh, N.; Negi, D. S.; Rawat, S. Green Synthesis of Zinc Oxide Nanoparticles Using *Rubia cordifolia* Root Extract Against Different Bacterial Pathogens. *Indo Am. J. Pharm. Res.* **2017**, *7* (9), 759–765.

Pradell, T.; Climent-Font, A.; Molera, J.; Zucchiatti, A.; Ynsa, M. D.; Roura, P.; Crespo, D. Metallic and Nonmetallic Shine in Luster: An Elastic Ion Backscattering Study. *J. Appl. Phys.* **2007**, *101* (10), 103518–103518. https://doi.org/10.1063/1.2734944

Prasad, A. S. Green Synthesis of Nanocrystalline Manganese (II, III) Oxide. *Mater. Sci. Semicond. Process.* **2017,** *71*, 342-347. https://doi.org/10.1016/j.mssp.2017.08.034

Prasad, K. S.; Patra, A. Green Synthesis of MnO_2 Nanorods Using *Phyllanthus amarus* Plant Extract and Their Fluorescence Studies. *Green Process. Synth.* **2017,** *6* (6), 549-554. https://doi.org/10.1515/gps-2016-0132

Prasad, R. *Advances and Applications Through Fungal Nanobiotechnology. Springer, International Publishing Cham* (ISBN: 978-3-319-42989-2), **2016**.

Prasad, R. Synthesis of Silver Nanoparticles in Photosynthetic Plants. *J. Nanopart.* **2014**, 2014, Article ID 963961. https://doi.org/10.1155/2014/963961

Prasad, R.; Bhattacharyya, A.; Nguyen, Q. D. Nanotechnology in Sustainable Agriculture: Recent Developments, Challenges, and Perspectives. *Front. Microbiol.* **2017**, *8*, 1014. https://doi.org/10.3389/fmicb.2017.01014

Prasad, R.; Pandey, R.; Barman, I. Engineering Tailored Nanoparticles with Microbes: Quo Vadis? *Wiley Interdiscip. Rev. Nanomed. Nanobiotechnol.* **2016**, *8* (2), 316–330. https://doi.org/10.1002/wnan.1363

Prasad, S.; Selvam, A. P.; Reddy, R. K.; Love, A. Silicon Nanosensor for Diagnosis of Cardiovascular Proteomic Markers. *J. Lab. Autom.* **2013**, *18* (2), 143–151. https://doi.org/10.1177/2211068212460038

Pugazhendhi, A.; Kumar, S. S.; Manikandan, M.; Saravanan, M. Photocatalytic Properties and Antimicrobial Efficacy of Fe Doped CuO Nanoparticles Against Pathogenic Bacteria and Fungi. *Microb. Pathog.* **2018,** *122*, 84–89. https://doi.org/10.1016/j.micpath.2018.06.016

Pugazhendhi, A.; Prabhu, R.; Muruganantham, K.; Shanmuganathan, R.; Natarajan, S. Anticancer, Antimicrobial and Photocatalytic Activities of Green Synthesized Magnesium Oxide Nanoparticles (MgONPs) Using Aqueous Extract of *Sargassum wightii*. *J. Photochem. Photobiol. B Biol.* **2019**, *190*, 86–97. https://doi.org/10.1016/j.jphotobiol.2019.02.009

Puttoo, B. L. A New Defoliation Disease of Apple in Kashmir. *Indian J. Mycol. Plant Pathol.* **1987**, *17*, 109–110.

Qanash, H.; Bazaid, A. S.; Alharazi, T.; Barnawi, H.; Alotaibi, K.; Shater, A. R.; Abdelghany, T. M. Bioenvironmental Applications of Myco-Created Bioactive Zinc Oxide Nanoparticle-Doped Selenium Oxide Nanoparticles. *Biomass Convers. Biorefin.* **2024,** *14* (15), 17341–17352. https://doi.org/10.1007/s13399-023-03809-6

Qazi, N. A.; Ahmad, K.; Beig, M. A.; Munshi, N. A.; Khan, N. A. Impact of Inoculum Distance on the Initiation and Spread of Apple Scab Infection [*Venturia inaequalis* (Cke.) Wint.] to Isolated Apple Plantation. *Appl. Biol. Res.* **2008**, *10*, 40–43.

Quester, K.; Avalos-Borja, M.; Castro-Longoria, E. Biosynthesis and Microscopic Study of Metallic Nanoparticles. *Micron* **2013**, *54–55*, 1–27. https://doi.org/10.1016/j.micron.2013.07.003

Quimio, T. H.; Chang, S. T.; Royse, D. J. Technical Guidelines for Mushroom Growing in the Tropics; FAO: Rome, **1990**; pp. 155.

Raab, C.; Simko, M.; Fiedeler, U.; Nentwich, M.; Gazso, A. Production of Nanoparticles and Nanomaterials. *NanoTrust-Dossier* **2011**; pp. 1–4.

Radhi Devi, K.; Bruno Chandrasekar, L.; Kasirajan, K.; Karunakaran, M.; Divya Gnaneswari, M.; Usha, S. Enhanced In Vitro Antibacterial Activity of ZnO and Mn–Mg Co-Doped ZnO Nanoparticles: Investigation of Synthesis, Characterization, and Impact of Dopant. *Appl. Phys. A* **2022**, *128* (5), 368. https://doi.org/10.1007/s00339-022-06569

Radwan, M.; Moussa, M. A.; Manaa, E. A.; El-Sharkawy, M. A.; Darweesh, K. F.; Elraey, S. M.; Saleh, N. A.; Mohammadein, A.; Al-Otaibi, W. M.; Albadrani, G. M.; Al-Ghadi, M. Q. Synergistic Effect of Green Synthesis Magnesium Oxide Nanoparticles and Seaweed Extract on Improving Water Quality, Health Benefits, and Disease Resistance in Nile Tilapia. *Ecotoxicol. Environ. Saf.* **2024**, *280*, 116522. https://doi.org/10.1016/j.ecoenv.2024.116522

Ragab, G. A.; Saad-Allah, K. M. Green Synthesis of Sulfur Nanoparticles Using *Ocimum basilicum* Leaves and Its Prospective Effect on Manganese-Stressed *Helianthus annuus* (L.) Seedlings. *Ecotoxicol. Environ. Saf.* **2020,** *191*, 110242. https://doi.org/10.1016/j.ecoenv.2020.110242

Ragavendran, C.; Kamaraj, C.; Alrefaei, A. F.; Priyadharsan, A.; de Matos, L. P.; Malafaia, G.; Thirugnanasambandam, S. Green-Route Synthesis of ZnO Nanoparticles via *Solanum surattense* Leaf Extract: Characterization, Biomedical Applications, and Their Ecotoxicity Assessment in a Zebrafish Embryo Model. *South Afr. J. Bot.* **2024**, *167*, 643–662. https://doi.org/10.1016/j.sajb.2024.02.049

Raghupathi, K. R.; Koodali, R. T.; Manna, A. C. Size-Dependent Bacterial Growth Inhibition and Mechanism of Antibacterial Activity of Zinc Oxide Nanoparticles. *Langmuir* **2011**, *27* (7), 4020–4028. https://doi.org/10.1021/la104825u

Rahman, M. M.; Rahaman, M. S.; Islam, M. R.; Hossain, M. E.; Mannan Mithi, F.; Ahmed, M.; Sobarzo-Sánchez, E. Multifunctional Therapeutic Potential of Phytocomplexes and Natural Extracts for Antimicrobial Properties. *Antibiotics* **2021**, *10* (9), 1076. https://doi.org/10.3390/antibiotics10091076

Rai, M.; Bonde, S.; Golinska, P.; Trzcińska-Wencel, J.; Gade, A.; Abd-Elsalam, K. A.; Shende, S.; Gaikwad, S.; Ingle, A. P. *Fusarium* as a Novel Fungus for the Synthesis of Nanoparticles: Mechanism and Applications. *J. Fungi* **2021**, *7* (2), 139. https://doi.org/10.3390/jof7020139

Rai, M.; Ingle, A. Role of Nanotechnology in Agriculture with Special Reference to Management of Insect Pests, Pathogens, and Weeds. *Appl. Microbiol. Biotechnol.* **2012**, *94* (2), 287–293. https://doi.org/10.1007/s00253-012-3969-4

Rai, M.; Yadav, A.; Bridge, P. D.; Gade, A. Chapter 14. Myconanotechnology: A New and Emerging Science. **In** *Appl Mycology*; Rai, M., Bridge, P. D., Eds., **2009**, pp. 258. https://doi.org/10.1079/9781845935344.0258

Rajan, A.; Cherian, E.; Baskar, G. Biosynthesis of Zinc Oxide Nanoparticles Using *Aspergillus fumigatus* JCF and Its Antibacterial Activity. *Int. J. Mod. Sci. Technol.* **2016,** *1* (2), 52-57.

Rajasingam, M.; Gopinath, S. C.; Anbu, P.; Vijayakumar, S. Biological Synthesis of Zinc-Oxide Nanoparticle Using Wide-Spread *Lentinus sajor-caju* Extract as a Carrier for Natural Compounds. *Mater. Today Commun.* **2023**, *35*, 105973. https://doi.org/10.1016/j.mtcomm.2023.105973

Rajendran, S. P.; Sengodan, K. Synthesis and Characterization of Zinc Oxide and Iron Oxide Nanoparticles Using *Sesbania grandiflora* Leaf Extract as Reducing Agent. *J. Nanoscience* **2017**, *2017* (1), 8348507. https://doi.org/10.1155/2017/8348507

Rajiv, P.; Rajeshwari, S.; Venckatesh, R. Bio-Fabrication of Zinc Oxide Nanoparticles Using Leaf Extract of *Parthenium hysterophorus* L. and Its Size-Dependent Antifungal Activity Against Plant Fungal Pathogens. *Spectrochim. Acta A Mol. Biomol. Spectrosc.* **2013,** *112*, 384–387. https://doi.org/10.1016/j.saa.2013.04.072

Rajput, V.; Minkina, T.; Mazarji, M.; Shende, S.; Sushkova, S.; Mandzhieva, S.; Burachevskaya, M.; Chaplygin, V.; Singh, A.; Jatav, H. Accumulation of Nanoparticles in the Soil-Plant Systems and their Effects on Human Health. *Ann. Agric. Sci.* **2020**, *65*, 137–143. https://doi.org/10.1016/j.aoas.2020.09.008

Rajwade, J. M.; Chikte, R. G.; Paknikar, K. M. Nanomaterials: New Weapons in a Crusade Against Phytopathogens. *Appl. Microbiol. Biotechnol.* **2020,** *104* (4), 1437-1461. https://doi.org/10.1007/s00253-019-10334-y

Raliya, R.; Saharan, V.; Dimkpa, C.; Biswas, P. Nanofertilizer for Precision and Sustainable Agriculture: Current State and Future Perspectives. *J. Agric. Food Chem.* **2018**, *66* (26), 6487–6503. https://doi.org/10.1021/acs.jafc.7b02178

Raliya, R.; Tarafdar, J. C.; Choudhary, K.; Mal, P.; Raturi, A.; Gautam, R.; Singh, S. K. Synthesis of MgO Nanoparticles Using *Aspergillus tubingensis* TFR-3. *J. Bionanoscience* **2014,** *8* (1), 34-38.

Ramanujam, K.; Sundrarajan, M. Antibacterial Effects of Biosynthesized MgO Nanoparticles Using Ethanolic Fruit Extract of *Emblica officinalis*. *J. Photochem. Photobiol. B Biol.* **2014**, *141*, 296–300. https://doi.org/10.1016/j.jphotobiol.2014.10.013

Ramesh, M.; Anbuvannan, M.; Viruthagiri, G. Green Synthesis of ZnO Nanoparticles Using *Solanum nigrum* Leaf Extract and Their Antibacterial Activity. *Spectrochim. Acta A Mol. Biomol. Spectrosc.* **2014**, *136*, 864–870. https://doi.org/10.1016/j.saa.2014.09.105

Ramezani Farani, M.; Farsadrooh, M.; Zare, I.; Gholami, A.; Akhavan, O. Green Synthesis of Magnesium Oxide Nanoparticles and Nanocomposites for Photocatalytic Antimicrobial, Antibiofilm and Antifungal Applications. *Catalysts* **2023**, *13* (4), 642. https://doi.org/10.3390/catal13040642

Rana, S.; Sharma, S.; Kalia, A.; Kapoor, S. Functionalization with Bio-Molecules Derived from Oyster Mushroom (*Pleurotus florida*) Diminished the Antibacterial Potential of the Mycogenic Metal Oxide Nanoparticles (NPs). *Mushroom Res.* **2021**, *30* (1).

Rani, B. J.; Ravina, M.; Ravi, G.; Ravichandran, S.; Ganesh, V.; Yuvakkumar, R. Synthesis and Characterization of Hausmannite (Mn3O4) Nanostructures. *Surface Interface* **2018**, *11*, 28–36. https://doi.org/10.1016/j.surfn.2018.02.007

Rani, P.; Kaur, G.; Rao, K. V.; Singh, J.; Rawat, M. Impact of Green Synthesized Metal Oxide Nanoparticles on Seed Germination and Seedling Growth of *Vigna radiata* (Mung Bean) and *Cajanus cajan* (Red Gram). *J. Inorg. Organomet. Polym. Mater.* **2020**, *30*, 4053–4062. https://doi.org/10.1007/s10904-020-01602-0

Raut, S.; Thorat, P. V.; Thakre, R. Green Synthesis of Zinc Oxide (ZnO) Nanoparticles Using *Ocimum tenuiflorum* Leaves. *IJSR* **2015**, *4* (5), 1225–1228.

Raut, S.; Thorat, P. V.; Thakre, R. Green Synthesis of Zinc Oxide (ZnO) Nanoparticles Using *Ocimum tenuiflorum* Leaves. *Int. J. Sci. Res.* **2013**, *14*, 2319–7064.

Raza, M. A.; Kanwal, Z.; Rauf, A.; Sabri, A. N.; Riaz, S.; Naseem, S. Size- and Shape-Dependent Antibacterial Studies of Silver Nanoparticles Synthesized by Wet Chemical Routes. *Nanomaterials (Basel)* **2016**, *6* (4), 74. https://doi.org/10.3390/nano6040074

Rekha, K.; Nirmala, M.; Nair, M. G.; Anukaliani, A. Structural, Optical, Photocatalytic and Antibacterial Activity of Zinc Oxide and Manganese Doped Zinc Oxide Nanoparticles. *Phys. B* **2010,** *405*, 3180–3185. https://doi.org/10.1016/j.physb.2010.04.042

Rickman, D.; Luvall, J.; Mask, P.; Shaw, J.; Kissel, D.; Sullivan, D. Precision Agriculture: Changing the Face of Farming. *Geotimes*, **2003**.

Rico, C. M.; Majumdar, S.; Duarte-Gardea, M.; Peralta-Videa, J. R.; Gardea-Torresdey, J. L. Interaction of Nanoparticles with Edible Plants and Their Possible Implications in the Food Chain. *J. Agric. Food Chem.* **2011**, *59* (8), 3485–3498. https://doi.org/10.1021/jf104517j

Rilda, Y.; Ummah, K. K.; Septiani, U.; Syukri, S.; Agustien, A.; Pardi, H.; Sofyan, N. Biosynthesis of Zinc Oxide Nanorods Using *Agaricus bisporus* and Its Antibacterial Capability Enhancement with Dodecyltriethoxyl on Cotton Textiles. *Mater. Sci. Eng. B* **2023**, *298*, 116910. https://doi.org/10.1016/j.mseb.2023.116910

Roberts, J. W. Morphological Characters of *Alternaria mali* Roberts. *J. Agric. Res.* **1924**, *27*, 699–708.

Ruffolo, S. A.; La Russa, M. F.; Malagodi, M.; Oliviero Rossi, C.; Palermo, A. M.; Crisci, G. M. ZnO and ZnTiO3 Nanopowders for Antimicrobial Stone Coating. *Appl. Phys. A* **2010,** *100*, 829–834. https://doi.org/10.1007/s00339-010-5658-4

Saad, E. L.; Azab, M. S.; Saied, E. Study of the Optimal Factors for Biosynthesis of Magnesium Oxide Nanoparticles Using *Aspergillus* sp. **2018**.

Safaei, G. J.; Zahedi, S.; Javid, M.; Ghasemzadeh, M. MgO Nanoparticles: An Efficient, Green and Reusable Catalyst for the Onepot Syntheses of 2,6-Dicyanoanilines and 1,3-Diarylpropyl Malononitriles Under Different Conditions. *J. Nanostruct.* **2015**, *5*, 153–160. https://doi.org/10.22052/JNS.2015.07.008

Sagar, P. V.; Ramadevi, D.; Basavaiah, K.; Botsa, S. M. Green Synthesis of Silver Nanoparticles Using Aqueous Leaf Extract of *Saussurea obvallata* for Efficient Catalytic Reduction of Nitrophenol, Antioxidant, and Antibacterial Activity. *Water Sci. Eng.* **2024**, *17* (3), 274–282. https://doi.org/10.1016/j.wse.2023.09.004

Salavati-Niasari, M.; Esmaeili-Zare, M.; Gholami-Daghian, M. Synthesis and Characterization of Mn2O3 Nanorods Using a Novel Manganese Precursor. *Adv. Powder Technol.* **2014**, *25* (3), 879–884. https://doi.org/10.1016/j.apt.2014.01.007

Salcido-Martinez, A.; Sanchez, E.; Licon-Trillo, L. P.; Perez-Alvarez, S.; Palacio-Marquez, A.; Amaya-Olivas, N. I.; Preciado-Rangel, P. Impact of the Foliar Application of Magnesium Nanofertilizer on Physiological and Biochemical Parameters and Yield in Green Beans. *Not. Bot. Horti Agrobot. Cluj-Napoca* **2020**, *48* (4), 2167–2181. https://doi.org/10.15835/nbha48412090

Salem, S. S.; EL-Belely, E. F.; Niedbała, G.; *et al.* Bactericidal and In-Vitro Cytotoxic Efficacy of Silver Nanoparticles (Ag-NPs) Fabricated by Endophytic Actinomycetes and Their Use as Coating for the Textile Fabrics. *Nanomaterials* **2020,** *10* (10), 2082. https://doi.org/10.3390/nano10102082

Salem, S. S.; Fouda, A. Green Synthesis of Metallic Nanoparticles and Their Prospective Biotechnological Applications: An Overview. *Biol. Trace Elem. Res.* **2020,** *199*, 344–370. https://doi.org/10.1007/s12011-020-02138-3

Samsoon, S.; Azam, M.; Khan, A.; Ashraf, M.; Bhatti, H. N.; Alshawwa, S. Z.; Iqbal, M. Green-Synthesized MnO_2 Nanofertilizer Impact on Growth, Photosynthetic Pigment, and Non-Enzymatic Antioxidant of *Vigna unguiculata* Cultivar. *Biomass Convers. Biorefin.* **2024**, *14* (21), 26943–26952. https://doi.org/10.1007/s13399-022-03686-5

Sardul, S. S.; Harshita, S.; Shyamji, S. Biosynthesis of Silver Nanoparticles by Endophytic Fungi: Its Mechanism, Characterization Techniques and Antimicrobial Potential. *Afr. J. Biotechnol.* **2017,** *16* (14), 683-698. https://doi.org/10.5897/ajb2017.15873

Sawai, J.; Yoshikawa, T. Quantitative Evaluation of Antifungal Activity of Metallic Oxide Powders (MgO, CaO and ZnO) by an Indirect Conductimetric Assay. *J. Appl. Microbiol.* **2004**, *96*, 803–809. https://doi.org/10.1111/j.1365-2672.2004.02223.x

Sedefoglu, N. Green Synthesis of ZnO Nanoparticles by *Myrtus communis* Plant Extract: Investigation of Effect of Precursor, Calcination Temperature, and Study of Photocatalytic Performance. *Ceram. Int.* **2024**, *50* (6), 9884–9895. https://doi.org/10.1016/j.ceramint.2024.01.387

Senapati, U. S.; Jha, D. K.; Sarkar, D. Structural, Optical, Thermal, and Electrical Properties of Fungus-Guided Biosynthesized Zinc Sulphide Nanoparticles. *Res. J. Chem. Sci.* **2015**, *5* (6), 1-7.

Shahzad, A.; Bhat, G. N.; Mir, N. A. *Alternaria mali* – A New Pathogen of Apple in Kashmir. *SKUAST J. Res.* **2002**, *4*, 96–98.

Shamim, A.; Mahmood, T.; Abid, M. B. Biogenic Synthesis of Zinc Oxide (ZnO) Nanoparticles Using a Fungus (*Aspergillus niger*) and Their Characterization. *Int. J. Chem.* **2019**, *11* (2), 119. https://doi.org/10.5539/ijc.v11n2p119

Sharkey, T. D. What Gas Exchange Data Can Tell Us About Photosynthesis. *Plant, Cell Environ.* **2016**, *39* (6), 1161–1163. https://doi.org/10.1111/pce.12641

Sharma, D.; Kanchi, S.; Bisetty, K. Biogenic Synthesis of Nanoparticles: A Review. *Arab. J. Chem.* **2015**, *12*, 3576–3600. https://doi.org/10.1016/j.arabjc.2015.11.002

Sharma, D.; Rajput, J.; Kaith, B. S.; Kaur, M.; Sharma, S. Synthesis of ZnO NPs and Study of Their Antibacterial and Antifungal Properties. *Thin Solid Films* **2010,** *519*, 1224–1229. https://doi.org/10.1016/j.tsf.2010.08.073

Sharma, I. M. Antagonistic Effect of Fungi Associated with Apple Scab Lesions on Growth of Its Pathogen *Venturia inaequalis* (Cke.) Wint. *Res. J. Agric. Sci.* **2010**, *1*, 245–248.

Sharma, J. L.; Dhayal, V.; Sharma, R. K. White-Rot Fungus Mediated Green Synthesis of Zinc Oxide Nanoparticles and Their Impregnation on Cellulose to Develop Environmentally Friendly Antimicrobial Fibers. *3 Biotech* **2021,** *11* (6), 269. https://doi.org/10.1007/s13205-021-02840-6

Sharma, N.; Jandaik, S.; Kumar, S.; Chitkara, M.; Sandhu, I. S. Synthesis, Characterisation and Antimicrobial Activity of Manganese- and Iron-Doped Zinc Oxide Nanoparticles. *J. Exp. Nanosci.* **2016,** *11* (1), 54–71. https://doi.org/10.1080/17458080.2015.1025302

Sharma, P.; Jha, A. B.; Dubey, R. S. Utilizing Manganese-Based Nanoparticles for Enhancing Environmental Stress Resilience and Productivity of Plants. *Environ. Sci.: Nano* **2025**. https://doi.org/10.1039/D5EN00292C

Sharma, R.; Garg, R.; Kumari, A. A Review on Biogenic Synthesis, Applications, and Toxicity Aspects of Zinc Oxide Nanoparticles. *EXCLI J.* **2020**, *19*, 1325–1340. https://doi.org/10.17179/excli2020-2842

Sharvelle, E. G. *The Nature and Uses of Modern Fungicides*; Burgess Publishing Company: Minneapolis, **1961**.

Shobana, N.; Prakash, P.; Samrot, A. V.; Saigeetha, S.; Dhiva, S.; Thirumurugan, A.; Abirami, S. Natural Biopolymer Mediated Green Synthesis of Silver Nanoparticles and Its Applications in Environmental Remediation. *Biomass Convers. Biorefin.* **2024**, *1*–14. https://doi.org/10.1007/s13399-024-05282-1

Siddiqi, K. S.; Husen, A. Green Synthesis, Characterization and Uses of Palladium/Platinum Nanoparticles. *Nanoscale Res. Lett.* **2016**, *11*, 482. https://doi.org/10.1186/s11671-016-1695-z

Siddiqui, Z. A.; Khan, M. R.; Aziz, S. Use of Manganese Oxide Nanoparticle (MnO_2 NPs) and *Pseudomonas putida* for the Management of Wilt Disease Complex of Carrot. *Exp. Parasitol.* **2024**, 257, 108698. https://doi.org/10.1016/j.exppara.2024.108698

Sierra-Fernandez, A.; Gomez-Villalba, L. S.; De la Rosa-García, S. C.; Gomez-Cornelio, S.; Quintana, P.; Rabanal, M. E.; Fort, R. Inorganic Nanomaterials for the Consolidation and Antifungal Protection of Stone Heritage. *Adv. Mater. Conserv. Stone* **2018,** 125–149. https://doi.org/10.1007/978-3-319-72260-3_6

Sikong, L.; Kongreong, B.; Kantachote, D.; Sutthisripok, W. Photocatalytic Activity and Antibacterial Behavior of Fe3+-Doped TiO2/SnO2 Nanoparticles. *Energy Res.* **2010,** *1*, 120–125. https://doi.org/10.4028/www.scientific.net/JNanoR.12.89

Silva, S.; Dias, M. C.; Silva, A. M. Potential of MgO and $MgCO_3$ Nanoparticles in Modulating Lettuce Physiology to Drought. *Acta Physiol. Plant.* **2023**, *45* (2), 31. https://doi.org/10.1007/s11738-022-03507-2

Silva-Perez, V.; Molero, G.; Serbin, S. P.; Condon, A. G.; Reynolds, M. P.; Furbank, R. T.; Evans, J. R. Hyperspectral Reflectance as a Tool to Measure Biochemical and Physiological Traits in Wheat. *J. Exp. Bot.* **2017**, *69* (3), 483–496. https://doi.org/10.1093/jxb/erx421

Silver, L. T.; Phung, B. Bacterial Heavy Metal Resistance: New Surprises. *Annu. Rev. Microbiol.* **1996**, *50*, 753–789. https://doi.org/10.1146/annurev.micro.50.1.753

Singaram, G. M. P.; Selvaraj, R. Photocatalytic Degradation of Acid Violet Dye by Sunlight Exposure Using Green Synthesized Magnesium Oxide Nanoparticles. *Chem. Phys. Impact* **2024**, *8*, 100628. https://doi.org/10.1016/j.chphi.2024.100628

Singh, A.; Joshi, N. C.; Ramola, M. Magnesium Oxide Nanoparticles (MgONps): Green Synthesis, Characterizations and Antimicrobial Activity. *Res. J. Pharm. Technol.* **2019,** *12* (10), 4644-4646. http://dx.doi.org/10.5958/0974-360X.2019.00799.6

Singh, G.; Chandra, S. Insights on Microbes-Mediated Greener Synthesis of Nanoparticles: Advantages and Challenges. **In** *Applications of Nanotechnology in Microbiology*; Springer Nature Switzerland: Cham, **2024**; pp. 41–57. https://doi.org/10.1007/978-3-031-49933-3_2

Singh, J.; Dutta, T.; Kim, K. H.; Rawat, M.; Samddar, P.; Kumar, P. Green Synthesis of Metals and Their Oxide Nanoparticles: Applications for Environmental Remediation. *J. Nanobiotechnol.* **2018**, *16*, 84. https://doi.org/10.1186/s12951-018-0408-4

Singh, P.; Kim, Y. J.; Zhang, D.; Yang, D. C. Biological Synthesis of Nanoparticles from Plants and Microorganisms. *Trends Biotechnol.* **2016,** *34* (7), 588-599. https://doi.org/10.1016/j.tibtech.2016.02.006

Singh, R. P.; Shukla, V. K.; Yadav, R. S.; Sharma, P. K.; Singh, P. K.; Pandey, A. C. Biological Approach of Zinc Oxide Nanoparticles Formation and Its Characterization. *Adv. Mater. Lett.* **2011,** *2* (4), 313–317. http://dx.doi.org/10.5185/amlett.INDIAS.204

Singh, S.; Gade, J. V.; Verma, D. K.; Elyor, B.; Jain, B. Exploring ZnO Nanoparticles: UV–Visible Analysis and Different Size Estimation Methods. *Opt. Mater.* **2024**, *152*, 115422. https://doi.org/10.1016/j.optmat.2024.115422

Singh, A.; Jain, D.; Upadhyay, M. K.; Khandelwal, N.; Verma, H. N. Green Synthesis of Silver Nanoparticles Using *Argemone mexicana* Leaf Extract and Evaluation o f Their Antimicrobial Activities. *Digest J. Nanomater. Biostruct.* **2010**, *5*, 483-489.

Sirelkhatim, A.; Mahmud, S.; Seeni, A.; Kaus, N. H. M.; Ann, L. C.; Bakhori, S. K. M.; Hasan, H.; Mohamad, D. Review on Zinc Oxide Nanoparticles: Antibacterial

Activity and Toxicity Mechanism. *Nano-Micro Lett.* **2015**, *7*, 219–242. https://doi.org/10.1007/s40820-015-0040-x

Sobańska, Z.; Roszak, J.; Kowalczyk, K.; Stępnik, M. Applications and Biological Activity of Nanoparticles of Manganese and Manganese Oxides in In Vitro and In Vivo Models. *Nanomaterials* **2021,** *11* (5), 1084. https://doi.org/10.3390/nano11051084

Soni, J.; Revathi, D.; Dhanraj, G.; Ramasubburayan, R. Bioinspired Green Synthesis of ZnO Nanoparticles by Marine-Derived *Streptomyces plicatus* and Its Multifaceted Biomedicinal Properties. *Microbial Pathogenesis* **2024**, 106758. https://doi.org/10.1016/j.micpath.2024.106758

South, D. B. Inorganic Pesticides. **In** *Encyclopedia of Pest Management*; Pimentel, D., Ed.; Marcel Dekker, Inc.: New York, **2002**; pp. 395–397.

Sowani, H.; Mohite, P.; Munot, H.; Shouche, Y.; Bapat, T.; Kumar, A. R.; Kulkarni, M. Green Synthesis of Gold and Silver Nanoparticles by an Actinomycete Gordonia amicalis HS-11: Mechanistic Aspects and Biological Application. *Process Biochem.* **2015**, *51*, 374–383. https://doi.org/10.1016/j.procbio.2015.12.013

Spoehr, H. A.; McGee, J. M. Investigations in Photosynthesis. *Ind. Eng. Chem.* **1924**, *16* (2), 128–130. https://doi.org/10.1021/ie50172a004

Stamets, P. *Growing Gourmet and Medicinal Mushrooms*; Ten Speed Press: Berkeley and Toronto, **2000**; pp. 339.

Stensvand, A.; Gadoury, D. M.; Amundsen, T.; Semb, L.; Seem, R. C. Ascospore Release and Infection of Apple Leaves by Conidia and Ascospores of *Venturia inaequalis* at Low Temperatures. *Phytopathology* **1997**, *87*, 1046–1053. https://doi.org/10.1094/PHYTO.1997.87.10.1046

Stoimenov, P. K.; Klinger, R. L.; Marchin, G. L.; Klabunde, K. J. Metal Oxide Nanoparticles as Bactericidal Agents. *Langmuir* **2002,** *18* (17), 6679–6686. https://doi.org/10.1021/la0202374

Strain, B. R. Seasonal Adaptations in Photosynthesis and Respiration in Four Desert Shrubs Growing *in situ*. *Ecology* **1969**, *50* (3), 511–513. https://doi.org/10.2307/1933910

Sugirtha, P.; Divya, R.; Yedhukrishnan, R.; Suganthi, K. S.; Anusha, N.; Ponnusami, V.; Rajan, K. S. Green Synthesis of Magnesium Oxide Nanoparticles Using *Brassica oleracea* and *Punica granatum* Peels and Their Anticancer and Photocatalytic Activity. *Asian J. Chem.* **2015,** *27* (7), 1549-1553. http://dx.doi.org/10.14233/ajchem.2015.17965

Sui, M.; Zhang, L.; Sheng, L.; Huang, S.; She, L. Synthesis of ZnO-Coated Multi-Walled Carbon Nanotubes and Their Antibacterial Activities. *Sci. Total Environ.* **2013**, *452–453*, 148–154. https://doi.org/10.1016/j.scitotenv.2013.02.050

Sumanth, B.; Lakshmeesha, T. R.; Ansari, M. A.; Alzohairy, M. A.; Udayashankar, A. C.; Shobha, B.; Almatroudi, A. Mycogenic Synthesis of Extracellular Zinc Oxide Nanoparticles from *Xylaria acuta* and Its Nanoantibiotic Potential. *Int. J. Nanomedicine* **2020,** 8519-8536.

Suresh, J.; Pradheesh, G.; Alexramani, V.; Sundrarajan, M.; Hong, S. I. Green Synthesis and Characterization of Zinc Oxide Nanoparticle Using Insulin Plant (*Costus pictus* D. Don) and Investigation of Its Antimicrobial and Anticancer Activities. *Adv. Nat. Sci. Nanoscience Nanotechnology* **2018**, *9* (1), 015008. https://doi.org/10.1088/2043-6254/aabf85

Sutton, D. K.; MacHardy, W. E.; Lord, W. G. Effects of Shredding or Treating Apple Leaf Litter with Urea on Ascospore Dose of *Venturia inaequalis* and Disease Buildup. *Plant Dis.* **2000**, *84*, 1319–1326. https://doi.org/10.1094/PDIS.2000.84.12.1319

Sweet, M. J.; Chessher, A.; Singleton, I. Metal-Based Nanoparticles; Size, Function, and Areas for Advancement in Applied Microbiology. *Advances in Applied Microbiology* **2012**, *80*, 113–142. https://doi.org/10.1016/B978-0-12-394381-1.00005-2

Swihart, M. T. Vapor-Phase Synthesis of Nanoparticles. *Curr. Opin. Colloid Interface Sci.* **2003**, *8*, 127–133. https://doi.org/10.1016/S1359-0294(03)00007-4

Tahir, K.; Haroon, U.; Akbar, M.; Elahi, M.; Quraishi, U. M. Tetragonal crystalline MnO nanoparticles alleviate Pb stress in wheat by modulating antioxidant enzymes in leaves. *Physiol. Mol. Biol. Plants* **2024**, 1-11. https://doi.org/10.1007/s12298-024-01488-9

Takcı, D. K.; Ozdenefe, M. S.; Huner, T.; Takcı, H. A. M. Plant-Mediated Green Route to the Synthesis of Zinc Oxide Nanoparticles: In Vitro Antibacterial Potential. *J. Aust. Ceram. Soc.* **2024**, *1*, 1-9. https://doi.org/10.1007/s41779-024-01064-0

Talib, A.; Wu, H. F. Biomimetic Synthesis of Lotus Leaf Extract-Assisted Silver Nanoparticles and Shape-Directing Role of Cetyltrimethylammonium Bromide. *J. Mol. Liq.* **2016**, *220*, 795–801. https://doi.org/10.1016/j.molliq.2016.04.100

Talie, M. D.; Wani, A. H.; Ahmad, N. U. S. R. A. T.; Bhat, M. Y.; War, J. M. Green Synthesis of Silver Nanoparticles (AgNPs) Using *Helvella leucopus* Pers. and Their Antimycotic Activity Against Fungi Causing Fungal Rot of Apple. *Asian J. Pharm. Clin. Res.* **2020**, *13* (4), 161–165. http://dx.doi.org/10.22159/ajpcr.2020.v13i4.37024

Taourati, R.; Khaddor, M.; Laghzal, A.; El Kasmi, A. Facile One-Step Synthesis of Highly Efficient Single Oxide Nanoparticles for Photocatalytic Application. *Sci. Afr.* **2020**, *8*, e00305. https://doi.org/10.1016/j.sciaf.2020.e00305

Tari, V.; Kannan, K.; Das, J. G. K. J.; Gurushankar, K.; Wahyuni, D. K. Influence of Zinc Oxide (ZnO) Nanomaterials on the Crop: A Perspective Analysis. In *Nanomaterials in Agroforestry Systems*; Springer Nature Singapore: Singapore, **2025**; pp 171–193. https://doi.org/10.1007/978-981-96-1337-3_8

Thakkar, K. N.; Mhatre, S. S.; Parikh, R. Y. Biological synthesis of metallic nanoparti cles. *Nanomed. Nanotechnol. Biol. Med.* **2010**, *6*, 257-262. https://doi.org/10.1016/j.nano.2009.07.002

Thakur, V. S.; Sharma, R. D. Apple scab and its management, diseases of horticultura l crops. **In** *Diseases of Horticultural Crops: Fruits*; Indus Publication Co.: New Delhi, **1999**.

Thankalekshmi, R. R.; Dixit, S.; Rastogi, A. C.; Samanta, K.; Katiyar, R. S. Closed-Space Flux Sublimation Growth and Properties of (Cu-Mn)-Doped ZnO Films in Nanoneedle-Like Morphologies. *Integr. Ferroelectr.* **2011,** *125* (1), 130-140. https://doi.org/10.1080/10584587.2011.558648

Theivasanthi, T.; Alagar, M. Studies of Copper Nanoparticles Effects on Micro-Organisms. *arXiv* **2011**.

Theivsanthi, T.; Alagar, M. Electrolytic synthesis and characterization of silver nanopowder. *Nano Biomed. Eng*. **2012**, *4*, 58-65.

Thomas, M. D.; Hill, G. R. The Continuous Measurement of Photosynthesis, Respiration, and Transpiration of Alfalfa and Wheat Growing Under Field Conditions. *Plant Physiol.* **1937**, *12* (2), 285–307. https://doi.org/10.1104/pp.12.2.285

Thomas, T. S.; Kumar, S. N.; Cherian, V. K.; Rajagopal, V. Gas Exchange Parameters and Canopy Area in Relation to Coconut Productivity in Two Agro-Climatic Regions of India. *Trop. Agric.* **2008**, *85* (1), 34.

Thunugunta, T.; Channa Reddy, A.; Kodthalu Seetharamaiah, S.; Ramanna Hunashikatti, L.; Gowdra Chandrappa, S.; Cherukatu Kalathil, N.; Dhoranapalli Chinnappa Reddy, L. R. Impact of Zinc Oxide Nanoparticles on Eggplant (*S. melongena*): Studies on Growth and the Accumulation of Nanoparticles. *IET Nanobiotechnol.* **2018**, *12* (6), 706–713. https://doi.org/10.1049/iet-nbt.2018.5121

Titus, D.; Samuel, E. J. J.; Roopan, S. M. Nanoparticle Characterization Techniques. **In** *Green Synthesis, Characterization and Applications of Nanoparticles*; Roopan, S. M., Ed.; Elsevier: **2019**; pp. 303–319. https://doi.org/10.1016/B978-0-08-102579-6.00012-5

Tiwari, A. K.; Jha, S.; Tripathi, S. K.; Shukla, R.; Awasthi, R. R.; Bhardwaj, A. K.; Singh, A. K.; Dikshit, A. Spectroscopic Investigations of Green Synthesized Zinc Oxide Nanoparticles (ZnO NPs): Antioxidant and Antibacterial Activity. *Discover Appl. Sci.* **2024a**, *6* (8), 399. https://doi.org/10.1007/s42452-024-06049-z

Tiwari, V.; Bambharoliya, K. S.; Bhatt, M. D.; Nath, M.; Arora, S.; Dobriyal, A. K.; Bhatt, D. Application of Green Synthesized Copper Oxide Nanoparticles for Effective Mitigation of Fusarium Wilt Disease in Roots of *Cicer arietinum*. *Physiol. Mol. Plant Pathol.* **2024b**, *131*, 102244. https://doi.org/10.1016/j.pmpp.2024.102244

Tominaga, J.; Shimada, H.; Kawamitsu, Y. Direct measurement of intercellular CO_2 concentration in a gas-exchange system resolves overestimation using the standard method. *Journal of experimental botany*, **2018**, *69* (8), 1981-1991.

Treasure, U. N.; Christiana, A. C.; Maduabuchi, E. P.; Nnamdi, O. A.; Ebiye, E. C.; Chigozie, U. M.; Chiedu, O. F. B.; Okechukwu, E. C. The Isolation, Identification and Antimicrobial Activities of Endophytic Fungi from *Azadirachta indica*. *GSC Biol. Pharm. Sci.* **2020**, *11* (3), 115–124. https://doi.org/10.30574/gscbps.2020.11.3.0171

Tripathy, N.; Ahmad, R.; Song, J. E.; Ko, H. A.; Hahn, Y. B.; Khang, G. Photocatalytic Degradation of Methyl Orange Dye by ZnO Nanoneedle Under UV Irradiation. *Mater. Lett.* **2014,** *136*, 171–174. https://doi.org/10.1016/j.matlet.2014.08.064

Turner, M. L.; MacHardy, W. E.; Gadoury, D. M. Germination and appressorium formation by *Venturia inaequalis* during infection of apple seedling leaves, **1986**.

Usha, R.; Prabu, E.; Palaniswamy, M.; Venil, C. K.; Rajendran, R. Synthesis of Metal Oxide Nanoparticles by *Streptomyces* Sp for Development of Antimicrobial Textiles. *Glob. J. Biotechnol. Biochem.* **2010,** *5* (3), 153-160.

Vaidyanathan, R.; Kalishwaralal, K.; Gopalram, S.; Gurunathan, S. NanoSilver—The Burgeoning Therapeutic Molecule and Its Green Synthesis. *Biotechnol. Adv.* **2009**, *27*, 924–937. https://doi.org/10.1016/j.biotechadv.2009.08.001

Vanaja, M.; Annadurai, G. *Coleus aromaticus* Leaf Extract Mediated Synthesis of Silver Nanoparticles and Its Bactericidal Activity. *Appl. Nanosci.* **2013,** *3*, 217-223. https://doi.org/10.1007/s13204-012-0121-9

Vandeputte, P.; Ferrari, S.; Coste, A. T. Antifungal Resistance and New Strategies to Control Fungal Infections. *Int. J. Microbiol.* **2012**, *2012*, Article ID 713687, 1–27. https://doi.org/10.1155/2012/713687

Varshney, S.; Gupta, A. Forest Industrial Biomass Residue-Mediated Green Synthesized Multifunctional Copper Oxide Nanoparticles for Efficient Wastewater Treatment and Biomedical Applications. *J. Cleaner Prod.* **2024**, *434*, 140109. https://doi.org/10.1016/j.jclepro.2023.140109

Veeramani, H.; Aruguete, D.; Monsegue, N.; Murayama, M.; Dippon, U.; Kappler, A.; Hochella, M. F. Low-Temperature Green Synthesis of Multivalent Manganese Oxide Nanowires. *ACS Sustainable Chem. Eng.* **2013**, *1* (9), 1070–1074. https://doi.org/10.1021/sc400092v

Venkatachalam, P.; Priyanka, N.; Manikandan, K.; Ganeshbabu, I.; Indiraarulselvi, P.; Geetha, N.; Muralikrishna, K.; Bhattacharya, R. C.; Tiwari, M.; Sharma, N. Enhanced Plant Growth Promoting Role of Phycomolecules Coated Zinc Oxide Nanoparticles with Phosphorus Supplementation in Cotton (*Gossypium hirsutum* L.). *Plant Physiol. Biochem.* **2017**, *110*, 118–127. https://doi.org/10.1016/j.plaphy.2016.09.004

Villa, F.; Cappitelli, F.; Cortesi, P.; Kunova, A. Fungal biofilms: Targets for the development of novel strategies in plant disease management. *Front. Microbiol*. **2017**, *8*, 654. https://doi.org/10.3389/fmicb.2017.00654

Vinothini, A.; Conceptulaization, A. M.; Arulkumar, E.; Vedhi, C.; Thanikaikarasan, S. Green Route Synthesis of Transition Metal Doped V_2O_5 Nanoparticles, with Emerging Biomedical Applications. *Results Chem.* **2024**, *7*, 101373. https://doi.org/10.1016/j.rechem.2024.101373

VS, S.; Magar, S. J.; Somwanshi, S. D. In Vitro Antifungal Efficacy of Silver Nanoparticles Against *Fusarium oxysporum* f. sp. *Lycopersici* in Tomato. *Microbiol. Res. J. Int.* **2024**, *34* (3), 1–9. https://doi.org/10.9734/mrji/2024/v34i31432

Wadhwa, P.; Sharma, S.; Sahu, S.; Sharma, A.; Kumar, D. A Review of Nanoparticles Characterization Techniques. *Curr. Nanomater.* **2022**, *7* (3), 202–214. https://doi.org/10.2174/2405461507666220405113715

Wandati, T. W.; Kenji, G. M.; Onguso, J. M. Phytochemicals in Edible Wild Mushrooms from Selected Areas in Kenya. *J. Food Res.* **2013**, *2* (3), 137–144. https://doi.org/10.5539/jfr.v2n3p137

Wang, G.; Cao, X.; Ma, X.; Guo, M.; Liu, C.; Yan, L.; Bian, Y. Diversity and Effect of *Trichoderma* spp. Associated with Green Mold Disease on *Lentinula edodes* in China. *MicrobiologyOpen* **2016a**, *5* (4), 709–718. https://doi.org/10.1002/mbo3.366

Wang, H.; Qiao, X.; Chen, J.; Ding, S. Preparation of Silver Nanoparticles by Chemical Reduction Method. *Colloids Surf. A Physicochem. Eng. Asp.* **2005**, *256* (2–3), 111–115. https://doi.org/10.1016/j.colsurfa.2004.12.058

Wang, N.; Wolf, J.; Zhang, F. S. Towards Sustainable Intensification of Apple Production in China-Yield Gaps and Nutrient Use Efficiency in Apple Farming Systems. *J. Integr. Agric.* **2016b**, *15* (4), 716–725. https://doi.org/10.1016/S2095-3119(15)61099-1

Wang, X.; Yang, X.; Chen, S.; Li, Q.; Wang, W.; Hou, C.; Gao, X.; Wang, L.; Wang, S. Zinc Oxide Nanoparticles Affect Biomass Accumulation and Photosynthesis in *Arabidopsis*. *Front. Plant Sci.* **2016c**, *6*, 1243. https://doi.org/10.3389/fpls.2015.01243

Wani, A. H.; Shah, M. A. A Unique and Profound Effect of MgO and ZnO Nanoparticles on Some Plant Pathogenic Fungi. *J. Appl. Pharm. Sci.* **2012**, *3*, 40–44.

Wasser, S. P.; Weis, A. L. Medicinal Mushrooms, *Lentinus edodes* (Berk.) Singer; Nevo, E., Ed.; Peledfus Publ. House: Haifa, Israel, **1997**; pp. 95.

Waxman, M. F. *The Agrochemical and Pesticide Safety Handbook*; CRC Press, **1998**; pp. 616.

Wei, Y.; Salih, K. A. M.; Rabie, K.; Elwakeel, K. Z.; Zayed, Y. E.; Hamza, M. F.; Guibal, E. Development of Phosphoryl-Functionalized Algal-PEI Beads for the Sorption of Nd(III) and Mo(VI) from Aqueous Solutions–Application for Rare Earth Recovery from Acid Leachates. *Chem. Eng. J.* **2020**, *412*, 127399. https://doi.org/10.1016/j.cej.2020.127399

Willner, B.; Katz, E.; Willner, I. Electrical Contacting of Redox Proteins by Nanotechnological Means. *Curr. Opin. Biotechnol.* **2006,** *17*, 589–596. https://doi.org/10.1016/j.copbio.2006.08.007

Xu, J.; Huang, Y.; Zhu, S.; Abbes, N.; Jing, X.; Zhang, L. A Review of the Green Synthesis of ZnO Nanoparticles Using Plant Extracts and Their Prospects for Application in Antibacterial Textiles. *J. Eng. Fiber. Fabr.* **2021**, *16*, 1–14. https://doi.org/10.1177/15589250211046242

Xu, J.; Luo, X.; Wang, Y.; Feng, Y. Evaluation of Zinc Oxide Nanoparticles on Lettuce (*Lactuca sativa* L.) Growth and Soil Bacterial Community. *Environ. Sci. Pollut. Res.* **2018**, *25*, 6026–6035. https://doi.org/10.1007/s11356-017-0867-7

Xu, J.; Yang, X.; Yang, Q.; Zhang, W.; Lee, C. S. Phase Conversion from Hexagonal CuS y Se1–y to Cubic Cu2–x S y Se1–y: Composition Variation, Morphology Evolution, Optical Tuning, and Solar Cell Applications. *ACS Appl. Mater. Interfaces* **2014,** *6* (18), 16352–16359. https://doi.org/10.1021/am5046247

Yadav, A.; Jangid, N. K.; Khan, A. U. Biogenic Synthesis of ZnO Nanoparticles from *Evolvulus alsinoides* Plant Extract. *J. Umm Al-Qura Univ. Appl. Sci.* **2024**, *10* (1), 51-57. https://doi.org/10.1007/s43994-023-00076-z

Yadav, A.; Kon, K.; Kratosova, G.; Duran, N.; Ingle, A. P.; Rai, M. Fungi as an Efficient Mycosystem for the Synthesis of Metal Nanoparticles: Progress and Key Aspects of Research. *Biotechnol. Lett.* **2015**, *37* (11), 2099–2120. https://doi.org/10.1007/s10529-015-1901-6

Yah, C. S.; Simate, G. S. Nanoparticles as potential new generation broad spectrum a ntimicrobial drugs. *DARU J. Pharm. Sci.* **2015**, *23*, 43. https://doi.org/10.1186/s40199-015-0125-6

Yamamoto, A.; Nakamura, T.; Adu-Gyamfi, J. J.; Saigusa, M. Relationship between chlorophyll content in leaves of sorghum and pigeon pea determined by extraction method and by chlorophyll meter (SPAD-502). *Journal of Plant Nutrition*, **2002**, *25* (10), 2295-2301.

Yamamoto, O. Influence of Particle Size on the Antibacterial Activity of Zinc Oxide. *Int. J. Inorg. Mater.* **2001**, *3*, 643–646. https://doi.org/10.1016/S1466-6049(01)00197-0

Yang, J. H.; Lin, H. C.; Mau, J. L. Non-Volatile Taste Components of Several Commercial Mushrooms. *Food Chem.* **2001**, *72*, 465–471. https://doi.org/10.1016/S0308-8146(00)00262-4

Youtie, J.; Shapira, P.; Porter, A. L. Nanotechnology Publications and Citations by Leading Countries and Blocs. *J. Nanopart. Res.* **2008**, *10*, 981–986. https://doi.org/10.1007/s11058-008-9436-y

Yuan, S.; Yan, J.; Wang, M.; Ding, X.; Zhang, Y.; Li, W.; Cao, J.; Jiang, W. Transcriptomic and metabolic profiling reveals 'Green Ring' and 'Red Ring' on jujube fruit upon postharvest Alternaria alternata infection. *Plant Cell Physiol*. **2019**, *60*, 844-861. https://doi.org/10.1093/pcp/pcz079

Yue, L.; Feng, Y.; Ma, C.; Wang, C.; Chen, F.; Cao, X.; Xing, B. Molecular Mechanisms of Early Flowering in Tomatoes Induced by Manganese Ferrite ($MnFe_2O_4$) Nanomaterials. *ACS Nano* **2022**, *16* (4), 5636–5646. https://doi.org/10.1021/acsnano.1c10602

Yulizar, E.; Kusrini, D. O. B.; Apriandanu, N.; Nurdini, D. *Datura metel* L. Leaves Extract Mediated CeO2 Nanoparticles: Synthesis, Characterizations, and Degradation Activity of DPPH Radical. *Surf. Interfaces* **2020a**, *19*, 100437. https://doi.org/10.1016/j.surfin.2020.100437

Yulizar, Y.; Apriandanu, D. O. B.; Ashna, R. I. *La2CuO4*-Decorated ZnO Nanoparticles with Improved Photocatalytic Activity for Malachite Green Degradation. *Chem. Phys. Lett.* **2020b**, *755*, 137749. https://doi.org/10.1016/j.cplett.2020.137749

Yusof, H. M.; Mohamad, R.; Zaidan, U. H.; Rahman, N. A. A. Microbial Synthesis of Zinc Oxide Nanoparticles and Their Potential Application as an Antimicrobial Agent and a Feed Supplement in Animal Industry: A Review. *J. Anim. Sci. Biotechnol.* **2019**, *10*, 57. https://doi.org/10.1186/s40104-019-0368-z

Zahera, M.; Mishra, K.; Fatima, F. Exploiting the Bioprospecting Potential of Nanoparticles with Micro-Organisms. **In** *The Nanotechnology Driven Agriculture*; CRC Press: **2024**; pp. 245–263.

Zaker, M. Natural plant products as eco-friendly fungicides for plant diseases control: A review. *The Agricu*. **2016**, *14* (1), 134-141. https://doi.org/10.3329/agric.v14i1.29111

Zaki, M. I.; Hasan, M. A.; Pasupulety, L.; Kumari, K. Thermochemistry of manganes e oxides in reactive gas atmospheres: Probing catalytic MnOx compositions in the atmosphere of CO+O2. *Thermochim. Acta* **1998**, *311* (1-2), 97. https://doi.org/10.1016/S0040-6031(97)00417-6

Zaragosa, G. P.; Ilem, C. N. D.; Conde, B. I. C.; Garcia, J. Plant-Mediated Synthesis of Mn_3O_4 Nanoparticles: Challenges and Applications. *Nanotechnology* **2024**, *35* (34), 342001. https://doi.org/10.1088/1361-6528/ad4c71

Zayed, M. F.; Eisa, W. H. *Phoenix dactylifera L.* Leaf Extract Phytosynthesized Gold Nanoparticles; Controlled Synthesis and Catalytic Activity. *Spectrochim. Acta A Mol. Biomol. Spectrosc.* **2014,** *121*, 238-244. https://doi.org/10.1016/j.saa.2013.11.084

Zayed, M. F.; Eisa, W. H.; Hezma, A. M. Spectroscopic and Antibacterial Studies of Anisotropic Gold Nanoparticles Synthesized Using *Malva parviflora*. *J. Appl. Spectrosc.* **2017,** *83*, 1046-1050. https://doi.org/10.1007/s10812-017-0444-1

Zhang, F.; Li, S.; Wang, L.; Li, X. An Innovative Approach to Alleviate Zinc Oxide Nanoparticle Stress on Wheat through Nanobubble Irrigation. *Int. J. Mol. Sci.* **2024**, *25* (3), 1896. https://doi.org/10.3390/ijms25031896

Zhang, H. Y.; Su, W. H. Classification, Uptake, Translocation, and Detection Methods of Nanoparticles in Crop Plants: A Review. *Environ. Sci.: Nano* **2024**. https://doi.org/10.1039/D4EN00059E

Zhang, R.; Zhang, H.; Tu, C.; Hu, X.; Li, L.; Luo, Y.; Christie, P. Phytotoxicity of ZnO Nanoparticles and the Released Zn(II) Ion to Corn (*Zea mays* L.) and Cucumber (*Cucumis sativus* L.) During Germination. *Environ. Sci. Pollut. Res.* **2015,** *22*, 11109–11117. https://doi.org/10.1007/s11356-015-4325-x

Zhang, X.; Saravanakumar, K.; Sathiyaseelan, A.; Wang, M. H. Biosynthesis, Characterization, Antibacterial Activities of Manganese Nanoparticles Using *Arcopilus globulus* and Their Efficiency in Degradation of Bisphenol A. *Inorg. Chem. Commun.* **2022,** *141*, 109521. https://doi.org/10.1016/j.inoche.2022.109521

Zhang, X.; Yan, S.; Tyagi, R. D.; Surampalli, R. Y. Synthesis of Nanoparticles by Microorganisms and Their Application in Enhancing Microbiological Reaction Rates. *Chemosphere* **2011a**, *82*, 489–494. https://doi.org/10.1016/j.chemosphere.2010.10.023

Zhang, X.; Yin, K.; Huo, R.; Wang, Z.; Fan, S.; Ma, Q.; Wang, L.; Zhai, S.; Wang, J. Phytotoxic Effects of Different Concentrations of Zinc Species on Lettuce. *Water Air Soil Pollut.* **2023**, *234*, 569. https://doi.org/10.1007/s11270-023-06540-7

Zhang, Y.; Li, S.; Wang, X.; Zhang, L.; Cheung, P. C. Advances in Lentinan: Isolation, Structure, Chain Conformation and Bioactivities. *Food Hydrocolloids* **2011b**, *25* (2), 196–206. https://doi.org/10.1016/j.foodhyd.2010.03.012

Zhao, L.; Sun, Y.; Hernandez-Viezcas, J. A.; Hong, J.; Majumdar, S.; Niu, G.; Duarte-Gardea, M.; Peralta-Videa, J. R.; Gardea-Torresdey, J. L. Monitoring the

Environmental Effects of CeO2 and ZnO Nanoparticles through the Life Cycle of Corn (Zea mays) Plants and in Situ μ-XRF Mapping of Nutrients in Kernels. *Environ. Sci. Technol.* **2015**, *49* (5), 2921–2928. https://doi.org/10.1021/es5060226

Zhao, X.; Zhou, L.; Rajoka, M. S. R.; Yan, L.; Jiang, C.; Shao, D.; Zhu, J.; Shi, J.; Huang, Q.; Yang, H.; Jin, M. Fungal Silver Nanoparticles: Synthesis, Application, and Challenges. *Crit. Rev. Biotechnol.* **2018**, *38* (6), 817–835. https://doi.org/10.1080/07388551.2017.1414141

Appendices

Appendix 1

Media

1. Potato Dextrose Agar (PDA)

Ingredients	gm/L
Potato infusion	200 gm
Dextrose	20 gm
Agar	15 gm
Distilled water	1 L

2. Potato Dextrose Broth (PDB)

Ingredients	gm/L
Potato infusion	200 gm
Dextrose	20 gm
Distilled water	1 L

3. Water Agar (WA)

Ingredients	gm/L
Agar	20 gm
Distilled water	1 L

Appendix 2

Reagents

1. Sodium hypochlorite (2.5 %)

Ingredients	Quantity
Sodium hypochlorite	2.5 gm
Distilled water	100 mL

2. Zinc acetate dihydrate (0.005 M)

Ingredients	Quantity
Zinc acetate dihydrate	1.09 gm
Distilled water	1 L

3. Magnesium nitrate hexahydrate (0.005 M)

Ingredients	Quantity
Magnesium nitrate hexahydrate	1.28 gm
Distilled water	1 L

4. Manganese dioxide (0.005 M)

Ingredients	Quantity
Manganese dioxide	0.43 gm
Distilled water	1 L

5. Combination metal salt (0.005 M)

Ingredients	Quantity

Zinc acetate dihydrate	0.12 gm
Magnesium nitrate hexahydrate	0.14 gm
Manganese dioxide	0.05 gm
Distilled water	1 L

6. Methylene cotton blue stain

Ingredients	Quantity
Lactophenol cotton blue	0.125 gm
Distilled water	50 ml

Appendix 3

Instruments used

Serial No.	Instrument
1	Autoclave
2	Refrigerator
3	Hot air oven
4	Centrifuge
5	Weighing balance
6	Laminar air flow
7	BOD incubator
8	Magnetic stirrer with hot plate
9	Sonicator
10	Pipettes
11	Inoculation loop
12	Mortar and Pestle
13	Water bath
14	Light microscope
15	UV-Vis Spectrophotometer
16	FT-IR Spectrophotometer
17	X-Ray Diffractometer
18	Scanning Electron Microscope with EDX

Publications

Papers:

- **Anjum S**, Vyas A, Sofi TA. 2023. Fungi-mediated synthesis of nanoparticles: characterization process and agricultural applications. Journal of the Science of Food and Agriculture. 103(10): 4727-4741.
- **Anjum S**, Vyas A, Sofi TA. 2024. Mycogenic fabrication of zinc nanoparticles for their antifungal activity against *Alternaria mali*. Indian Journal of Microbiology 9: 1-19.
- **Anjum S**, Sofi TA, Vyas A, 2024. Mycogenic fabrication of Magnesium nanoparticles for antifungal activity against *Alternaria mali* infecting apple crop.

Book chapters:

- **Anjum S**, Vyas A, Sofi TA, Mirza U, Bera S, Chakraborty S. Fungal-Based Nanoparticles. In: Microbial Processes for Synthesizing Nanomaterials. 2023, pp. 81-111.
- **Anjum S**, Mirza U, Shafi N, Parray JA. Natural therapeutics—unexploited potential from endophytes associated with medicinal plants. In: Plant Endophytes and Secondary Metabolites. 2023.
- **Anjum S**, Nazir A, Farooq B, Farooq M, Yousuf S. Methanogenesis and its Role in Climate-Change Alleviation. In: Climate Change and Microbiome Dynamics: Carbon Cycle Feedbacks. Springer, 2023, ISBN: 978-3-031-21079-2.
- **Anjum S**, Wani NA, Ji A, Gupta V, Sharma R. Role of Nanoparticles in Plant Disease Detection. In: Impact of Climate Change Socio-Economics and Ecological Transformation in Himalayan Region. 2023. ISBN: 978-81-965883-7-3
- **Anjum S**, Mirza U, Shafi N, Parray JA. Plant–microbe interactions: perspectives in promoting plant health. In: Microbiome Drivers of Ecosystem Function. 2024, pp. 79-90.

Conferences/Seminars attended

Oral presentation on topic "**Potentialities of nanotechnology to control plant pathogenic fungi**" in the International Conference on "Nanotechnology for Better Living NBL-2023" organized by National Institute of Technology, Srinagar, held on 25-29 May, 2023.

Received Best Oral Presentation Award on topic entitled "**Activity of *Acmella oleracea* on muli-drug resistant human pathogens- *E. coli* and *S. aureus***" in the International Conference on "Impact of Climate Change on Socio-Economics and Ecological Transformation in Himalayan region" organized by Mahima Research Foundation and Social Welfare, Banaras Hindu University, Varanasi, UP, India in collaboration with Faculty of Horticulture, SKUAST-Kashmir, J&K, India, held on 21-22 September 2023.

Oral presentation on topic "**Mycogenic biofabrication of zinc nanoparticles: characterization and antifungal evaluation against *Alternaria mali***" in the International Conference on "Microbial Bioprospecting Towards Sustainable Development Goals" organized by Association of Microbiologist of India-LPU Unit and Society of Chemical and Synthetic Biology at Lovely Professional University, Punjab, held on 24- 25 November 2023.

Completed a five days Hands-on Training Program on "**Bioinformatics**" organized by Institutional Biotech Hub, Bahona College, Jorhat, held on 19-23 December 2023.

Oral presentation on topic "**Nanotechnology in the 21st Century: A Frontier Beyond Imagination**" in the International Conference on "Fundamentals and Applications of Nanotechnology (ICFAN 2024)" organized by Department of Physics, Chevalier T. Thomas Elizabeth College for Women, University of Madras in collaboration with IQAC, held on 05 January 2024.

Oral presentation on topic "**Botanical breakthroughs: exploring the green frontier with recent advancements in plant-nanotechnology integration**" in the International Marmara Scientific Research and Innovation Congress organized by International

Science and Art Research Center (ISARC), Istanbul, Turkey, held on 27-28 January 2024.

Oral presentation on topic "**Fungal-mediated synthesis of magnesium nanoparticles and evaluation as novel antifungal agents**" in the 5th International Conference on "Recent Advances in Fundamental and Applied Sciences (RAFAS-2024)" organized by School of Chemical Engineering and Physical Sciences, Lovely Professional University, Punjab, held on 19-20 April, 2024.

Oral presentation on topic "**Biological synthesis of metal oxide nanoparticles of zinc, magnesium and manganese using cell-free extracts of edible fungi**" in the 1st International Conference on "Emerging Technologies in Agriculture and Allied Sciences (ETAAS-2024)" organized by Society for Agriculture, Allied Sciences & Technology (SAAST), Odisha, School of Agriculture, SR University, Warangal & Meadow Agriculture Pvt. Ltd., UP, held on 10-11 August, 2024.